Author:
Flew, S. R. G

Title:
Extensional strain analysis of the onset of elasticity in polyacrylamide solutions flowing through porous media

EXTENSIONAL STRAIN ANALYSIS OF THE ONSET OF ELASTICITY IN POLYACRYLAMIDE SOLUTIONS FLOWING THROUGH POROUS MEDIA

by

S. R. G. Flew

A thesis submitted in fulfilment for the degree of
Doctor of Philosophy at the University of Bristol.

Department of Civil Engineering
University of Bristol

April 1990

Summary

Quantification of the rheological effects of polymer solutions flowing through a porous matrix must be achieved if high molecular weight polymers are to be used as an effective agent in augmenting oil recovery. Polymers are used both for their viscosifying effect, and as a buffer for other chemical floods. Numerical simulation is used to design these floods requiring an accurate viscosity/shear rate relationship - this, for flexible coil molecules such as polyacrylamide, is not a simple pseudoplastic expression because of the dependence on the extensional flow term at higher flowrates.

This work investigates the extensional flow of polyacrylamide solutions, at dilutions around those used in oilfield practice, in a variety of flow geometries, including planar and axi-symmetric contractions and through glass bead packs.

Polymer solutions at 100, 250 and 500 wppm, were made up in 0%, 0.05% and 3% NaCl brines to test for the effect of polymer concentration and salinity on the magnitude of this elongational behaviour.

The contraction geometries were analysed and a theory developed whereby an effective extensional strain rate could be developed which allowed the results from **all** geometries to be compared enabling the effects of size scaling and different shear strain regimes to be analysed.

It was clearly shown that polyacrylamides can exhibit resistance to flow many times that predicted by shear viscometry alone. Evidence of extensional behaviour was detected in solutions as low as 10 wppm polyacrylamide.

Visualisation of the flow patterns, using a laser to illuminate the seeded flow, highlighted the effect of polymers in changing the flow from an inertia dominated solvent flow to one dominated by extensional entrance effects.

The importance of this work to the application of high molecular weight polymers in oilfield chemistry can be clearly seen in relation to the injection of such solutions into the reservoir, through the well perforations, where very high extensional strains can be developed leading to a pressure many times those expected, hence lowering injectivity. Thus full quantification of the extensional characteristics must be undertaken before topside equipment may be sized and the polymer flood designed.

DECLARATION

I confirm that this thesis is based on my original work except as indicted in by acknowledgement and reference to published work. The work was carried out during the period May 1986 to April 1989 under the supervision of Dr. R.H.J. Sellin at the Civil Engineering Department of the University of Bristol.

No part of the work contained herein has been submitted for a degree or award to this or any other University or examining body.

Some of the material presented here has been presented to the Sponsors of this work, BP Research, in the form of yearly progress reports. These reports are unavailable to the general public.

The author is willing that this thesis should be made available for interlibrary loan or photocopying at the discretion of the Librarian of the University.

Signed : 

April 1990

ACKNOWLEDGEMENTS

My thanks go to my supervisors, Dr Robert Sellin at The University of Bristol and Dr Alistair Fletcher at the BP Research Centre in Sunbury, for the information and guidance they provided throughout the project.

Special thanks go to Phil Leonard, who constructed the intricate apparatus used here, and to Ken Jones who helped with the setting up of the apparatus. Without Phil's engineering expertise several of the experiments would not have been possible.

Thanks also go to my friends and colleagues, both in Bristol and at BP for their help and support, and to my wife, Julia, who accepted my late nights and long hours with understanding and encouragement.

CONTENTS

3. Flow mechanics

4. Experimental apparatus and technique

7. Conclusions

Appendices

FIGURES

List of Tables.

List of Plates.

NOMENCLATURE

Symbol		units	introduced on page
a	Mark Houwink exponent	-	2.13
A	Flow cross sectional area	m^2	3.3
A_h	Area of hexagon	m^2	3.38
b	Stretch parameter in FENE dumbell model	-	2.6
b	rod spacing	m	3.15
$\dot{\beta}$	strain rate	sec-1	6.10
C	Polymer concentration	g/l or ppm	2.12
c_c	Inverse contraction ratio	-	3.12
D	Column diameter	m	4.36
d_b	Bead diameter	m	3.17
d_c	Capillary diameter	m	3.17
$\Delta P, \delta p$	Differential Pressure	Pa	3.3
ϕ	Porosity of porous media	-	3.1
f_o	Fractional flow ratio	-	1.4
$\dot{\gamma}$	Shear strain rate	sec^{-1}	2.1
Γ	Polymer Relaxation time	sec	2.7
g	Acceleration due to gravity	m/s^2	
η	Non-Newtonian shear viscosity	mPa.s	2.2
h	static head loss	m	3.3
h	Characteristic height	m	3.27
h^*	Piezometric head	m	
η_a	apparent shear viscosity	mPa.s	2.2
η_∞	High shear rate viscosity	mPa.s	
η_{eff}	Observed viscosity	mPa.s	6.10
η_{ext}	Extensional Viscosity	mPa.s	6.10
η_o	Low shear rate viscosity	mPa.s	
η_{red}	Reduced shear viscosity	l/g	2.12
η_s	Solvent shear viscosity	mPa.s	2.12
j	Capillary bundle constant	-	3.18
J	Capillary bundle constant = 36j	-	3.18
j_1	Carman model constant	-	3.19
j_o	Carman model constant	-	3.18
k	Rock permeability	m^2	1.3
κ	Fluid consistency in Power Law	var	2.3
K	Hydraulic conductivity	sec/m	3.3
k'	Huggins Constant	-	2.13
K'	Mark Houwink constant	l/g	2.13
λ	Extensional viscosity constant	var	5.14,6.10
L'	Tortuosity	-	3.5
L,l	Characteristic length	m	3.3
l_e	Actual distance travelled	m	3.18

Symbol		units	introduced on page
M	Mobility ratio	-	1.3
μ	Newtonian shear viscosity	mPa.s	1.3,2.1
m	Extensional viscosity exponent	-	5.14,6.10
M_v	Viscosity average Molecular weight	mol/g	2.13
n	Shear viscosity thinning index	-	2.3
n_c	Inverse contraction ratio	-	3.12
N_{De}	Deborah Number	-	2.7
N_{Re}	Reynolds Number	-	3.18
OOIP	Original oil in place	bbl	1.10
Q	Total flowrate	m^3/sec	3.3
ρ	Fluid density	kg/m^3	3.3
R'	Gas Constant	J/kg K	2.7
R,r	Characteristic radius	m	3.9
ρ_b	Bead density	kg/m^3	4.36
R_G	Polymer radius of gyration	cm	2.13
σ_r	Rouse relaxation time	sec	2.13
τ	Shear stress	Pa	2.1
t	Carreau model time constant	sec	2.4
T	Absolute Temperature	K	2.7
U	Superficial or Darcy velocity	m/sec	3.3
ū	Average pore velocity	m/sec	3.9
f	Friction factor	-	3.18
V_s	Solid Volume	m^3	3.17
V_v	Void volume	m^3	3.17
W1	Empty column weight	kg	4.36
W2	Column weight when packed	kg	4.36
$\dot{\xi}$	Extensional strain rate	sec^{-1}	3.24
$[\eta]_o$	Intrinsic shear viscosity	l/g	2.12

var indicates units are dependant on an exponent

1. HYDROCARBON RECOVERY

1.1 Recovery Processes

The recovery of hydrocarbons from their porous rock reservoirs, many thousands of feet beneath the surface, or deep underneath the bed of the sea, poses a number of challenges as the World's easily recoverable reserves begin to decline. Normal primary recovery procedures involve the drilling of a number of wells, penetrating the reservoir, some to act as injectors, receiving fluid pumped to maintain, or enhance the natural driving pressure gradient, and some which act as producers, situated so as to maximise the extraction of the hydrocarbons from the reservoir. The injection of water or gas, to maintain the drive pressure, ensures recovery of reserves not accessible under natural conditions - as the reservoir pressure drops toward the static overpressure less hydrocarbons will be produced. Water injection also ensures that the recovery can be carried out at an economically desired rate. In practice, reservoirs exist in heterogeneous permeable rock, with the immiscible highly saline connate water and oil mutually occupying the pore spaces formed. Although less dense than the water, it is unlikely that the formation will be totally oil saturated, as the oil will typically have migrated into an initially water wet zone, where an impervious cap rock has trapped it. Most reservoir rocks are water wet, resulting in the oil globules, encompassed with water, occupying the pore voids.

The stratified nature of the reservoir results in a less than even waterflood with early breakthrough occurring along high permeability strata, leading to only a portion of the recoverable reserves being lifted. The production of water at the riser results in a far lower efficiency as only a percentage of the energy expended in injecting the water is actually leading to an increase in recovered oil. As this water cut increases the operation becomes much less efficient, and will, at some point, cease to be economically viable.

Typical oil recovery factors lie in the range 20→50% of the total original oil in place, whereas gas recoveries achieve 70→95%.

It can be easily seen then, that there is considerable scope for enhancing the recoverable reserves of oil by adopting any process that increases this yield.

1.2 Enhanced or Improved hydrocarbon Recovery

Improved recovery (IHR) processes include the stimulation of the reservoir through fracturing, or by infill drilling, whereas enhanced recovery (EOR) usually applies to processes which improve the displacement or sweep efficiencies. These secondary recovery processes, which augment primary recovery, include chemical, thermal and miscible methods. The injection of water and/or gas to maintain the reservoir pressure is usually considered a primary recovery process.

1.2.1 Thermal Processes

The recovery of heavy oil, where the high viscosity causes difficulties, can be aided by reducing its viscosity through raising the reservoir temperature. Several methods have been utilized, including steam or hot water injection, and by causing combustion to occur in situ.(1)

1.2.2 Miscible Methods

The injection of hydrocarbon solvents or lean hydrocarbon gases, or the high pressure injection of gases such as CO_2 and N_2 are generally classified miscible methods. These methods reduce the density of the oil by dissolving in it, thereby swelling the volume, and hence increasing downhole pressure.(1)

1.2.3 Chemical Processes

Chemical processes, dependent on changes in viscosity, interfacial tension or wettability, include the injection of surfactants, polymers and alkalis. Surfactants are added to decrease the interfacial tension between the oil and the water, whilst alkalis are injected to control the rock-fluid wettability, leading to a reduction in residual oil saturation.(15,27) Polymer augmented secondary recovery, using high ($>10^6$) molecular weight water soluble polymers, centres on the thickening of water for use either as diverting agents, or by the consequent improvement in mobility ratio in increasing sweep efficiency.(27,51,52) Polymer solutions are also

used as buffers, preceding or following a surfactant or alkali flood, to control the permeability or to protect the chemicals from the highly saline formation fluids.

1.3 Polymer Flooding

The displacement of oil from a reservoir by water, when the two fluids are immiscible, results in a residual oil saturation (ROS). As mentioned above reservoirs tend to be water wet, with the oil existing as globules in the pore spaces. The migration of the oil into these pores occurs over a long time span, and the globule inside the pore is likely to enlarge as more, smaller droplets migrate into the pore. The resulting globule can grow until it is larger than the surrounding pore throats, thus trapping it. (Surface tension forces will not allow the oil to deform enough to allow it to pass through the water wet throat).

Polymer flooding does not reduce the ROS, as do alkali and miscible floods, but enables the residual limit to be reached more quickly, or economically through modifying the method of displacement.

The improvement in the recovery process can occur in two ways:

1. Mobility Control.

Real reservoirs cannot be swept uniformly - even if homogeneous reservoirs existed 100% areal sweep efficiency could not be achieved at water breakthrough because of gravity and other effects.

The mobility ratio, M, is defined as

$$M = \frac{k_p \mu_o}{\mu_p k_o} \qquad - 1.1$$

where k_p and k_o are the rock relative permeabilities to the polymer solution and oil respectively, and μ_p and μ_o the fluid viscosities.

In a given situation, a high M leads to less oil being recovered before water breakthrough - particularly apparent if μ_o is high. Any change that reduces M will improve the economic recovery. Polymers achieve this by increasing the water viscosity (μ_p), and, where adsorption of the polymer molecules on to the reservoir rock occurs, by decreasing the relative permeability to water (k_p).

The fractional flow of the oil moving through a reservoir during waterflood can be represented (after applying Darcy's Law to both water and oil) by

$$f_o = \frac{1}{1 + M} \qquad - 1.2$$

where M is the mobility ratio defined above.

Any change that reduces M here will improve the rate of oil recovery, again polymers achieve this by increasing μ_p, or by decreasing k_p through adsorbed polymer.

2. Fluid Diversion

Mobility control can only be effective in the polymer flooded zone. Most reservoirs contain significant heterogeneities in the areal sense, and particularly in the vertical sense. This leads to preferential water entry into the highly permeable thief zone, depriving the majority of the reservoir, as shown in figure 1.1. The injection of polymer into a thief zone may itself produce very little extra oil, but will be highly beneficial because of the fluid diversion it produces. The penetration of the polymer into the high permeability zones will cause an increase in flow resistance here (through both viscosity increase and permeability reduction), causing water subsequently injected to flow into the unswept areas.

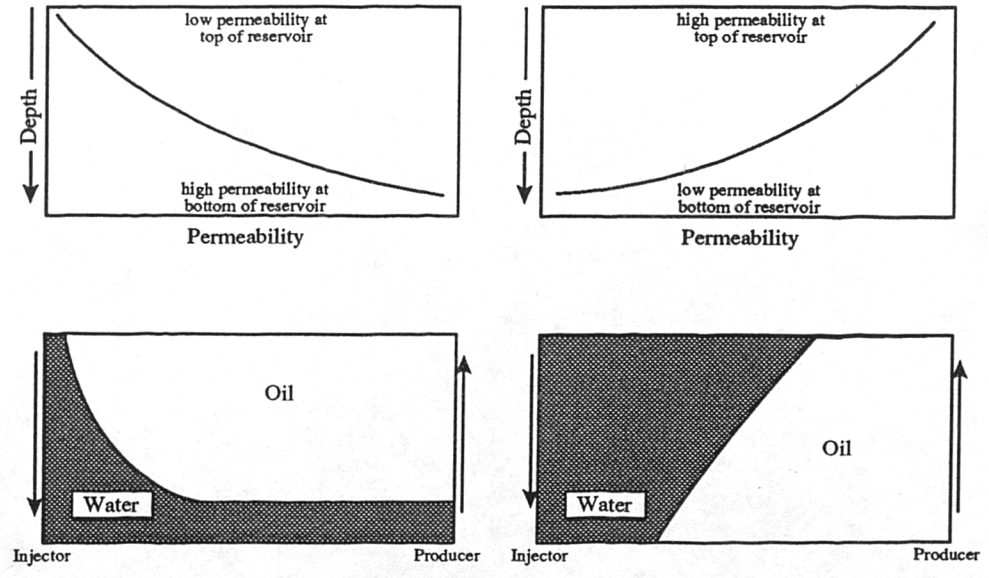

Unfavourable distribution Favourable distribution

Figure 1.1 Effect of vertical permeability distribution in waterflooding. (1)

The ability to block the thief zones maybe enhanced if the polymer is gelled. This occurs when the polymers are crosslinked to form a highly viscous fluid. In situ crosslinking can be achieved in a number of ways, including the use of organic compounds and multivalent cations, such as Cr^{3+}. The unlinked polymer solution can be initially injected into the thief zone, followed by the reagent slug, and the well closed in until the reaction is complete.

1.4 Polymers in field use.

Polymers have been used in the USA oilfields since the 1960's, initially being used for mobility control, but since then as buffers to protect other chemical floods. Much literature and field data has been published about polymer flooding, particularly in the United States, resulting in the publication of review papers (60) to compare the field effectiveness of such recovery enhancement methods. It is difficult to interpret many of the field results, as factors such as oil price, taxes, additional equipment and polymer costs have to be considered before a result can be deemed an economic success. Many of the floods have been technically successful, with an increase in the oil recovery, but as the majority of these have been tertiary operations, little experience has yet been gained in the injection into unswept reservoirs. Tertiary recovery usually applies to a process which is applied to a field which is only just economic in a hope to stimulate greater economic recovery. Typical field results are shown in table 1.1, from which it can be seen that the majority of the reservoirs have been flooded with the polymers mixed in low salinity waters, either softened formation waters, or injected from nearby rivers. Reservoir conditions have ranged from permeabilities of less than 10 mD to greater than 4 D, with temperature ranges from 15-100°C, although the majority have lain in the range 20-45°C. Polyacrylamides appear to have been the most widely used, although the availability of almost fresh water makes their choice more likely. Biopolymers have been used, particularly where the waters have had a high salinity, although problems with bacterial attack have occurred. Table 1.2 briefly outlines some of the advantages and disadvantages of the two polymer types.

Project	Start Date	Flood type	Polymer	Reservoir properties T (°C)	k (mD)	φ (%)	Result	Ref
Vernon KS, USA	1963	-	Pusher Fresh	24	27	20	S 8.6% OOIP	76
Wilmington CA, USA	1967	T	Pusher Fresh?	-	-	37.5	F	60
N Burbank OK, USA	1970	T	Pusher 0.12% TDS	47	1000-2000	11-32	S 1.6% OOIP	76
Pembina Canada	1971	T	Pusher 0.027% TDS	48	45	10-12	F	60
Bradford PS, USA	1974	T	Pusher Fresh	-	8-311	13-19	ES	77
N Stanley OK, USA	1976	-	Pusher Fresh	41	200	18	**	76
Chateaurenard France	1977	S	HPAM	30	1000	30	S	76
E Coalinga CA, USA	1978	-	Kelzan 0.071% TDS	38	50-480	26.5	** 2.8% OOIP expected	76
N Burbank OK, USA	1977	T	PAM 0.1% TDS	-	24	15.5	TS	78
Hanckenbuettel Germany	1977	S	PAM 0.017% TDS	58	300-4000	28	S ~60% OOIP total	60
Byron WY, USA	1982	T	-	50	13.9	-	* expect 20% increase	79

Note:

- indicates information unavailable

Result:
S indicates success (increase in yield)
TS indicates technical success
ES indicates economic success
* indicates too early to tell
** indicates encouraging results to date
F indicates failure (no change or decrease in yield)

Flood type:
S indicates a secondary operation
T indicates a tertiary operation

Table 1.1 Field results of polymer floods in the USA

Xanthan	Polyacrylamide
Advantages:	
Shear degradation resistant Insensitive to high salinity brines	Higher viscosity at a given polymer concentration in water, hence lower cost Good injectivity Not susceptible to microbial attack
Disadvantages:	
Well bore plugging due to high cell debris and microgels Microbial degradation *	Susceptible to shear degradation Reduction in viscosity in high salinity brines Susceptible to flocculation and degradation in presence of divalent ions Thermal instability in the presence of oxygen *

Note : * The addition of biocides and/or oxygen scavengers can limit these problems.

Table 1.2 Advantages and disadvantages of polyacrylamides against xanthan. (after 80)

1.4.1 Flooding of North Sea reservoirs

The technology applied to reservoirs in the USA, and elsewhere, cannot be applied directly to the North Sea, as conditions are generally more severe. The requirement that seawater, with a salinity of 3.2% TDS, be the injection fluid limits the application of polymer injection to those polymers that can give adequate properties in such saline waters. This can be further limited when formation brines of up to 25% TDS are encountered. Divalent metal ions (Mg^{2+} and Ca^{2+}) are detrimental to the polymer performance and can account for up to 35% of the total dissolved solids. The application could also be further limited by prolonged exposure to the very high reservoir temperatures (up to 110°C) and pressures (up to 450 bar), although initial injection temperatures will obviously be much lower. The injection of filtered seawater, and in some instances the re-injection of produced gas, have been widely used, almost since startup in some fields, to recover the oil at as high a rate as possible. Table 1.3 lists some of the possible fields where enhanced recovery techniques could be applied. A major constraint upon the application of these techniques is our inability to predict accurately the flow of these diverse fluids. The present research programme into the flow behaviour of polymer solutions, and hence improving our predictions of behaviour, is an essential step in solving this problem.

1.4.2 Economics of polymer flooding

Whilst polymer flooding can be used as either a secondary or as a tertiary recovery process, analysis of field results indicate that it has a much higher potential in secondary applications. The review paper by Needham and Doe (60), which considers some 27 case histories, concludes that secondary floods recover significantly more oil for less polymer usage than tertiary applications - polymer flooding is best therefore applied early in the life of a waterflood, before the high permeability zones become watered out.

Field	rock type	Reservoir properties T(°C)	k(mD)	φ(%)	Handling Capacity Production BOPD	Injection BWPD
Forties	s/s	-	1-753	20-29	500,000	450,000
					seawater injection since Dec 1976	
Piper	s	79	1500	24	300,000	250,000
					seawater since early 1978	
Thistle	s	-	?	?	216,000	250,000
					seawater since 1979, gas planned	
Brent	s	-	1500	29	600,000	1,000,000
					seawater injection since 1979	
Beryl A	?	-	?	?	-	-
					gas since 1977, seawater 1979	

where : s/s refers to sandstone and shale
s refers to sandstone

Table 1.3 Characteristics of some North Sea Oilfields (15)

Beyond a WOR of 10 the performance of polymer floods appears significantly lower.
Comparison of secondary and tertiary applications indicate that about four times the potential recovery is achieved by a secondary flood. Tertiary floods also require about 6 times more polymer per barrel of oil recovered.

The newer technology of crosslinking appears to further enhance yields - reported recoveries from secondary operations are about 1.5 times higher than for non-crosslinked operations per pound of polymer used.

As the ultimate ROS is the same for polymer and water floods, the economic advantage of using polymers is the ability to recover more oil (incremental oil recovery) for a given WOR, as shown in figure 1.2 (60)

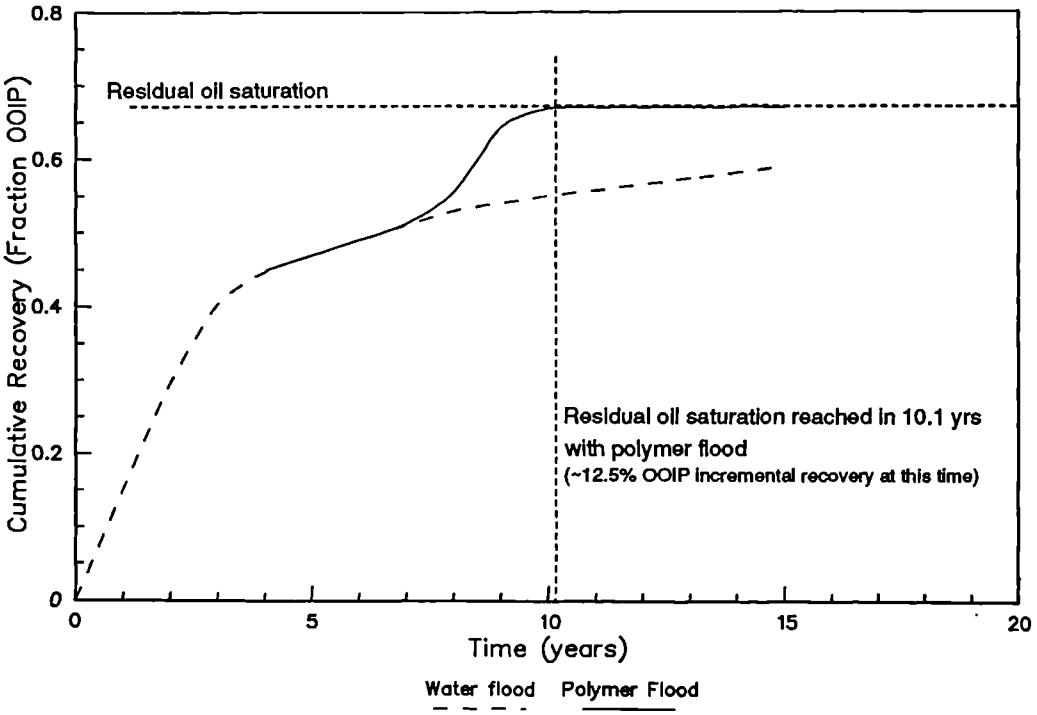

Figure 1.2 Incremental advantage of polymer flooding

2. SOLUTION MECHANICS

2.1 FLUID CHARACTERISTICS

Fluids are usually characterised by how the coefficient of their resistance to change of form (viscosity) varies with the rate of flow, and are classified as either Newtonian, or non-Newtonian, depending on whether the viscosity varies with strain rate or not.

2.1.1 Newtonian behaviour

A fluid can be considered Newtonian when a linear relationship, passing through the origin, exists between the shear stress and the rate of shear strain, as shown in figure 2.1. The relation, based on Newton's third law for flow between two parallel plates, is commonly written;

$$\tau = \mu \frac{\delta u}{\delta y} = \mu \dot{\gamma} \qquad -2.1$$

where: τ = fluid shear stress (N/m^2),

$\delta u/\delta y$ (or $\dot{\gamma}$)) = rate of shear strain (s^{-1}),

and, μ = the coefficient of proportionality (Ns/m^2), more commonly known as the absolute, or dynamic viscosity.

The viscosity of a Newtonian liquid is, by definition, constant for all rates of shear strain (at a constant temperature), and is usually measured in centiPoise (cP), where;

$$1\ cP = 10^{-3} Pa.s$$

$$(1Pa\ (\equiv Pascal) \equiv 1\ Nsm^{-2})$$

2.1.2 Non-Newtonian behaviour

Fluids that do not obey the simple relationship between shear stress and shear strain are termed non-Newtonian. Several classes of non-Newtonian fluids exist, which in general can be grouped as;

1. Time independent fluids,

where the shear rate is a unique, but non-linear function of shear stress. This group includes fluids that have a yield stress.

2. Time dependent fluids,

which have a more complex shearing stress-strain relationship. With these fluids the shear strain rate is not a single valued function of shear stress, but is dependent on shearing time or on the previous shear rate history of the fluid.

3. Viscoelastic fluids,

where some of the energy of deformation may be recoverable when the shear stress is removed.

A non-Newtonian fluid may have a combination of the above attributes, leading to a far more complex stress-strain relationship than is the case for a Newtonian (linear) fluid. Figure 2.1 illustrates some of the most common time independent fluid characteristics.

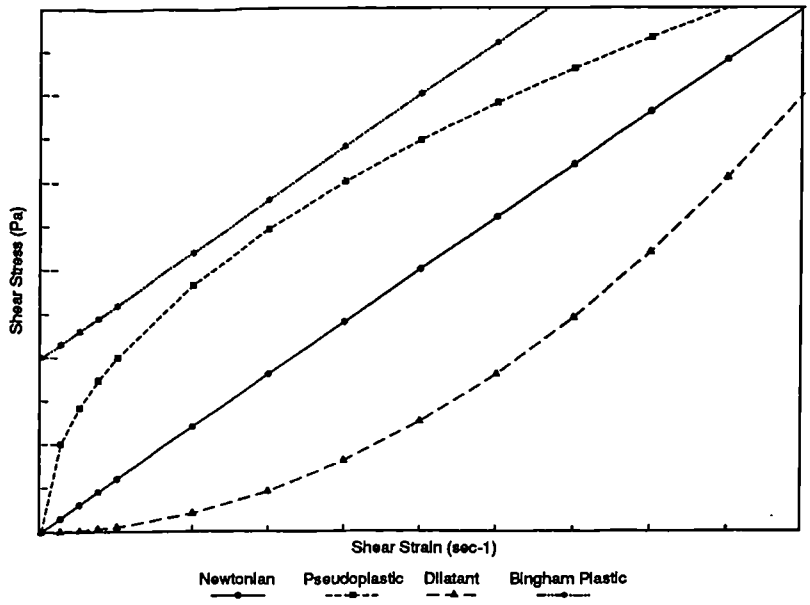

Figure 2.1 Stress-strain relationships for different (time independent) fluid types.

2.1.3 Pseudoplastic fluids

These fluids, known more simply as shear thinning fluids, are characterised by a progressively decreasing slope of shear stress vs shear strain rate - this slope being defined as the apparent viscosity;

$$\eta_a = \tau/\dot{\gamma} \qquad \text{- 2.2}$$

For most pseudoplastic fluids the apparent viscosity is constant at very low and very high rates of shear and equal to η_0 and η_∞ respectively [see footnote]. In the majority of applications only the central, shear thinning region, where the apparent viscosity is decreasing with increasing shear strain, is of interest, and so the simplest of the proposed, empirical relationships can be used. This relationship, the power law, or Ostwald-de Waele model may be written as;

$$\tau = \kappa\dot{\gamma}^n \qquad \text{(where } n<1\text{)} \qquad \text{- 2.3}$$

For a given fluid, κ and n are assumed constant over the range considered. κ is a measure of fluid consistency, and n, the exponent, a measure of how the fluid deviates from Newtonian behaviour. For a Newtonian fluid n=1 and $\kappa=\mu$, the viscosity.

Using equ 2.2 for apparent viscosity, and equ 2.3 for the shear stress/strain rate relationship, we may write;

$$\eta_a = \kappa\dot{\gamma}^{n-1} \qquad \text{- 2.4}$$

Several objections exist to the use of this model;

1. when the shear rate is zero, the apparent viscosity is infinite,
2. the value of n is not constant over the entire flow range,
3. κ has dimensions dependent on n.

However, due to the simplicity, and applicability to the shear thinning region normally encountered, it is the most widely used of all the models.

Note: In 2.1.1 μ was used to signify (Newtonian) viscosity, which is strain rate independent - where the viscosity of the fluid is rate dependent it will be represented by η

When it is required to model the entire shear rate range, a model which has found wide acceptance is the Carreau model, which can be written;

$$\eta = \eta_\infty + \frac{\eta_O - \eta_\infty}{[1 + (\dot{\gamma}t)^2]^{(1-n)/2}} \qquad - 2.5$$

where; η_O and η_∞ are the low and high shear rate viscosity plateau values,
n is the power law index governing behaviour in the shear thinning region,

and, t is a time constant - usually the inverse of the shear rate at the departure from the lower Newtonian plateau.

Two variations of this model exist - model A, where $\eta_\infty = 0$, and model B, where η_∞ is usually given the value of the solvent viscosity. A comparison of the viscosity predictions using both Carreau models, and the power law is shown in figure 2.2. Several other models, as shown in table 2.1 exist but, because of the increasing complexity, usually require extensive computation to calculate the values of the model constants.

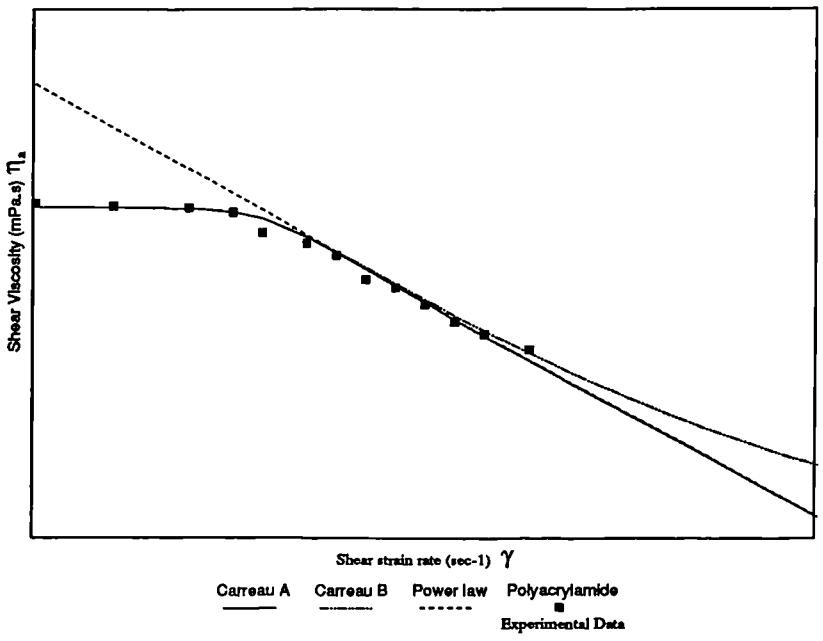

Figure 2.2 Comparison of model viscosity predictions

Model Name	Expression	Comments
Ellis	$\eta = \eta_o/[1+(\tau/\tau_*)^{1-A}]$	
Oldroyd (81)	$\eta = \eta_o(1+a_1\gamma^2)/(1+a_2\dot{\gamma}^2)$	
Jones (83)	$\eta = a - b\dot{\gamma}^2$	$a \approx \eta_o$
Van Wazer (82)	$\eta = \eta_\infty + (\eta-\eta_\infty)/(1+c_1\tau+c_2\tau^m)$	empirical
Sisko (81)	$\eta = A + B\dot{\gamma}^{(n-1)}$	
Prandtl-Eyring (81)	$\tau = A.\sinh^{-1}(\dot{\gamma}/B)$	$\sinh^{-1}x = 0.5(e^x-e^{-x})$
Harris (81)	$\eta = \eta_o[1-a(1-\exp(-\lambda^2\dot{\gamma}^2)]$	

Table 2.1 Shear stress/strain/viscosity models

2.1.4 Dilatent Fluids

Dilatent fluids differ from pseudoplastic fluids in that the apparent viscosity increases with intensifying shear strain rate, and are commonly known as shear-thickening fluids. These fluids are far less common than shear thinning fluids, and if represented by a power law have an exponent n greater than unity.

2.1.5 Viscoelastic Fluids

These fluids have both viscous and elastic properties. The most simple type is one which is Newtonian in viscosity behaviour, and obeys Hooke's Law for the elastic region, for which we can write :

$$\dot{\gamma} = \tau/\mu + \dot{\tau}/k \qquad -2.6$$

where k is a rigidity modulus.

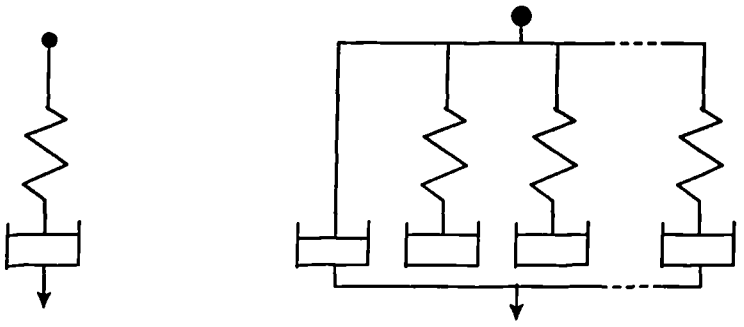

Figure 2.3 Schematic representation of Maxwell and generalised viscoelastic fluid models

Under steady flow $\dot{\gamma} = \tau/\mu$ and the fluid behaves as a Newtonian liquid. However, if the shear stress is changed, an elastic effect is noticed. Fluids that obey equ 2.6 are known as Maxwell liquids (see figure 2.3), although he proposed the relation in the form:

$$\mu\dot{\gamma} = \tau + (\mu/k)\dot{\tau} \qquad -2.7$$

where the constant $(\mu/k)^{-1}$ is known as the relaxation time - the time constant for exponential decay at a constant strain.
(If the motion is stopped the stress relaxes as $e^{-tk/\mu}$).

Other approaches have been based on the apparent ability to model the major properties of a polymer solution using a finite-extensible, nonlinear-elastic dumbbell to represent the polymer molecule, as proposed by Warner (86). His ideas, as illustrated in figure 2.4, consist of two spheres, representing the total molecular mass, connected by a massless spring with a non-linear force-displacement law. At small extensions, z, the model reacts linearly, but gets stiffer and stiffer as the spring is further extended up to its maximum extension of z_o.

FENE-Dumbbell (Warner)

Solvent (μ_s), FENE-Dumbbell

$$F = \text{const} \times \frac{z}{1-(z/z_o)^2}$$

$$\tau = \frac{b+5}{b}\frac{[\eta]\mu_s M}{AkT}$$
(see below)

Figure 2.4 Molecular models using Warner's FENE dumbbells, after (23)

If these finite extensible, nonlinear elastic (FENE) dumbbells are suspended in a Newtonian solvent of viscosity η_s, then a viscoelastic model of the polymer solution is obtained, which is characterised by the viscous properties of the solvent and the elastic nature of the dumbbells.

Combining these two properties in the definition of a relaxation time, Γ, produces:

$$\Gamma = \frac{[\eta]\eta_S M}{R'T} \qquad - 2.8$$

where, $[\eta]$ is the intrinsic viscosity, M the molecular weight, T the absolute temperature and R' the gas constant. Equation 2.8 holds for very large values of the stretching parameter $b=(z_o/z)^2$.

The Deborah number, N_{De}, is usually used to characterise the onset of viscoelastic behaviour. This is defined as the ratio of the relaxation time of the solution to the characteristic flow time;

$$N_{De} = \frac{\text{Relaxation time of the liquid}}{\text{Characteristic time of flow}} = \frac{\Gamma}{(1/\dot{\xi})}$$

hence,

$$N_{De} = \Gamma.\dot{\xi} \qquad - 2.9$$

where, in the case of extensional flows, the characteristic time of the flow may be expressed as the inverse of the elongational rate, $\dot{\xi}$.

2.2 POLYMERS FOR SECONDARY RECOVERY

The two main types of polymers used for enhanced oil recovery are synthetics, such as polyacrylamides (PAM or HPAM), and biopolymers, such as Xanthan (a polysaccharide).

2.2.1 Polyacrylamides

These synthetic polymers, consist of long, flexible chains of molecules that are free to extend and contract depending on the solvent and flow conditions. The structure of polyacrylamide is shown in figure 2.5a; however the samples used in this work have been partially hydrolysed, with a resulting modification to the structure of some of the monomer units (the number depending on the degree of hydrolysis) as shown in figure 2.5b.

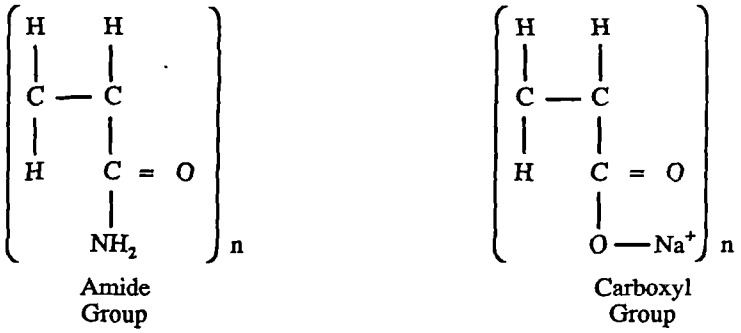

(a) Polyacrylamide structure (b) Modified hydrolysed structure

Figure 2.5 Structure of polyacrylamide molecules.(80)

The greater the degree of hydrolysis, the higher the viscosity at any given polymer concentration and salt content. Both groups (amides and carboxyls) are highly polar, which gives the polymer a high affinity for water (hydrophillic), but not for oil. In addition to being soluble in water, these groups have a strong attraction to sandstone and limestone surfaces. Solutions of polyacrylamides yield very high viscosities at low shear rates when the solvent is of zero ionic strength, but this decreases rapidly with increasing salt content, the electrolytes screening the

interaction of charges along the polymer molecule. The flexible nature of these polymers results in a viscoelastic response when moving through an accelerating flow field. The stronger the accelerating forces the more unravelled the chain becomes until a point when the chain starts to stretch. If stretching continues the chains will break, leading to a reduction in (apparent) viscosity. The unravelling and stretching of the chains leads to high viscous forces initially between the chains, and then to elastic forces as the chain is stretched. The presence of salt in the solvent enhances this increase in (viscoelastic) pressure loss, as the polymers already exist in a more relaxed, uncoiled state when the solvent is of low ionic strength.

2.2.2 Biopolymers

Biopolymers usually exist as rigid molecules with few ionizable groups, so that increasing ionic strength, or flow accelerations have little effect on the apparent solution viscosity. As these polymers are a 'natural' fermentation product they are usually supplied in the form of a broth, of which only a percentage will be active polymer. To disperse the molecules into a homogeneous solution high speed shear blending is used, the inactive cell debris from the broth is then filtered off. This is in complete contrast to PAMs which are often supplied as a high purity powder which is then dissolved in the solvent, whilst being slowly stirred.

2.2.3 Application to oil recovery

To be of use in secondary recovery processes a polymer solution must exhibit a high viscosity under reservoir conditions after being injected. Conditions near the well bore, including the perforations, could result in a shear rate greater than $1000sec^{-1}$, whilst deep in the reservoir the rates would significantly drop to less than $0.001sec^{-1}$ (72).

The variation of the solution's viscosity, higher at the lower shear rates found deep in the reservoir than at the large shear rates near the well bore is very significant. A comparable viscosity variation will also exist between low and high permeability zones where differing pore sizes result in different shear rates at a given flowrate. The inclusion of the elastic element could also significantly control the flow - the high extensional rates found near the well bore could induce the shear thickening response of many synthetic polymers. Conditions within some reservoirs could reach 90-100°C with a salinity of 25% TDS (52), although prior waterflooding of reservoirs usually greatly reduces both the temperature and salinity in the direction of the injected fluid conditions of 3.2% TDS at 10°C if seawater is injected. Long term stability is also an important factor as the polymer slug will be required to enhance recovery throughout its passage through the reservoir, which could take years to complete. It is therefore desirable to use a polymer which is not susceptible to excessive shear degradation, or chain scission caused by high extensional rates. It is quickly realised that to provide useful information on how the solution is likely to react to flow through the tortuous porous medium the solution characteristics of how its viscosity (both shear and extensional) varies with the rate of deformation is required.

2.3 Bulk Solution Properties

A solution may be described by its overall properties, for example by its molecular weight or intrinsic viscosity rather than by conditions specific to particular values of shear or extensional viscosity.

2.3.1 Viscosity as a function of deformation rate

As has been shown above (2.1.3), the shear viscosity of most polymer solutions is characterised by three regions - a low shear rate Newtonian plateau (I), a region of shear thinning (II), and a high shear rate plateau (III). Extensional viscosity on the other hand exhibits a constant resistance until the onset of stretching behaviour is reached as shown in figure 2.6.

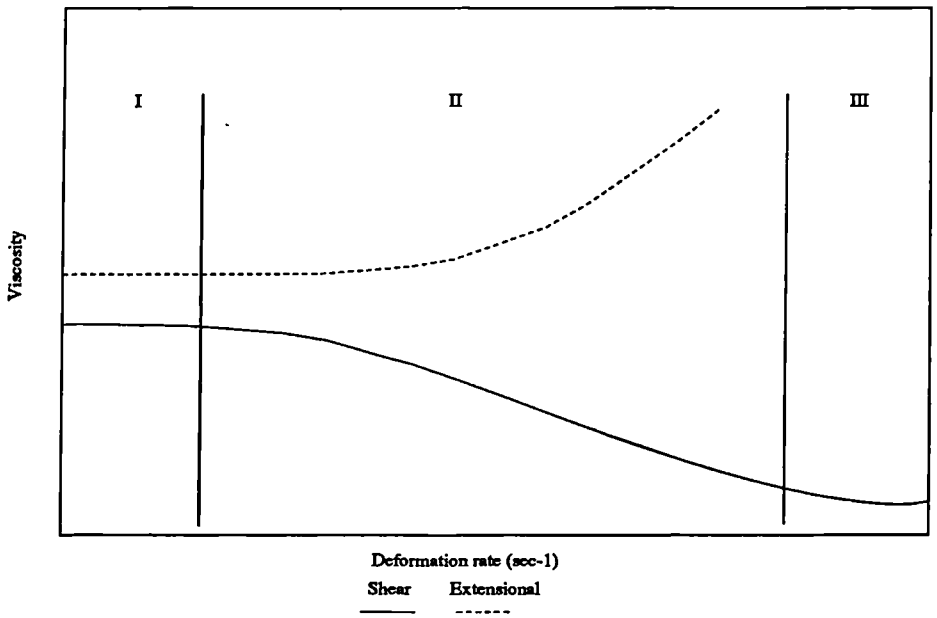

Figure 2.6 Variation of viscosity with deformation rate

2.3.2 Intrinsic Shear Viscosity

The intrinsic viscosity (IV) of a polymer solution is a useful measure of its viscosifying effect - the higher the IV the greater the solution's shear viscosity at a given concentration. The nature of the intrinsic viscosity - independent of shear (see below) and concentration - results in a single parameter which can be used to compare the viscosifying effect of different polymers.

As polymer solutions are, in general, shear thinning, the value of the IV will depend on the shear rate used to determine the solution viscosity. At low shear rates the IV approaches a limiting value $[\eta]_o$, which is known as the zero shear rate IV, through the low shear Newtonian plateau. Obviously, in the shear thinning region the IV is highly sensitive to shear rate, whilst in the high shear rate Newtonian plateau only small deviations from the solvent viscosity are encountered resulting in lower accuracy.

The low shear IV, $[\eta]_o$ is found by extrapolating the reduced viscosity (η_{red}) vs concentration curve back to zero concentration, which cannot be calculated directly because of the division by zero encountered in :

$$\eta_{red} = \left(\frac{\eta - \eta_s}{C\eta_s} \right) \qquad \text{- 2.10}$$

where η is the polymer solution viscosity, η_s is the solvent viscosity and C the concentration (g/l).

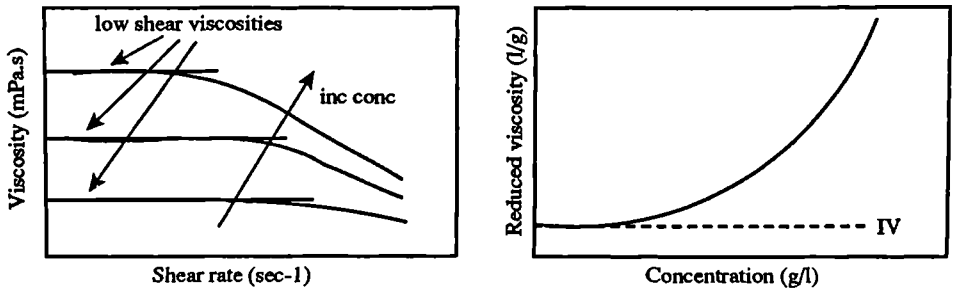

Figure 2.7 Comparison of Intrinsic and shear viscosities

Thus the IV is given by :

$$[\eta]_o = \lim_{\substack{C \to 0 \\ \dot{\gamma} \to 0}} [\eta_{red}] = \lim_{\substack{C \to 0 \\ \dot{\gamma} \to 0}} \left(\frac{\eta - \eta_s}{C\eta_s} \right) \qquad \text{- 2.11}$$

It is worthwhile to note the importance of the IV, as this can be used in other relationships to predict, for example, a viscosity-average molecular weight. The intrinsic viscosity function itself is based on the fact that a solution's viscosity can be expressed by a Taylor series in the concentration C ;

$$\frac{\eta}{\eta_s} = 1 + [\eta]C + k'[\eta]^2C^2 + \ldots \qquad - 2.12$$

where $[\eta]$ and k' (the Huggins constant) are independent of concentration.
As was mentioned above, the IV gives a measure of the polymer molecular weight (the viscosity average molecular weight) through the Mark-Houwink relation :

$$[\eta]_o = K'M_v^a \qquad - 2.13$$

where K' and a (the Mark-Houwink exponent) are dependent on the polymer solvent pair.
Thus, by monitoring the IV it is possible to establish the degree of chain scission undergone by a solution. (Note: the molecular weight of any polymer is not a single value, a distribution of molecular weights will naturally exist, with the quoted value being the average.)
The zero shear rate IV has also been related to the polymer molecular dimensions (82), through the Flory-Fox relationship, to determine the hydrodynamic radius of gyration R_G:

$$[\eta]_o = \Phi'\frac{\langle R_G \rangle^3}{M} \qquad - 2.14$$

where Φ', a nearly universal constant $\simeq 4.2 \times 10^{24}$, when R_G is given in cm, and $[\eta]_o$ in cm^3/g. The Rouse equation predicts the longest molecular relaxation time, σ_r, and has been written by Chauveteau (7) as:

$$\sigma_r = 6\eta_s(\eta_{redo} - 1)M/\pi^2CR'T \qquad - 2.15$$

where η_s is the solvent viscosity and R' is the gas constant. This equation is applicable for solutions that are not strictly dilute - where a limited amount of chain interactions are possible.

2.3.3 Molecular conformation

The changes undergone by the polymer chains in solution can be considered as either reversible, caused by changes in temperature or electrolyte concentration, or irreversible, caused by chemical degradation or depolymerisation due to high temperatures. The former, reversible changes in conformation, will be considered here; details of factors influencing degradation may be found later.

2.3.3.1 Effect of temperature

The viscosity of polymer solutions decreases with a rise in temperature and can be modelled by an Arrhenius type equation:

$$\eta = \text{const} \times e^{(Ea/R'T)} \qquad - 2.16$$

where Ea is the activation energy, T the temperature (in K) and R' the gas constant. Polyacrylamides have two activation energies, resulting in very little change in viscosity with temperatures up to ~35°C, and a higher rate of reduction beyond this point. Xanthan, in contrast, exhibits a constant viscosity reduction at a rate similar to the polyacrylamide's higher temperature rate.

2.3.3.2 Effect of solvent ionic strength

Solvent conditions have a strong effect on the viscosity of polymer solutions, with high ionic strength formation waters causing a large conformational change to the molecular chains (of ionic polymers). Polyacrylamides are very sensitive to salt (43), with xanthan and solutions of HEC less so. In fresh waters the ionic dissociation of the polyelectrolytes results in large repulsive forces among the charged groups present along the chain length leading to greatly expanded conformations and hence large molecular dimensions. Electrolytes in the solvent solution shield the charges, resulting in a decrease in molecular dimensions, and hence viscosity. Once all the available charged sites on the polymer chains are shielded any additional electrolytes are relatively ineffective at decreasing the viscosity. The presence of bi- and tri- valent cations affects the viscosity to a greater extent than monovalents as they are more effective at shielding the polymer. Xanthan, being much less ionic than PAMs, is affected to a much lower degree by salt concentration.

2.3.4 Degradation

Polymer solutions are susceptible to degradation through both mechanical (chain scission) and chemical (thermal or oxidative) means. Mungan (59) clearly illustrated the existence of a limiting temperature, beyond which severe degradation occurred as shown in figure 2.8.

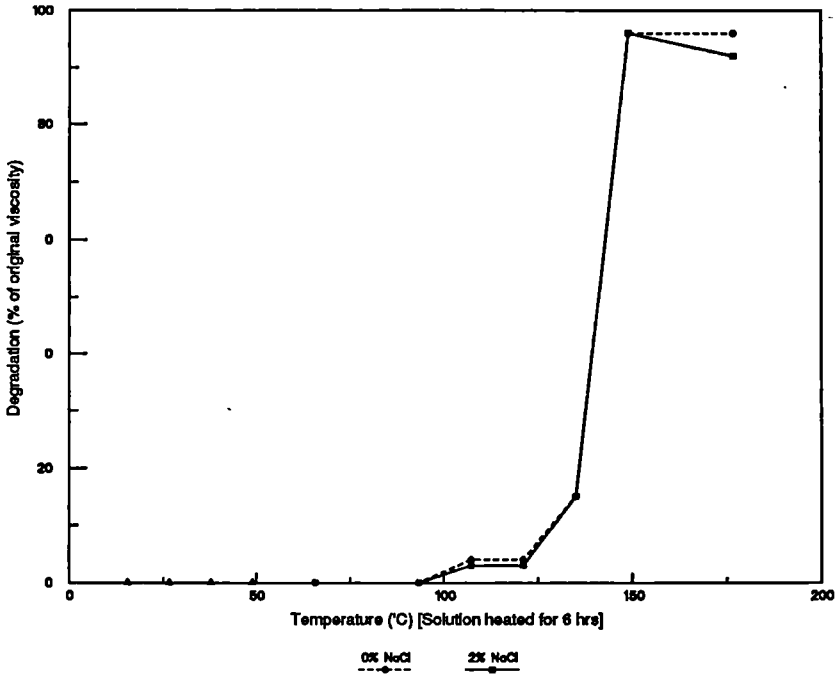

Figure 2.8 Effect of temperature on viscosity (after 59)

Below this limiting temperature, both the works by Mungan and that of Morris (89) report no degradative loss of solution (shear) viscosity. It can be seen then, that the resultant loss of viscosity from temperature alone will not be significant. However, particularly in the case of PAMs prolonged exposure at temperatures in excess of 40°C in the presence of magnesium or calcium ions can cause precipitation (19,62,85) of the polymer from solution. Chemical degradation, in the case of synthetic polymers results in the breakdown of the molecule into its base units. Free radical initiators, particularly O_2 and Fe^{2+} cause removal of the hydrogen atoms, and eventually results in decomposition (57,34,88). The addition of an

oxygen scavenger, such as sodium hydrosulphite, can stabilise the make-up water, but equal care must be taken to limit the exposure to metal ions, which can be dissolved in the connate water, may be present in the process equipment or found on the reservoir rock surface. Mechanical degradation, that is physical damage to the molecular chains, can occur in a variety of situations, from the pumping equipment through to the reservoir rock pores themselves. Synthetic polymers are particularly sensitive to this type of degradation as opposed to biopolymers which can be safely mixed at high shear. Many authors (84,87) have commented on the inaccuracies encountered by just equating shear viscosity loss to degradation. Jennings et al (43) suggested that screen factors are more sensitive to chain breakup, as it is the long molecular chains that contribute most to the elastic behaviour of the solution. High extensional rates can cause degradation, and as these are highest in the well bore/perforation region care must be taken to ensure injection rates do not induce chain scisson.

2.3.5 Polymer retention

Several mechanisms have been identified as causing retention of polymer molecules in porous media, which can lead to a reduction in effectiveness the further the polymer solution travels. Three major mechanisms are adsorption of molecules onto solid surfaces, mechanical entrapment in small pores, and hydrodynamic retention which is flowrate dependent.

Adsorption of the polymer onto rock surfaces is beneficial when controlling the mobility of the displacing fluid. The adsorbed molecule may attach itself onto the rock at a few points along its length, leaving the rest to protrude into the flow stream, allowing entrapment of other molecules, thus building up a layer much thicker than the molecular dimensions. This polymer layer increases the flow resistance in those passages, diverting the flow elsewhere. Figure 2.9a illustrates this phenomenon. It is known (14,57,85) that in waters of salinities up to 10% TDS calcium ions can cause a higher level of polyacrylamide adsorption than sodium ions. It is therefore important to carefully establish conditions prior to injection, particularly in carbonate reservoirs, or areas where the connate water is particularly hard.

Mechanical entrapment will occur where the dimensions of a molecule are of the same size as the pore. Figure 2.9b shows some of the possible sites where molecules could become trapped during their flow. As mentioned above the presence of an adsorbed polymer layer can enhance mechanical retention as there will be a level of interaction between the chains of a flowing molecule and the adsorbed one, as illustrated in figure 2.9c.

Hydrodynamic retention, or molecular trapping due to flow forces, is a reversible process. Several authors (19,90) have noted that the amount of retained polymer increases with decreasing mobility, and that at the inception of a higher flowrate significantly more polymer is retained than before the increase. This increase in retention, however, tends to reduce as, it is thought, all available sites become occupied. A decrease in flowrate leads to a lowering of hydrodynamic pressures which allows some of the molecules to uncoil slightly and get flushed out. A recent study by Cohen and Christ (14) concluded that adsorption (of a HPAM) accounted for ~35% of the total polymer retention in their packed beds, attributing the remainder to mechanical and/or hydrodynamic retention. Their results predicted an effective hydrodynamic thickness (EHT) of 0.57μm at their lowest flowrate, and decreasing with increasing flowrate. More importantly for flow deep in a reservoir, where the flow will be slow, the EHT increased with lower interstitial velocities.

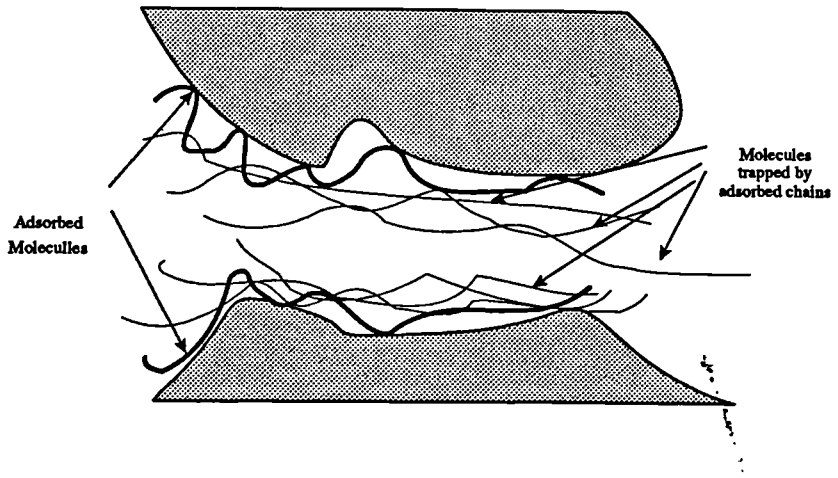

Figure 2.9a Illustration of adsorbed molecules aiding further retention

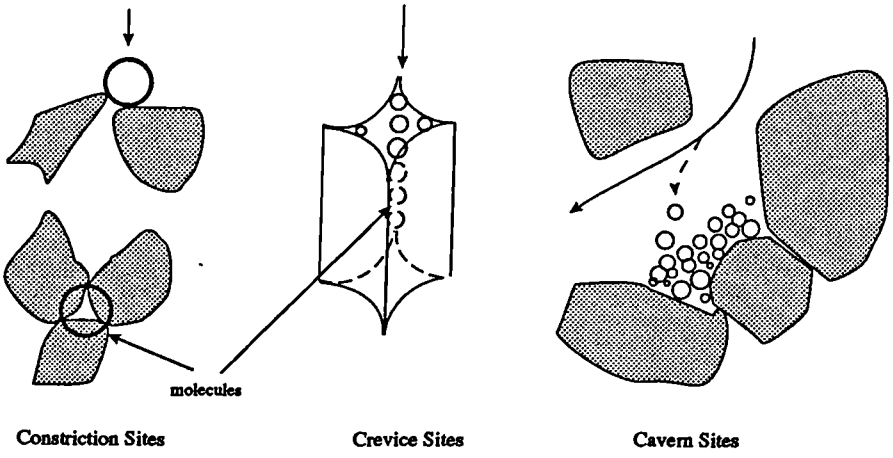

Figure 2.9b Adsorption sites within a porous medium

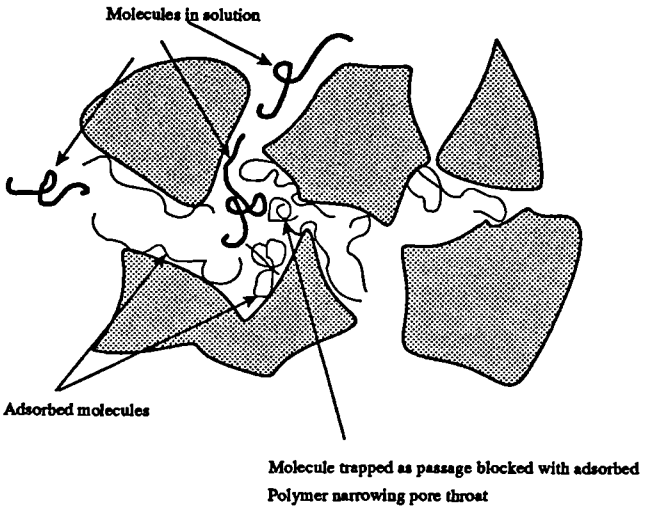

Figure 2.9c Fluid diversion effects through adsorbed polymer

3. FLOW MECHANICS

3.1 Porous Media

A porous material can be considered as containing a series of interconnected voids, the shape and size of these determining the medium's intrinsic properties of porosity and permeability, although the two are not readily relatable due to the dependence of permeability on passage shape (pore geometry). This description of porous media applies equally to consolidated media, such as porous rock or sintered glass discs, and unconsolidated media, such as glass bead packs, uncemented sands, gravels and soils. It is the flow of liquids through the pores in these media that is the current area of study, and how to *define the flow regimes* that exist therein. Models exist that attempt to define the flow but, in the main, fail in that no account is taken of the continuously changing flow cross sectional area. The most useful of these models will be reviewed briefly, and a new analysis presented to predict the extensional strain rate inherent in these passages.

3.1.1 Porosity

Porosity can be considered the most basic definition of a porous medium. Generally symbolised by ϕ, it is defined as the ratio of void volume to bulk volume.

$$\phi = \frac{\text{volume of voids}}{\text{total volume}} \qquad - 3.1$$

The porosity of commercial oil reservoir rocks are usually in the range 0.1 to 0.3 (10 to 30% of total volume), unconsolidated glass bead packs range from 0.2795 (for close hexagonal packing) to 0.4764 (open cubic packing) in porosity for monodisperse beads.

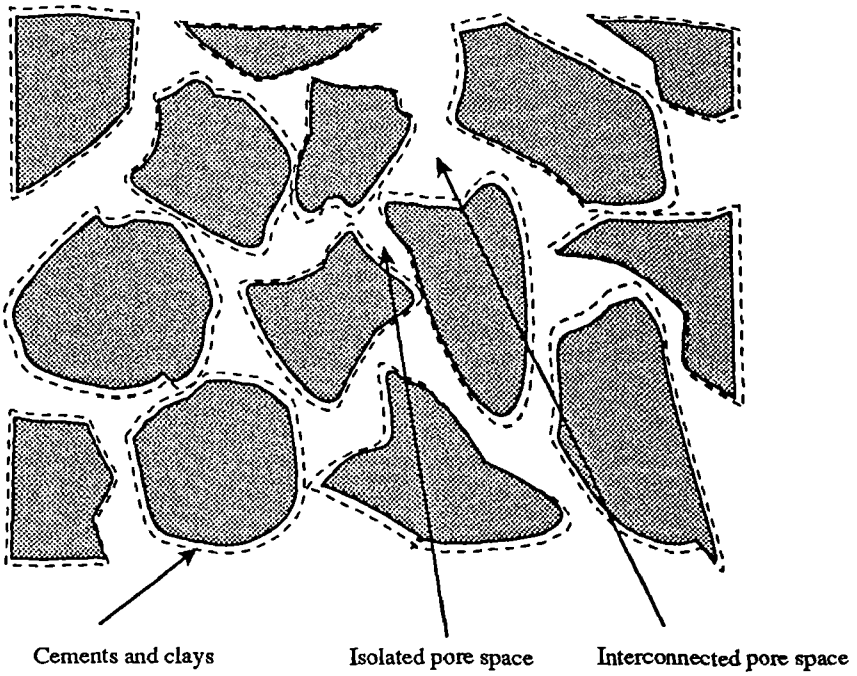

Figure 3.1 Representation of Porosity.

Porosity can be measured in a variety of ways in the lab., or estimated insitu in the reservoir by wireline logs. Measurement of porosity in the lab can be effected by a material balance, by mercury porosimetry (displacement or infusion) or by estimating the grain volume via Boyle's Law in a gas pressurisation system. Some of these methods will only measure the 'effective porosity' ϕ_e - that is passages that are interconnected and provide a flow path in the matrix - blocked or inaccessible pore space being the difference between ϕ_e and ϕ. In an unconsolidated medium no passages should be blocked, so $\phi_e = \phi$. In the case of an artificially constructed medium, such as a glass bead pack, the porosity maybe more easily calculated from compacting a known volume of the solid, to produce a measurable bulk volume of medium, the difference being the volume of voids. As mentioned above, glass bead pack porosities should lie between a maximum of 0.4764 and a minimum of 0.2795 for monodisperse beads, the two extremes indicating the limits of ordered packing. When a media is randomly packed the porosity has been estimated at between 0.36 to 0.42, depending on the method of packing (28). For random packing of beads with a narrow size distribution, the porosity has been estimated at between 0.39 to 0.42 - the smaller beads too large still to fill the voids formed by the larger beads. For monodisperse spheres the porosity is not a function of diameter, only of packing arrangement.

3.1.2 Permeability

The permeability of a medium is a measure of its specific flow capacity (either resistance at constant flowrate, or produced flow under constant driving pressure). As mentioned above, porosity and permeability are not directly related, as permeability is a measure of pore space continuity, and not of the relative volumes of the pores themselves. However a high porosity is required for a high permeability, and conversely a zero porosity must result in a zero permeability. For unconsolidated media it is possible to establish some form of relationship between porosity, apparent pore diameter (or specific surface) and permeability . Darcy (92) in 1856 originally studied the vertical filtration of water, and experimentally derived the relation :

$$\frac{Q}{A} = U = -\text{constant} \times \frac{dh^*}{dl} \qquad -3.2$$

The constant in this relation (negative as dh^*/dl is -ve in the direction of flow) is usually called K - the hydraulic conductivity, and is dependent on the fluid used (and therefore is also temperature dependent). The intrinsic permeability k is related to the hydraulic conductivity by the relationship :

$$k = \frac{K\mu}{\rho g} = \frac{\mu Q}{A\rho g(dh^*/dl)} = \frac{Q\mu L}{A\Delta P} \qquad -3.3$$

where ΔP is the pressure drop over length L when passing a fluid of viscosity μ through the porous media of bed cross sectional area A at a flowrate Q. This definition makes the permeability k independent of the fluid, measuring only the porous media properties. (Note: Gas permeabilities will differ slightly due to fluid compressibility).

The unit of permeability in the oil industry is the Darcy, and is defined as:

A rock has a permeability of 1 Darcy if a potential gradient of 1 atm/cm induces a 1 cm^3/s flowrate of a 1 cP viscosity fluid through a 1 cm^2 cross sectional area of rock 1 cm in length.

1 Darcy	$= .98 \times 10^{-12} m^2$	$= .98 \times 10^{-8} cm^2$	symbol D
1 milliDarcy	$= .98 \times 10^{-15} m^2$	$= .98 \times 10^{-11} cm^2$	symbol mD

Permeabilities can range from several Darcys for bead and unconsolidated sand packs to less than 1 mD for a very tight layer in a reservoir, typical reservoir rock permeabilities lie in the range 10 → 500 mD. In the laboratory permeabilities must be measured by flow tests, either under constant pressure or constant flow, producing a relationship between flow and pressure loss. Insitu, permeability can be estimated by electrical or pumping means (1). Unlike porosity, the permeability of an artificially constructed porous media is highly dependant on the average particle size, as illustrated in figure 3.2 - smaller particles leading to smaller pores which induce higher frictional resistance and therefore decrease the permeability.

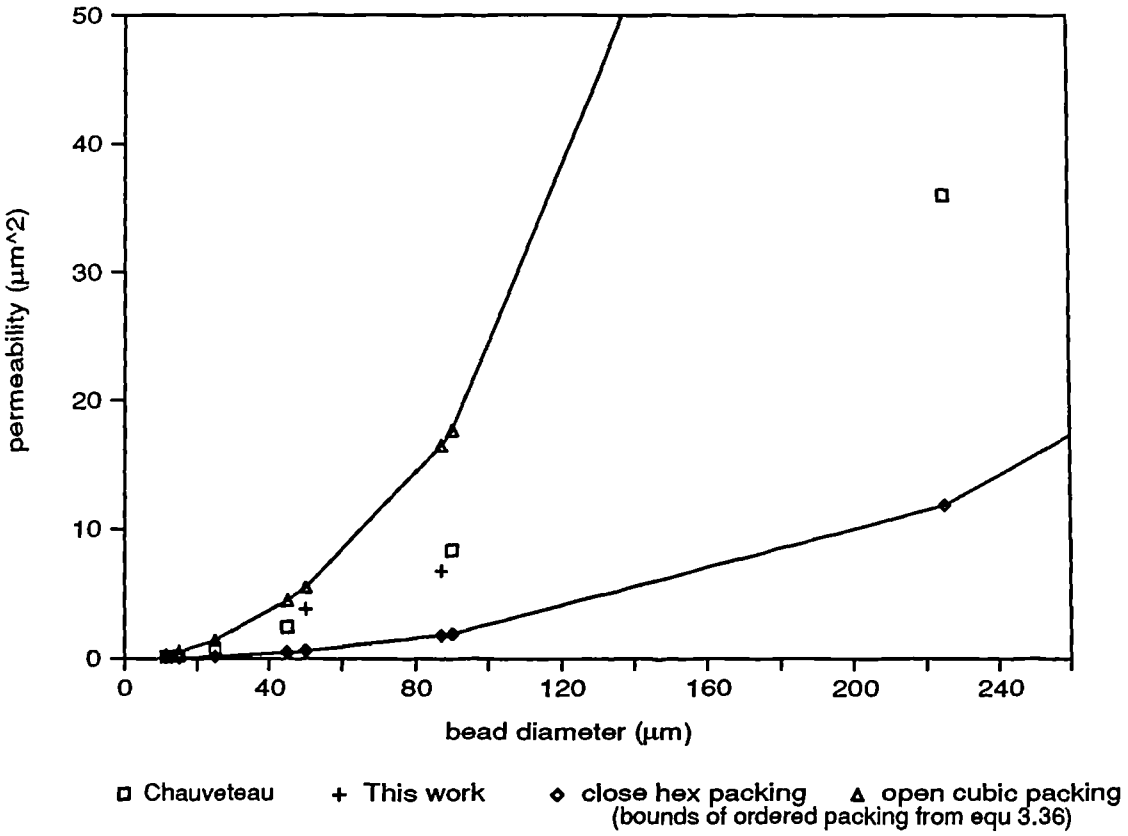

Figure 3.2 Variation of permeability with average particle diameter

In reservoirs this is usually further complicated by the lack of isotropy, ($k_x \neq k_y \neq k_z$) - this is important as averaging techniques have to be applied to reservoir flows to estimate the regional (direction specific) flowrates. Stratification of reservoirs leads to more problems, here permeability modification systems, such as polymer gelling are used to divert flow from the higher permeability strata into the tighter payzones.

3.1.3 Tortuosity

Tortuosity is defined as the ratio of the actual distance travelled by the fluid to the overall linear length of the porous medium, as shown in figure 3.3. Tortuosity, L', is thus dependant on pore geometry.

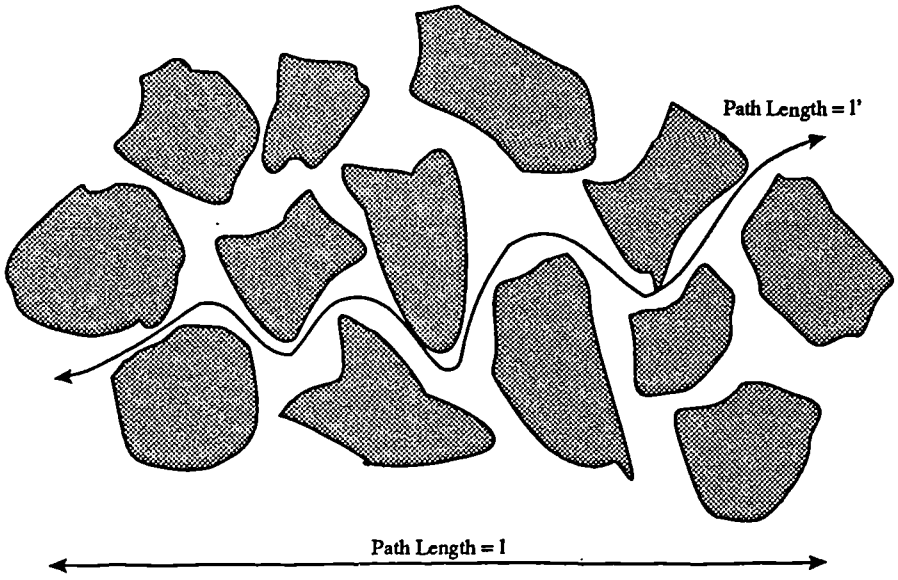

Figure 3.3 Representation of tortuosity

3.1.4 Pore Geometry

The geometry of the flow passages occurring in rock can be best described as a tube whose cross sectional area, shape and direction is constantly changing, with additional side tubes forming intersections with other equally complex pores. It is impossible to quantify the dimensional variation along a single pore as being representative of the sample as a whole.

Artificially constructed porous media have, however, better defined flow passages, from the straight cylindrical pore of a Nuclepore© filter to the constantly changing tricuspid passages of a monodisperse glass bead pack. The precise flow geometry of pores in a multidisperse bead pack are less well defined, but can be assumed to be close to those obtained from close hexagonal packing (each bead in contact in one layer with its 6 neighbours), the geometry of which is easily defined. In a column, packed tightly in close hexagonal arrangement with glass beads (in at least 2 dimensions) a combination of two pore types may exist:

1. The most simple case is known as ABA packing; this, illustrated in figure 3.4a, results in continuous pores the length of the column (hence tortuosity=1). The pore geometry formed consists of a tricuspid throat formed between three beads, opening out into an expansion chamber, where parallel pores interconnect, before contracting to another tricusp, in the opposite orientation to the first, as in figure 3.4b. This contraction - expansion - rotate - contraction - expansion is replicated every two layers.

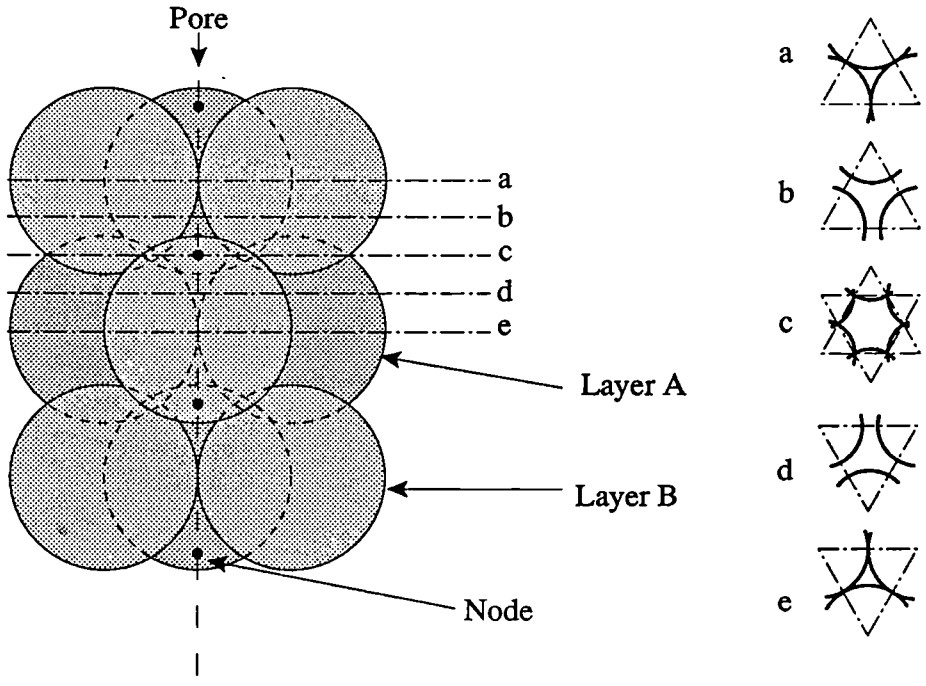

Figure 3.4a Side elevation of ABA packing

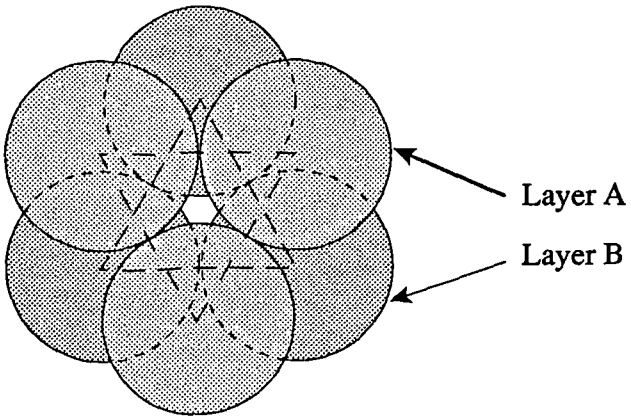

Figure 3.4b Plan view of ABA packing

2. The more complex geometry arises when beads are packed in an ABCA array. This arrangement, figure 3.5a, consists of a single unit of AB packing, whose central pore is then blocked by the 'C' bead, causing the pore to divide at the three cusps (and hence resulting in a tortuosity > 1). The geometry of the pore formed thus again starts from a tricuspid throat, but before full expansion can occur, the pore is divided by the blocking bead, causing 3 tricuspid throats to form connecting passages to adjacent pores. This contraction - expansion - divide can be repeated every three layers.

In random packing, either ABA or ABC packing statistically may occur, as both are equilibrated lowest energy packing states. However, in a heterogeneous pack, the packing will not be perfect and slip planes are likely to occur.

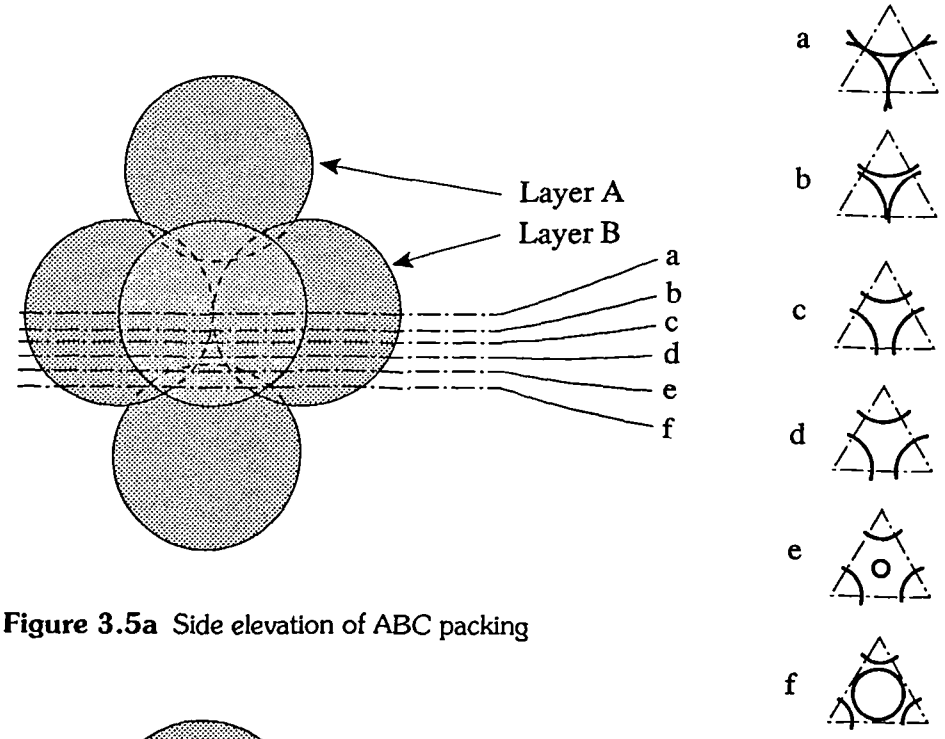

Figure 3.5a Side elevation of ABC packing

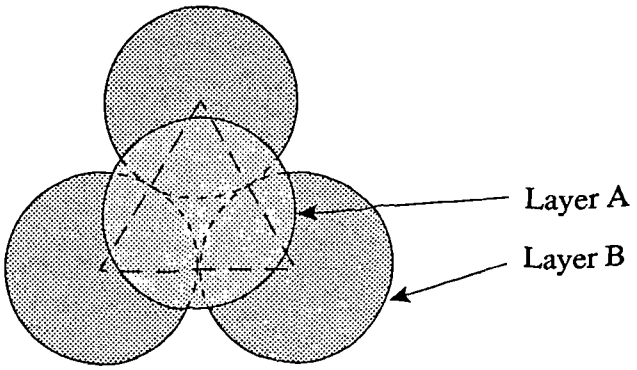

Figure 3.5b Plan view of ABC packing

3.1.5 Velocity

The superficial or Darcy velocity, U, is defined as the rate of flow per unit area of empty bed (ϕ = 1.0). Therefore for a bed of cross sectional area A, we have:

$$U = \frac{Q}{A} \qquad - 3.4$$

where Q is the volume flowrate.
The 'frontal advance rate', or average pore velocity, $\bar{u}$, which is dependant on porosity, is given by the Dupuit-Forchheimer relation (91):

$$\bar{u} = \frac{U}{\phi} \qquad - 3.5$$

3.2 Fluid Flow models

In order to predict the flow of fluids through a porous medium, the precise nature of the pore geometry dimensions and variations are required. As has been outlined above, a medium is highly complex with constantly varying flow cross sectional areas and shapes - this results in the requirement to model average fluid characteristics in an idealised situation. The flow of polymer solutions is further complicated by their departure from Newtonian behaviour and in some cases, for example polyacrylamides, their visco-elasticity.
In a long, straight, circular capillary of radius R, the Hagen-Poiseuille relationship holds :

$$Q = \frac{\pi R^4}{8\mu} \left(- \frac{dp}{dx} \right) \qquad - 3.6$$

where (dp/dx) is the pressure gradient in the flow direction.
However, when the continuously changing cross sectional area of a porous bed pore is considered the equation ceases to be applicable. Indeed, equ 3.6 cannot be considered totally applicable for the flow in the interrupted capillary apparatus of this work, except for the slower flows, as it assumes fully developed laminar flow which implies a constant velocity profile.

3.3 Shear Flow

Shear flow can be considered to dominate all flows up to the onset of elongational behaviour, assuming that fluid inertia is not significant. Simple steady shear, as found in rotary viscometers for example, is used to measure how the viscosity of a solution varies with the rate of shear. When a real fluid flow field is considered, however, such linear velocity gradients are almost unrepeated, the majority of flows possessing a curvilinear velocity profile. Indeed, even this curvilinear profile need not be constant unless the flow is fully developed, which may take many pipe diameters to achieve. In a porous medium, as in the flow between any converging (or diverging) boundaries, local steady state conditions will not exist as the flow will be periodic, thus globally averaged variables have to be used, which smooth these local fluctuations out.

3.3.1 Pipe Flow

As mentioned above, the fluid may take several pipe diameters to settle - a simple expression of $[0.057N_{Re}(2R)]$ proposed by Langhaar (53) is often used to estimate the entry length (for profiled contractions). This expression indicates, for the interrupted capillary apparatus, that only solutions where the experimental flowrate is less than 150 ml/hr can be assumed to have fully developed flow for more than half the length of the interconnecting capillary pore. For the case of polymer solutions this limiting flowrate will be increased in line with the increase of solution shear viscosity (greater viscous stabilizing forces). With this restriction in mind, it is now possible to derive an expression for the velocity profile (and hence wall shear rate) for a fluid flowing through a tube. It will be assumed that the shear rate range experienced allows the power law model to be used to predict non-Newtonian behaviour.

Consider $\tau = \kappa \left(\frac{\delta u}{\delta r}\right)^n$ is representative for the fluid

For flow in a circular tube we have ;

$$\tau = \frac{-r}{2}\frac{dP}{dl} \qquad -3.7$$

substituting for the power law model gives;

$$\frac{\delta u}{\delta r} = r^{1/n}\left(\frac{-1}{2\kappa}\frac{dP}{dl}\right)^{1/n} \qquad (= \dot{\gamma}) \qquad -3.8$$

which, upon integration and application of boundary conditions gives;

$$u = \left(\frac{-1}{2\kappa}\frac{dp}{dl}\right)^{1/n}\frac{n}{(n+1)}\left(R^{(n+1)/n} - r^{(n+1)/n}\right) \qquad -3.9$$

where r is the local radius (distance from tube centre)

Now, as most data is measured in the form of ΔP vs Q, we need to integrate over the tube cross sectional area to obtain the flowrate as $\bar{u} = \delta Q/(2\pi r \delta r)$

$$\int_0^Q \delta Q = \left(\frac{-1}{2\kappa}\frac{dP}{dl}\right)^{1/n}\frac{n}{(n+1)}\int_0^R \left(R^{(n+1)/n} - r^{(n+1)/n}\right)2\pi r\,\delta r \qquad -3.10$$

which gives :

$$Q = \left(\frac{-1}{2\kappa}\frac{dP}{dl}\right)^{1/n}\frac{n\pi}{(3n+1)}R^{(3n+1)/n} \qquad -3.11$$

which, for Newtonian liquids ($\kappa = \mu$, $n = 1$) reduces to :

$$Q = \frac{-\pi R^4}{8\mu}\frac{dP}{dl} \qquad -3.12$$

which is the Hagen-Poiseuille equation.

The mean velocity $\bar{u}$ can be expressed as

$$\bar{u} = \left(\frac{-1}{2\kappa}\frac{dP}{dl}\right)^{1/n}\frac{4n}{(3n+1)}R^{(n+1)/n} \qquad -3.13$$

If the capillary is now divided up into short (10mm) sections, and are separated from each other by a chamber of equal length but of 10 times the capillary diameter, extra pressure loss terms must be added to take account of the losses encountered at the sudden contractions and expansions. (See section 4.1.3 for more information on the capillary geometries)

1. Abrupt enlargement

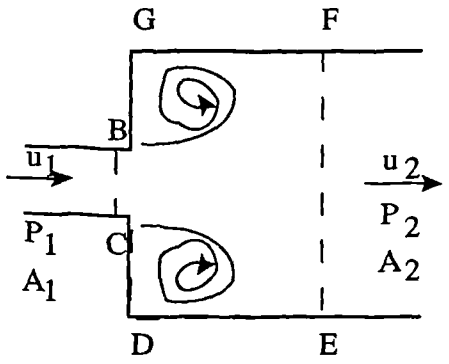

Figure 3.6 Abrupt Enlargement

From the energy equation, we get:

$$p_1 - p_{loss} + 1/2\rho u_1^2 = p_2 + 1/2\rho u_2^2 \qquad -3.14$$

and from equating the force over BCDEFG we get:

$$p_1 - p_2 = \rho u_2(u_2 - u_1) \qquad -3.15$$

substituting equ 3.15 into 3.14 we get:

$$p_{loss} = 1/2\rho(u_1 - u_2)^2 \qquad -3.16$$

or, as $A_1u_1 = A_2u_2$;

$$p_{loss(e)} = 1/2\rho u_1^2(1 - n_c)^2 \qquad -3.17$$

where n_c is the inverse contraction ratio (A_1/A_2), and $p_{loss(e)}$ is the pressure loss at a sudden enlargement.

2. Abrupt contraction.

Following a similar approach to the enlargement case, the pressure loss at a contraction may be estimated by:

$$p_{loss(c)} = 1/2\rho u_c^2(c_c - 1)^2 \qquad -3.18$$

where c_c is the inverse contraction ratio (A_1/A_c) (A_c being the area of the vena contracta formed by the fluid as it enters the capillary bore), and $p_{loss(c)}$ being the pressure loss at a sudden contraction.

As the contraction ratio (tube to capillary) increases the value of $(c_c - 1)^2 \rightarrow 0.455$. A ratio of 10:1 gives the value of $\simeq 0.453$.

Therefore the **total** extra pressure loss for a 10:1 contraction/expansion system may estimated as:

$$P_{loss(e+c)} = 0.722 \rho u_c^2 \qquad - 3.19$$

or over 10 pores,

$$P_{loss(e+c)} = 7.22 \rho u_c^2 \qquad - 3.20$$

where u_c is the average capillary velocity.

If the loss in the capillaries and bores is now reconsidered, we get:

$$P_{loss(total)} = \underbrace{\left\{ \frac{(3n+1)Q}{\pi n R_2^3} \right\}^n \frac{2\kappa L}{R_2}}_{\text{(term 1)}} + \underbrace{7.22 \frac{\rho Q^2}{R_2^4}}_{\text{(term 2)}} + \underbrace{\left\{ \frac{(3n+1)Q}{\pi n R_1^3} \right\}^n \frac{2\kappa L}{R_1}}_{\text{(term 3)}} \qquad - 3.21$$

where; term 1 is due to the pressure lost in the capillary bores (of radius R_2)
term 2 is the pressure lost during contraction and expansion
term 3 is due to the pressure lost in the tube bore (of radius R_1).

In order to compare the relative viscosity (ΔP(polymer)/ΔP(solvent)) obtained in the interrupted capillaries to the relative viscosity predicted from the viscometer an estimate of the wall shear strain rate is required. If we now substitute for γ from equ 3.8, into equ 3.11, we get:

$$\dot{\gamma}_w = \left\{ \frac{3n+1}{4n} \right\} \frac{4Q}{\pi R_2^3} \qquad - 3.22$$

where R_2 is the capillary radius.

3.3.2 Planar Contraction Flow

If flow through an array of vertical rods is contemplated, then it may be considered to be planar, that is varying in one plane only. The flow regimes that exist however are a good two dimensional approximation of the complex three dimensional flow experienced by fluids in a bead pack (See section 4.1.4 for more details). The shear flow in this planar case can never be considered fully developed as straight parallel boundaries do not exist. However, the continual convergence - divergence of the passages will lead to a time averaged steady state, where the average wall shear rate will be dependant on flowrate. Let us consider the flow through a single group of three rods;

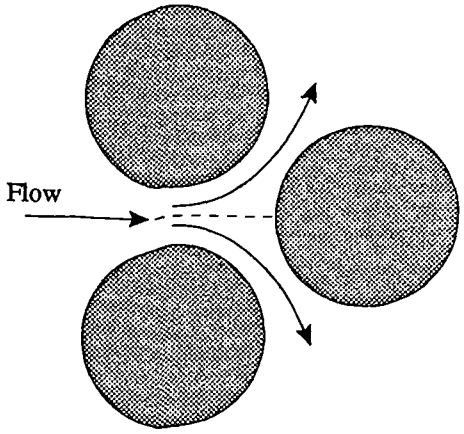

Figure 3.7 Planar Contraction

As fully developed conditions do not exist, it is likely that the velocity profile will be flatter as there will be less time, at a given velocity, for the wall shear stresses to slow the bulk of the fluid down.

In order to calculate the wall shear stress from a theoretical basis and from this deduce the pressure loss, an acceleration term must be included in the force balance, based on a constant change in velocity.
If an elemental force balance is considered (see Appendix B) we get;

$$\frac{\delta \tau}{\delta y} = \rho u \frac{\delta u}{\delta x} + \frac{\delta p}{\delta x} \qquad \text{- 3.23}$$

Now, if $(\delta u/\delta x)$ is assumed independent of y (that is a constant velocity over the cross section - flat velocity profile) and that the power law is representative of the fluid over the shear strain range encountered we get;

$$\frac{\delta u}{\delta y} = \left(\frac{\delta u}{\delta x}\frac{\rho u y}{\kappa} \frac{\delta p}{\delta x}\frac{y}{\kappa} + \frac{A}{\kappa}\right)^{1/n} \qquad - 3.24$$

which is considered beyond the scope of this work to solve accurately due to the split infinitive. However, if a Newtonian fluid is assumed equ 3.24 becomes somewhat simpler, with the substitutions $\kappa = \mu$ and $n = 1$. This assumption, although precluding any polymer pressure drop calculations does allow the shear strain rate to be estimated with some degree of accuracy for fluids with a shear thinning index $n>0.7$. Thus equ 3.24 now becomes;

$$\frac{\delta u}{\delta y} = \left(\frac{\delta u}{\delta x}\frac{\rho u y}{\mu} \frac{\delta p}{\delta x}\frac{y}{\mu} + \frac{A}{\mu}\right) \qquad - 3.25$$

If we assume the distance between the rods to equal 'b', then upon integration and application of boundary conditions we get ;

$$u = \left(\rho u \frac{\delta u}{\delta x} + \frac{(y-b)}{y}\frac{\delta p}{\delta x}\right)\frac{y^2}{2\mu} \qquad - 3.26$$

Again, in order to put this in terms of globally measured parameters, ΔP and Q, we must integrate the velocity over the cross section. If we let the rod height be h, then we can say that $u = \delta Q/(h\delta y)$, applying this to equ 3.26, and integrating over the range $0 \leq y \leq b$, we obtain;

$$Q = \frac{hb^3}{12\mu}\left(2\rho u \frac{du}{dx} - \frac{dP}{dx}\right) \qquad - 3.27$$

In order to estimate the shear strain rate, we can assume the acceleration term to be zero (in fact at the point of minimum cross section this assumption is momentarily valid).

We have then, at $y = 0$ (for wall strain rate);

$$\dot{\gamma} = \frac{-b}{2\mu}\frac{dp}{dx} \qquad - 3.28$$

which is negative as dp/dx is -ve in positive x direction. Now substituting for $\dot{\gamma}$ into equ 3.27, and imposing the no acceleration condition we obtain ;

$$Q = \frac{hb^2}{6}\dot{\gamma}_{max} \qquad - 3.29$$

3.3.3 Bead Pack Flow

Several fluid flow models have been developed to model flow through a porous medium. They can be divided into three main categories;

1. Network Models.

These can be considered microscopic models, where the flow through individual passages is considered and then statistically correlated with a pore size distribution to form an iterative method of predicting the flow through the network as a whole. Little literature has been published on these models, but a recent paper by Sorbie et al (71) illustrates that this approach could yield a much enhanced view of the displacement processes on the microscopic scale (see footnote). Studies carried out in Imperial College by Dawe et al (93) on the visualisation of the displacement processes in their models illustrate the usefulness of being able to physically view the differences, when for example wettability is changed.

2. Submerged Particle Models.

This approach considers the very slow flow of a sphere. Stoke's Law (for the sphere), together with the Navier-Stokes equation for an incompressible fluid and Darcy's Law were combined by Brinkman (94) in 1949. However the relationship relating pressure drop with velocity produced a minimum at a porosity $\phi = .333$. Brinkman regarded his model as unreliable for flow through packs where the porosity $\phi < 0.4$. Unfortunately this is around the porosities of most bead packs, so the model is considered unsuitable. Other attempts have been made with this approach, notably Wilkinson (95), who built up his porous media iteratively, by placing successively larger particles together into a continuum. However, again the author admits a poor correlation with experimental data.

3. Capillary Models.

The original model, proposed by Kozeny in 1927, considers the porous media to be made up of separate small particles, with no net flow normal to the principal flow direction. Although the fluid follows a somewhat tortuous path, Kozeny reasoned that in place of the porous material, a bundle of parallel, identical capillary tubes with their axis the x direction could be used.

Recent work by Sorbie on computer modelling of porous media flows through network modelling is very encouraging - shear thinning polymer solutions have been simulated in a highly heterogeneous network with results that can be matched to coreflood experiments (71)

To account for the porosity he reasoned that, since the resistance to flow results from frictional losses at the fluid/solid interface, the capillary tubes and porous medium would be truly equivalent if, for a given volume occupied by the fluid, the total surface area of the solid boundaries were the same. All recent criticisms of this model (17,18,22,29,39,21) focus on the fact that not all of the pressure loss can be accounted for by maintaining the same wetted surface area, as no account is then taken of the changes in cross sectional area and of continual fluid acceleration and deceleration. As indicated in equs 3.21 and 3.24 above, only a fraction of the total pressure loss is due to the friction losses at the solid boundaries. Deviations from the original model therefore introduce terms which should account for these extra losses. A brief summary of the capillary model follows below, for more detailed analyses references 5,12,18,25,49 should be read.

As discussed above, equating porosities gives;

$$\phi = \frac{V_v}{V_v + V_s} \qquad - 3.30$$

where V_v is the void volume and V_s is the solid volume.
If the total surface area A_s is now introduced, and rewriting equ 3.30 in terms of the void volume we obtain;

$$\frac{V_v}{A_s} = \frac{V_s\phi}{(1 - \phi)A_s} \qquad - 3.31$$

For a capillary tube of internal diameter d_c, and length l, the corresponding value is $d_c/4$. Therefore if a set of capillary tubes is to represent the porous bed each must have an internal diameter of

$$d_c = \frac{4V_s\phi}{(1 - \phi)A_s} \qquad - 3.32$$

Now the solid volume of a bead of diameter d_b is $\pi d_b^3/6$, whilst its surface area is πd_b^2. Putting these values into equ 3.32, we obtain an expression for an equivalent capillary diameter representing a bead array;

$$d_c = \frac{4d_b\phi}{6(1 - \phi)} \qquad - 3.33$$

If the fluid is now considered to move only in the x direction, then its velocity may be written as U/ϕ. As the actual paths, l_e, are longer than the linear distance l due to the sinuous nature of the bed, Carman pointed out that the mean velocity will therefore be greater than if the passages were straight and should be given by $(U/\phi)(l_e/l)$. If the Poiseuille relationship (equ 3.8) is considered to hold for this flow (which will be assumed Newtonian at this point) then;

$$\frac{\Delta p}{l_e} = \frac{32\mu}{d_c^2}\frac{Q}{d_c^2\pi/4} = \frac{32\mu}{d_c^2}\frac{Ul_e}{\phi l} \qquad - 3.34$$

where Δp is the pressure drop inducing the flowrate Q. Substituting from equ 3.33 into 3.34 and rearranging gives;

$$U = \frac{\Delta p \phi^3 d_b^2}{l(1-\phi)^2 \mu(36j)} \qquad - 3.35$$

where $j = 2(l_e/l)^2$ and has to be empirically derived.
Comparing equ 3.35 with Darcy's Law (equ 3.3) it is possible to obtain a relationship between average particle size, permeability and porosity. By inspection then;

$$k = \frac{\phi^3 d_b^2}{36j(1-\phi)^2} \qquad - 3.36$$

The value of j is subject to much contention. The work by Kemblowski and Michienwicz (49) reviews the range of values (of 36j) chosen in the literature. Most porous materials have values of j in the range $4 \rightarrow 6$, with $j \approx 5$ the most common. In considering flow through a bed of spherical particles, the maximum value of tortuosity is $0.5\pi d_b/d_b$ (=1.57) which produces a value of $j = 4.93$ ($36j = 177.65$). Ergun (25) proposed two dimensionless groups, f & N_{Re}, to describe the flow. These are usually defined such that;

$$f = \frac{J}{N_{Re}} \qquad - 3.37$$

where;

$$f = \frac{d_b\phi^3}{(1-\phi)}\frac{1}{\rho U^2}\frac{\Delta p}{l} \qquad - 3.37a$$

$$N_{Re} = \frac{Ud_b\rho}{\mu(1-\phi)} \qquad - 3.37b$$

and $J = 36j$.

It can be seen that the bed Reynolds number N_{Re} is still the ratio of inertial to viscous forces. Ergun proposed that equ 3.37 be valid whilst the viscous forces dominate the inertial forces, beyond this limit he proposed the relationship became;

$$f = \frac{J}{N_{Re}} + 1.75 \qquad - 3.38$$

which simplifies at high N_{Re} (>> J) to $f = 1.75$.

All of the above assume a Newtonian fluid, if as in 3.3.1 and 3.3.2 above, the power law relationship is considered to hold for non-Newtonian behaviour a similar derivation may be followed to develop equations for non-elastic polymer solution flow through porous media.

This derivation will follow a similar route to that chosen by Kemblowski & Michniewicz (49), as opposed to the more usual Christopher & Middleman (12) (or Bird et al (5)) approach. The difference between the approaches being how and where to introduce the tortuosity factor (l_e/l). The author believes that the correction of the velocity term, as introduced by Carman, as well the length correction is more reasonable. Thus for a given pressure drop the Carman approach predicts a lower flowrate, some 76% different if his method is followed exactly. [He further divided the constant j into j_o (a shape factor which equals 2 for circular cross-section, and 3 for parallel plates {Carman chose the value 2.5 for bead packs}), and j_1 (which equals the tortuosity L', for which he chose L' = $\sqrt{2}$), such that $j=j_o j_1^2$.] Thus, we obtain;

$$U = \frac{4n}{3n+1} \frac{d_b\phi^2}{6j_o j_1(1-\phi)} \left(\frac{\Delta p d_b \phi}{3j_o j_1 l(1-\phi)\kappa} \right)^{1/n} \qquad - 3.39$$

As the average velocity in a capillary is simply the flowrate divided by the cross sectional area, a relationship predicting the flowrate at a given pressure drop may be developed.

$$Q = \frac{4n}{3n+1} \frac{d_b\phi^2 A}{15j_1(1-\phi)} \left(\frac{\Delta p d_b \phi}{6j_1 l(1-\phi)\kappa} \right)^{1/n} \qquad - 3.40$$

where A is the bed cross sectional area. Again, using the same definition (3.37) for the $f.N_{Re}$ relation, we get;

$$N_{Re} = \frac{d_b^n \rho U^{2-n}}{\kappa (1-\phi)^n} \left(\frac{4n}{3n+1} \right)^n \left(\frac{15j_1}{\phi^2} \right)^{n-1} \qquad - 3.41$$

where $j_1 = (l_e/l)$, and the definition of f remains unchanged, and into which equ 3.36 converting bead diameter into permeability may be used.

It can be seen by inspection that when $\kappa = \mu$, and n = 1 this reduces to the Newtonian case. Combining equations 3.40 for Q, and 3.8 for the wall shear rate when $r=d_c/2$, the effective capillary diameter, and the pressure differential $\delta P/\delta L=\Delta P/l_e$, gives;

$$\dot{\gamma} = \left(\frac{1}{2\kappa j_1}\frac{\Delta P}{l}\right)^{1/n}\left(\frac{d_c}{2}\right)^{1/n}$$

$$= \frac{3n+1}{4n}\frac{15j_1(1-\phi)Q}{d_b\phi^2 A}\left(\frac{3(1-\phi)}{\phi\ d_b}\right)^{1/n}\left(\frac{d_c}{2}\right)^{1/n} \qquad - 3.42$$

Substituting for U, and for d_c (from equ 3.33) we get;

$$\dot{\gamma} = \frac{(3n+1)}{4n}\ \frac{1-\phi}{\phi^2}\ \frac{12j_1U}{d_b} \qquad - 3.43$$

or, putting in general terms of k and ϕ, and using the Carman value of $\sqrt{2}$ for the tortuosity;

$$\dot{\gamma} = \frac{(3n+1)}{4n}\ \frac{15\sqrt{2}\,U}{[180(k\phi)]^{0.5}} \qquad - 3.44$$

Chauveteau (8), however, used the shear thinning behaviour of xanthan gum to produce an empirically derived constant, which he called an α factor, where;

$$\dot{\gamma} = \frac{\alpha\ 4U}{(8k\phi)^{1/2}} \qquad - 3.45$$

In matching the onset of pseudoplasticity of xanthan solutions over a range of concentrations and bead sizes, he proposed that the constant α have a value of 1.7. This results in a shear rate prediction some 50% higher than that predicted by the Carman approach. Thus we have, after applying the Rabinoswitch-Mooney factor,

$$\dot{\gamma} = \left(\frac{3n+1}{4n}\right)\frac{2.4U}{(k\phi)^{1/2}} \qquad - 3.46$$

Chauveteau also noted that when solutions were flowed through core samples the value of the constant had to be increased, with values of $\alpha \simeq 2$ for sand packs, and $\alpha \simeq 4.5$ for sandstone.

In an attempt to include the extra pressure losses at the contractions and expansions of the passages in a porous media, modified capillary models have been proposed which are either based on an abrupt change of cross section (as in the interrupted capillary work), or on a sinusoidally varying cross section. Sheffield and Metzner (96) proposed a model with a sinusoidal variation (figure 3.8a), limiting their analyses to purely viscous liquids only, their predictions of the flowrate/pressure drop relationship indicated a far higher accuracy than the plain parallel capillary model for shear thinning fluids. For Newtonian fluids the improvement was only slight - indicating the sensitivity of the capillary approach to how the shear viscosity element, through predicted strain rates, is introduced. Their model takes account of the deviation from the Newtonian streamlines by non-linear liquids by the inclusion of an empirical factor b', which represents the effective pore dimensions when a non-linear liquid is flowing through. This parameter, however, significantly complicates their approach as b' is N_{Re} dependant, and combined with the need for numerical integration of the pressure gradient through the pore, limits the analysis by requiring extensive computation. The abrupt approach, outlined by Duda et al (21), illustrates the need for a model to include terms to account for the losses at the changes in cross section, and as they conclude if a model which accurately predicts these kinetic energy losses is derived, then the porous media itself should be able to be better characterised.
By adjusting the model geometric characteristics as defined in figure 3.8b, so that a better fit with the experimental data was obtained, the converging/diverging nature of the medium could be determined, which would aid investigation into other topics such as trapped oil, multiphase flow and dispersion. If the model thus accurately predicted the converging nature of the medium then the analysis could then be extended to include viscoelastic effects through the extensional strain rate.

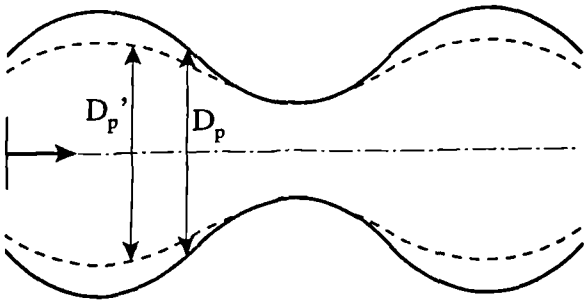

$$D_p = D_{min}\frac{1+b\sin x}{1-b}$$

$$D_p' = D_{min}\frac{1+b'\sin x}{1-b'} \quad b' < b$$

$$\text{where } b = \frac{D_{max}-D_{min}}{D_{max}+D_{min}}$$

Figure 3.8a Alternative pore model of Sheffield and Metzner

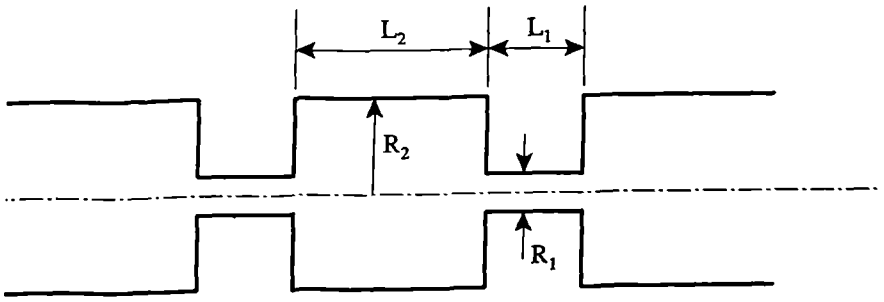

Figure 3.8b Alternative pore model of Duda et al

3.4 Elongational Flow

Elongational flows are experienced by fluids undergoing a change in velocity, that is where there is a region of acceleration (or conversely deceleration). The apparent onset of viscoelastic behaviour is characterised by a sudden, rapid increase in the resistance to flow, that can, in certain circumstances, lead to an effective viscosity many times that of the pre-onset value. As mentioned in chapter 2, not all polymers are susceptible to viscoelastic behaviour, only those polymers where the molecular chains can be considered flexible exhibit this apparent shear thickening region. The onset of the apparent elongational effects is important to quantify. For example, too high a polymer solution injection rate for an oil reservoir could lead to pressures many tens of times those predicted by shear viscosity alone. These overpressures could lead to formation fracture, or to the solutions being diverted from their intended path. It is the goal of this work to provide a means of predicting the extensional strain in a variety of geometries so that one experiment may be used to determine the onset elongational rate which could be used to determine maximum injection rates for example.

3.4.1 Determination of rate of elongation

Consider a free stream flow element of length l, cross sectional area A, as illustrated in figure 3.9. After a time δt, the element has travelled a distance δx, and the length has been stretched to $l + \delta l$, and the area changed to $A + \delta A$.

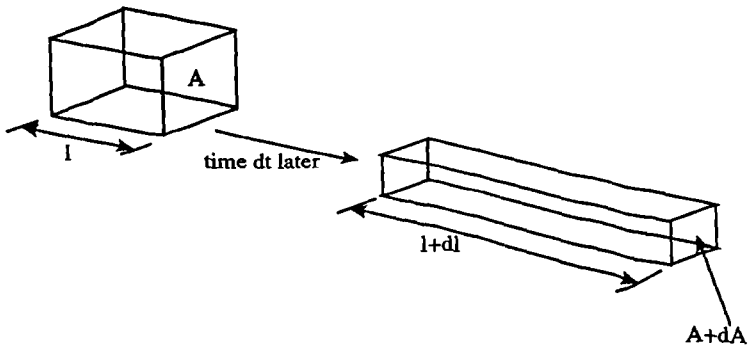

Figure 3.9 Elemental elongation

By considering the conservation of elemental volume, we get;

$$Al = (A + \delta A)(l + \delta l) \qquad - 3.47$$

re-arranging this gives;

$$(A + \delta A)\,\delta l = - l\,\delta A \qquad - 3.48$$

or;

$$\frac{\delta l}{l} = \frac{-\delta A}{A + \delta A} \qquad - 3.49$$

We can define the rate of extensional strain as the rate of increase in elemental length per unit time, so that;

$$\dot{\xi} = \frac{\delta l}{l}\,\frac{1}{\delta t} \qquad - 3.50$$

If the average elemental velocity is considered, such that $\bar{u} = \delta x/\delta t$, then equ 3.50 may be rewritten;

$$\dot{\xi} = \frac{-\delta A}{A+\delta A}\,\frac{\bar{u}}{\delta x} \qquad - 3.51$$

If the axes are chosen such that $A = f(x)$, then we can represent the average velocity $\bar{u}$ by q/A, where q is the flowrate through cross sectional area A. Substituting for $\bar{u}$ in equ 3.51, and neglecting small multiples, in the limit as $\delta x \to 0$, we get ;

$$\dot{\xi} = \frac{-q}{A^2}\,\frac{dA}{dx} \qquad - 3.52$$

Thus, provided the relationship dA/dx is known, or can be found, any pore geometry may be solved. The only assumption made is that all elements are travelling at a velocity represented by the average. Clearly this will not be the case, but as discussed earlier, the converging/diverging nature of the passages should result in a flatter velocity profile than pertains for fully developed flow. (Note : for flows of non-Newtonian fluids where $n<1$ the velocity profile also becomes flatter). This analysis will now be applied to the geometries of this work, to enable cross-correlations to be made.

3.4.2 Pipe Flow

The abrupt nature of some of the capillaries used cannot be directly compared in this way, due to the discontinuity at the change in area. However, the analysis can be applied, if instead of the physical boundaries, fluid boundaries are considered. When any fluid flows through an abrupt contraction recirculation zones (vorticies) will develop. The funnel effect formed can then be analysed using this method, by assuming the vortex limits to be the boundaries. Other approaches to this geometry have recently been published. The paper by Binding (4), considers an energy balance over the contraction, combining the shear and elongational components to form a maximum extensional rate, dependant on the vortex length, the polymer power law indicies (assuming shear and elongational viscosities can be represented by power laws), and an integral relating the shear and extensional power law indicies. The analysis requires the predetermination of the indicies of the elongational power law, which are not determinable in the majority of laboratories. The paper also points out that here, as is common with most contractions, the rate of extension will not be a simple function, but will vary through the contraction, further complicating the mathematics. The analysis developed here, whilst not determining the precise rate of elongational strain, will allow comparison between geometries to be easily made.

If we consider the profiled contraction of the capillary apparatus (see also 4.1.3), then we may use the physical boundaries as our limits until vortex formation occurs. We have therefore;

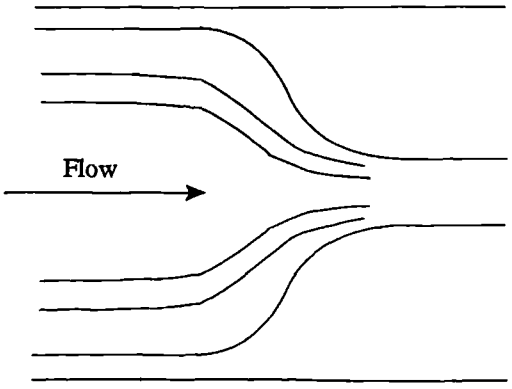

Figure 3.10 Axi-symmetric profiled contraction

From equ 3.52, in order to predict an elongational rate, the relationship between flow cross sectional area and distance is required. For this case the relationship can be simply found from geometry.

$$A = f(x) = 5.73\cos^2(\pi x/2)+14\cos(\pi x/2)+8.55 \qquad - 3.53$$

where $0 \le x \le 2$, and is measured in mm.

This function was obtained after regressing measurements taken from one contraction.

Therefore, after differentiation, and substitution into equ 3.52, we get;

$$\dot{\xi} = \frac{0.5q\pi[5.726\sin(\pi x) + 14\sin(\pi x/2)]}{[5.73\cos^2(\pi x/2)+14\cos(\pi x/2)+8.55]^2} \qquad - 3.54$$

where q, the flowrate, is in mm^3/s.

This function, figure 3.11, illustrates the change in extensional rate whilst passing the contraction region. The maximum rate can be found by differentiating again, however, as this value is only attained for a short period, and is very sensitive to flow boundary geometry in the region shown below an average rate may be more representative.

$$\dot{\xi}_{max} = 9.65\ q\ (mm^3/s) = 2.68\ q\ (ml/hr) \qquad - 3.55$$

$$\dot{\xi}_{av} = 3.36\ q\ (mm^3/s) = 0.933\ q\ (ml/hr) \qquad - 3.56$$

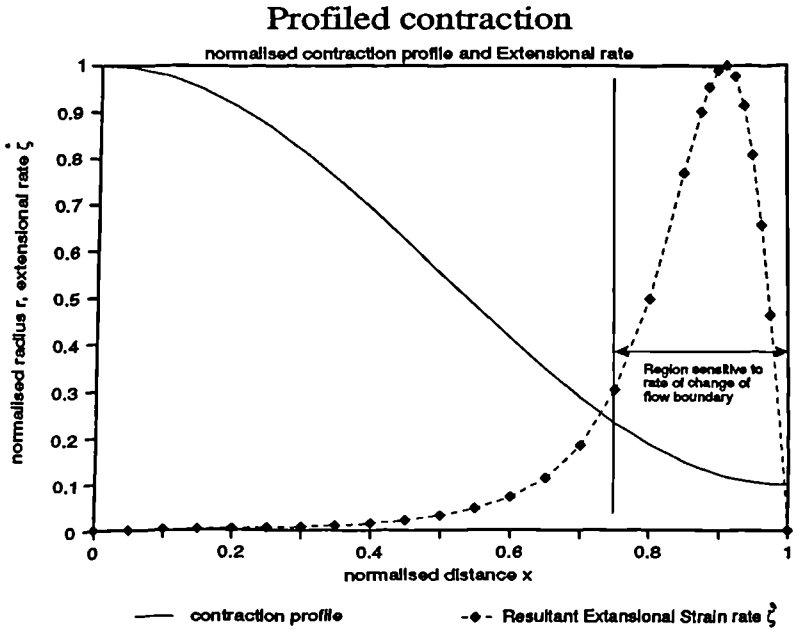

Figure 3.11 Variation of extensional rate and area through pore.

Now, as stated above, this equation holds true only up until vortex formation occurs, beyond that point (and for all flows in the abrupt case) the vortex limits should be used in place of the physical boundaries. Visualisation studies, however, revealed that at higher flowrates the fluid tends to jump (see section 5.5) from the exit of one capillary to the entrance of the next, without undergoing any significant expansion. This would, of course, reduce the extensional component of the flow to almost nil, and render the analysis redundant.

3.4.3 Planar Contraction Flow

The steady contraction of the flow passing between two rods can be considered ideal for studying the onset of elongational behaviour because, as has been found in this work, little or no vortex formation occurs in flows which exhibit the rapid increase in effective viscosity. Consider two rods in a free stream, as shown in figure 3.12, of height h, diameter d_r, l distant from each other at the narrowest point.

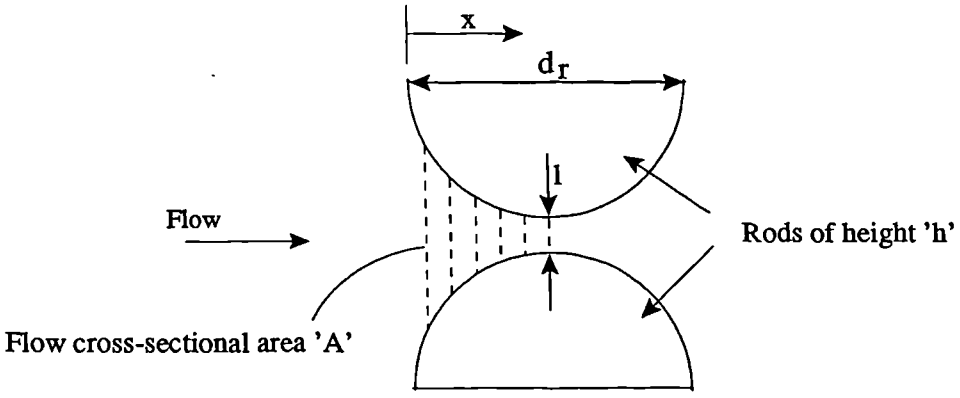

Figure 3.12 Planar Contraction Flow (2 rod case)

Now we can write the flow cross sectional area A as;

$$A = h[(d_r+l) - 2(x(d_r-x))^{0.5}] \qquad - 3.57$$

and therefore;

$$\frac{dA}{dx} = h[x/(d_r-x)]^{0.5}[1-(dr-x)/x] \qquad - 3.58$$

Substituting equs 3.57 and 3.58 into 3.52 gives;

$$\dot{\xi} = \frac{-q[1-(d_r-x)/x][x/(dr-x)]^{0.5}}{h[(d_r+l) - 2(x(d_r-x))^{0.5}]2} \qquad - 3.59$$

where q is the flowrate between these two rods only.

The results of this can be seen in figure 3.13 for the rod arrangements used in this work. As was the case for the axisymmetric contraction, a maximum value is reached, but is maintained for a longer period of time, therefore;

$$\dot{\xi}_{max} = 0.575q(ml/hr)\ sec^{-1} \text{ for the 0.5mm array} \quad - 3.60$$
$$= 3.017q(l/hr)\ sec^{-1} \text{ for the 5mm array (8mm high)}$$

$$\dot{\xi}_{av} = 0.426q(ml/hr)\ sec^{-1} \text{ for the 0.5mm array} \quad - 3.61$$
$$= 2.23q(l/hr)\ sec^{-1} \text{ for the 5mm array (8mm high)}$$

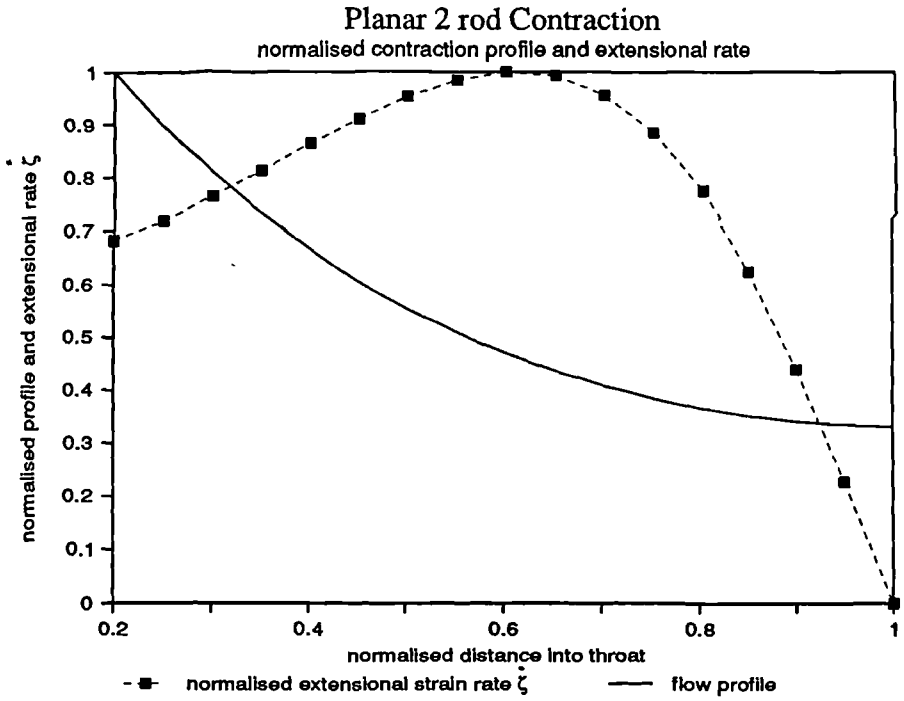

Figure 3.13 Variation of elongational rate through 2 rod planar contraction.

If rather than the arrangement above, a rotational fluid motion is assumed, as shown in figure 3.14, where the fluid is approaching the contraction at an angle, rather than head on, a slightly different result is obtained.

If the distance, x, is assumed to be the average distance travelled by the plane (that is the linear distance travelled by the mid point of the plane) then we get:

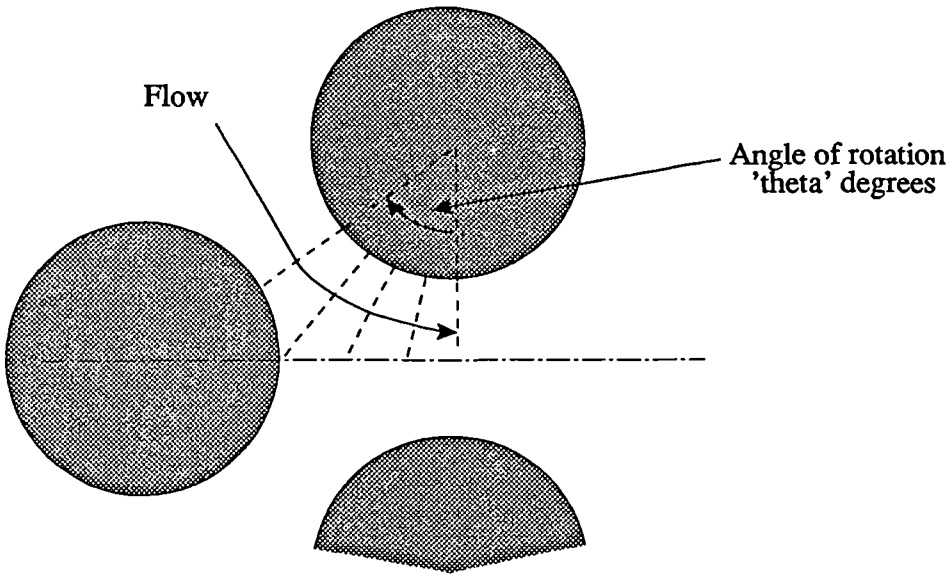

Figure 3.14 Planar contraction with rotation (3 rod case)

Rather than attempting to fully define an equation for A the evaluation of dA/dx, the slope of the variation of cross sectional area with distance was carried out numerically.

theta	area	distance	dA/dx mid point	$\dot{\varepsilon}$ (s^{-1}) (q=1)
60	0.01h	0		
			-0.089h	-6973/h
56.3	0.0105h	0.00195		
			-0.102h	-7229.2/h
53.1	0.011h	0.00366		
			-0.169h	-10436/h
49.4	0.012h	0.00573		
			-0.22h	-10984/h
45	0.0136h	0.00827		
			-0.05h	-2319.6/h
39.8	0.014h	0.01117		
			0.286h	14808/h
33.7	0.011h	0.01483		
			0.232h	18824/h
28.1	0.009h	0.01793		
			0.193h	21500/h
25	0.0081h	0.01955		
			0.167h	22931/h
21.8	0.0073h	0.02021		
			0.141h	23711/h
18.4	0.0066h	0.02292		
			0.115h	23442/h
14.9	0.0061h	0.02467		
			0.0894h	21531/h
11.3	0.0056h	0.02645		
			0.0638h	17675/h
7.59	0.0053h	0.02825		
			0.038h	11628/h
3.81	0.0051h	0.03007		
			0.0128h	4124.2/h
0	0.005h	0.0319		

Table 3.1 Variation of extensional rate through 3 rod array, calculated using 0.5mm rods

As can be seen from table 3.1 and figure 3.14a, a maximum value of $\dot{\zeta}$ is reached and is maintained for the majority of the contraction flow.

So, for the apparatus configurations used in this work, we have;

$$\dot{\zeta}_{max} = 0.549 * q \text{ (ml/hr) for 0.5mm rods} \qquad - 3.62$$
$$\dot{\zeta}_{max} = 2.88 * q \text{ (l/hr) for 5mm rods (8mm high)}$$
$$\dot{\zeta}_{max} = 1.77 * q \text{ (l/hr) for 5mm rods (13mm high)}$$

$$\dot{\zeta}_{av} = 0.476 * q \text{ (ml/hr) for 0.5mm rods} \qquad - 3.63$$
$$\dot{\zeta}_{av} = 2.19 * q \text{ (l/hr) for 5.0mm rods (8mm high)}$$
$$\dot{\zeta}_{av} = 1.35 * q \text{ (l/hr) for 5.0mm rods (13mm high)}$$

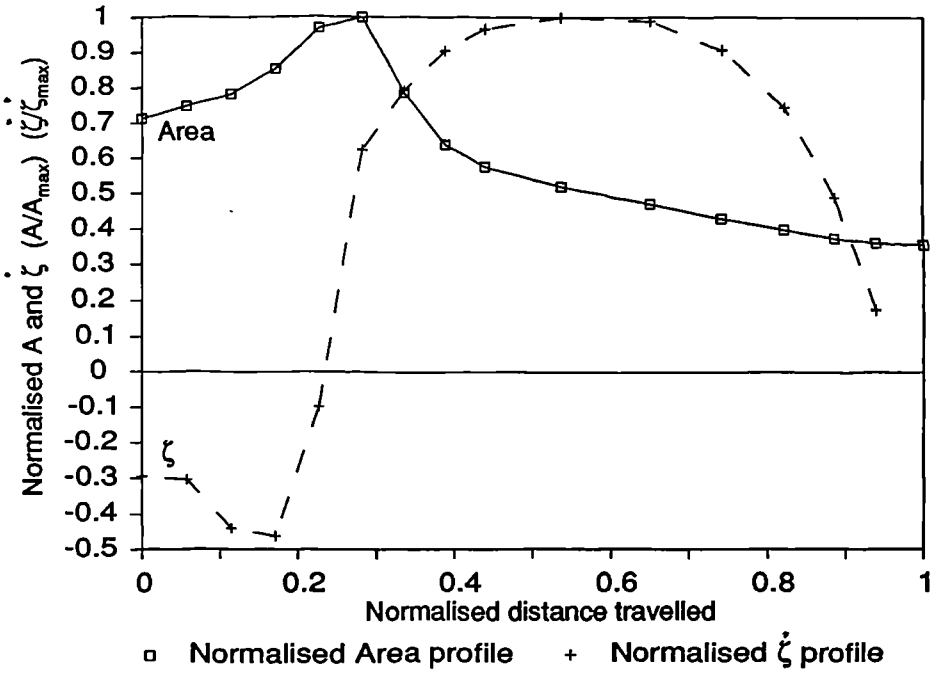

Figure 3.14a Variation of elongational rate through a 3 rod planar contraction

3.4.4 Bead Pack Flow

James and Mclaren (39) in 1975 were the first to attempt to derive a porous media extensional strain rate. Their work does analyse the flow through ABA and ABC bead packing types. Rather than analysing the exact geometry they assumed the actual passage shape could be represented by the inside of a sphere which fills the cavity. They produced a relationship proposing that
extensional strain = constant *superficial velocity/bead diameter
for which they found the constant was equal to 150. This produced values for the onset of extensional behaviour of the order 10^2. More recently work by Durst and Haas (31) has analysed cubic and orthorhombic (ABA) geometries. They have not however considered ABC packing. Again the same functional form was adopted for the equation, but this time a constant of 4 was obtained semi empirically.

In considering the flow through a bead pack consideration must be given to the variety of pore types that may occur. Having assumed already that although randomly packed, the bead packing is likely to approximate to hexagonal, we must consider the extensional rate through two passage types - one caused by the ABA packing arrangement, the other by the ABC arrangement.
If we consider the former first;

1. Derivation for ABA packing.

Consider the three beads, of diameter d_b, shown in figure 3.15, packed hexagonally together.

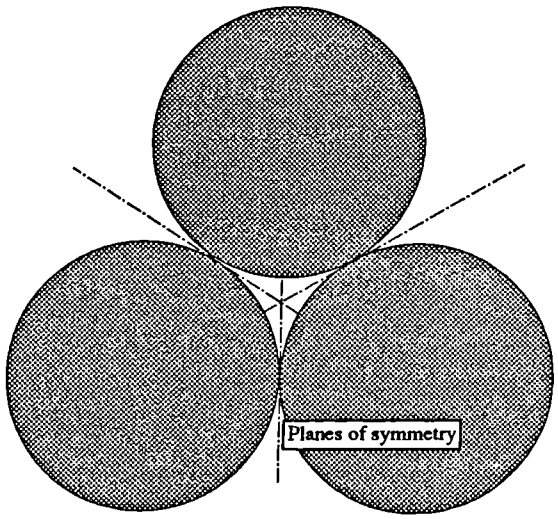

Figure 3.15 ABA packing with planes of symmetry.

If the flow is considered normal to planes parallel to the plane containing the bead centres, then it can be shown that the area A, and the rate of change of area, dA/dx, are represented by;

$$A = \frac{\sqrt{3}d_b^2}{4} - \frac{\pi(d_b-x)x}{2} \qquad - 3.64$$

and;

$$\frac{dA}{dx} = \pi(x-d_b/2) \qquad - 3.65$$

If these definitions are now substituted in equ 3.52 we get;

$$\dot{\zeta} = \frac{-q\ 16\pi(x-d_b/2)}{[\sqrt{3}\ d_b^2-2\pi(d_b-x)x]^2} \qquad - 3.66$$

The results of which are shown in figure 3.16.

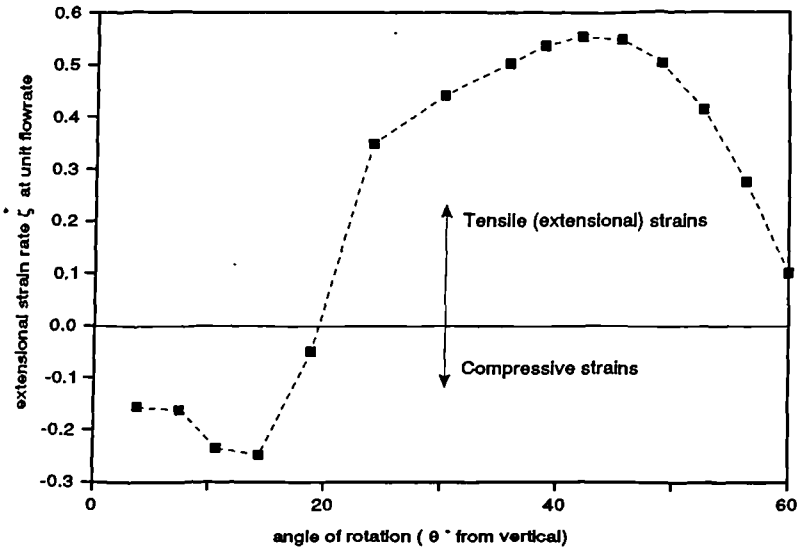

Figure 3.16 Variation of extensional strain through ABA pore

Again, as with the previous cases, the maximum value is maintained only for a short period. It is interesting to note, however, that the position of the maximum is only $\sim 0.1\ d_b$ away from the pore throat, rather than more distant where the greatest rate of change of area lies. The maximum elongational rate can be expressed therefore as;

$$\dot{\zeta}_{max} = 100.57\ \frac{q}{d_b^3} \qquad - 3.67$$

and the average rate as;

$$\dot{\zeta}_{av} = 32.9\ \frac{q}{d_b^3} \qquad - 3.68$$

2. Derivation for ABC packing.

The analysis of this configuration is hindered by the inclusion of the C bead, as illustrated in figure 3.17. For convenience the flow will be assumed to flow in through the three pores on the top layer, and out through the central pore on the base. As was the case for the array of three rods above, we will consider the flow to rotate around the beads, so that the plane normal to the surface of the bead is perpendicular to the direction of flow as explained by figure 3.18, a scheme which does produce obvious problems in the vicinity of the axial stagnation point.

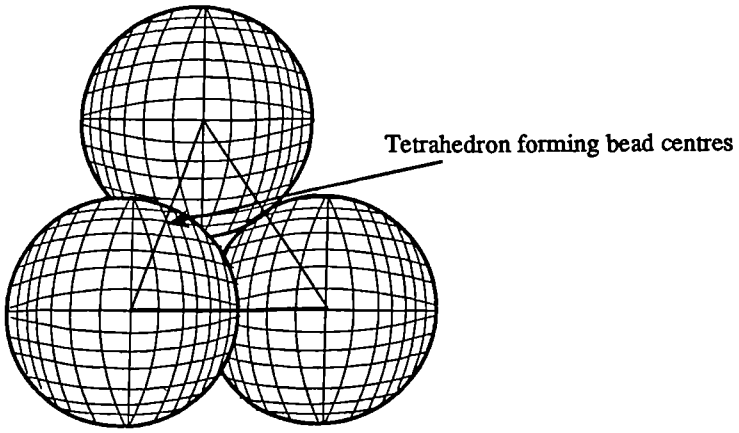

Figure 3.17 Schematic layout of ABC packing

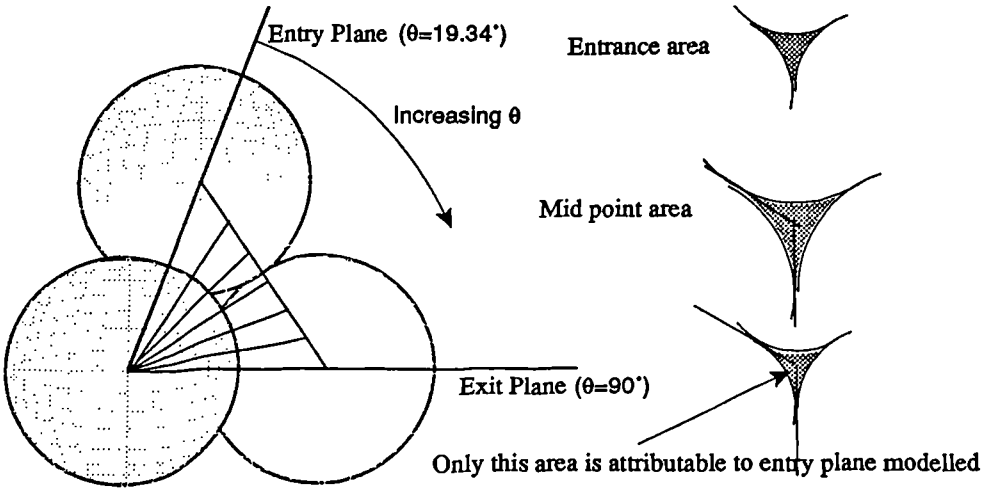

Figure 3.18 Planes of rotation for ABC packing

Due to the symmetry of the packing, it is only necessary to model 1/6 of the outlet pore arrangement, although calculating 1/3 was considered easier. (This meant that one whole pore could be modelled as it passed through the packing arrangement). It was first attempted to calculate the flow areas using computer graphics on an Apollo workstation. These flow areas, contained by the plane rotated about a line joining the centres of two of the beads, proved to be too complex for the software, and lower accuracy was obtained than was expected. The exercise was therefore repeated geometrically, the results from both analyses contained in table 3.2.

Angle of plane from vertical	Values of A		% diff
	Computer simulation	Geometrical calculations	
19.47	not attempted	$0.04031d_b^2$	-
20	$0.04072d_b^2$	not calc'd	-
25	$0.04078d_b^2$	$0.04174d_b^2$	-2.3
30	$0.04322d_b^2$	$0.04372d_b^2$	-1.1
35	failed	$0.04428d_b^2$	-
40	$0.0403d_b^2$	$0.04096d_b^2$	-1.6
45	$0.3344d_b^2$	$0.03296d_b^2$	+1.5
50	$0.02738d_b^2$	$0.02696d_b^2$	+1.6
55	$0.02308d_b^2$	$0.02272d_b^2$	+1.6
60	not attempted	$0.01966d_b^2$	-
65	$0.0179d_b^2$	$0.01746d_b^2$	+2.5
70	not attempted	$0.01586d_b^2$	-
75	$0.01512d_b^2$	$0.01474d_b^2$	+2.6
80	not attempted	$0.01400d_b^2$	-
85	$0.01386d_b^2$	$0.01358d_b^2$	+2.1
90	$0.01378d_b^2$	$0.01344d_b^2$	+2.5

Table 3.2 Comparison of flow areas calculated by the two methods.

The data in table 3.2 forms the basis of our (numerical) relationship $A=f(\theta)$, we now need to define a mean flow path in order to obtain the $\theta=f(x)$ relation. If we consider an element entering the matrix at the centroid of one of the upper pores, and then flows such that it passes through the centroid of each areal plane calculated, then we can calculate the distance travelled, and hence the relation $\theta=f(x)$.

Plane Angle $\theta°$	distance travelled x_i/d_b (m)	Cumulative distance $\Sigma x_i/d_b$ (m)	time taken t_i/q (s)	Cumulative time $\Sigma t_i/q$ (s)
19.47°	0	0	0	0
25°	0.02809	0.02809	0.00039	0.00039
30°	0.02504	0.05313	0.00036	0.00076
35°	0.02495	0.07808	0.00037	0.00112
40°	0.02485	0.10293	0.00034	0.00146
45°	0.02476	0.12769	0.00027	0.00174
47.63°	discontinuity - departure of top bead			
50°	0.02466	0.15235	0.00022	0.00196
55°	0.02457	0.17692	0.00019	0.00214
60°	0.02429	0.20140	0.00016	0.00230
65°	0.02438	0.22578	0.00014	0.00245
70°	0.02429	0.25007	0.00013	0.00257
75°	0.02420	0.27427	0.00012	0.00269
80°	0.02411	0.29838	0.00011	0.00280
85°	0.02401	0.32239	0.00011	0.00291
90°	0.02392	0.34631	0.00011	0.00302

Table 3.3 Determination of h=f(x), where q is the flowrate *per exit plane pore* (that is only q/3 flows through the section modelled)

Therefore the relation A=f(x) may now be predicted, as shown by figure 3.19. Table 3.3 also provides data on the tortuosity of the flow;

$$L' = l_e/l = \Sigma x/y = 0.34631d_b/0.272d_b = 1.272 \qquad -3.69$$

where y is the equivalent vertical distance travelled.

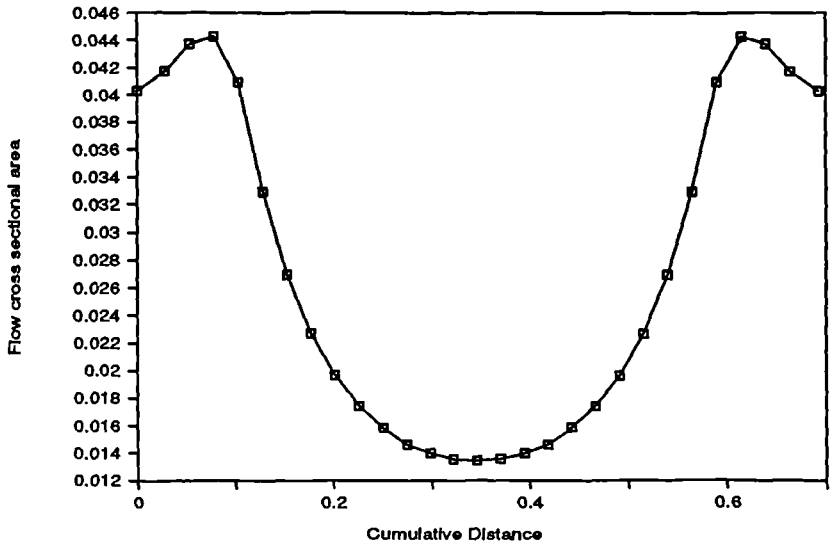

Figure 3.19 Variation of flow cross sectional area through pore with distance x

It is interesting to note that at the point of departure of the top bead from the analysis, no discontinuity occurs in the area function.
Also, the point of maximum extensional rate does not necessarily occur at $(\delta A/\delta x)_{max}$, because of the inclusion of the $(1/A^2)$ term. Due to the complex nature of the relationship obtained, it was decided to interpolate linearly between each of the calculated points, and to take the gradient of this line to represent the function dA/dx at x = mid way between the points, as shown in table 3.4.

distance into pore x (m)	**gradient of line dA/dx (m)**	**linear interpolated area (m)**	**extensional rate (s^{-1})**
$0.01404d_b$	$0.0506d_b$	$0.041d_b^2$	$-10\ q/d_b^3$
$0.0406d_b$	$0.0791d_b$	$0.0427d_b^2$	$-14.4\ q/d_b^3$
$0.0656d_b$	$0.0244d_b$	$0.044d_b^2$	$-3.9\ q/d_b^3$
$0.0905d_b$	$-0.134d_b$	$0.0426d_b^2$	$24.5\ q/d_b^3$
$0.1153d_b$	$-0.323d_b$	$0.0369d_b^2$	$78.8\ q/d_b^3$
$0.1400d_b$	$-0.243d_b$	$0.0299d_b^2$	$90.4\ q/d_b^3$
$0.1646d_b$	$-0.173d_b$	$0.0248d_b^2$	$93.2\ q/d_b^3$
$0.1892d_b$	$-0.125d_b$	$0.0212d_b^2$	$92.8\ q/d_b^3$
$0.2136d_b$	$-0.090d_b$	$0.0186d_b^2$	$87.3\ q/d_b^3$
$0.2379d_b$	$-0.066d_b$	$0.0167d_b^2$	$79.1\ q/d_b^3$
$0.2622d_b$	$-0.046d_b$	$0.0153d_b^2$	$65.9\ q/d_b^3$
$0.2863d_b$	$-0.031d_b$	$0.0144d_b^2$	$49.5\ q/d_b^3$
$0.3104d_b$	$-0.017d_b$	$0.0137d_b^2$	$30.6\ q/d_b^3$
$0.3344d_b$	$-0.058d_b$	$0.0135d_b^2$	$10.7\ q/d_b^3$
$0.3583d_b$	$0.058d_b$	$0.0135d_b^2$	$-10.7\ q/d_b^3$

Table 3.4 Calculation of dA/dx and $\dot{\varepsilon}$.
(Note: q is total flow out of base tricuspid pore)

These results may now be plotted to show the variation in extensional strain rate as a fluid passes through the pore. (figure 3.20)

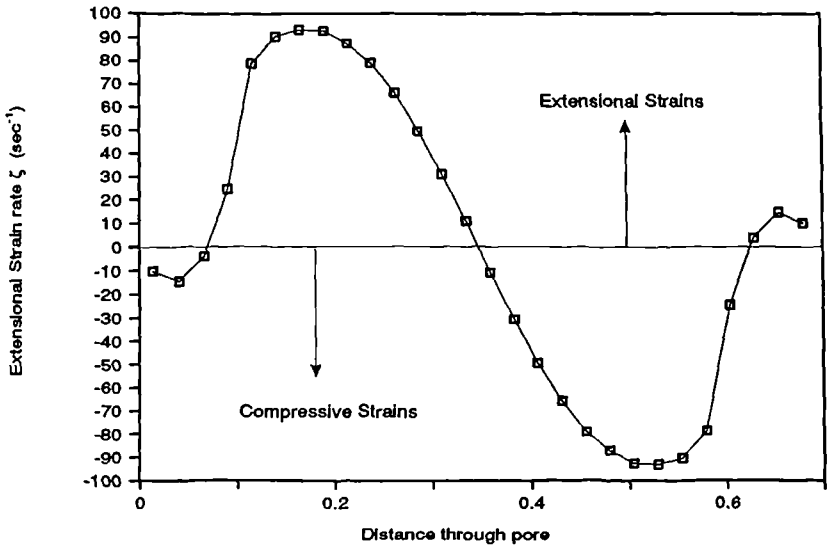

Note : Distances and areas based on unit bead diameter, strain rates on unit flowrate

Figure 3.20 Variation of extensional strain through ABC pore.

As was the case with the other geometries, the solution is not simple, that is the elongational rate varies greatly as a molecule passes through the pore. Although in this case the maximum value is attained rapidly upon entering the pore and is maintained for ~1/3 of the length of the pore. We can now say, therefore, that the maximum elongational strain rate attained in an ABC pore can be predicted by;

$$\dot{\xi}_{max} = 93.2 \frac{q}{d_b^3} \qquad - 3.70$$

and by numerical integration;

$$\dot{\xi}_{av} = 46 \frac{q}{d_b^3} \qquad - 3.71$$

These rates are also the rates of compressive strains found in a similar pore with the opposite orientation, that is flow in through the single throat, and out through the three exits.

3.5 Conversion of local to global parameters.

The above analyses for bead pack flow all depend on the ability to predict the number of pores, and hence the flow per pore from the global flowrate. The dependence of the function on the bead diameter d_b, also limits the usefulness, a far more useful form would be such that $\zeta = f(U,\phi,k)$.

3.5.1 Conversion of pore flowrate into superficial (or Darcy) velocity

If we now consider a single sphere, hexagonally packed in the arrangement of figure 3.21a, then the area occupied by the bead, and its share of the surrounding voids can be shown to be represented by hexagon with the bead at its centre, in contact with all the sides, as shown in figure 3.21b.

We can say that;

$$U = \frac{\Sigma q}{\text{(total csa)}} = m.q \qquad \text{- 3.72}$$

where m = pore density (m^{-2})
q = single pore flowrate (m^3/s)

therefore we have;

$$m = \frac{2}{A_h} = \frac{4\sqrt{3}}{3d_b^2} \qquad \text{- 3.73}$$

where A_h = area of hexagon occupied by bead.

By substituting equ 3.73 into 3.72, we obtain a relation linking the superficial velocity U, with the pore flowrate q;

$$q = \frac{\sqrt{3}Ud_b^2}{4} = \frac{\sqrt{3}Qd_b^2}{4A} \qquad \text{- 3.74}$$

where; $Q = \Sigma q$ = total pack flowrate (m^3/s)
A = bed cross sectional area (m^2)

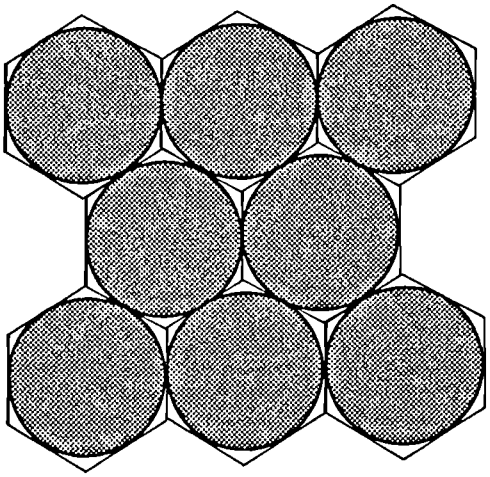

Figure 3.21a Monolayer of beads in hexagonal packing

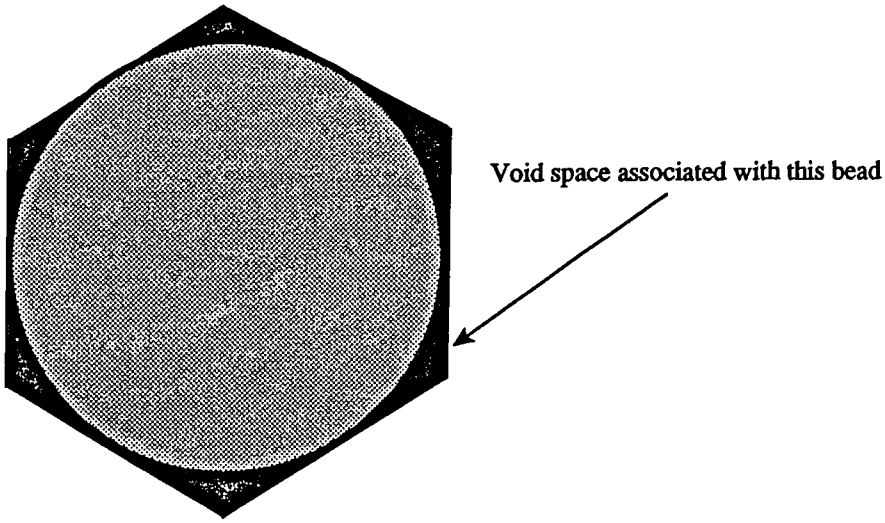

Figure 3.21b Flow area associated with a single bead

3.5.2 Conversion of bead diameter to permeability/porosity function

The relationship developed for the capillary bundle (equ 3.36), called the Blake-Carmen-Kozeny equation, will be used here to convert the bead diameter, d_b, into terms of permeability and porosity. Therefore, from equ 3.36, in terms of d_b we have;

$$d_b = \frac{(Jk)^{0.5}(1-\phi)}{\phi^{3/2}} \qquad - 3.75$$

3.5.3 Conversion of (q/d_b^3) to global parameters

Using the results obtained in the above two subsections, it is now possible to replace the ratio (q/d_b^3) in the extensional rate relationships. From equs 3.74 and 3.75 above, we have;

$$\frac{q}{d_b^3} = \frac{\sqrt{3}\, U\, \phi^2}{4(1-\phi)(180k\phi)^{1/2}} \qquad - 3.76$$

Thus we have, in comparison to the earlier work of Durst and Haas, and James and McLaren, for the average extensional strain in a bead pack;

$$\dot{\xi}_{av} = \frac{46\sqrt{3}\, U\, d_b^2}{4d_b^3}$$

$$= 19.9\ \frac{U}{d_b} \qquad - 3.77$$

(compared to their values for the constant of 4 and 150)

For flow in consolidated media, such as rock, the extensional strain may be estimated by;

$$\dot{\xi}_{max} = \frac{3U\phi^{3/2}}{(1-\phi)k^{1/2}} \qquad - 3.78$$

or,

$$\dot{\xi}_{av} = \frac{1.48U\phi^{3/2}}{(1-\phi)k^{1/2}} \qquad - 3.79$$

4. Experimental Apparatus and Technique

4.1 Objectives

The design objective of the apparatus used in this work was to produce an extensional flow field, related to porous media flow, and of sufficient strength that it will be possible to study the onset of elongational behaviour in dilute polymer solutions.

Much of the previous work in the investigation of polymer solution flow has centred on flow through columns tightly packed with glass beads (ballotini) (55,31,12,8,3,38,40,46). Durst and Haas (31,22), among others (26,9) have also used apparatus whose flow passages are similar to those found between hexagonally packed beads, and have empirically derived expressions for the rate of extension (or elongational strain rate) for these passages.

The present study differs from these previous works by attempting to correlate data from several different experimental configurations onto a single plot of resistance factor against elongational strain rate, and hence predict the onset in one case from the results of another.

The main programme of tests in the bead pack here was supported by tests in other flow cells designed to give axi- and non axi-symmetrical extensional and compressive flows. For each of these supporting experiments a similar set-up existed designed for visualisation of the resulting flow patterns.

4.1.1 Design Constraints and Requirements

Several design objectives applied in common to all of the apparatus. These were, in addition to the requirement to produce an extensional flow field of sufficient magnitude:

1. That the Reynolds Number should be as low as possible so that inertia effects would not affect the results. Typical Reynolds numbers are of the order of 0.01 to 1.0 in an oil reservoir. In this work solvent N_{Re} were of the order 0.0001 to 0.1 in the bead pack and typically 0.1 to 100 in the fine bore capillary apparatus (0.03 to 30 for the corresponding expansion chambers).
2. Keep shear strain rates to a minimum in order to reduce shear degradation of the polymer samples. Sorbie (72) estimates that γ is less than 10 sec^{-1} at a distance of 30m or greater from the well bore. This restraint presents problems as the rate of extension is dependant on similar parameters, hence a reduction in shear strain rate (via a reduction in flowrate) leads to a reduction in the elongational strain rate.
3. Wherever possible the use of metals should be avoided in order to reduce the levels of ion contamination (which aid degradation).
4. The apparatus should be as 'simple' as possible so that faults could be quickly diagnosed and corrected. Transparent materials should be used wherever appropriate to allow visual inspection.

4.1.2 Main experiment - bead pack

As can be seen from plate 4.1, the apparatus was placed horizontally in a large waterbath, with a constant head device at the outlet providing a system overpressure of 1m head of fluid. It was decided that this experiment would be performed by measuring the pressure drop at various flowrates (ie flowrate control) at a constant temperature. This was achieved by delivering the test solutions to the bead pack by way of an infusion pump, and measuring the resulting pressure drops using differential pressure transducers (figure 4.1).

4.1.2.1 Pack Design

Large (53mm) diameter acrylic (Perspex) tube, with a 6mm wall thickness was used for the body of the bead packs.
This large diameter ensured that the low shear rates found in a reservoir could be achieved in the interstices of the beads when supplying the pack with a flowrate of 1ml/hr, the minimum the pump would supply. Using a large tube diameter also ensured a high column-to-bead diameter ratio (>500 in this case) so that edge effects were not too serious a problem.

The main pack was 1.0m in length, with pressure tappings 0.25, 0.45 and 0.75m from the inlet. This produced a maximum test length of 0.5m , with the shorter sections available to be monitored to check pressure drop continuity or to be used when the differential pressure over the longer section exceeded the transducer limit.

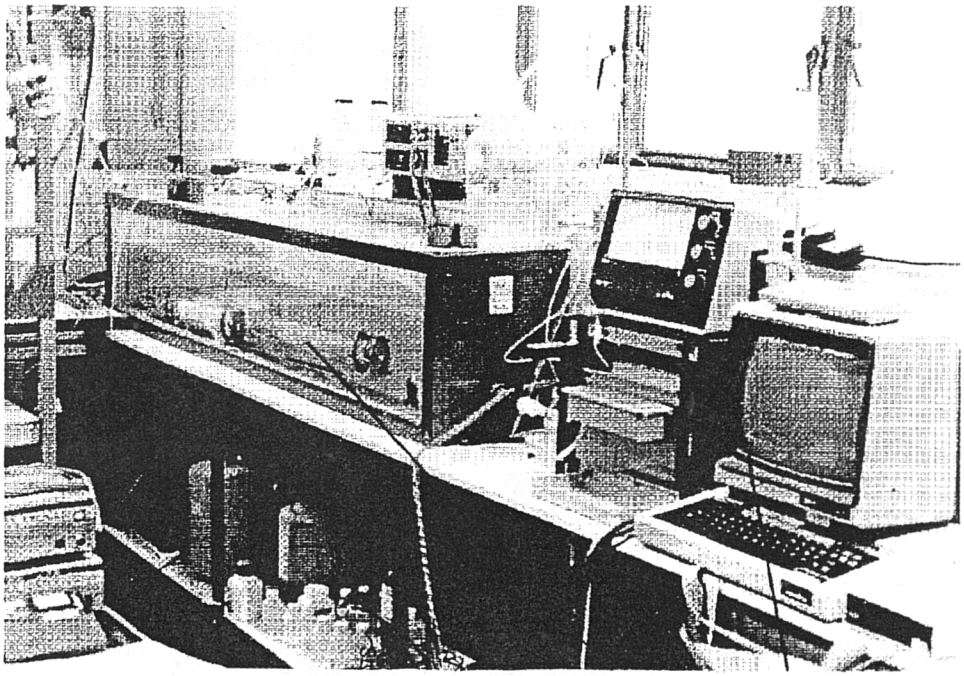

Plate 4.1 Apparatus Layout

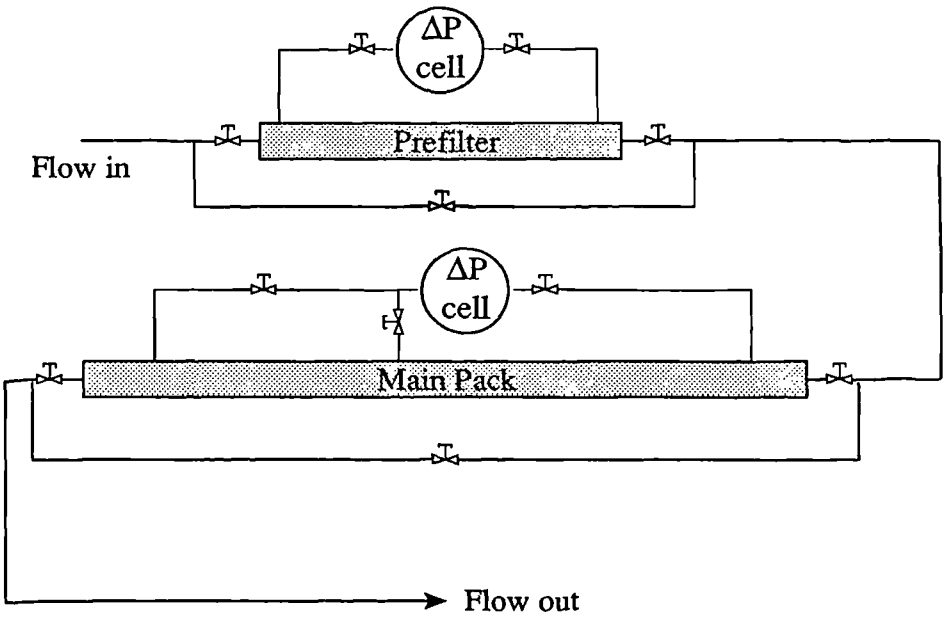

Figure 4.1 Schematic Apparatus Design

The ends of the column were designed to ensure the solutions enter the pack diffused across the full diameter, and also to contain and compress the beads. Both end pieces, as shown in figure 4.2, consist of a solid acrylic piston machined to give a good sliding fit in the pipe internal diameter. Through the centre of the pistons, two holes were drilled, one acting as the fluid delivery line, the other to take a platinum resistance thermocouple in order to record the fluid temperature just prior to it entering the pack. Two 'O' rings, the first acting as a wiper, the second as the seal, make a continuous pressure tight joint between the piston and the pipe. On the inner (bead) face a series of concentric grooves were machined with interconnecting passages to enable the fluid to spread before passing through a sintered glass disc which acted as a bead retainer. As neither end piston is fixed it was possible to vary the length of the bead column by up to 8cm. This facility enabled one piston to be fitted in place, a known weight of beads added, then the other piston fitted. By vibrating the pack and tightening from both ends the beads were firmly compacted and clamped in place.

By knowing the weight and density of the glass beads, and being able to measure the total bead filled length it was possible to calculate pore volume and column porosity.

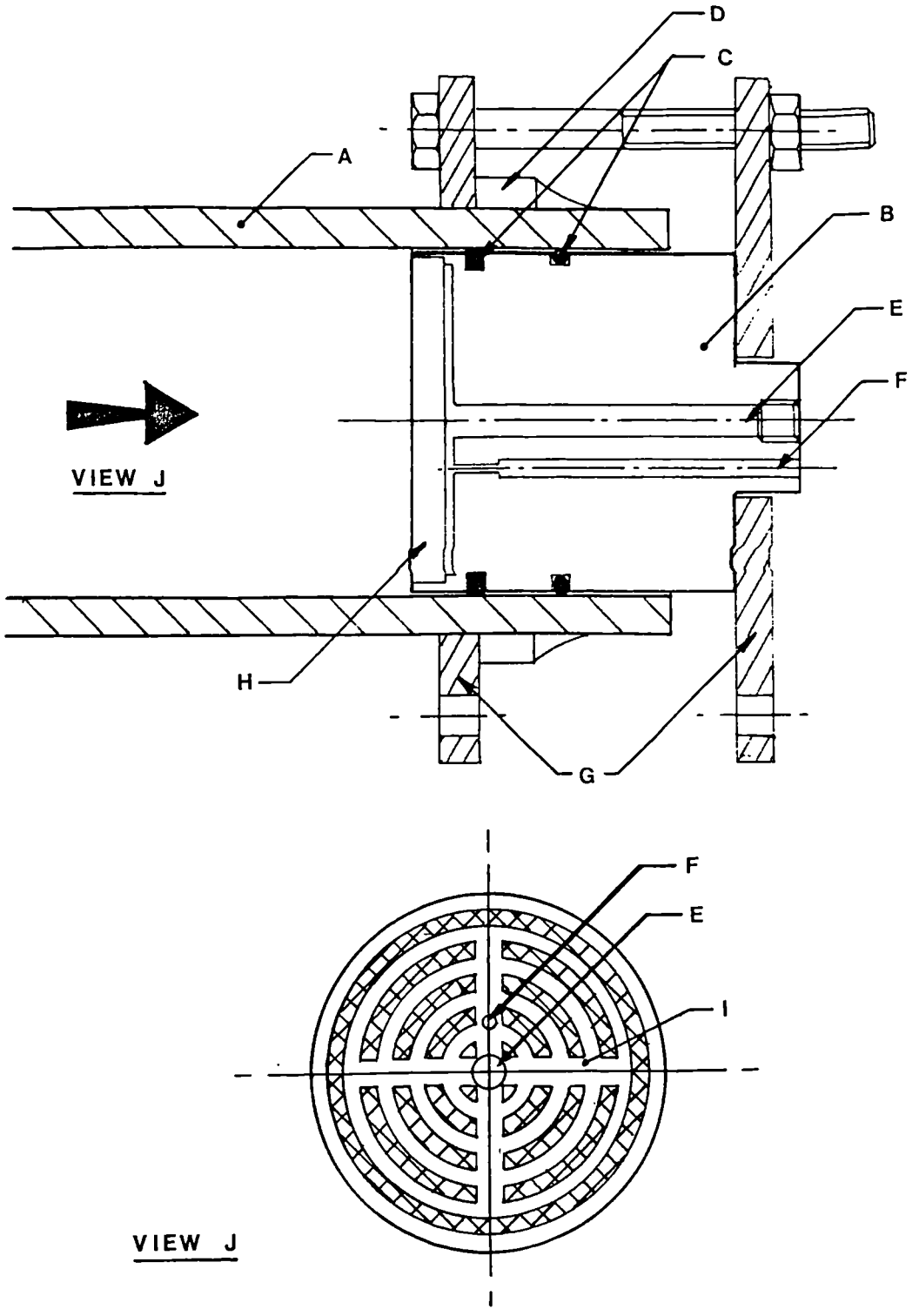

Legend

A. 53mm (id) clear acrylic pipe
B. Clear acrylic end piston
C. Nitrile 'O' rings
D. Bonded clamping ring
E. Fluid delivery bore
F. Thermocouple bore
G. Stainless Steel clamps
H. Sintered Glass disc
I. Fluid passages behind bead retainer

Figure 4.2 End piece design

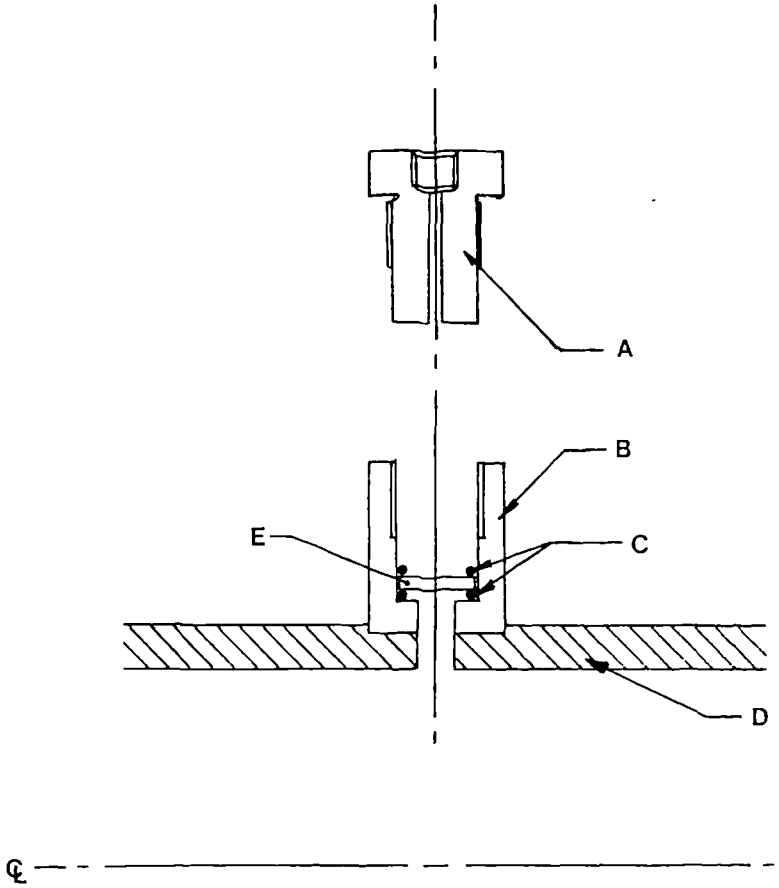

Legend

A. Threaded acrylic piston
B. Acrylic receiver
C. Nitrile 'O'rings
D. Bead Pack tube wall
E. Sintered glass disc

Figure 4.3 Pressure Tapping Design

The pressure tappings are similar in design (figure 4.3) to the end caps, with a hole machined in the side wall of the tubing and a receiver bonded in place. This receiver was then sealed with another sintered glass disc, sandwiched between 2 'O' rings, and clamped in place with a threaded acrylic piston.

Previous work carried out in this laboratory (55) encountered problems with a reaction occurring between the ballotini and the polymer solution itself. The effect of this was to block the injection end of the pack, and was not caused by adsorption. It was therefore decided to employ a shorter pack, of the same design, of length 0.5m to act as a 'prefilter' to the main pack. If any reaction did occur then it would not disrupt the main pack. Pressure drop and effluent viscosity were monitored across this shorter pack to check for signs of blockage.

As stated above the packs were made from clear acrylic, along with the end pistons and pressure tappings. Due to previous problems experienced when using high temperature highly saline solutions in metal pipes all connecting pipes, pressure lines, taps and valves used with the bead packs were made from either nylon or polyethylene.

4.1.2.2 Measurement of variables

As stated above, flow was supplied to the packs by an infusion (Pharmacia P-500) pump. Where the flowrate was greater than 500ml/hr two pumps were used in parallel. These pumps are equipped with flowrate control over the range $1 \rightarrow 499$ ml/hr in 1 ml/hr steps. The pumps were both calibrated to ensure that the indicated flowrate was correct - both pumps showed an error of <1% for all values in the range as shown in figure 4.4a. The flowrate was also measured at intervals over the tests to check for leakage and/or pump error.

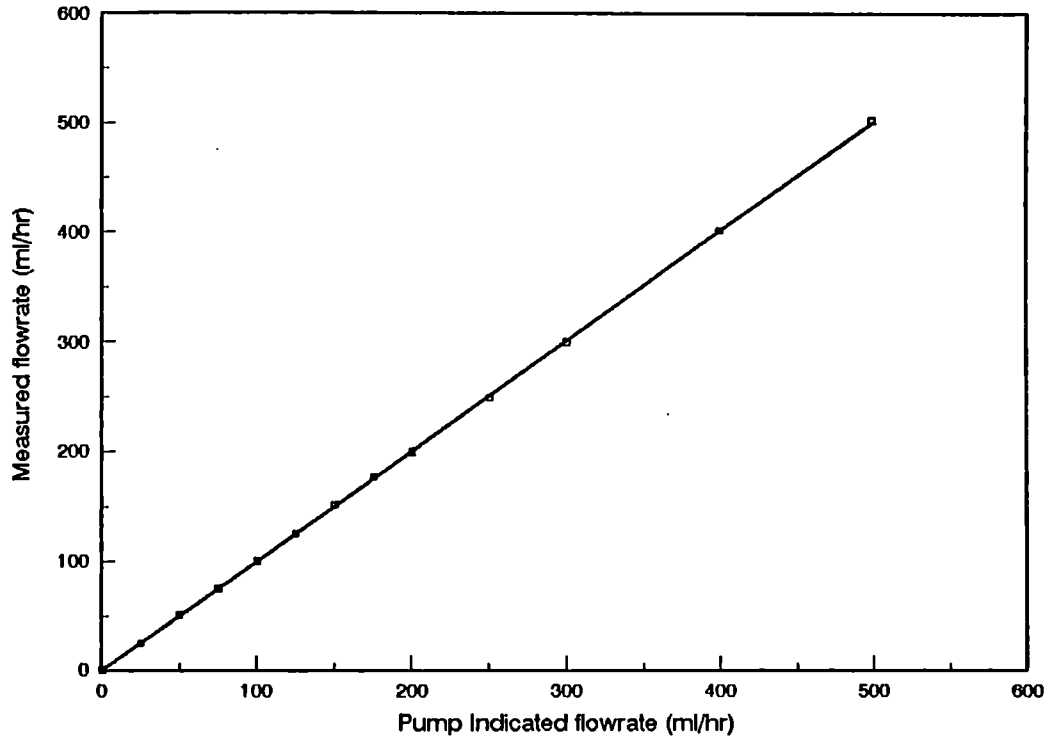

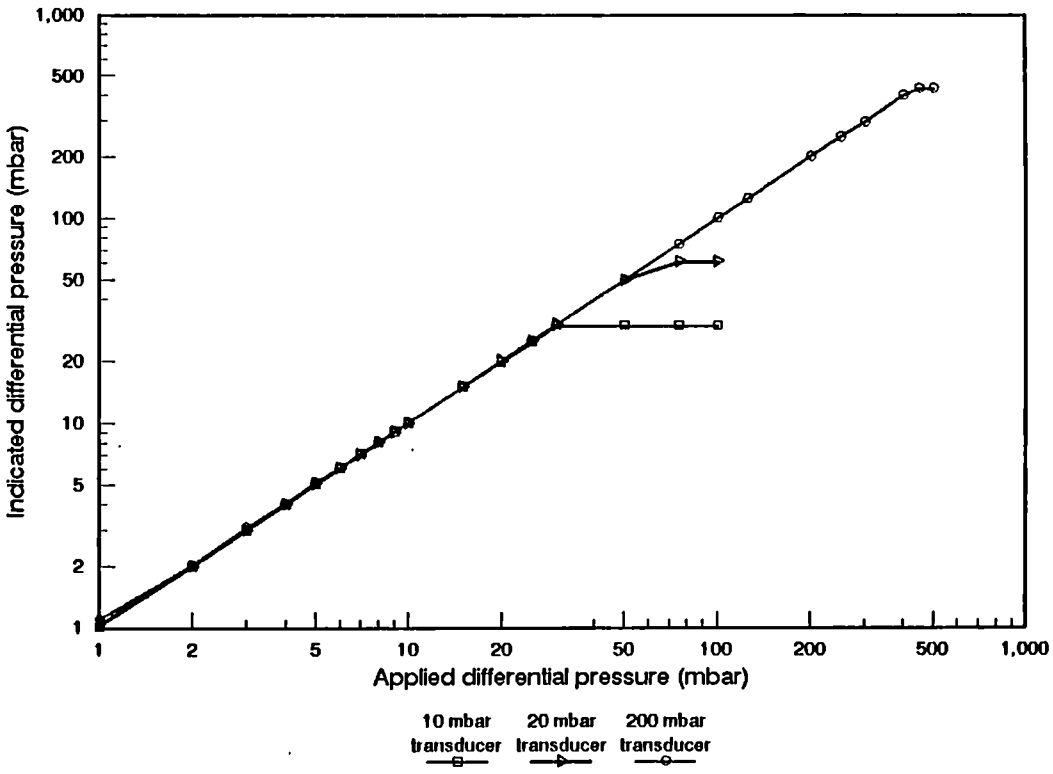

Figure 4.4a (top) Pump Calibration Curve

Figure 4.4b (bottom) Pressure Transducer Calibration Curves

Pressure drops were measured using Electorr differential pressure transducers. These robust transducers are driven with 12 V dc and output a voltage between 0 to 1.5 V (0 to 5 V for later transducers) which is proportional to the differential pressure being monitored. In order to assess the accuracy and to recalibrate these transducers an accurate static differential water level gauge was designed (figure 4.5). The linear digital micrometer scales on both water level height recorders have an accuracy of 0.01 mm, which proved useful for calibrating 1mbar differential transducers. In the main the ranges of the transducers used in this work were of the 10, 20 and 200 mbar fsd differential type, a typical calibration being shown in figure 4.4b.

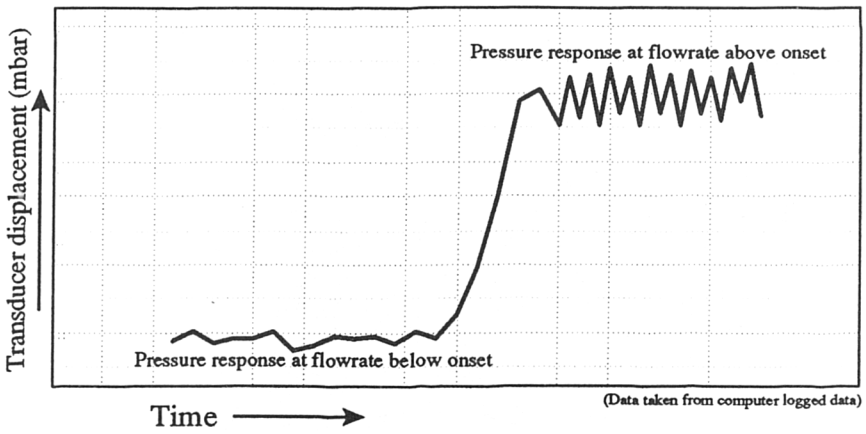

Figure 4.6 Pressure trace fluctuation at onset

Differential pressure across the pre- and main packs along with the injection fluid temperature were displayed digitally on voltmeters and also recorded on a chart recorder to assess time effects. Onset of elongational behaviour was usually indicated by a lack of stability on the pressure trace, with the pressure fluctuating between stable maxima and minima as illustrated in figure 4.6.

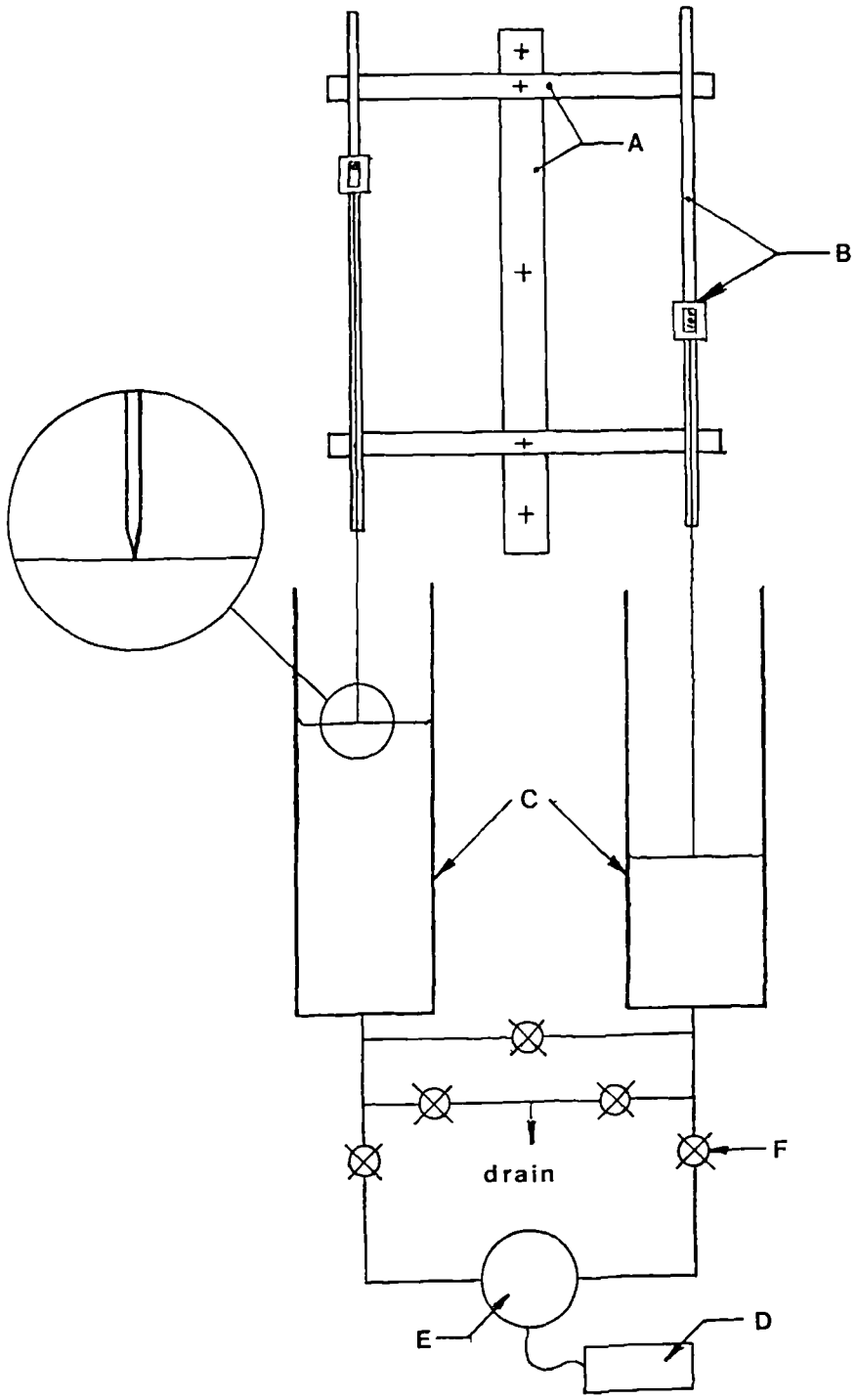

Legend

A. Wall mounted framework
B. Tracking and readout
C. Large diameter fluid vessels
D. Transducer readout
E. Pressure transducer
F. Fluid control taps

Figure 4.5 Pressure transducer Calibration Apparatus

It was initially hoped to automate the experiment, with a BBC microcomputer receiving flowrate and pressure data, incrementing the pump when stable conditions were reached and a time averaged pressure drop recorded. Due to cost constraints the internal Analogue to Digital converter was to have been used, but tests indicated that at the lower pressure drops the resolution was insufficient to accurately determine stability and hence record the differential pressure, so this plan was abandoned in favour of manual operation.

Settling times between flow increments depended on how large the flow increment was, with a bigger increase in flowrate requiring a proportionally longer settling time. Wherever possible times in excess of two hours were allowed (settling usually took up to one hour) before reading to ensure an equilibrated state. As wide a range of flowrates as the pressure transducer limits would allow was obtained for each polymer concentration/salinity combination.

As was the case with all the experiments, more than 5 pore volumes (usually >20 for the supporting experiments) were injected at a flowrate below onset to allow chemical equilibrium to occur. The experiment was then carried out with the lowest flows first, incrementally increasing to the highest. Early tests indicated the maximum injection rate for the first runs in the bead pack, but once the test procedure was established the results from the planar contraction apparatus were used to determine the maximum injection rate. To avoid onset in the 48 μm pack 7 days were taken to establish equilibrium.

4.1.2.3 Temperature Control

The temperature control system was based on a domestic central heating system as shown in figure 4.1b. The two bead packs sat horizontally in an insulated water bath, some 1.5 m in length, 0.3 m wide with a water depth of 0.3 m. Connected to one end of the bath was the top of an electric immersion type heater with a presettable thermostat, whilst the other end of the bath connected with a circulation pump which returned the water to the base of the immersion cylinder. In order to achieve temperature stability, a system with a large thermal inertia was required. For this reason the water bath in which the packs sat, and the immersion cylinder were chosen as large as possible. The total fluid volume of the system

when filled was some 300 litres (66 gallons), which when insulated with sheets of expanded polystyrene maintained the bead packs at a temperature of 30±1°C. Apart from keeping the bead packs at constant temperature, the water bath was also required to heat the polymer solution up to pack temperature. The prefilter here also acted as a heat exchanger in warming the test solution up. In all except the fastest flows the fluid took upward of an hour to travel the length of this shorter pack with its small pores, in which time the test solution was seen to have reached the water bath temperature. Platinum resistance thermocouples were incorporated into the inlet pistons of the prefilter and main pack to monitor the efficiency of this heat exchange.

As the polymer solutions were stored and usually pumped from a refrigerator at 3°C to reduce bacteriological attack the temperature of the solutions had to rise by some 27°C. This increase usually presented no problems as the solutions at the low to medium flowrates tended to warm up to laboratory temperature (22 to 23°C) before leaving the pumps, hence only some 7°C of heating was carried out in the prefilter.

In the case of the high flowrates (upwards of 600 ml/hr), the time allowed for heating from 3°C was insufficient, and the polymer reservoir had to be removed from the refrigerator and allowed to warm up to room temperature. This did not affect the degradation aspect as it was the high flows that were carried out last and so the solution was only un-refrigerated for a maximum of 24 hours before use. (At low flowrates of say 10 ml/hr the solution takes 35 hours to travel the length of the prefilter).

4.1.3 Axi-symmetric contraction flow apparatus

Several experimenters, including Chauveteau and Ghonheim (26,9,58,56), have used this type of apparatus to study the viscoelastic behaviour of dilute polymer solutions.
These experiments were originally performed under pressure control, setting the system pressure drop between an upper and lower constant head device, and recording the resultant flowrate and test section pressure drop.

4.1.3.1 Apparatus Design

The general design of this apparatus is shown in the schematic layout of figure4.7a. It was initially manufactured from lengths of 6mm o/d glass capillary with a 0.6mm bore, spaced at intervals along a piece of flexible polyethylene tube. Several methods of sealing the outside of the capillaries were tried, but a seal made by wire wrapped a few times around the flexible tube was found to be the most reliable. Pressure tappings were placed 50mm upstream of the first capillary and 50mm downstream of the last.

In order to find the required contraction ratio and capillary bore sizes to yield an onset condition three sizes were initially made up :-
a 3:1 contraction ratio with 6mm o/d tube with a 2mm bore
a 10:1 contraction ratio with 6mm o/d tube with a .6mm bore
a 20:1 contraction ratio with 6mm o/d tube with a .3mm bore.
Tests indicated that the apparatus with the contraction ratio of 10 was likely to yield the optimum results.
As an adaptation of this design, it was decided to attempt to glassblow another 'interrupted capillary' apparatus with a contraction ratio of 10 , but with profiled entrances to and from the capillary sections as shown in figure 4.7b. The conical nature of these entry/exit regions lends itself to mathematical analysis of the contraction induced extensional strain.
In order to carry out a control experiment, apparatus was designed that had the same total capillary length but was not 'interrupted' as shown in figure 4.7c. Pressure drop measurements were taken over the same total length of tube so that any losses occurring in the 6mm tube would also be accounted for. These control apparatus were glassblown for both abrupt and conical contractions.

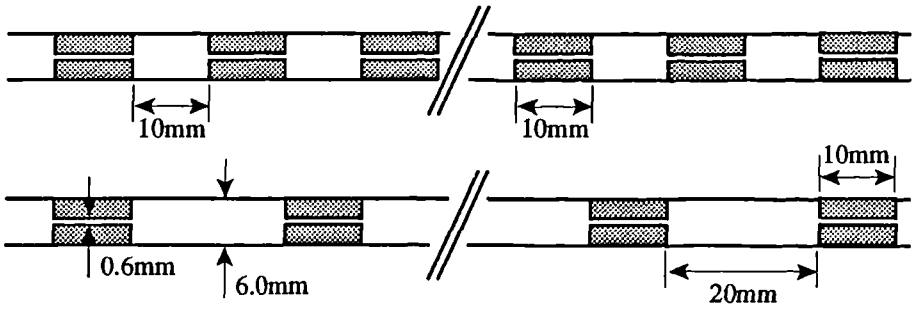

Figure 4.7a Arrangement and sizes of abrupt interrupted capillary apparatus

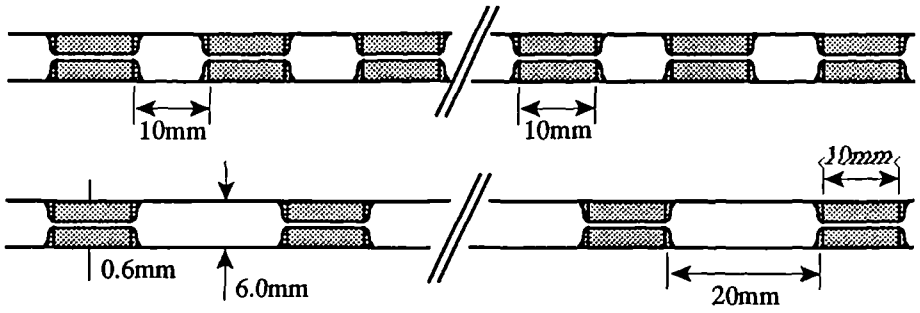

Figure 4.7b Schematic of profiled contraction interrupted capillary apparatus

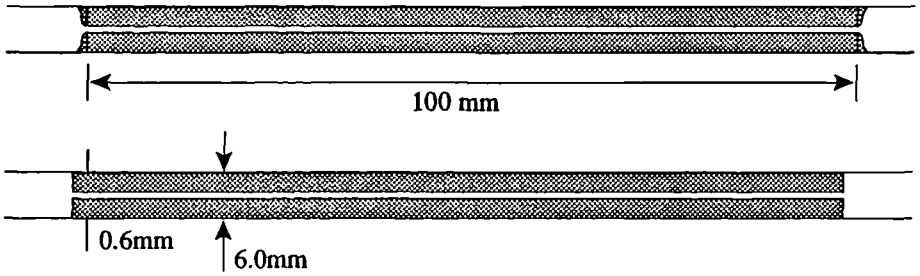

Figure 4.7c Sizes of Continuous Capillary Control Apparatus

4.1.4 Planar Contraction Apparatus

The extensional field produced by flow through a hexagonally arranged array of cylinders produces a similar flow domain to that found in bead packs, with constantly varying cross-sectional areas, and hence steady-state accelerations and compressions. The passage network formed ensures the ability for different flow routes through the array to be followed as is the case in any porous medium. The author feels that this property makes this apparatus very suitable for studying a 2d simplification of the flow through a bead pack.

Experiments using this apparatus were conducted under flowrate control using a Pharmacia pump to inject the fluid, and measuring the pressure drop over the cylinder array to calculate resistance factors.

4.1.4.1 Apparatus Design

The basic concept of this apparatus is illustrated in figure 4.8. It was decided to build two sizes of apparatus so that the effects of scale-up could be studied.

1. The smaller cell has passage widths of 100μm which simulate more closely the flow through the porous media used, where average pore diameters are 15μm. This was the smallest that could be manufactured given the tolerances of the machines available. The 0.5mm diameter glass rods were made by heating and drawing out a 2mm rod, and then carefully selecting the most accurate on size and concentricity. The top faces of these rods were then lapped to ensure a flat contact surface with the glass cover which acts as a seal to prevent fluid passing over the top of the rods. (The rods could not be polished due to their fragile nature).
As it was very difficult to trim the rods to the same length a novel support system was designed. As indicated in figure 4.9a, the inclusion of a thin layer of latex ensured that the rods were pushed against the top cover whilst being able to be pushed down to the same level. This small block was then fixed inside a larger block as shown in figure 4.9b, which incorporates a water jacket so that the rig could be run at various (constant) temperatures.

2. The larger flow cell, 10 times the size of the smaller one, consists of an array of 5mm glass rods at a 1mm nominal spacing. Although able to be used for measurement of resistance factors the main objective behind this apparatus was to provide a unit suitable for flow visualisation. A description of this apparatus can be found in section 4.1.6.1.

4.1.5 Screen Factor Apparatus

The flow of polymer solutions through fine meshed stainless steel screens has been studied by Prud'homme (54). Although very difficult to analyse numerically due to the woven nature of the screens, the screen factor apparatus as it is known is a useful and quick experiment to indicate the presence and magnitude of viscoelastic effects. Due to the random placing of the five screens on top of each other, it again provides a flow regime similar to that in a porous media with its tortuous passages.

4.1.5.1 Apparatus Design

This apparatus is based on five 100 mesh (100 wires/inch) stainless steel gauzes, placed randomly on top of each other. An acrylic housing was designed as in figure 4.10 in which the screens were sandwiched between 2 'O' rings. The experiment can be conducted either in the form of a capillary viscometer as in figure 4.11a, or under flowrate control as in figure 4.11b. Although useful results can be obtained in both configurations, the author agrees with Prud'homme that the operation over a wide flow range using an infusion pump for flowrate control provides the optimum results.

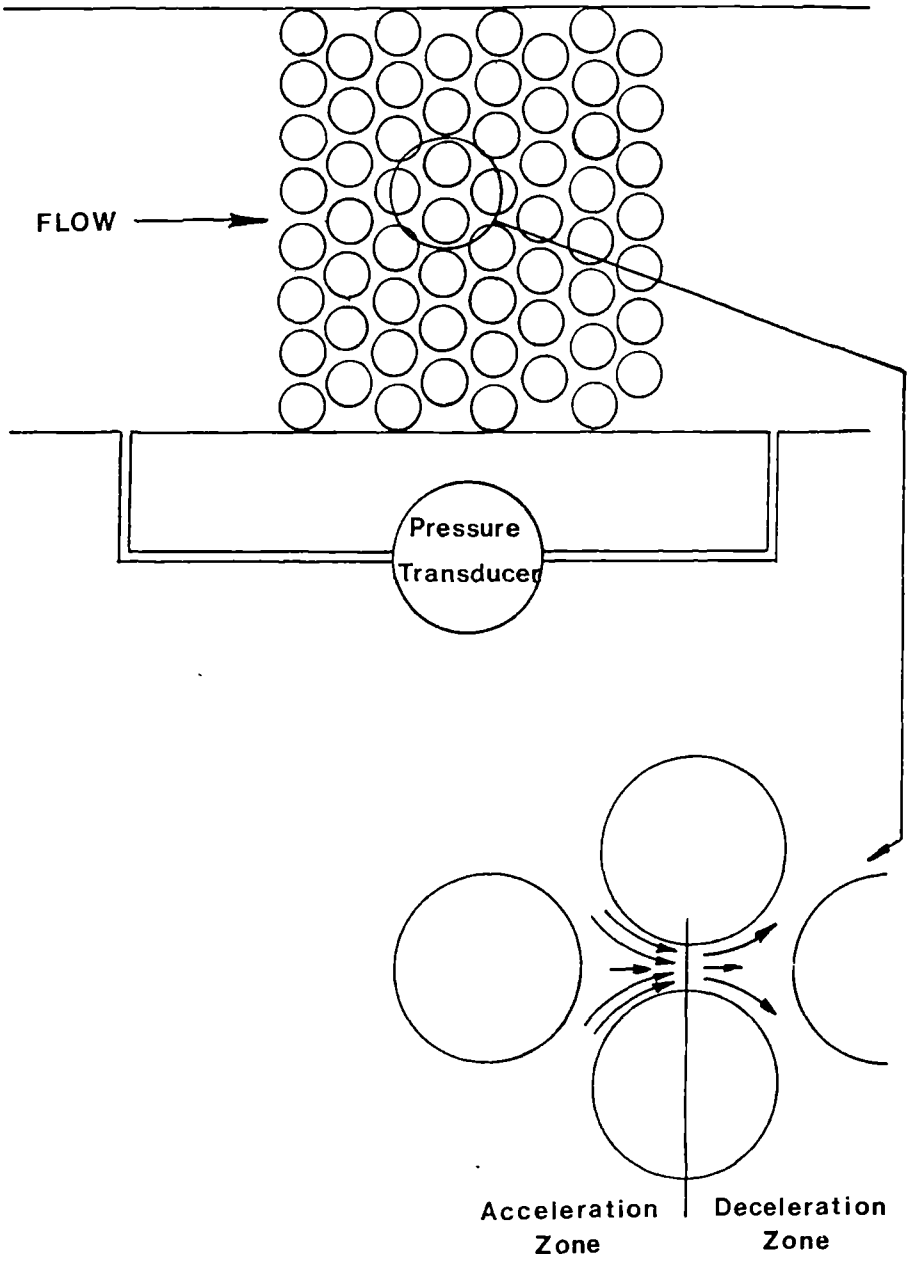

Figure 4.8 Planar Contraction Apparatus

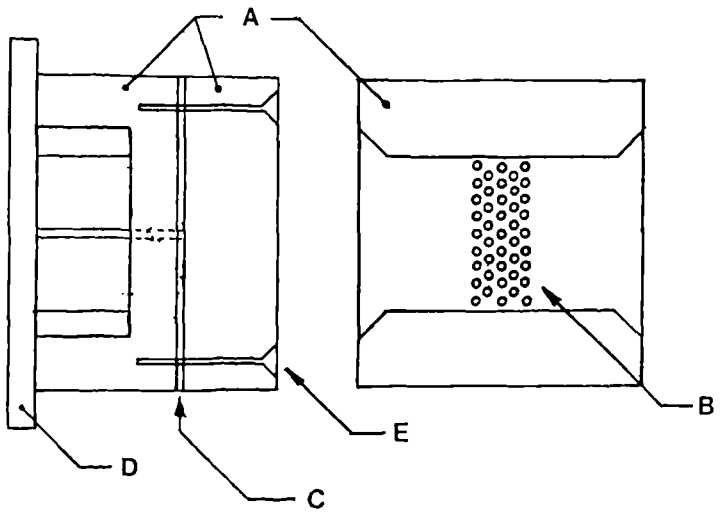

Legend

A. Solid brass housing
B. 0.5mm glass rods
C. Thin latex sheet
D. Glass cover plate
E. Fixing rivets

Figure 4.9a 0.5mm rod array holder

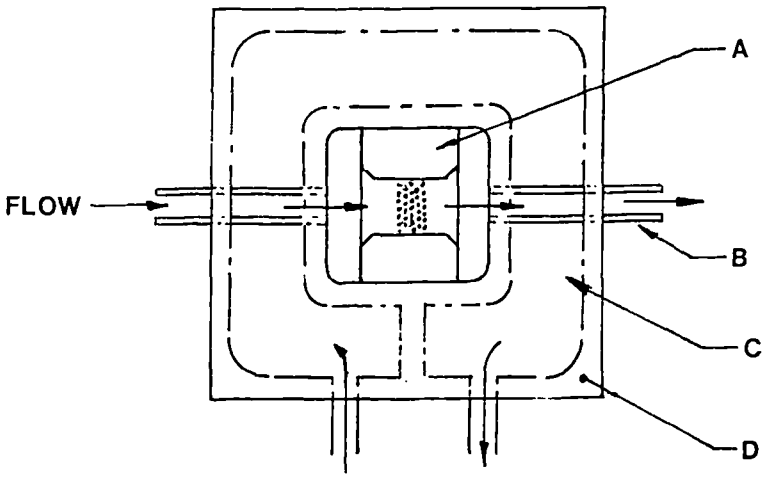

Legend

A. Rod holder (as above)
B. Test fluid inlet/outlets
C. Water jacket passages
D. Stainless steel block

Figure 4.9b 0.5 mm rod array casing detail (showing water jacket passages)

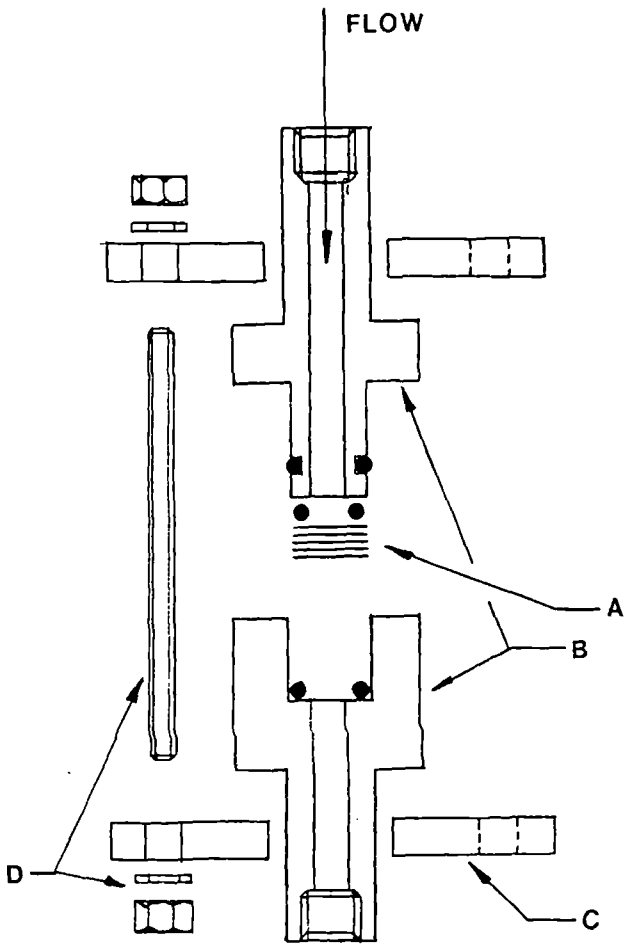

Legend

A. 5 stainless steel meshes
B. Clear acrylic housings
C. Acrylic clamping rings
D. Brass studs and nuts

Figure 4.10 Screen Factor Apparatus - Exploded view

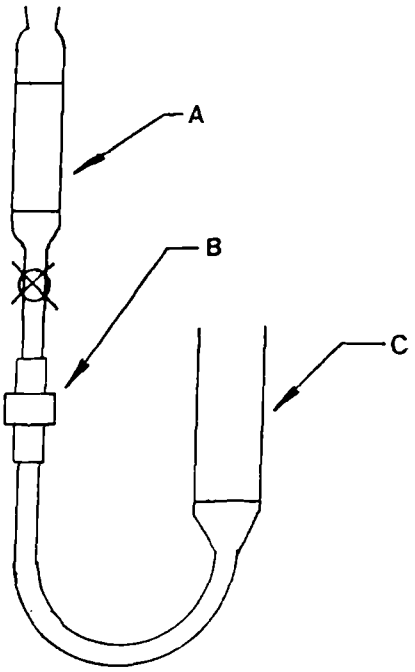

Legend

A. Graduated Buchner funnel

B. Screen factor housing

C. Graduated receiver

Figure 4.11a Screen 'Viscometer'

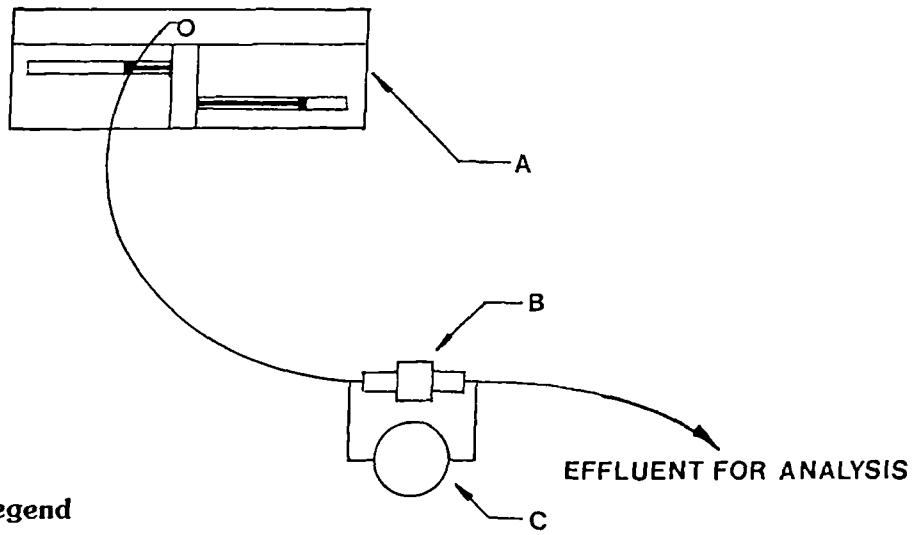

Legend

A. Pharmacia infusion pump

B. Screen factor housing

C. Pressure transducer

Figure 4.11b Screen Factor Apparatus under flowrate control

4.1.6 Flow Visualisation Apparatus

In order to study the flow patterns, visualisation studies were undertaken in both the planar and axi-symmetric contraction apparatus.

A thin (1mm) light sheet was provided by passing the beam from a 35mW Spectra-Physics Helium-Neon laser through a series of lenses as shown in figure 4.12. A stage which has controlled movement in 3 dimensions was fixed to an optical bench to provide a stable base for the apparatus to be attached to. The resulting visualisations were then recorded using either a Pentax SLR camera (with 100mm extension tubes) or a Panasonic VHS video camera (with an 18x close-up lens). The recording devices were fixed onto a vertical screw operated mount so that optimum focus and picture composition could be achieved.

4.1.6.1 Apparatus Design

For the case of the axisymmetric apparatus a similar design was employed with only six interrupted units. However, in order to investigate the dependence of expansion chamber length a second cell was built in which the chamber lengths were doubled to 20mm as indicated in figures 4.7a & 4.7b, leaving the capillary length unchanged at 10mm. For the case of the abrupt contraction set-up, which could not be glassblown, transparent glue with the same refractive index as glass (Loctite© Glass bond) was used to cement the capillary sections between the expansion chambers. This proved a very successful method of jointing the sections. The planar contraction apparatus, however, is ten times the size of that used for the majority of the planar supporting work. The rod diameter used here is 5mm, at a 1mm spacing as shown by figure 4.13. This apparatus was constructed with a glass top and clear acrylic sides, the rods being located in an aluminium base. Early tests with the cell indicated the need to blacken the rods totally except for the narrow illuminated test section - without this the light tended to be scattered across the total cell height after diffraction and reflection of the beam on the first few rods, which made visualisation of a single plane impossible.

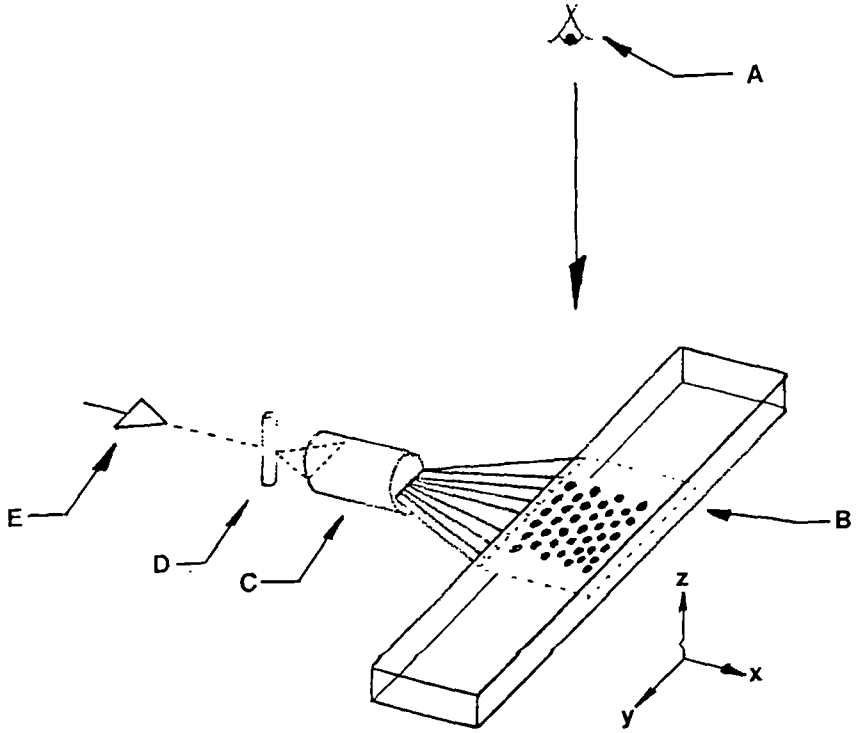

Legend

A. Viewing direction (also video and stills camera mounts)

B. Visualisation flow cell

C. Laser focussing lens

D. Beam spreader

E. Laser light sheet

Figure 4.12 Flow Visualisation Apparatus Arrangement

The visualisation experiments were usually conducted under pressure control, the high flows requiring the reservoir to be pressurised with nitrogen to provide a sufficiently high driving force.

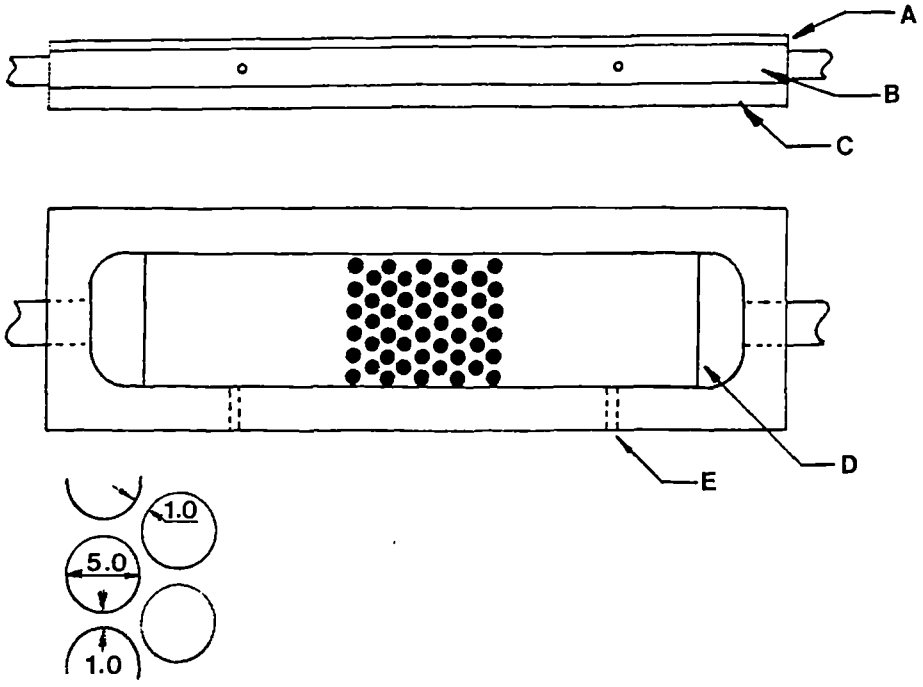

Legend

A. 2mm thick glass cover plate
B. Clear acrylic surround
C. Aluminium base
D. Flow baffles
E. Pressure tappings

Figure 4.13 Planar Visualisation Apparatus

4.2 POLYACRYLAMIDE SOLUTIONS

4.2.1 Polyacrylamide Solution Preparation

It has been noted that synthetic polymers are sensitive to the method of preparation, in particular high shear blending should be avoided. It was decided that in order to achieve consistent and well defined solutions a rigorous laboratory preparation procedure would be followed. The main steps involved were :-
preparation of the solvent (brine) solution,
weighing and mixing of a 2000wppm (nominal) Master solution in brine,
dilution of the master solution to final test concentration,
filtration of the test solution and deoxygenation.

4.2.1.1 Solvent preparation

The solvent solution consisted of analytical grade Sodium Chloride (NaCl) dissolved in deionised water with an initial conductivity of $< 1 \mu s/cm$, and initial dissolved salt content of < 0.0001 ppm.

It was first intended to use formaldehyde as a biocide, preventing bacteriological attack, but after consultation with the polymer manufacturer, it was decided that this could, in certain circumstances, aid crosslinking and so no biocide was added.

The salt was added to the centre of a vortex formed in the water by a magnetic stirrer, the stirring continuing until dissolution was apparently complete, ie the solution was clear. The solution was then shaken vigorously and stirred for a further 4 hours to ensure complete homogeneity. Batches of 20 kg (~20 litres) of solvent were made up at a time with no filtration of the brine solution occurring at this point.

4.2.1.2 Master solution preparation

The polyacrylamides used in this work are available in both liquid emulsion and powder form. In all tests only powdered formulations have been used. Polymer B powder was analysed by BP Sunbury (6) and found to have a water content of 13.8% by weight. Sufficient master solution was made up so that when diluted all of the concentrate would be used. Twenty kilograms (~20 l) of test solution was made prior to each run in the bead pack, so that for the case of a 500 wppm solution, 5 kg of 2000 wppm master would be made up.

The following method was adopted for preparation of the master concentrate:

1. After weighing a clean dry bottle to .001g, 25g of methanol was added. The methanol was then swirled around the bottle to wet all the sides to prevent the polymer sticking.
2. The correct weight of polymer was added, according to the final desired concentration. The powder was added slowly to ensure clumping did not occur. The bottle was then gently swirled to ensure all the polymer particles were individually methanol wetted.
3. 500 g of brine solution was added, the bottle then being capped and shaken to form a suspension of polymer particles.
4. Brine was then added to the correct weight, a dumbbell spinbar added and the bottle capped and inverted four times to mix the brine and suspension.
5. The bottle was placed on a magnetic stirrer at 30 RPM for 24 hours.
6. After stirring the 2000 wppm solution was placed for storage in a refrigerator at 3°C prior to being diluted to working strength.

Master solutions were kept for no longer than 14 days before dilution and use.

4.2.1.3 Test Solution Preparation

As mentioned above, 20 kg (~20 l) of solution was made up prior to each bead pack test. This large amount was required to be able to pass 7 pore volumes (1pv ≈ 1l) through the pack prior to any readings (4-5 pvs were sufficient to stabilise the pressure drop and effluent concentration). The dilution of the master to test strength was achieved by adding the master solution to a vortex formed in a 25 l vessel. Approximately half the required weight of brine was placed in the vessel, and a vortex formed by a magnetic stirrer. Master solution was then added to the vortex, with the remaining required brine being first washed around the master solution bottle to ensure transfer of all the polymer. The solution was then stirred for a further 24 hours to achieve homogeneity.

4.2.1.4 Filtration and deoxygenation of test solutions

Filtration of the solutions was achieved by pumping the solutions through 45mm diameter Millipore© MF filter papers with 5μm mean pore dimensions at 150 ml/hr. The pressure switch on the Pharmacia pump was set to stop the pump at a pressure of 0.25 MPa, after which the filter paper was changed. This usually resulted in three papers being used for the filtration - indicating reasonable filterability.

Removal of the oxygen from the polymer solution was effected by gently bubbling oxygen free nitrogen through the solution for 1 hour, causing nitrogen saturation. In order not to introduce a metallic object an acrylic gas diffuser head was built.

4.2.2 Polymer solution quality monitoring

As it is the viscosity of the polymer solution that most affects the experimental characteristics, close monitoring is important in order to cross relate results. Wherever possible samples of the solutions made up for the bead pack were used in the supporting experiments, but where this was not possible, and to assess polymer performance, its shear viscosity, pH and concentration were measured before, during and after their use.

4.2.2.1 Viscometric measurements

The intrinsic shear viscosity of a polymer solution is proportional to its molecular weight, and hence monitoring the low shear viscosity can indicate signs of mechanical degradation and also any gross errors in make-up. Polymer rheograms at all solvent salinity conditions were obtained from measurements taken on a Contraves Low Shear viscometer at BP Sunbury. These rheograms were compared to viscosity measurements obtained on the concentric cylinder type viscometer in the lab in Bristol. This viscometer, manufactured by UK Viscometers Ltd., is fitted with a low centipoise adapter and water jacket to enable readings to be taken at 30±0.5°C, the temperature at which the majority of experiments were conducted. The readings from this viscometer gave comparative rather than absolute readings due to the lower accuracy of the machine.

The viscosity of the test solutions was monitored at the end of its stirring period, and also after filtration. Master solution shear viscometry was not monitored due to lack of range on the viscometer. Figure 4.14a shows the range of viscosities obtained for a 100 wppm solution in 0.05% brine.

4.2.2.2 pH Analysis

The pH of the solutions was measured at 30°C using a Pye Unicam pH meter. Tests on unused polymer solutions were in the range 6.8 to 7.1, with the range for the solvent being 6.6 for 0% NaCl to 6.9 for the 3% salt solutions. Bead pack effluent pH was measured from samples collected for concentration analysis, however, no difference in values of the injection to effluent pH was found. This result indicates the inertness of the bead pack apparatus used.

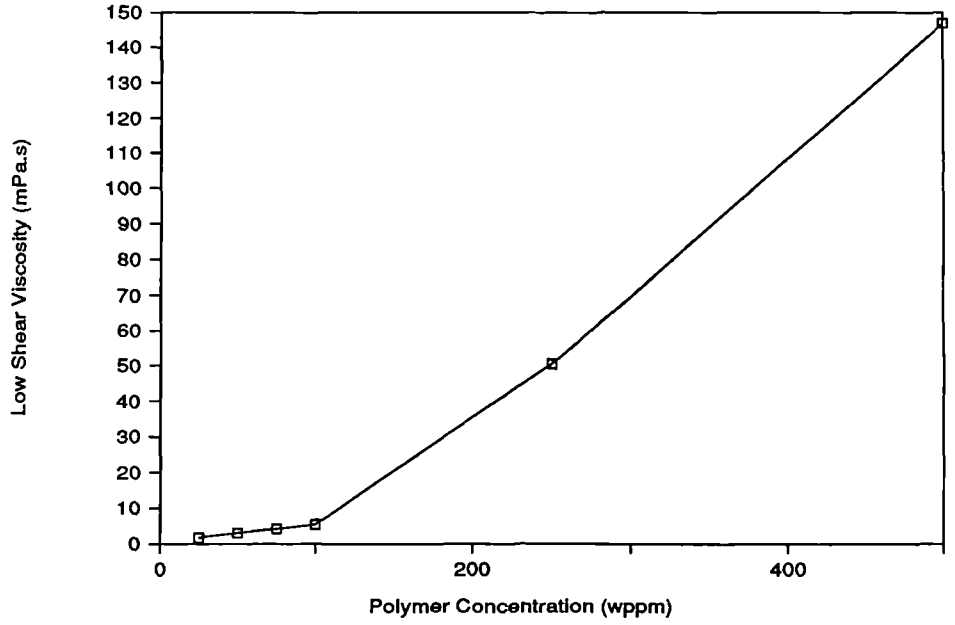

Figure 4.14a Viscosity variation for 100 wppm solutions in a 3% brine

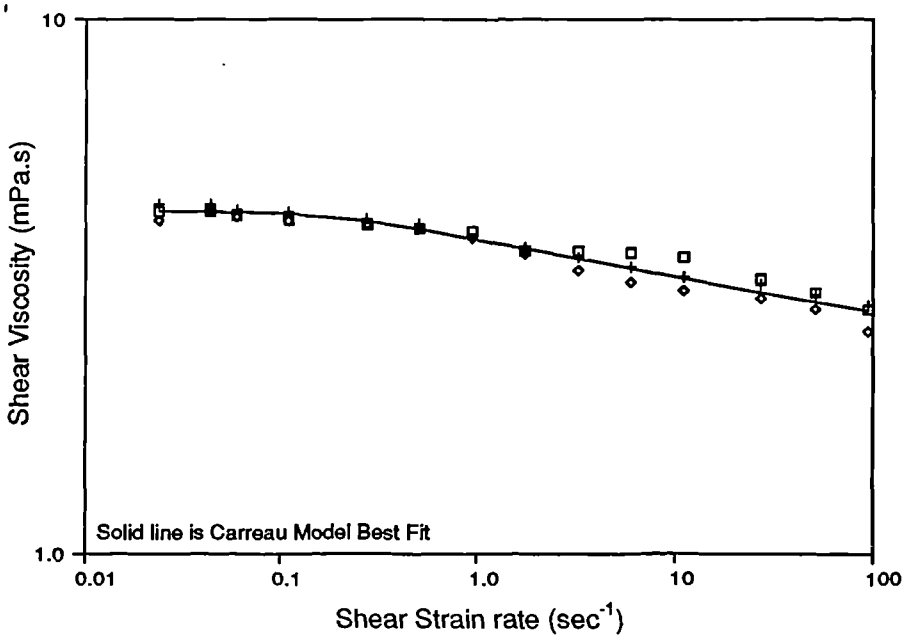

Figure 4.14b Relationship between low shear viscosity ($\gamma \rightarrow 0$ sec^{-1}) and polymer concentration in an 0.05% brine

4.2.2.3 Polymer Concentration Determination

As mentioned above, the polyacrylamide powder was found to contain 13.8% water by weight. The error this could cause should far outweigh any other concentration error. These could be introduced during solution make-up only during :

1. initial measurement of powder and brine for master solution,
2. measurement of brine when diluting master solution,
3. filtration, when polymer loss could occur by removal of any not fully dissolved polymer powder.

Errors due to weight measurement are unlikely to amount to >1% of the nominal concentration as even for a 100 wppm solution 2g of powder was added and weighed to 3 decimal places (maximum error of ±0.45% if 3rd decimal place read incorrectly). Viscometric monitoring of the solutions should indicate any gross errors in make-up; figure 4.14b shows the relationship between low shear rate viscosity and polymer concentration for a 0.05% NaCl solvent. Polymer losses during filtration are difficult to determine without chemical analysis, but viscometric measurements taken pre- and post- filtration indicated only a slight decrease as shown in figure 4.15.

It was hoped that refractometry would provide an analysis tool for polymer concentration. The deviation of a solution's refractive index from that of its solvent is proportional to the concentration of polymer molecules present. Tests, however, with a Knauer Differential Refractometer failed to yield consistent and reproducible results, even for the same solution. Absolute measurement of refractive indices was thought unlikely to have sufficient resolution so this approach was abandoned. (It is possible that an error existed either in the machine, or with operator ignorance - the instruction manual supplied was in German, and no English translation was available for the particular model).

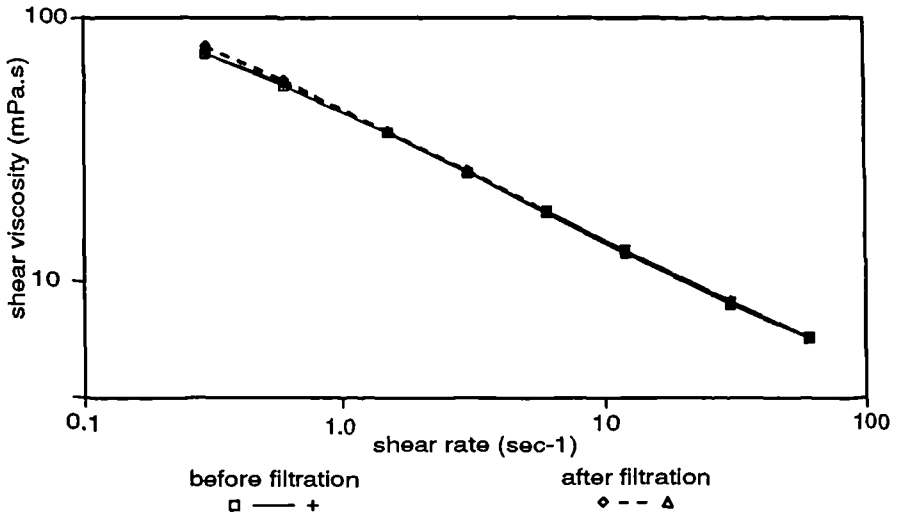

Figure 4.15 Comparison of Pre- and Post- Filtration shear viscosities

In order to obtain correlations between the nominal, post filtration and effluent concentrations, titration of samples was carried out at BP Sunbury.

4.3 PREPARATION AND PACKING OF THE BALLOTINI

The ballotini used in this work was supplied by English Glass Ltd.. Specially sieved beads were obtained with a narrow size distribution, typically with over 90% of the beads within a 10% band about the average diameter. The narrower the diametric distribution the greater the uniformity of the pack, and therefore the more regular and predictable the passage shapes and dimensions.

4.3.1 Bead Sizing

Although the beads were sized close to the required tolerances it was decided that a narrower range could be achieved by sieving the beads to remove the smallest and largest fractions. This was highly laborious and tedious as the spherical particles tended to wedge into the square sieve holes, which meant that the sieve screens had to be frequently cleaned. The removal of these tails was considered important as it is the beads with a large deviation in diameter that will disrupt the packing the most. It was found that the beads had a coating preventing them from sticking during the manufacturing process, which had to be removed before use. After

cleaning, as described below, the beads were magnified and photomicrographed to enable a sample average diameter to be calculated. This optical inspection process could obviously only examine a very small percentage of the beads used in filling the packs. Typically the diameters of some 500 beads were measured by enlarging photographs to 10"x8" plates which contained some 50 beads.

4.3.1.1 86 micron bead cleaning

The beads themselves were delivered as 'inert' - however because of previous problems with polymer → 'bead' reactions it was thought prudent to wash and then stabilise the beads in de-ionised water. Several methods of cleaning were initially tried including; washing in a sodium hypochlorite solution; boiling in acid; or copious washing in deionised water.
It was noticed that in all cases a precipitate was forming and rising to the surface, indicating the presence of a salt added as a free-running agent for the beads. A method was adopted where the beads were boiled in hydrochloric acid, then thoroughly and repeatedly washed in deionised water until a pH of 7 was reached. After drying in an oven at 80°C for 48 hours, the top layers of beads had formed a hard crust which had to be broken (with a hammer) to reach the clean beads below. These clean beads appeared to 'run' far easier and no precipitate was formed when washed again.

4.3.1.2 48 micron bead cleaning

The successful method for cleaning the packs between runs as detailed in 4.4.3 was adapted to initially clean this batch of beads. It had now been established that magnesium carbonate (a free running agent) had been sprayed onto the beads during manufacture.

A 1m column of 53mm internal diameter pipe was half filled with a 1% (w/v) solution of Hydrogen peroxide (H_2O_2). Beads were gradually introduced into the top end of the column in batches of ~1kg. A violent reaction ensued for about an hour with gas being given off (CO_2 and O_2), and a precipitate of a magnesium salt forming. Once the reaction had almost ceased, further beads were added with up to about 4kg being cleaned at a time. After the 4th kg of beads had been added a 0.5% (w/v) H_2O_2 solution was pumped at 500 ml/hr up through the base of the column, thus slowly permeating upwards. The purpose of this second 'washing' was to react with any salt still in place on the beads. This process usually produced as strong a reaction as with the 1% (w/v) solution. Once the reaction had stopped deionised water was pumped through until the water above the beads had cleared. The beads were then removed and thoroughly washed to remove any traces of precipitate, and then dried in the oven. No solid layer was found on removing these beads from the oven.

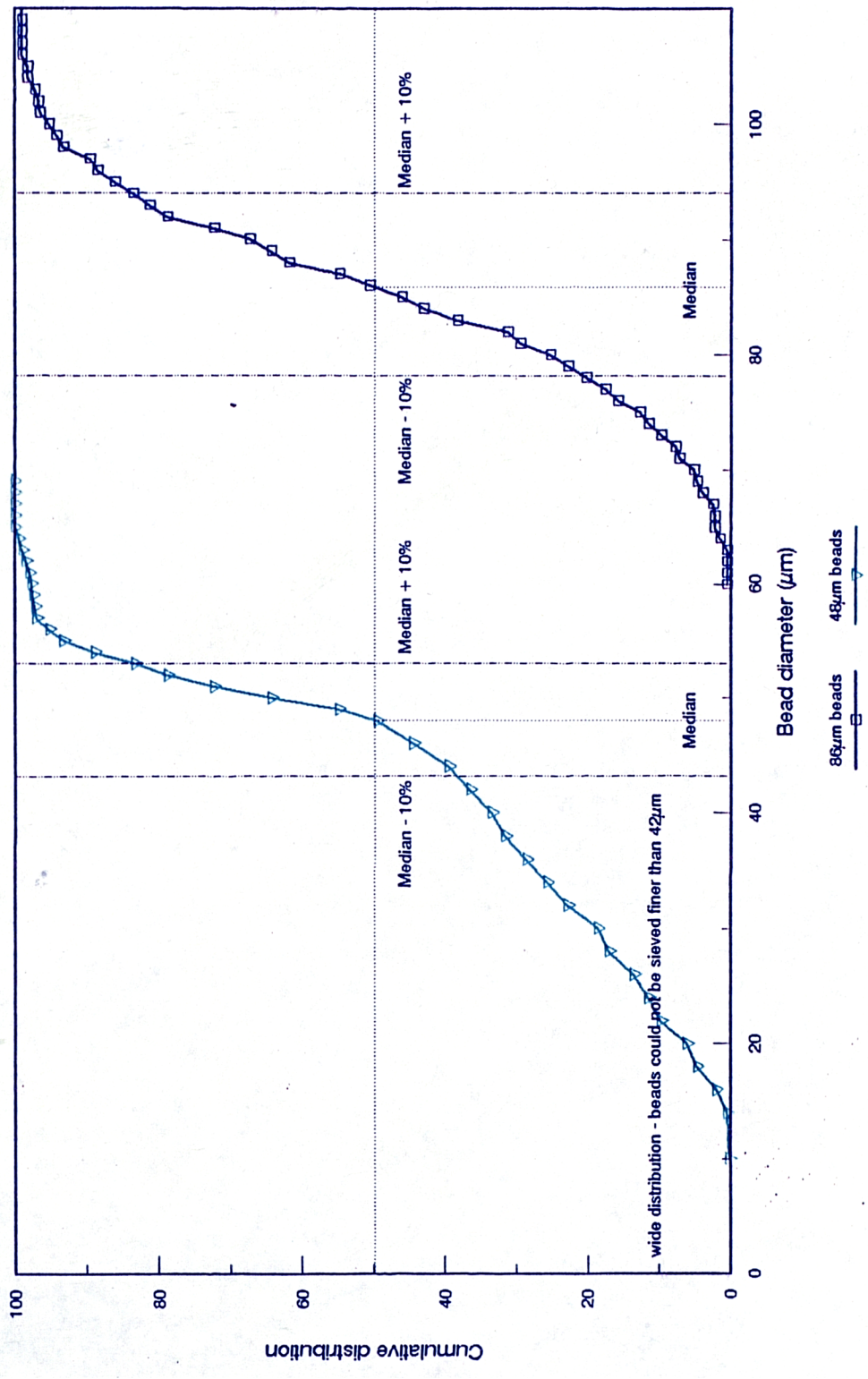

Figure 4.16 Bead Size Distribution for both bead sizes

4.3.2 Column Packing

The objective of this procedure is to pack the beads as closely and regularly together as is feasible. For monodisperse beads it should be possible to achieve a completely regular and hence repetitive pack. To ensure as good packing as possible, the following procedure was adopted :

1. The empty pack was weighed, with one end cap fitted, together with all fittings (tension rods, etc), and this weight recorded as W1.
2. The column was attached vertically to an oscillator, and vibrated at 50-60 Hz. A pressure line was attached to the bottom (fitted) end cap, and $C0_2$ was slowly pumped through as illustrated in figure 4.17.
3. Clean beads were slowly added, allowing the beads to fall separately - the upward flow of the gas aiding this separation.
4. When sufficient beads had been added to fill the column to within 25mm of the top, the second end piston was pushed into place.
5. By increasing the flow of CO_2, it was possible to produce an almost fluidised bead pack. By gradually reducing the CO_2 flow, the beads were seen to settle. This process usually resulted in a 10mm reduction in packed column length. The top piston was then loosely fixed in place.
6. The pack was then left to vibrate for several hours, reducing the pack length by a further few millimetres.
7. The length, L1, of the bead column was measured through the clear acrylic wall, and recorded, after fixing both end pistons tightly in place.
8. Finally the packed column was then weighed to determine the total weight, W2.

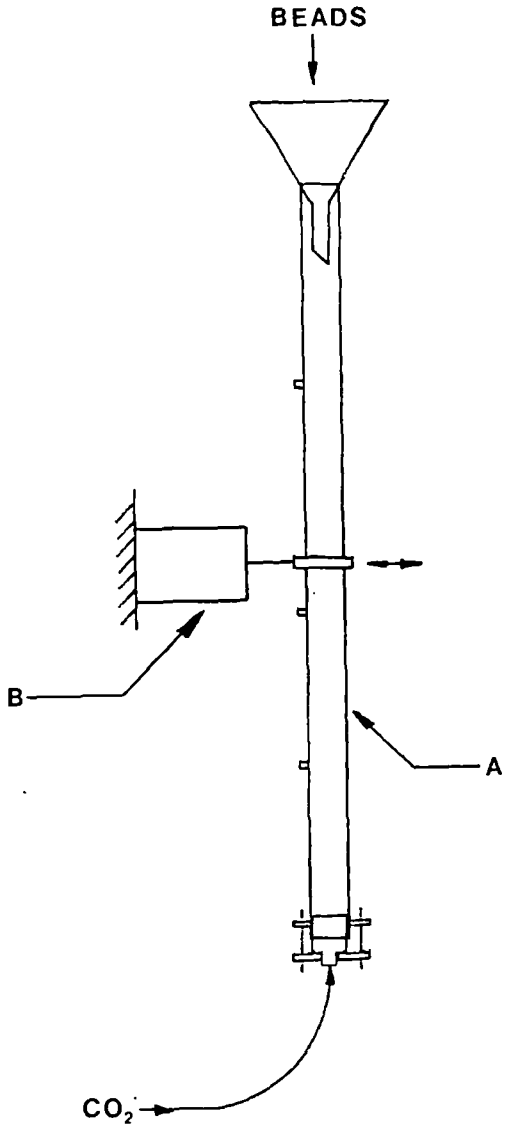

Legend

A. Bead Pack clamped vertically

B. Ling Dynamic Systems vibrator, oscillating at 50 - 60 Hz

Figure 4.17 Arrangement used for column packing

4.3.2.1 Porosity calculations

The porosity (void fraction) of the pack was determined from the net bead column weight (W2-W1), the bead density (ρ_b), and the total column volume ($0.25\pi D^2 L1$), where D is the column internal diameter (0.053m).

$$\therefore \text{Void fraction} = \frac{\text{total column volume - volume of beads}}{\text{total column volume}} \quad - 4.1$$

$$= \frac{0.25D^2\pi L1 - (W2-W1)/\rho_b}{0.25D^2\pi L1} \quad - 4.2$$

$$= 1 - \frac{4(W2-W1)}{\rho_b D^2 \pi L1} \quad - 4.3$$

4.4 PACK CALIBRATION

Unless the packs could be accurately calibrated and those calibrations reproduced, then little trust could be placed on the results produced. A careful calibration procedure was followed before each run in the pack as well as after the initial packing.

4.4.1 Initial pack flooding

When installed in the water bath, both packs were connected up in series and to their respective pressure lines. With the water bath at operating temperature a further flood of about 100 PVs of CO_2 was used to remove the air from the connecting and pressure lines. With the flooding occurring underwater, escapes of gas could be easily identified and corrected. To complete the leak testing the pack outlet was closed and the system pressurised to 5 bar; if no leaks occurred with a gas then a fluid with a viscosity some 100x greater would be unlikely to leak. Carbon dioxide is highly soluble in water, and so with all the air displaced by CO_2 waterflooding of the packs could occur. Deionised water was injected into the packs at a rate of 500ml/hr (1 PV every 2 hours). One of the advantages of using clear acrylic pipe was that it was now possible to observe the waterfront advancing along the columns. Also, the difference in refractive index of a water(bath)-perspex-water system is large compared to a water(bath)-perspex-gas system, so air bubbles

could be easily observed. If air was seen to exist, further flooding with CO_2 took place until the air was eradicated. The ability to view the shape of the advancing front also enabled pack homogeneity to be assessed, as illustrated in figure 4.18a. Waterflooding continued until about 25 PVs had been injected - this being more than adequate to obtain stable conditions.

4.4.2 Determination of Permeability to water

Darcy's Law can be applied to flow in a porous medium as shown in 3.1.2. Therefore by measuring pressure drops at a range of flowrates, the permeability of the pack relative to water (or other Newtonian calibrating fluid) can be determined. The range of permeabilities to water for the 86μm pack over its entire history are presented in figure 4.18b - it can be seen that the packing, cleaning and calibration procedures followed produced very stable results.

4.4.3 Recalibration procedure

After each polymer run in the packs, waterflooding took place to establish the post-polymer water permeability, an important parameter as this gives an indication of adsorption and polymer retention. Following this flood a 0.1% (w/v) solution of H_2O_2 was injected at 150 ml/hr (6.5 hrs per pv). The injection of hydrogen peroxide to degrade polyacrylamides by oxidation is adapted from the work of Ramsden and McKay (88) - in their case a catalyst of Iron (II) ammonium sulphate was added to produce hydroxyl radicals to degrade the polymer. It was decided that oxidation would be used as opposed to hydroxyls as the introduction of Fe^{2+} ions into the pack could lead to contamination problems later. It is worthwhile mentioning the fact that a stronger solution of H_2O_2 is not advised as the reaction, as well as being exothermic, produces rather copious amounts of gas, so its rate control within an enclosed environment its critical. After injecting 2 PVs of the H_2O_2 solution, deionised water was re-introduced to flush any unused reagents out. CO_2 flooding and re-calibrating as previously detailed were then carried out.

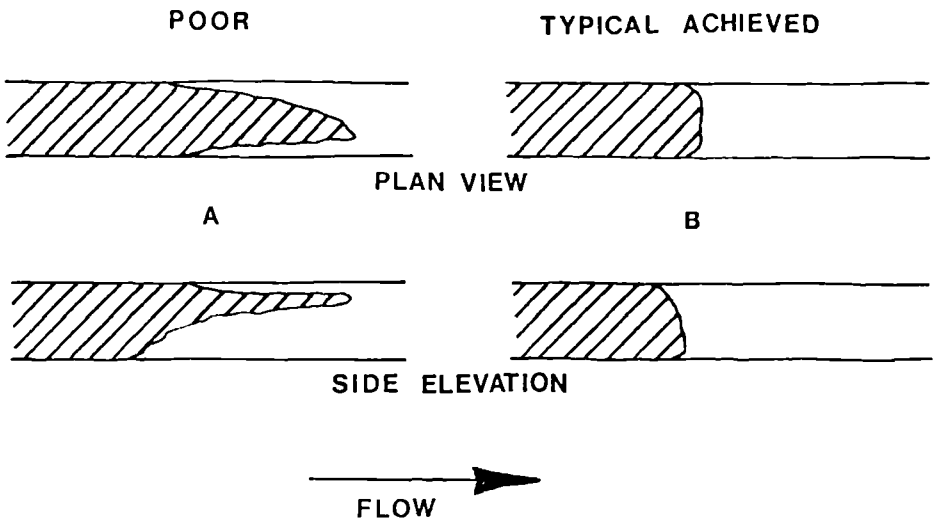

Legend

A. Poor *homogeneity of packing indicated by distorted waterfront (pack* fingering) - usually from insufficient pack tightening

B. Typically achieved waterfronts during initial flooding, showing good homogeneity

Figure 18a Visual inspection of pack homogeneity

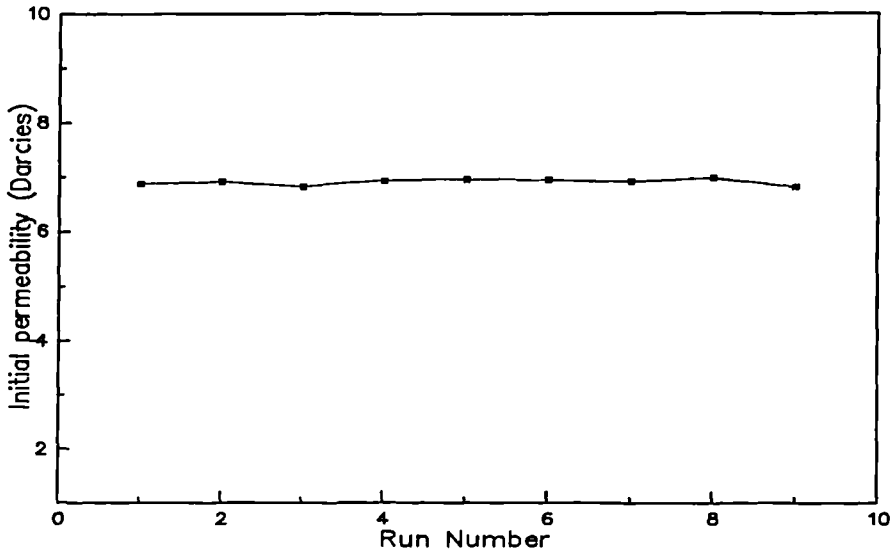

Figure 4.18b Range of initial permeabilities (to water) for 86μm pack

Previous work in this laboratory had involved the use of sodium hypochlorite to clean bead packs. When this was attempted here a colour change to reddish brown occurred throughout the beads, and although the permeability increased it was still some 50% lower than the initial value. One detrimental effect of using H_2O_2 as an oxidising agent to clean the pack was that the nitrile 'O' rings used for sealing suffered degradation and needed renewing when the pack was stripped down to be repacked with the smaller beads.

4.5 Cleaning and calibration of supporting experiments

As the duration (and surface areas) of the supporting experiments was much lower than that of the bead packs it was not expected that adsorption would present a problem. Indeed the cleaning procedure usually followed simply involved injecting large quantities of hot (80°C +) seawater to re-establish initial conditions. When low salt content solvent tests were carried out in the small planar apparatus a weak H_2O_2 solution had to be used to thoroughly clean the apparatus. Calibration of all the experiments followed a similar procedure to the one used for the bead packs, with differential pressures recorded at incremental flowrates. Calibration coefficients, equal to the ratio of the pressure differential to the flowrate were produced. This coefficient (dp/Q) was then used to calculate polymer resistance factors.

5. EXPERIMENTAL RESULTS

In order that bulk solution properties may be compared with experimental observations, effective viscosities must first be defined.
Where an apparatus has been calibrated using the flow of the solvent, and the pressure drop recorded for various test flowrates, then the effective viscosities (resistance to flow) can be represented by ;

$$\text{relative effective viscosity} = \frac{\Delta p_p}{\Delta p_s}\Big|_q \qquad \text{- 5.1}$$

$$\text{absolute effective viscosity} = \frac{\Delta p_p}{\Delta p_s}\Big|_q * \mu_s \qquad \text{- 5.2}$$

where $\Delta p \,|_q$ denotes the pressure at a given flowrate.

5.1 Bulk Solution Rheology

Shear rheology measurements were made on the solutions not only to provide rheological data but also to assess solution repeatability and reliability.

5.1.1 Shear Viscosity

All shear rheological data were obtained using a Contraves© LS-30 shear viscometer at BP Sunbury. For everyday and comparison work a lower accuracy machine (Viscometers UK Low Shear viscometer) was used - this machine recorded the same results as the Contraves but over a much narrower range as shown in figure 5.1. Despite its lower accuracy and smaller range the viscometer clearly highlighted any errors in make up or loss of viscosity over filtration.
Polymer A, a medium to high molecular weight polyacrylamide, was only used for a single series of tests in the 86μm bead pack in 0.05% NaCl solution. As can be seen from figure 5.2, the solutions are highly shear thinning, with values of n (the shear thinning index), and κ (fluid consistency) as shown in table 5.1.
Polymer B, a high to ultra high molecular weight polyacrylamide was used for the majority of experiments including the visualisation tests. Dilutions of this polymer were made in deionised water, 0.05% NaCl and 3% NaCl solutions with the shear rheograms obtained illustrated in figures 5.3 to 5.5 respectively.

The very high shear viscosity obtained in the deionised water solutions (The 500ppm solution was too viscous for the Contraves to measure) rapidly diminished with increasing salt concentration. The salt concentration dominates the shear viscosity because of the sensitivity of the molecules to ionic concentration - the **higher** the salt concentration the **less** uncoiled the molecules and hence the **lower** the shear viscosity as less interaction between chains occurs - this is clearly shown in figure 5.6. The viscosifying effect of polymer B was much greater than polymer A, due to polymer B's higher molecular weight. Table 5.1 compares the n and κ values for both polymers.

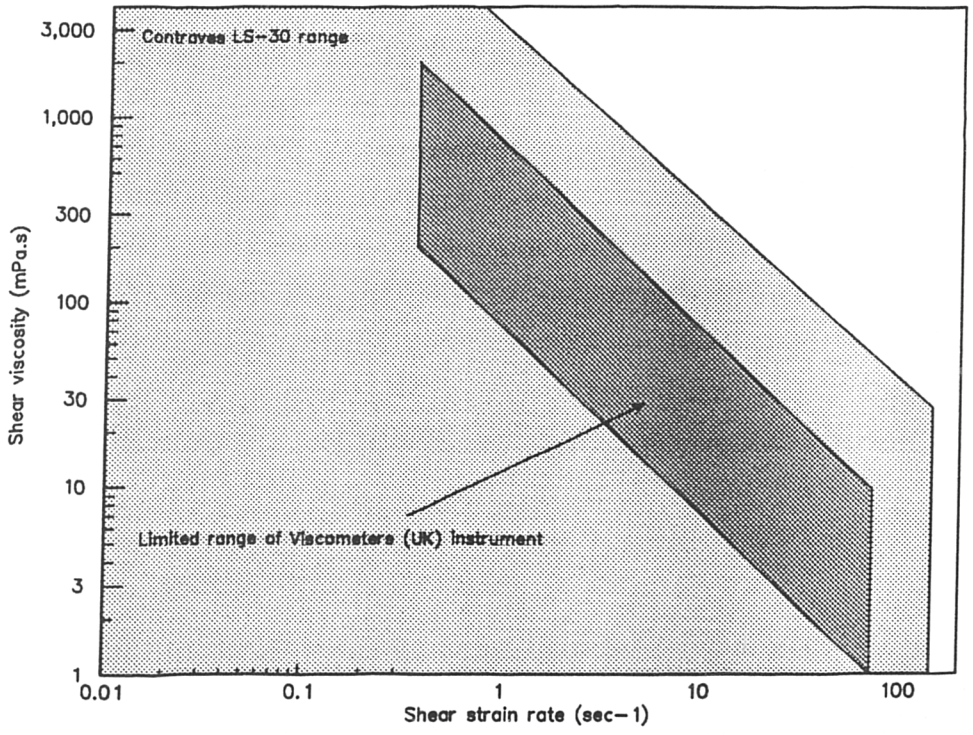

Figure 5.1 Comparisons of Viscometer ranges

The rheological data obtained in these experiments can be represented by Carreau type curves, with the values of η_∞, η_O, n and t determined from the rheograms. Intrinsic viscosity measurements were made on the polymer/solvent pairs used in this work, as shown in figure 5.8, and the Huggins constant k' calculated, with the values recorded in table 5.1.

Polymer/solvent pair	n	κ	η_o mPa.s	η_∞ mPa.s	t sec	$[\eta]_o$ l/g	k' av
Polymer A/deionised						191	0.0457
500 wppm	.521	.1307	410	0.8	10.5		
250 wppm	.575	.0446	112	0.8	9.07		
100 wppm	.578	.0213	42.7	0.8	4.35		
Polymer B/deionised						1508	0.026
250 wppm	.265	.1956	3300	0.8	47		
100 wppm	.33	.0674	915	0.8	50		
Polymer B/0.05% NaCl						26.4	0.9073
500 wppm	.595	.0606	147	0.8	9.09		
250 wppm	.651	.0252	50.6	0.8	7.7		
100 wppm	.801	.0047	5.36	0.8	1.953		
Polymer B/3% NaCl						5.83	0.972
500 wppm	.91	.0039	4.36	0.8	5		
250 wppm	.93	.0020	2.17	0.8	4		
100 wppm	.95	.0013	1.32	0.8	3		

Table 5.1 Rheological parameters for polymer/solvent pairs

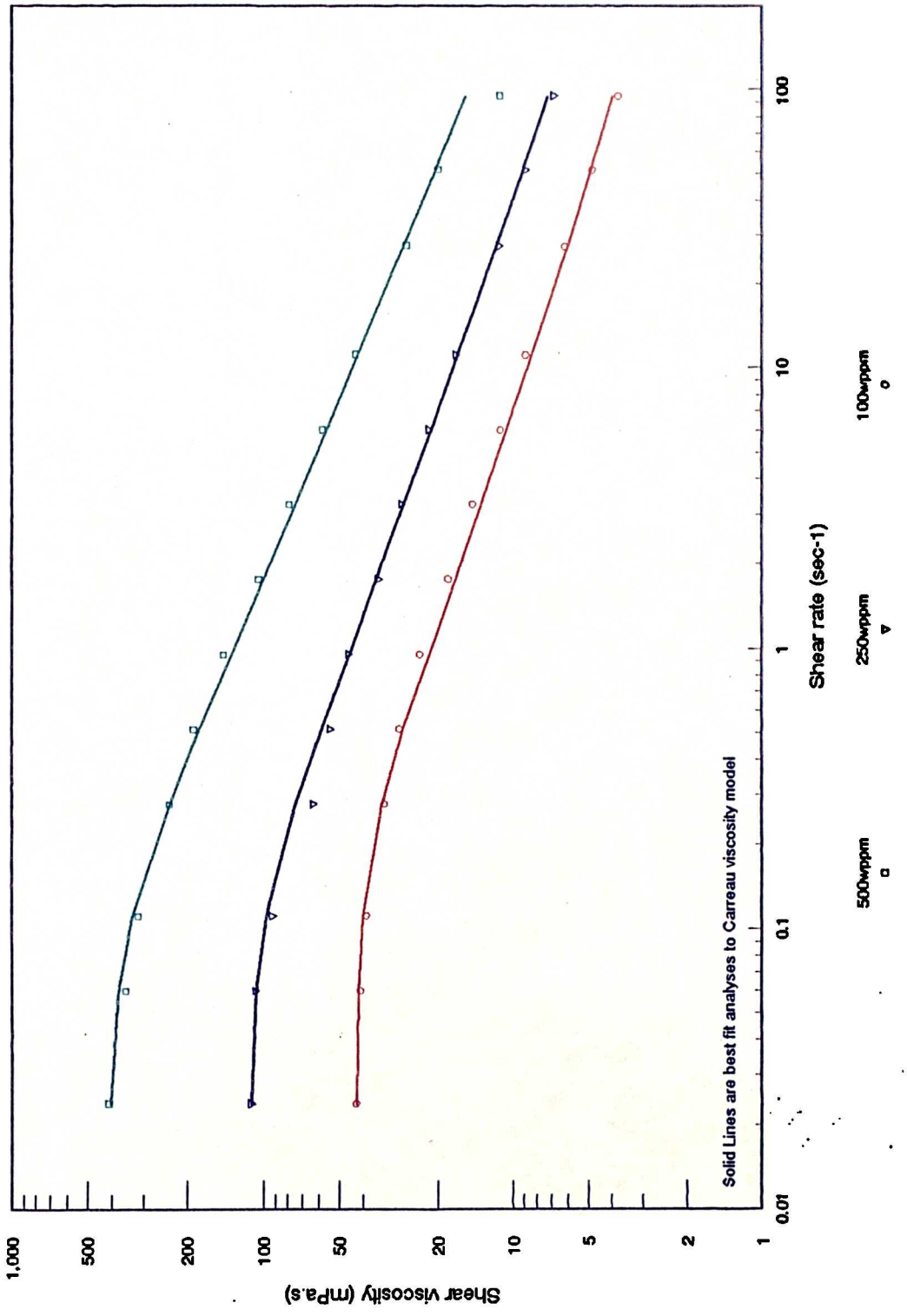

Figure 5.2 Polymer A rheogram in delonised water

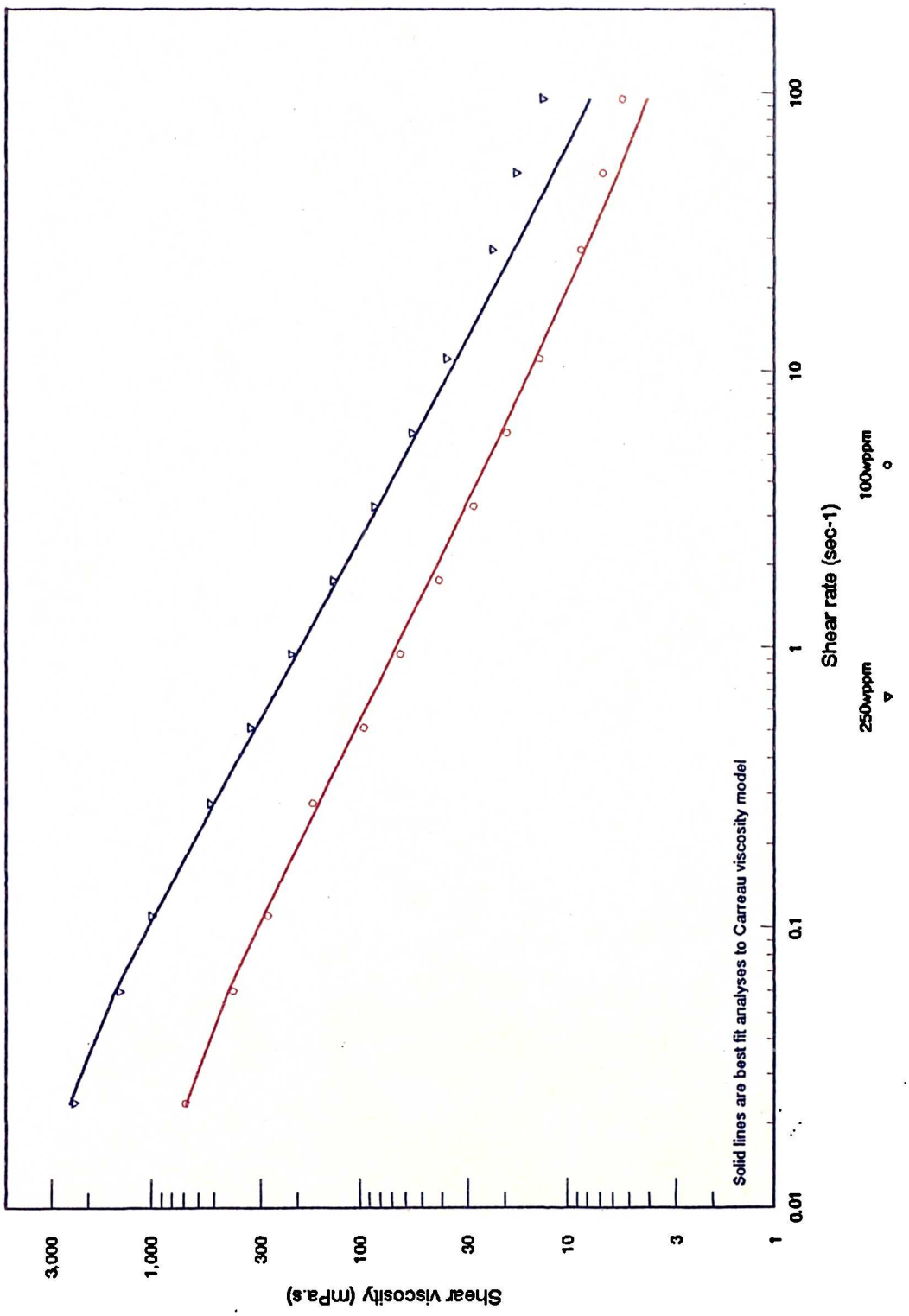

Figure 5.3 Polymer B rheogram in deionised water

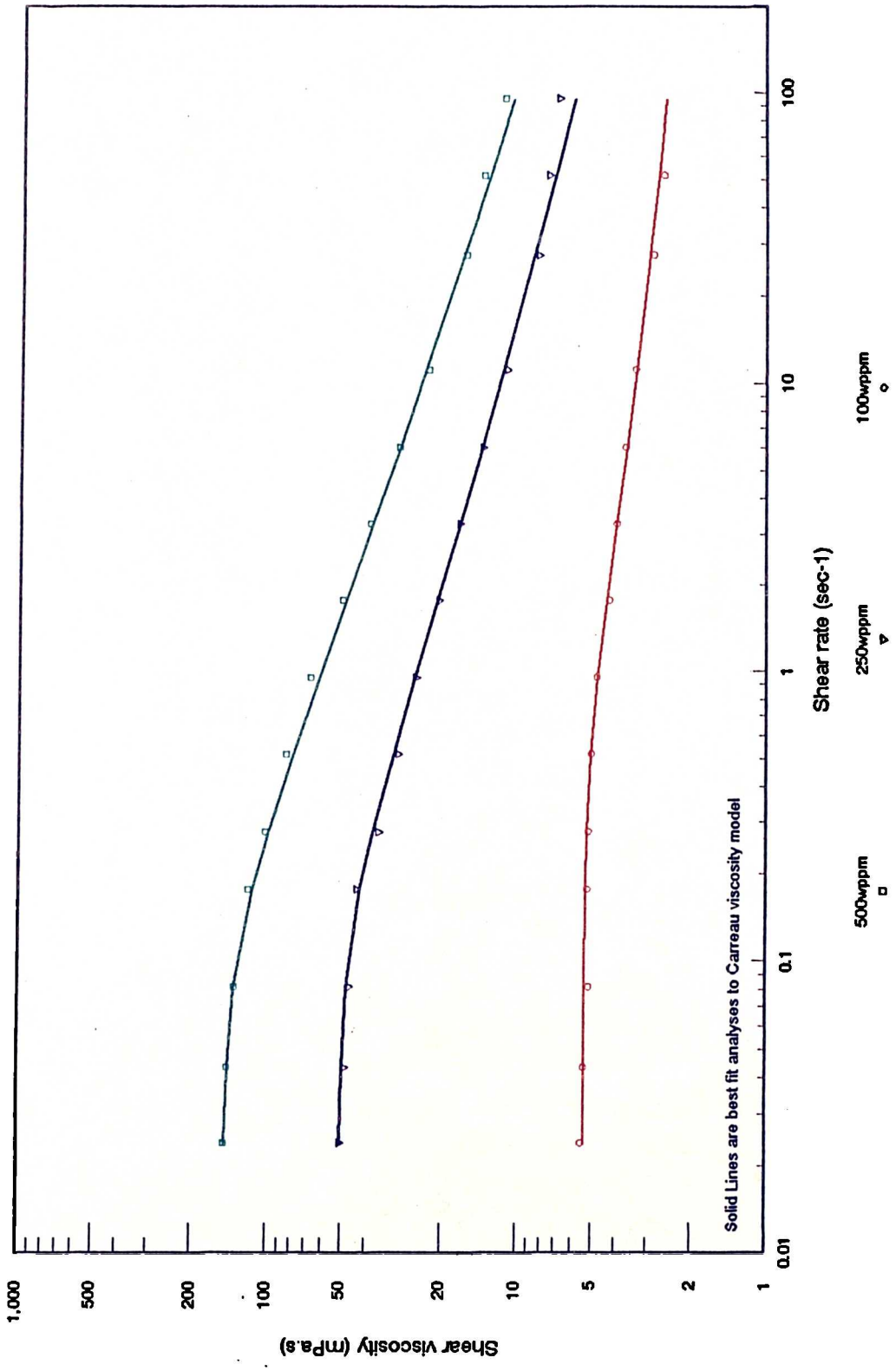

Figure 5.4 Polymer B rheogram in low salinity brine (0.05%wt NaCl)

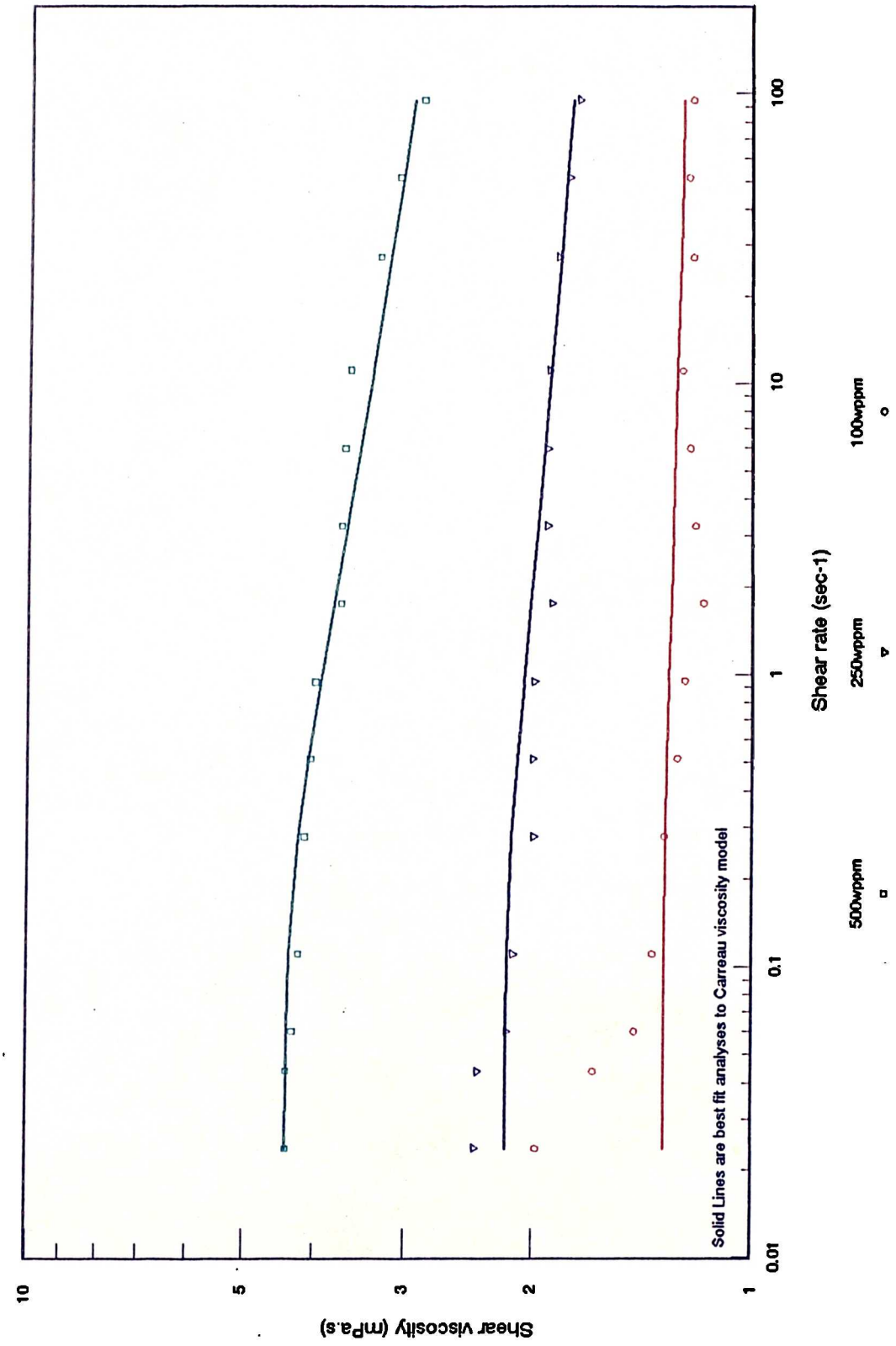

Figure 5.5 Polymer B rheogram in high salinity brine (3%wt NaCl)

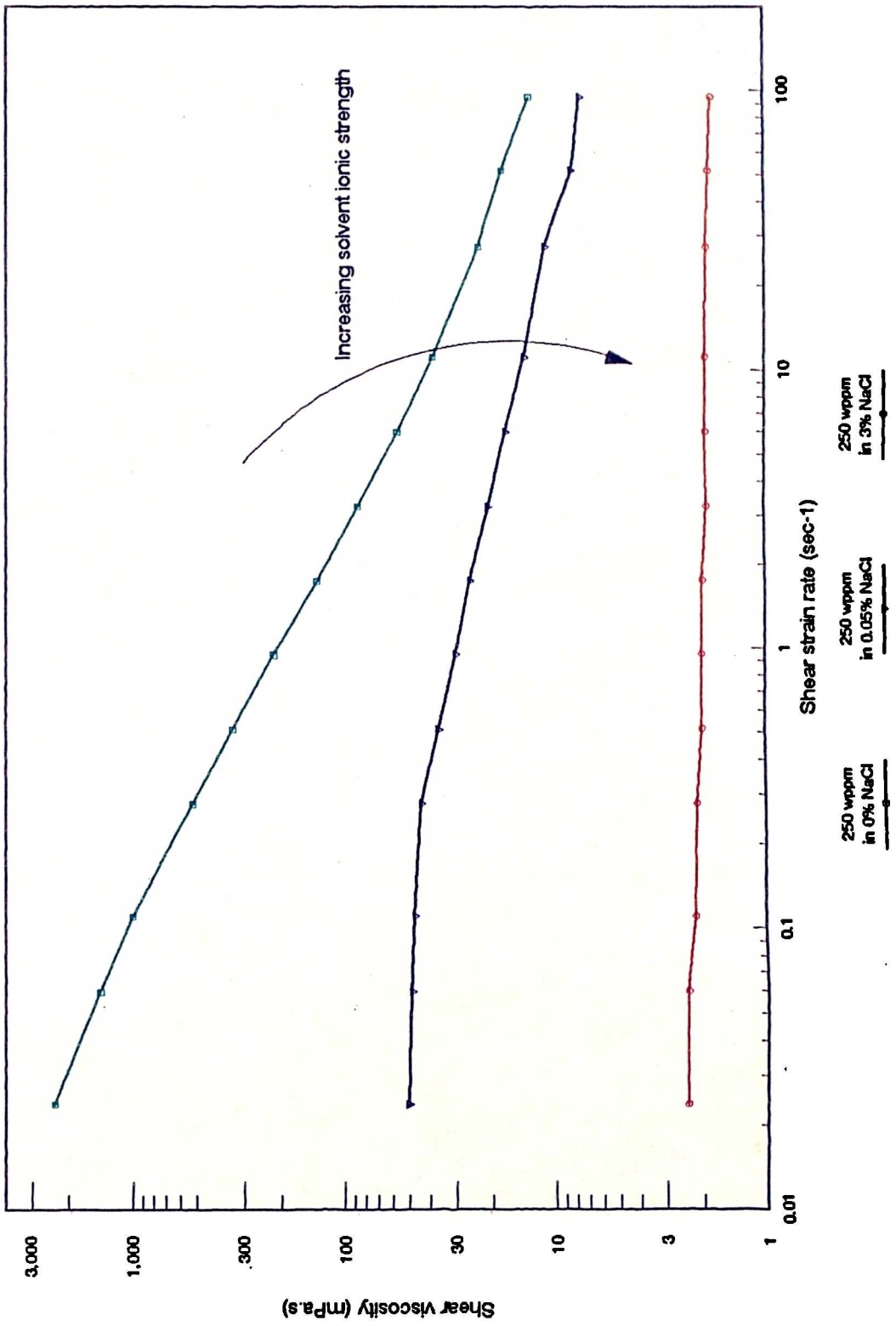

Figure 5.6 Effect of solvent ionic strength on polymer rheograms

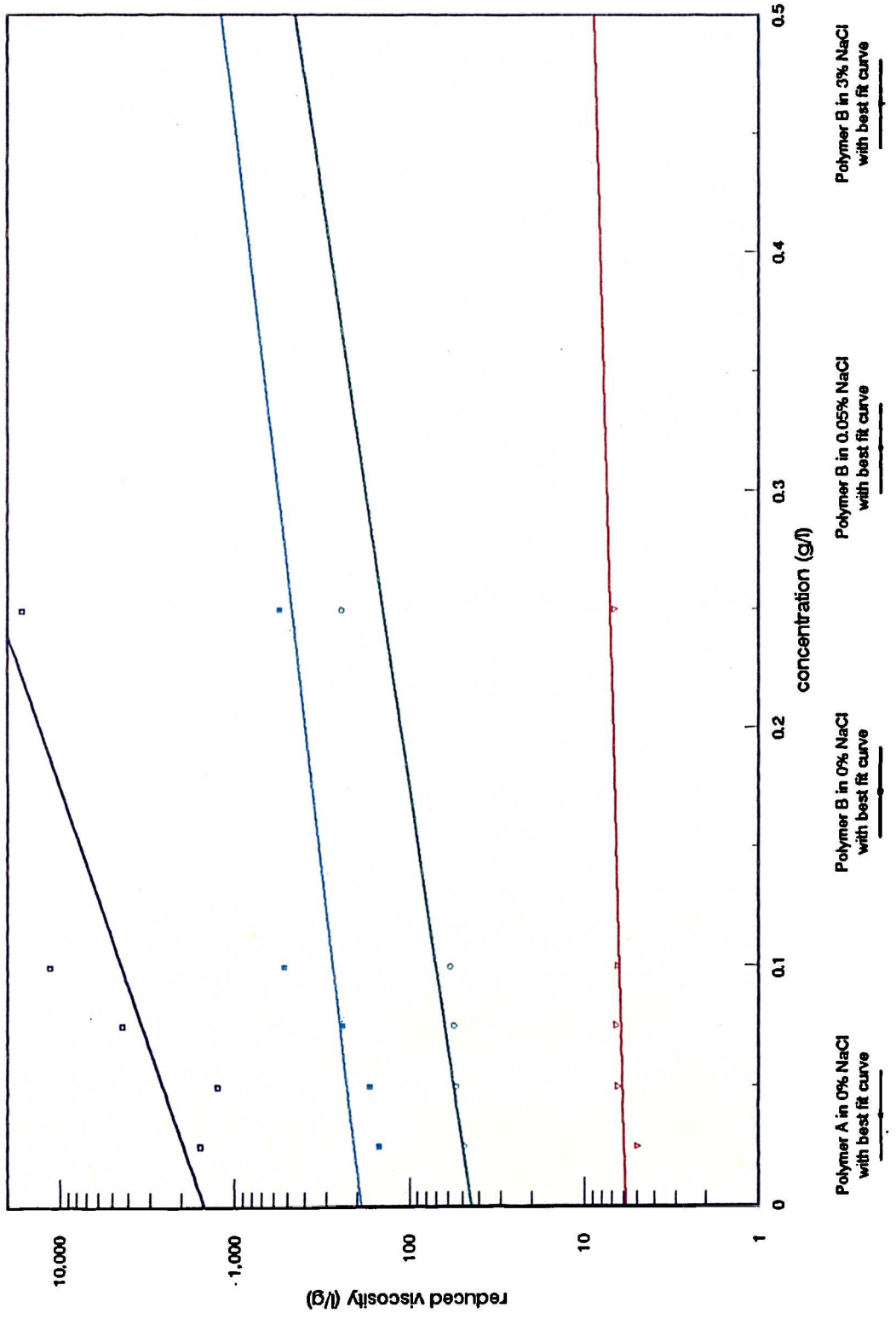

Figure 5.7 Variation in reduced viscosity of test solutions

5.1.2 Screen Factor

Screen factor measurements, where the fluid is subjected to a low shear but high extensional strain rate, were carried out only for polymer B in the two saline solvents. The high shear viscosity of polymer B in de-ionised water resulted in screen blockage and pressure transducer operating over-range and hence was impossible to test. Ideally, if no shear strain were present this apparatus should give a good indication of the extensional viscosity (η_{ext}) of the polymeric solution. The Trouton ratio (equal to 3 for Newtonian fluids) allows calculation of η_{ext} since $Tr = \eta_{ext}/\eta_{shr}$. However, as some shear stresses are induced, purely through friction with the pipe and apparatus walls as the solution flows, there will be an element of shear stress in the total measured stress. Hence the viscosity value calculated will be a combination of both effects, with the shear term dominating at flows lower than the critical onset.

Calibration of the apparatus was carried out prior to each run by recording the pressure loss at various flowrates over the range of the solvent alone. Typical results for a 0.05% NaCl brine are shown in figure 5.8, together with results for a 100wppm polymer B solution for comparison.

Figure 5.9 presents the screen factor results for polymer B in 0.05% NaCl solvent. It can be seen that beyond the critical flow rate the effective viscosity

$$[(\Delta P \text{ polymer})|_q * \mu_s)/(\Delta P \text{ solvent})|_q]$$

sharply increases. For given solvent conditions the **slope** of the viscosity vs flowrate curve was found to be constant for all polymer concentrations tested. This could be due the fact that it is the solvent which determines the conformation of the polyacrylamide molecules - the number of molecules present (the concentration) should only affect the magnitude of the stress, provided there are not extensive chain interactions. Thus the extensional behaviour should be able to be modelled by a power law with the exponent, m, **greater than** unity. Unfortunately the complex arrangement of the wire mesh cannot be easily converted into an extensional strain rate, so the exponent m will be based on q, the experimental flowrate (in ml/min), however the value of the m is not dependent on the units of q, as it is only a measure of the slope.

Table 5.2 presents the range of values of the exponent obtained from best fit analyses of the extensional behaviour of both the 0.05% NaCl and 3% NaCl solvent experiments. Figure 5.10, polymer B in 3% NaCl, again clearly shows the extensional behaviour but with a slightly greater slope (more energy has to be expended in extending the tightly coiled molecules at this ionic strength).

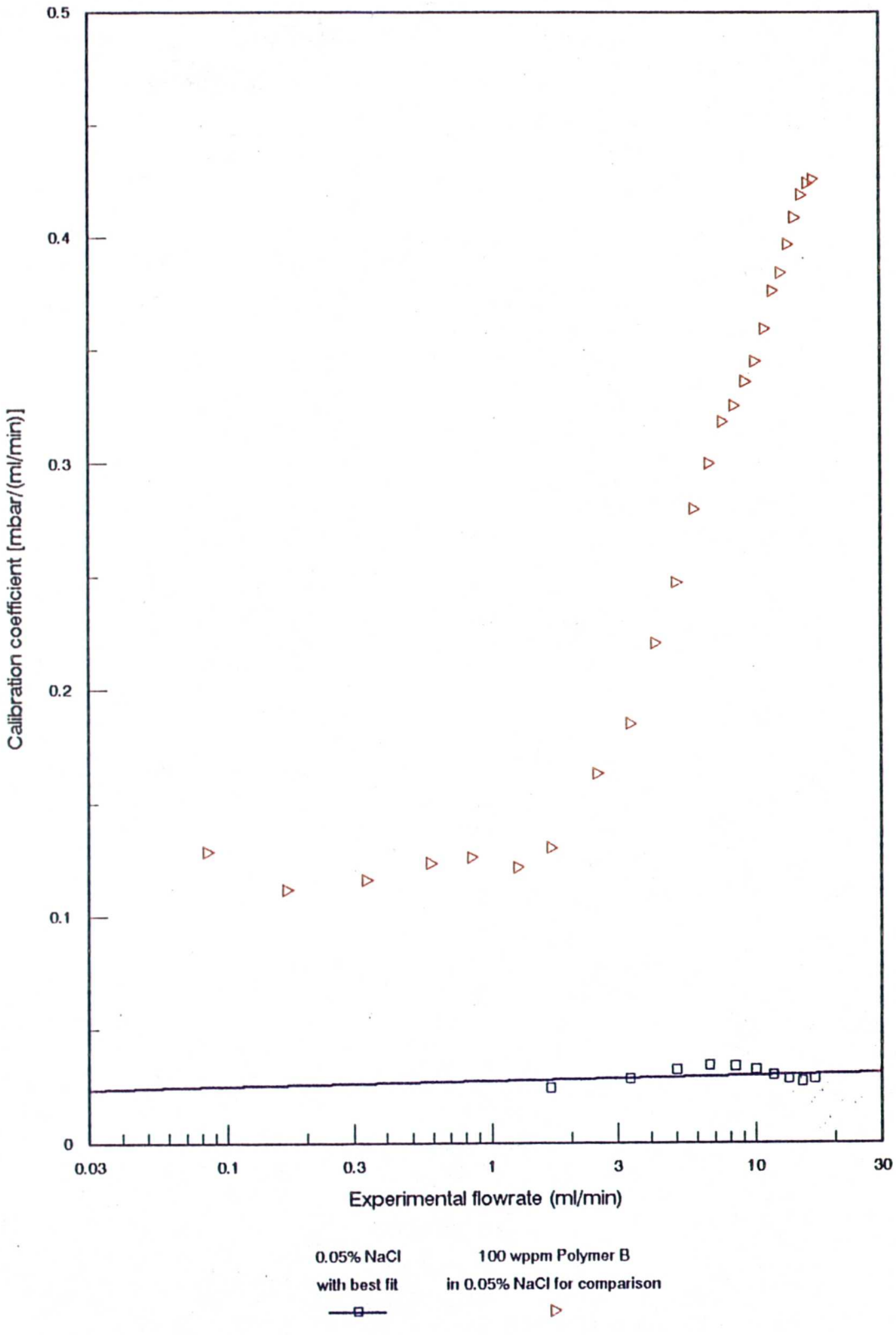

Figure 5.8 Calibration curve for screen factor apparatus

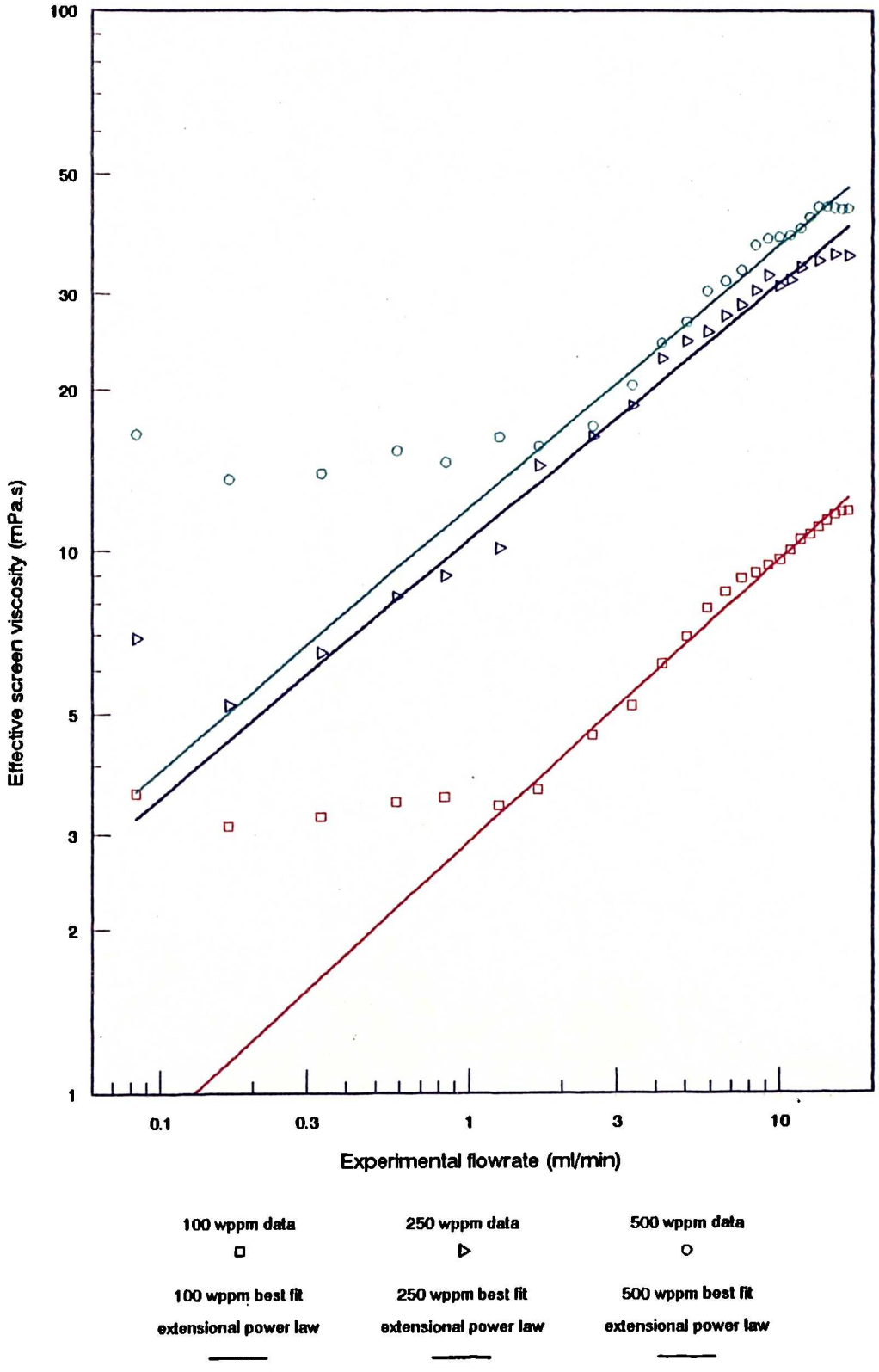

Figure 5.9 Flow characteristics of Polymer B (in 0.05% NaCl brine) in Screen Factor apparatus

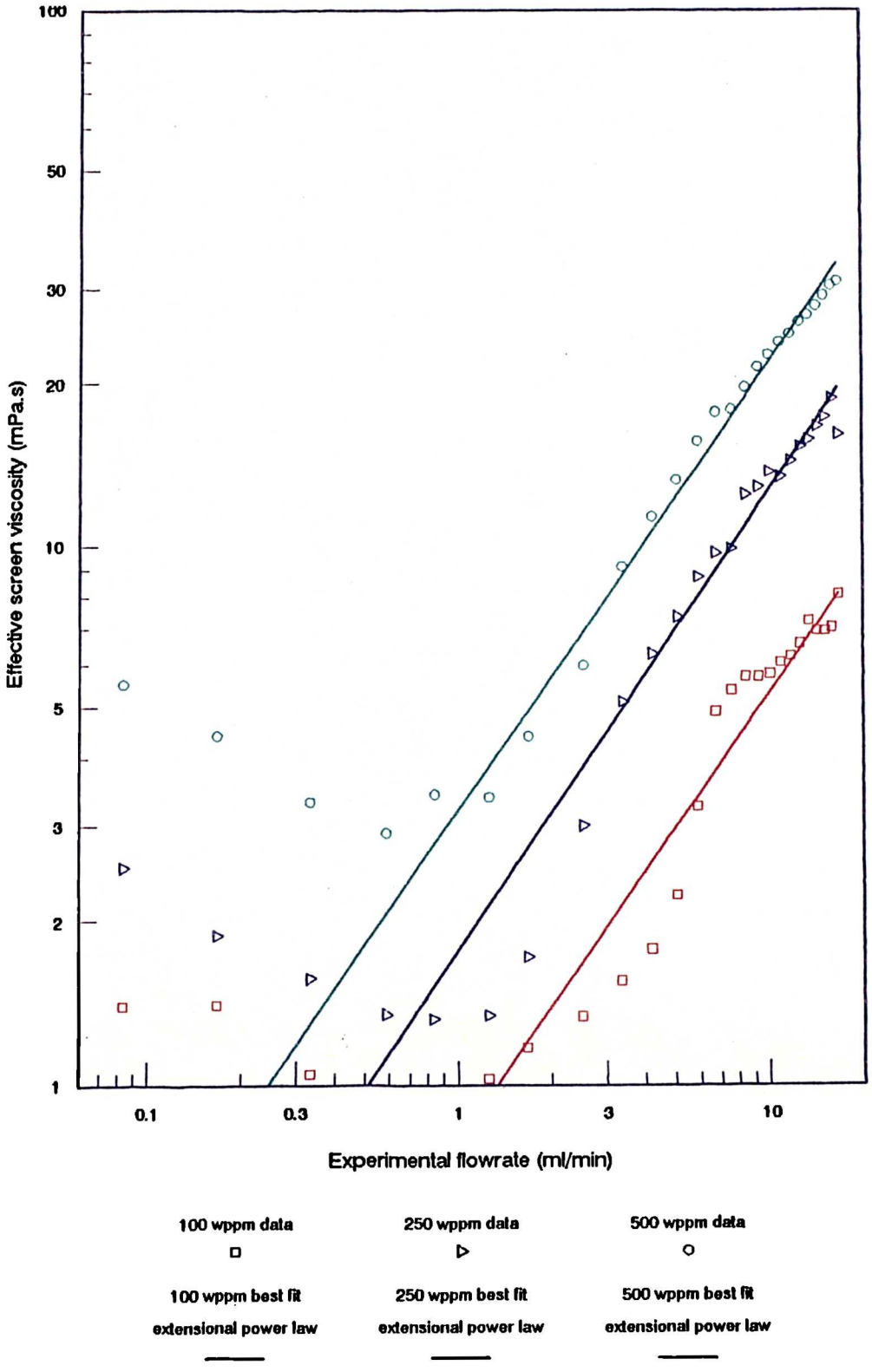

Figure 5.10 Flow characteristics of Polymer B (in 3% NaCl brine) in Screen Factor apparatus

	0.05% NaCl		3% NaCl	
	λ	m	λ	m
100 wppm	2.89	1.521	.785	1.83
250 wppm	10.45	1.476	1.764	1.855
500 wppm	11.99	1.486	3.207	1.833

Calculated from power law best fits in the form $\eta = \lambda q^{m-1}$, where q is in ml/min and η in mPa.s

Table 5.2 Variations in extensional power law exponent m for polymer B

The power law index m will be compared for each experimental apparatus used - however experiments where a large shear component exists are likely to confuse matters due to the shear thinning behaviour of these polymeric solutions.
As can be seen from both graphs the presence of an extensional component in the flow can result in effective viscosities many times that expected from shear rheometry alone. In the cases shown here, there was an 8 fold increase in the resistance to flow encountered whilst flowing the polymer solution in 0.05% NaCl solvent, and upto an 11 fold increase with the 3% NaCl solvent. There is no reason to suspect that these increases could not have been greater if a higher flowrate had been achievable. Increases such as these cannot be attributed to inertia in the flow - the Reynolds number of the solvent flow in this apparatus was never higher than 0.06 in the pipes approaching the screens and no more than approximately 0.1 in the screens themselves.

5.2 Axi-symmetric flow experiments

The axi-symmetric contraction apparatus allowed the effect of a single entrance/exit pair to be compared with a repeated unit, and visualisation of the resulting flow regimes (see section 5.5) to be conducted. The two geometries, a profiled entrance/exit and an abrupt entrance/exit proved useful in understanding the effect of vorticies and fluid inertia on the flow behaviour.
Calibration of these apparatus were carried out by passing solutions of the solvent through and recording the pressure differential at various flowrates and producing a calibration coefficient of $[(\Delta p/q)/\mu]$ as shown in figure 5.11. (The shear viscosity is included as some experiments were carried out at different temperatures). The predicted values of calibration coefficient were obtained using equation 3.21 for calculating the pressure drop at varying flowrate.

5.2.1 Polymer A solution results

Polymer A was tested in both interrupted capillary set-ups, that is both the profiled and abrupt entrance/exit pairs. Figure 5.12 illustrates the apparent results obtained if **constant** calibration coefficients were assumed as opposed to those of figure 5.11. Figures 5.13 shows the results, corrected with the variable calibration coefficients, obtained from the experiments along with the Carreau A representation of the bulk viscosities.

The results presented in figure 5.12 indicate a rapid rise in effective viscosity for the abrupt interrupted entrance/exit configuration which could be caused by extensional flow - however, this must, in the main, be attributed to the addition pressure loss caused by the formation of vorticies at the capillary entrances and exits, which occurs for the solvent as well. It can be seen though, that unless careful control experiments are conducted misleading results and conclusions can occur.

Figure 5.13 shows clearly the shear thinning behaviour of the three polymer concentrations, which are in reasonable agreement with the Carreau representation of the bulk solutions.

The results for the 100 wppm solution are inconclusive as a great deal of scatter is apparent. However, for the 250 and 500 wppm solutions it can be seen that an upturn does occur in the effective viscosity curve whilst flowing through the repeated contractions and expansions, which may be attributed to extensional behaviour. Due to the very limited data though, no firm conclusions can be drawn..

For the single entrance/exit apparatus no upturn in the viscosity was observed, however all three concentrations did show a change in slope, which may indicate another flow process occurring, such as vortex growth.

5.2.2 Polymer B solution results

Due to the uncertainty of the results of the abrupt interrupted apparatus the profiled entrance/exit apparatus was used in preference for this series of experiments.

Figures 5.14 through 5.16 present the comparison of the observed and bulk viscosities for solutions of polymer B in 0.05% NaCl solvent. Clear evidence can be seen here of extensional behaviour, particularly in the profiled repeated cell apparatus, where the elongational element of the flow is magnified over that of shear by the consecutive contractions and expansions.

However, unlike the screen factor results, all concentrations and geometries show a levelling off of the results at high flowrates. Subsequent testing of the effluent back through the apparatus showed no change in observed behaviour and thus ruled out degradation. Flow visualisation was then employed to try to solve this apparent anomaly. The results of this can be found later (5.5.1).
Figure 5.17 presents the only data obtained with polymer B in 3% NaCl solvent in this type of apparatus - comparing the effect of the profiled and abrupt repeated unit cells on a 250 wppm solution.
The point of departure (onset) from bulk shear behaviour occurs for both geometries at the same shear rate, indicating a similar process, however the abrupt geometry reaches a maximum less than half of the profiled case.

As was stated above, it would appear that the extensional behaviour of these dilute polymer solutions can be represented by a power law. The best fit slopes were again numerically regressed to determine the coefficient, m, as shown in table 5.3.

	m_{cap}	m_{sf}
100 wppm	1.385	1.521
250 wppm	1.338	1.476
500 wppm	1.432	1.486

Calculated from power law best fits in the form $\eta = \lambda\gamma^{m-1}$, where γ, the wall shear rate, is in sec^{-1} and η in mPa.s

Table 5.3 Comparisons of extensional power law exponent m for polymer B in 0.05% NaCl between capillary and screen factor apparatus.

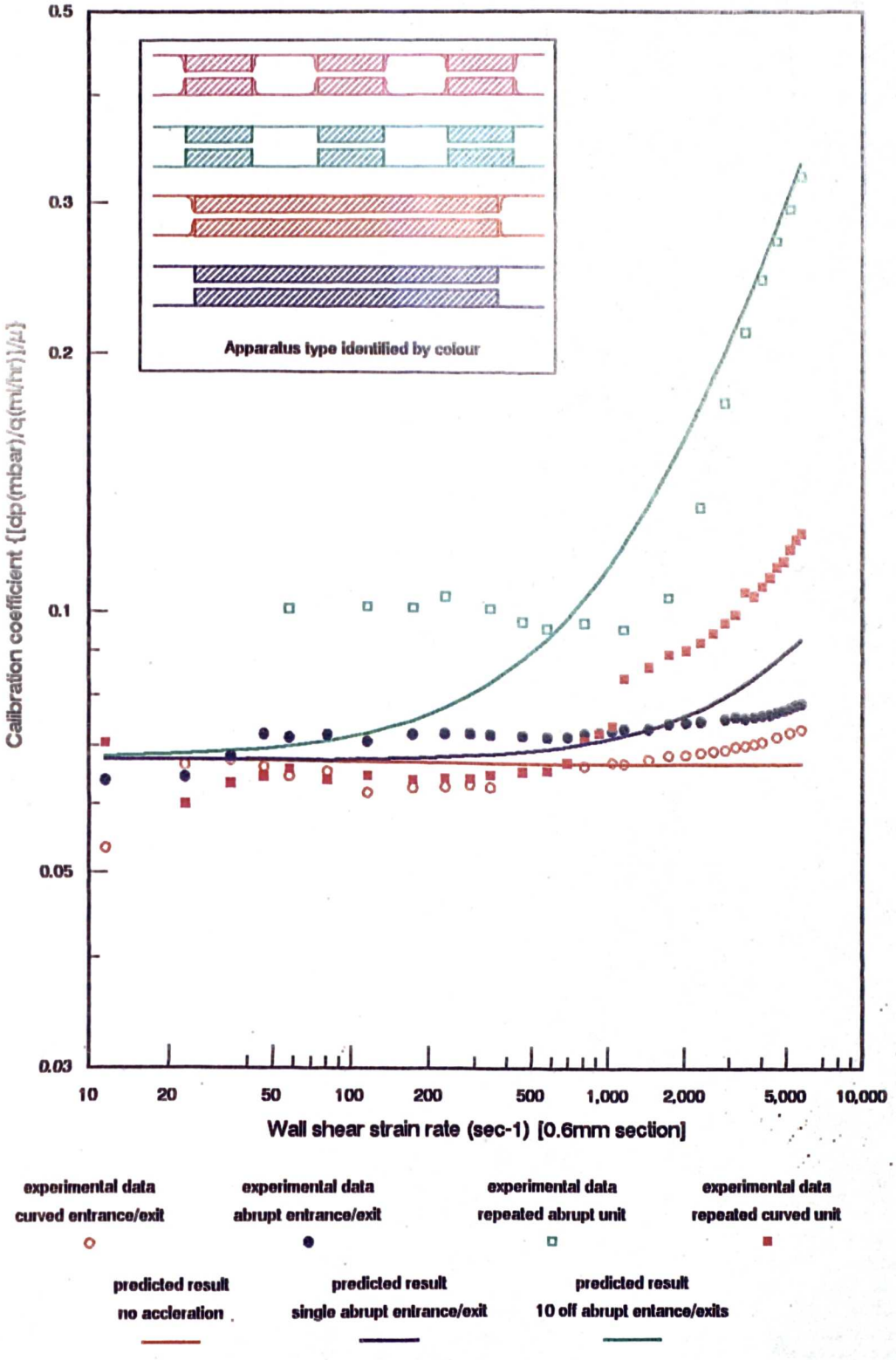

Figure 5.11 Comparison of predicted and experimental calibration coefficients for capillary apparatus

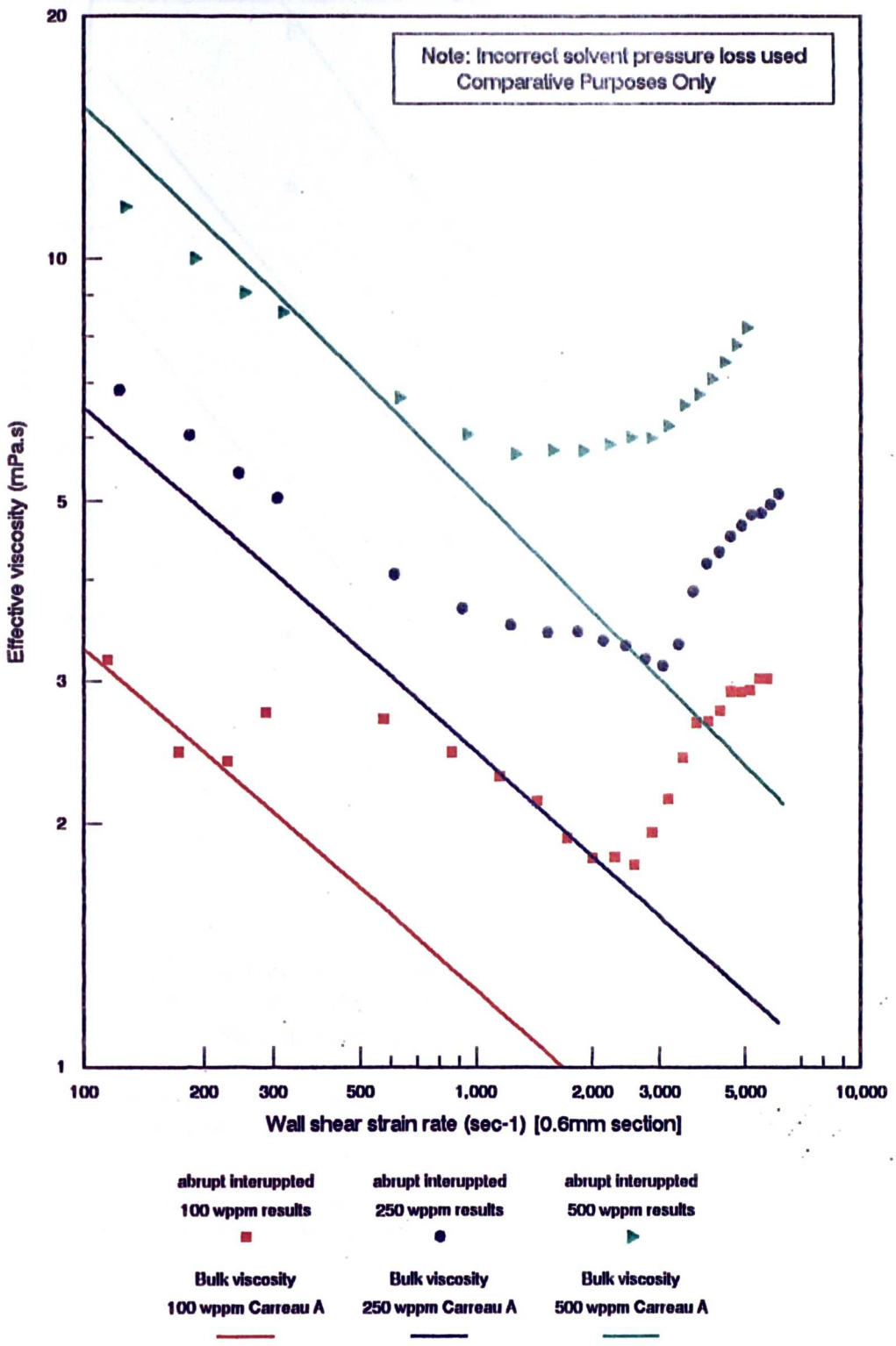

Figure 5.12 Effect of assuming a linear pressure variation with flowrate for the solvent on the apparent viscosity of Polymer A

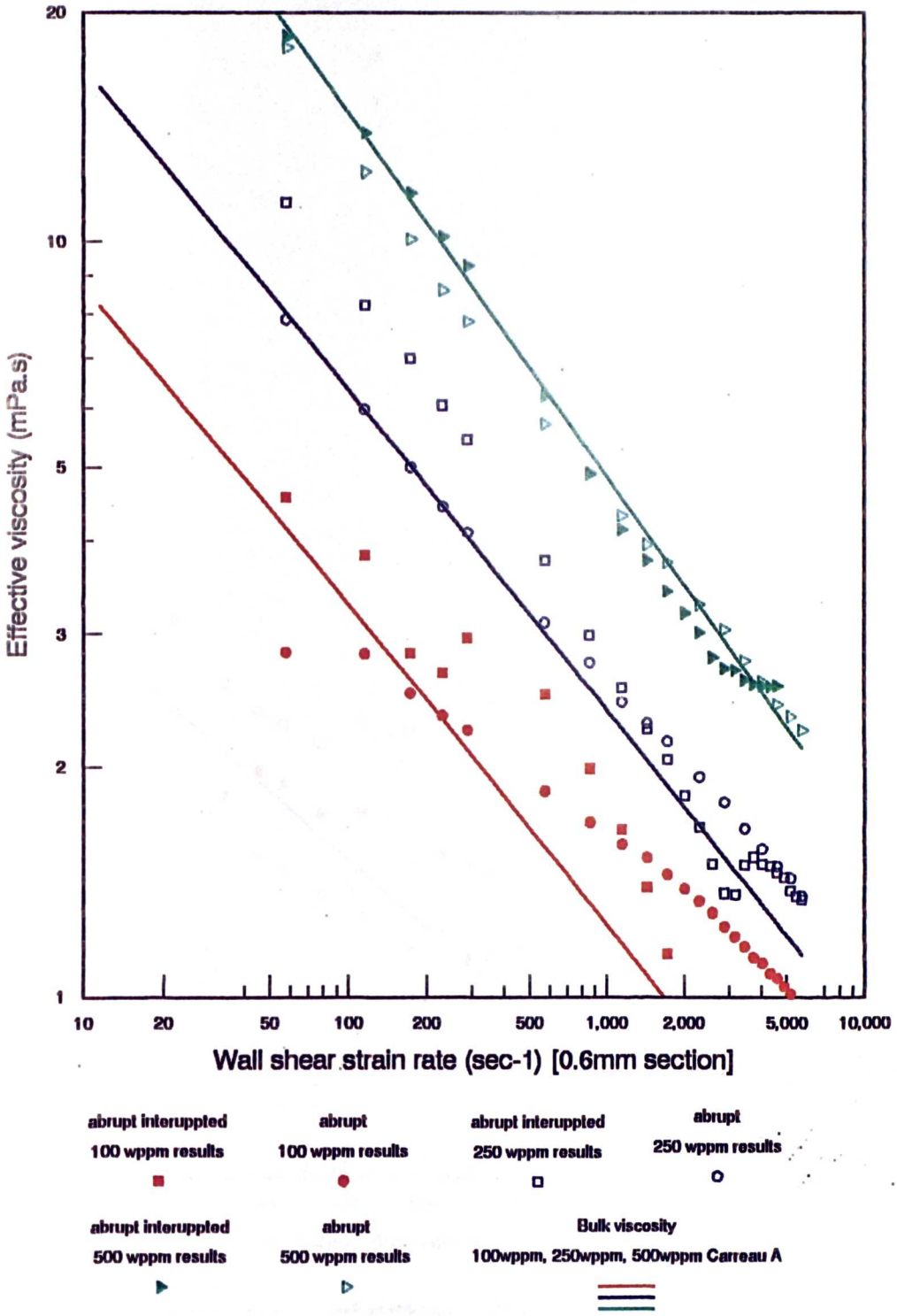

Figure 5.13 Variation in behaviour for Polymer A in deionised water between pure shear and capillary apparatus..

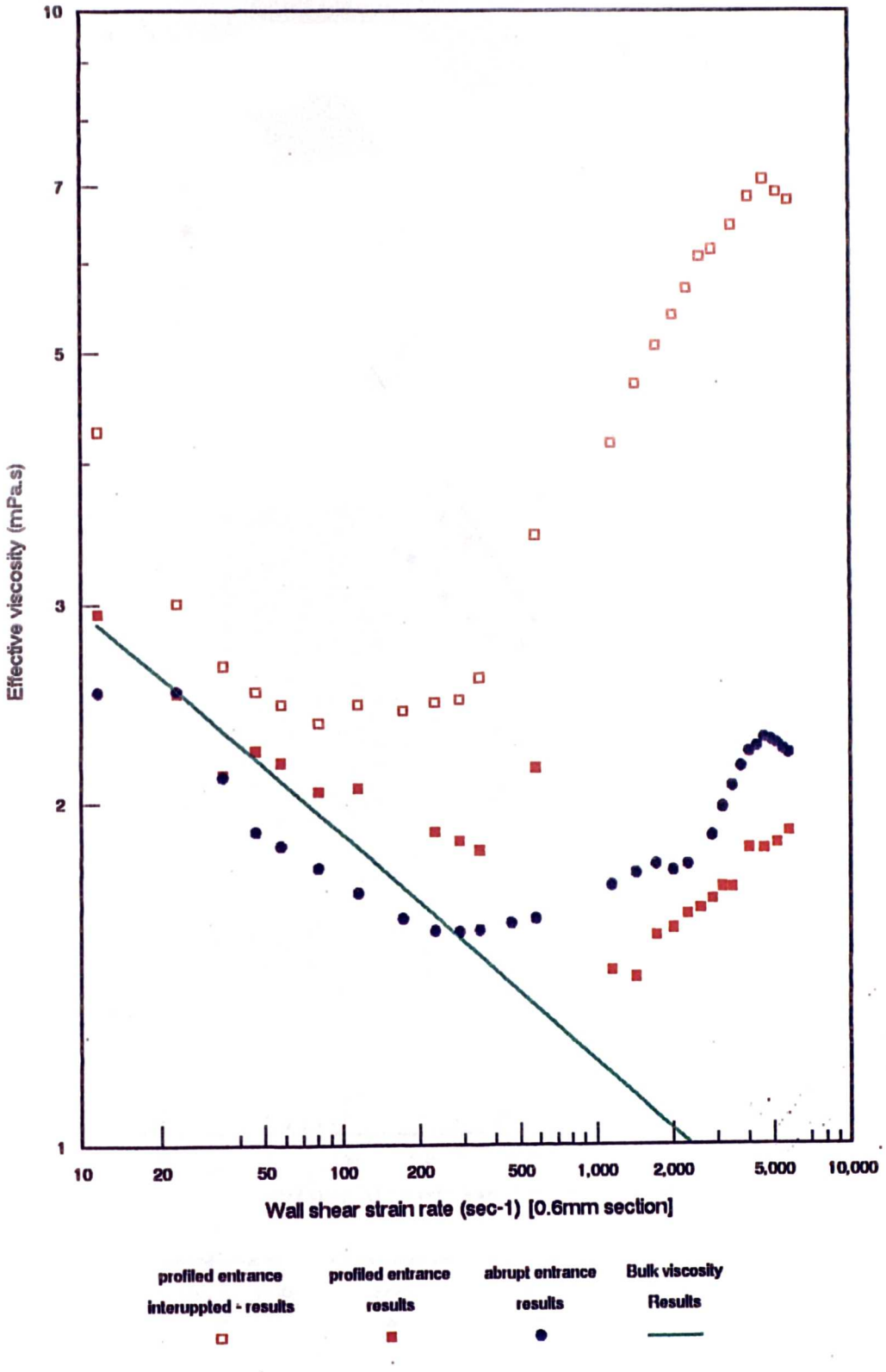

Figure 5.14 Variation in behaviour for 100wppm Polymer B in low salinity (0.05% NaCl) brine between pure shear and capillary apparatus

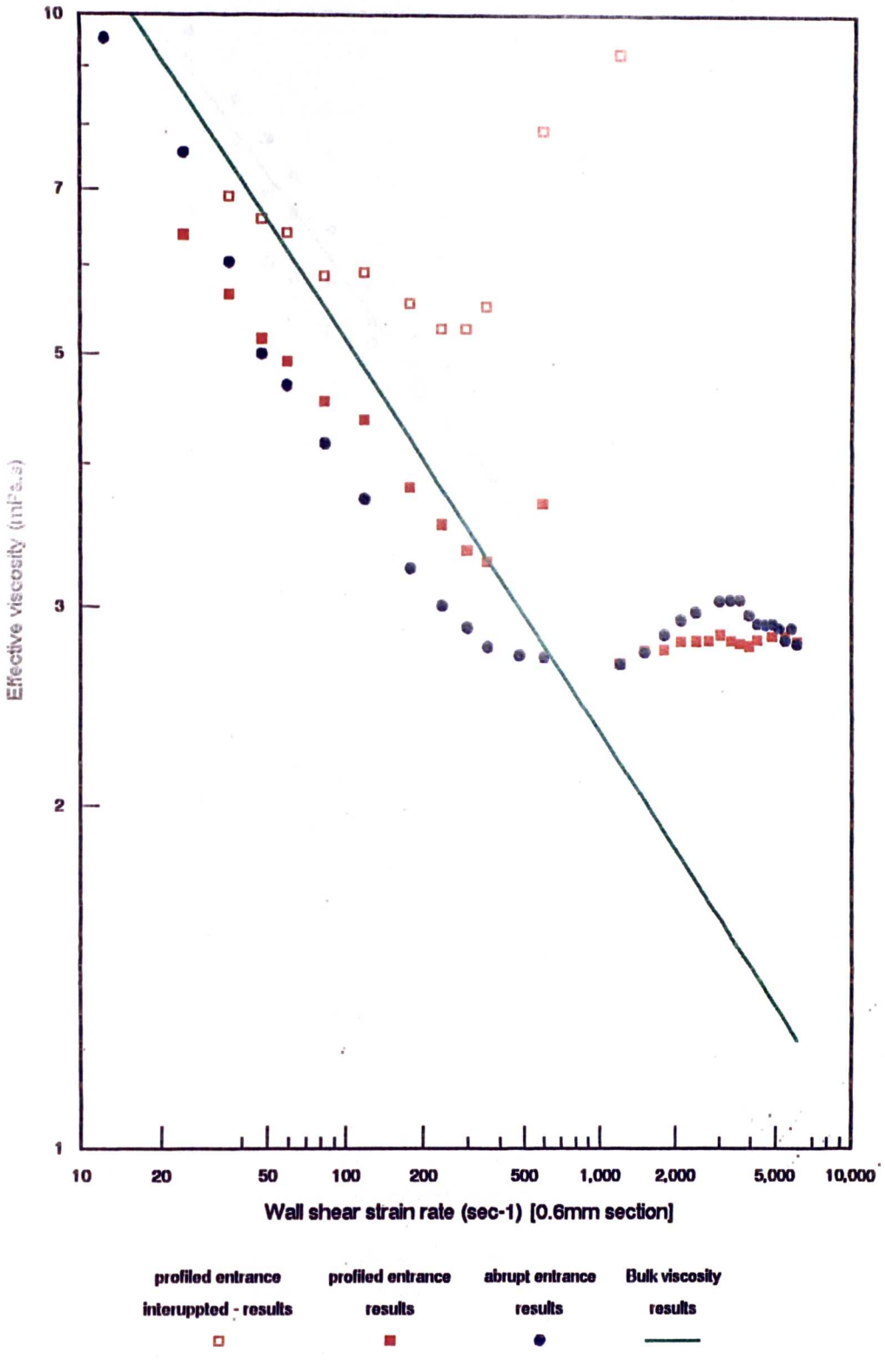

Figure 5.15 Variation in behaviour for 250wppm Polymer B in low salinity (0.05% NaCl) brine between pure shear and capillary apparatus

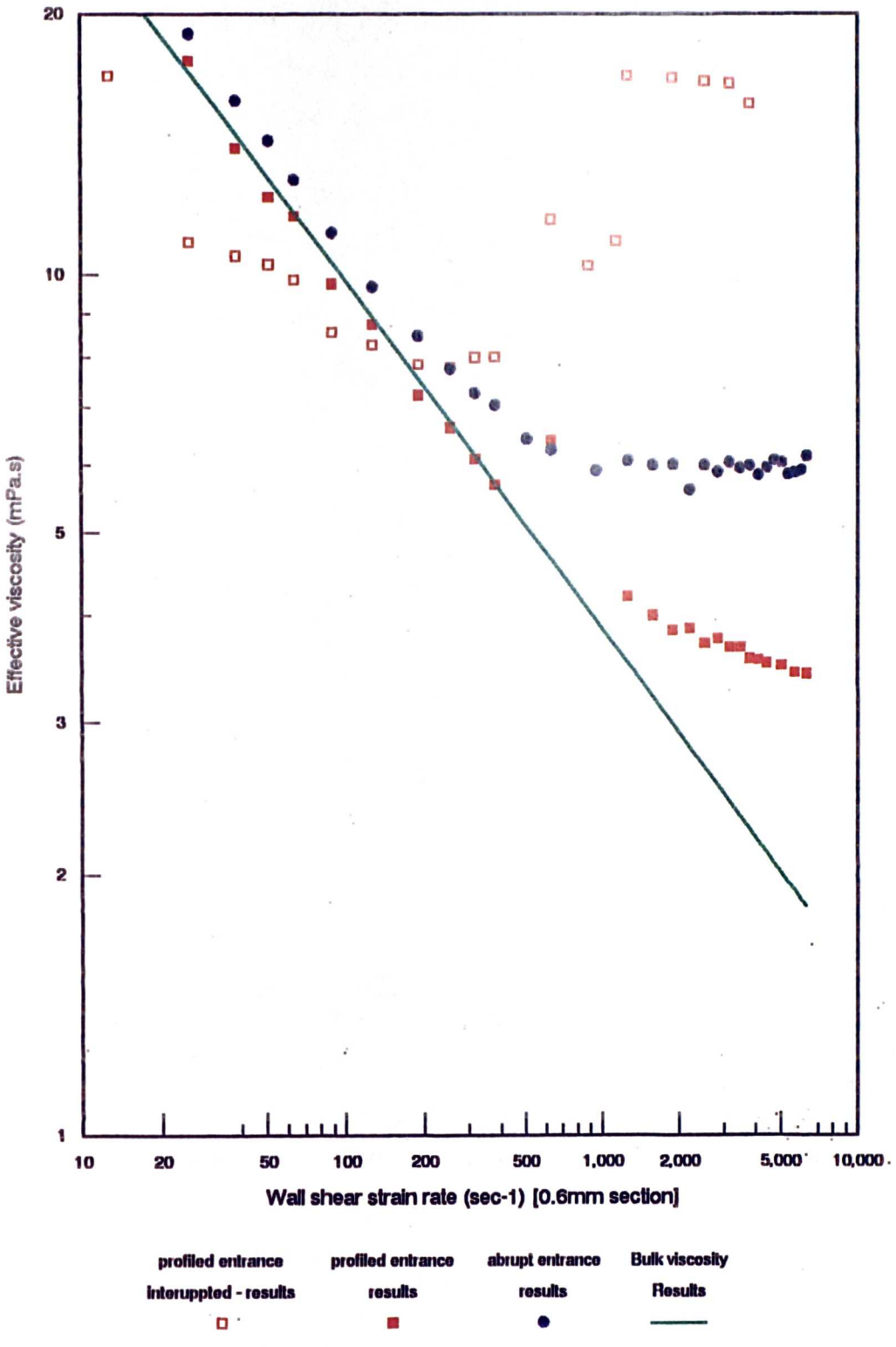

Figure 5.16 Variation in behaviour for 500wppm Polymer B in low salinity (0.05% NaCl) brine between pure shear and capillary apparatus

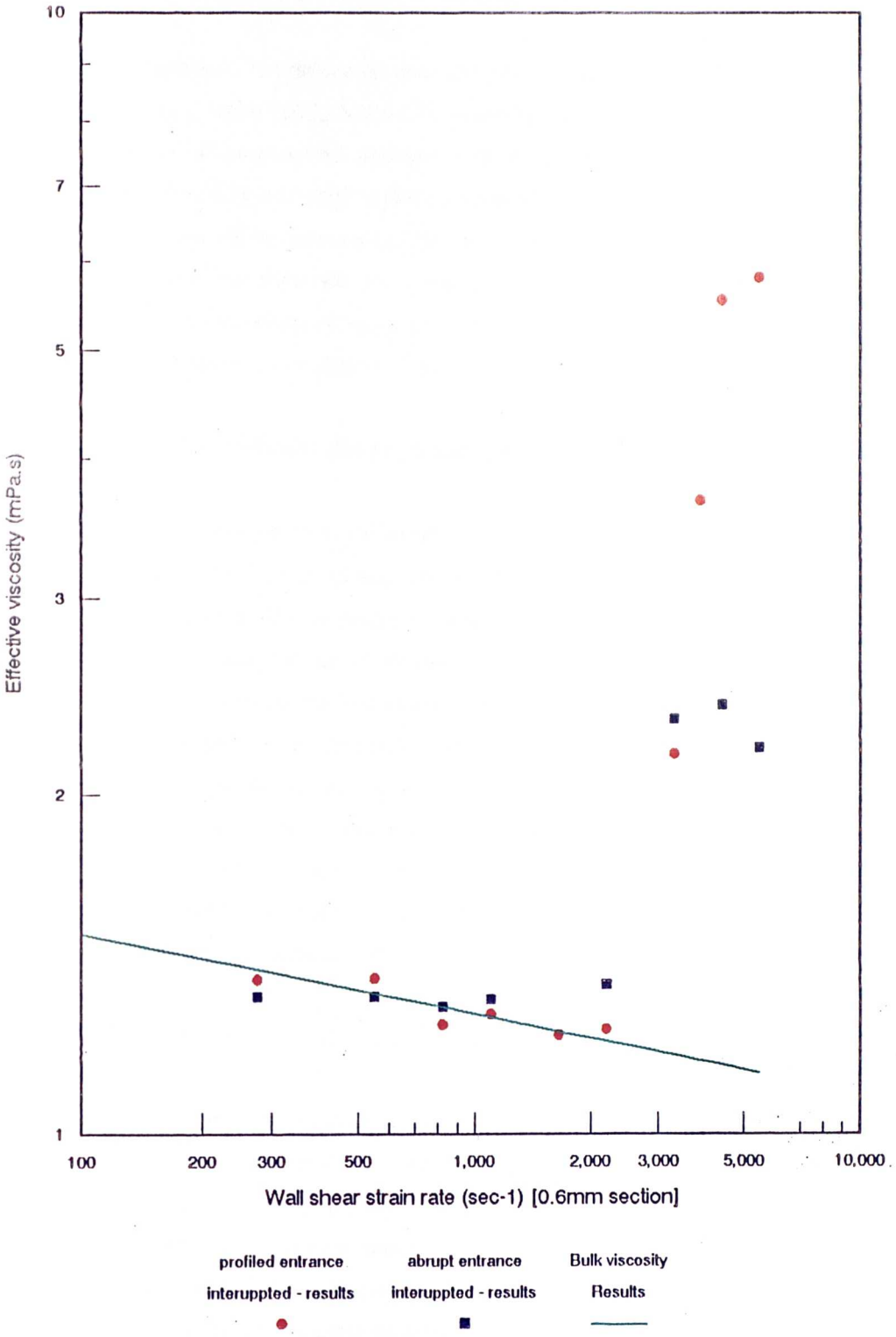

Figure 5.17 Variation in behaviour for 250wppm Polymer B in high salinity (3% NaCl) brine between pure shear and capillary apparatus

5.3 Planar contraction flow experiments

The same approach for calibration was used in this apparatus as was used above. However, here, unlike the calibration flows above, a calibration coefficient **independent** of flowrate was obtained, as shown in figure 5.18. This illustrates the usefulness of this geometry to studying extensional flows - only a slight amount of vortex activity will be generated at the rear side of the cylinders at the stagnation point. The use of two flowcells, one a tenth of the size of the other, allows some investigation into the effect of size scale on the flow. The actual size of the cells can be seen in relation to each other on figure 5.18.

5.3.1 Large (5.0mm) diameter rod array

Polymer B only was used in this apparatus, in both the 0.05% NaCl and 3% NaCl brines. However, this apparatus was also used for flow visualisation studies (see section 5.5). Figure 5.19, the results for polymer in the less saline brine, again clearly shows an onset, beyond which extensional behaviour is apparent. Due to the high volume flowrates involved in this apparatus, only a restricted shear rate range could be tested, which limited the extensional behaviour to that around the onset region. The small increases in flowrate possible with this apparatus, which was conducted under a constant pressure drop, resulted in a clear determination of the onset point, which was seen to vary with concentration.
Figure 5.20 presents the results for the high ionic strength brine dilutions, with table 5.4 containing the details of the extensional power law analysis.

5.3.2 Small (0.5mm) diameter rod array cell

Again, only polymer B in the saline solvents was tested in this apparatus.
For the lower salt content brine, the results, displayed in figure 5.21, again clearly show an increase in effective viscosity beyond a critical value. With no inertia present, this increase in flow resistance may be attributed to extensional behaviour of the polymer molecules in solution. The constantly changing passage dimensions do not lend themselves to accurate shear strain rate determination, and so comparisons will not be made directly to the Carreau representations of the bulk viscosities, other than confirm that the observed effective viscosities start from a reasonable value.

The polymer solutions made up in the 3% NaCl brine, give a very clear onset point, where the effective viscosity increases dramatically (figure 5.22). At the higher flowrates, all three polymer concentrations tend to a similar value of viscosity, around 20mPa.s, which, for the 100wppm solution is a 15 fold increase. Again, evaluation of the slopes of the extensional part of the flow was undertaken, with the values for the power law exponent, m, recorded in table 5.4.

0.05% NaCl solvent

	$m_{5.0mm}$	$m_{0.5mm}$	m_{cap}	m_{sf}
100 wppm	1.41	1.86	1.385	1.521
250 wppm	1.52	1.80	1.338	1.476
500 wppm	1.58	1.71	1.432	1.486

3% NaCl solvent

	$m_{5.0mm}$	$m_{0.5mm}$	m_{sf}
100 wppm	1.42	2.48	1.83
250 wppm		2.40	1.855
500 wppm	1.65	1.84	1.833

Calculated from power law best fits in the form $\eta = \lambda q^{m-1}$, where q, the flowrate, is in ml/min and η in mPa.s

Table 5.4 Comparisons of extensional power law exponent m for polymer B between experiments.

5.3.2.1 Investigation of concentration dependence

Experiments were conducted in the small flow cell to test the dependance of the onset point on polymer concentration. Solutions of 5 to 250wppm were diluted from a 500wppm master, so as to minimise concentration dilution errors. Only the 3% NaCl brine solvent was used for these studies. The results, figure 5.23, indicated increased flow resistance for solutions down to 10wppm. Clear onset points are difficult to assess for the lower concentrations, however the trend is clearly that increasing polymer concentration reduces the flowrate required for onset. The maximum value of the observed viscosity was also seen to vary with concentration, with, as expected, this value increasing with concentration. However, the large molecular weight of this polymer ($18x10^6$) means that only the 10wppm solution maybe considered 'dilute' - that is little or no inter-molecular

interference. Table 5.5 shows the variation in the ratio of the maximum observed viscosity to that of pure shear for the concentration used. For strictly dilute solutions the energy expended per chain should be constant, that is the increase divided by the number of chains present (the concentration) should be constant. The values displayed in table 5.5 indicate that as the molecular concentration decreases, the pressure drop attributable to each molecular chain increases. It is interesting to note that around a $Cx[\eta]$ value of 0.1 (ie the 25 and 10wppm solutions) the increase/concentration parameters are quite similar.

Concentration	**500**	**250**	**100**	**75**	**50**	**25**	**10**
increase in viscosity **	10.26	11.3	6.44	5.29	3.5	3.3	1.4
increase/concentration	0.02	0.045	0.06	0.071	0.07	.132	.14
$Cx[\eta]$	2.915	1.46	0.583	0.437	0.29	0.14	0.05

Notes: 1. ** increase calculated as :
maximum observed viscosity/shear viscosity
2. for dilute solutions $Cx[\eta]<<0.1$

Table 5.5 Observed viscosity increase per ppm polymer

5.3.2.2 Investigation of dependence on solvent ionic strength

The ionic strength of the solvent clearly has a strong effect on the shear viscosity of polymer solutions, particularly when the polymer is a polyelectrolyte. The screening of charges, reducing the repulsive forces, results in a more tightly coiled molecule which has less interactions on its neighbour reducing the bulk viscosity. Experiments were conducted to observe the effect solvent ionic strength has on the extensional behaviour of a 100wppm solution of Polymer B in solvents ranging from 0 to 10% NaCl by weight. The molecular radius of gyration over this range will decrease from ~0.2μm to less than 0.03μm, as predicted by equ 2.14, indicating changes in molecular dimensions. This 'coiling up' of the molecule results in greater stretch rates having to be applied before the solution starts to display elongational thickening behaviour, as seen in figure 5.24. These results displayed are based on the pressure drop to water after passing the polymer, as it was found that even after copious flushing with pure solvent, higher calibration factors than existed before the polymer solution test were recorded. This phenomena was only observed for the lower ionic strength solvents. Flushing with dilute solutions of H_2O_2, as detailed in Chapter 4, returned the cell to its original

cell to its original condition. It is unlikely that these residual effects can be attributed to filtration of the polymer, as the passage sizes are about two orders of magnitude larger than the molecular length. It is therefore probable that adsorption of a monolayer of molecules onto the glass rods subsequently trapped other molecules by entanglement to build up a layer thick enough to produce these effects. The tendency for all test solutions to reach a similar high stretch viscosity plateau can be explained by all molecules, irrespective of solvent conditions, reaching a similar conformation. It can be seen that as well as a lower onset point the solutions of the lower ionic strength solvent reach this plateau region more rapidly.

5.3.3 Comparison of results using extensional strain rate

Using the theory developed in Chapter 3, it is now possible to compare the results from the different flow cells. The dependence on salt concentration resulting in differing conformations means comparisons based on an extensional strain rate are not valid between the two solvent conditions. However, for a given solvent, direct comparison of all polymer concentrations should be possible.

In figure 5.25, which shows results for both flowcells using the 0.05% NaCl solvent, it can be seen that the viscosities observed in the small flow cell appear to follow on from the behaviour produced in the larger cell. This result implies that the onset of observable extensional behaviour (at a given solvent condition) is not constant but depends to some degree on the shear strain rate regime present for shear thinning polymers. Thus in a situation where a very high shear strain rate exists it would be expected that the onset of extensional behaviour would occur at a lower value of extensional strain rate than would be required to observe an onset in a system with a lower shear strain rate. However, the fact that the extensional viscosity behaviour appears continuous between the two cells does imply that the extensional viscosity-strain rate relationship is not shear strain rate dependant. In order to remove the dependance of onset on shear strain rate, a pseudo-onset point will be defined which will allow comparison of the extensional behaviour in systems with different shear strain rate regimes. This pseudo-onset point will be characterised by where the extensional power law, of exponent 'm' crosses the solvent viscosity curve ($\eta'=1$). This proposal can be seen in figure 5.26, the results for both flow cells in a 3%wt brine.

Note: If the extensional behaviour of a shear thinning polymer solution can be modelled by a power law then the definition of onset as the point at which departure from the apparent shear behaviour occurs is not strictly true, and could be misleading. Extensional stresses will exist below this rate but will be negligible compared to the shear stresses. In order to predict the behaviour fully an onset point must be defined which can allow for the existence of the extensional stresses below where they are observable. By extending the extensional power law behaviour below the polymer shear viscosity curve to where it crosses the (constant) solvent viscosity line, allows the removal of polymer shear viscosity from the onset point.

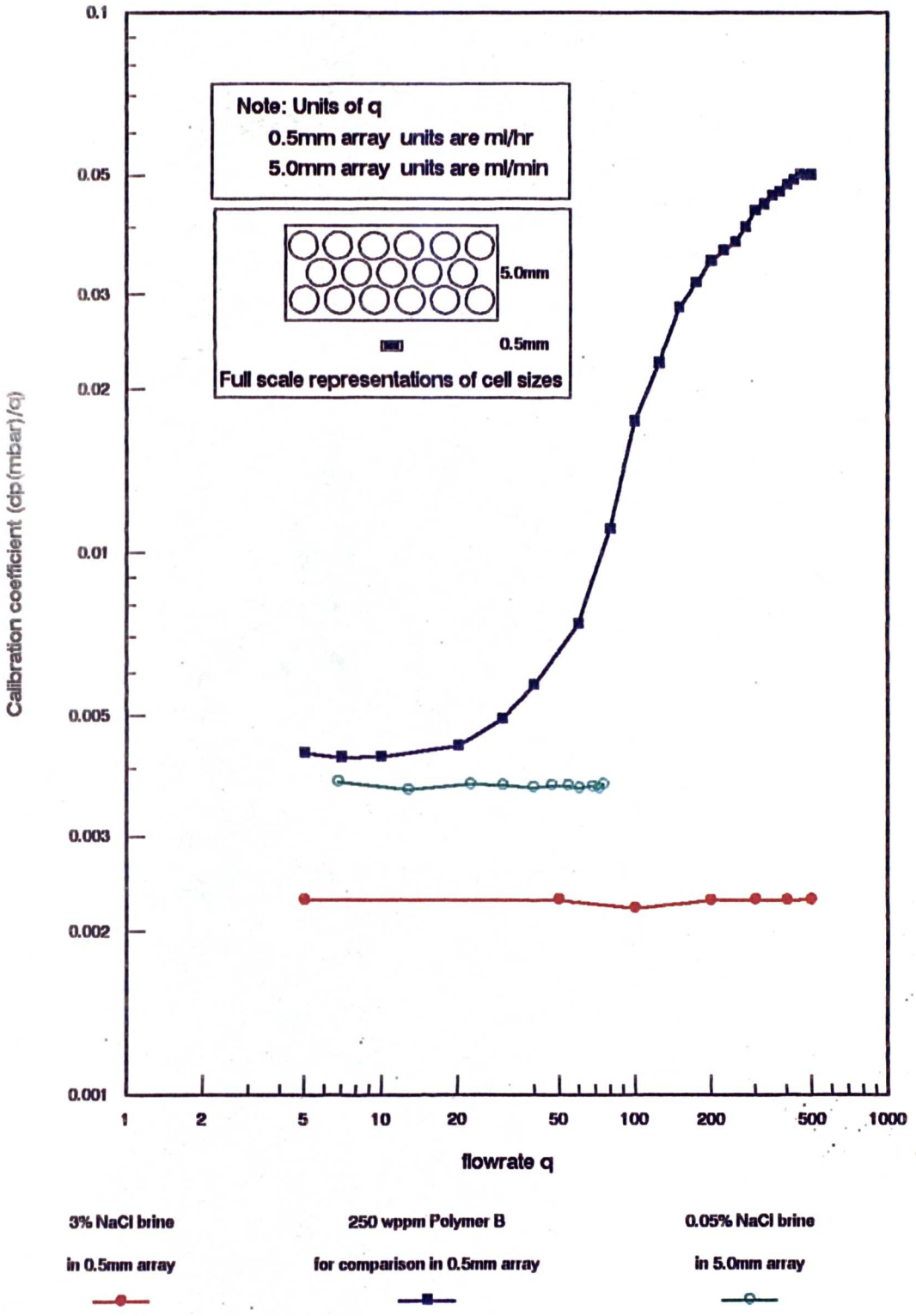

Figure 5.18 Calibration of planar contraction apparatus, including a full size representation of the two flow cell sizes used.

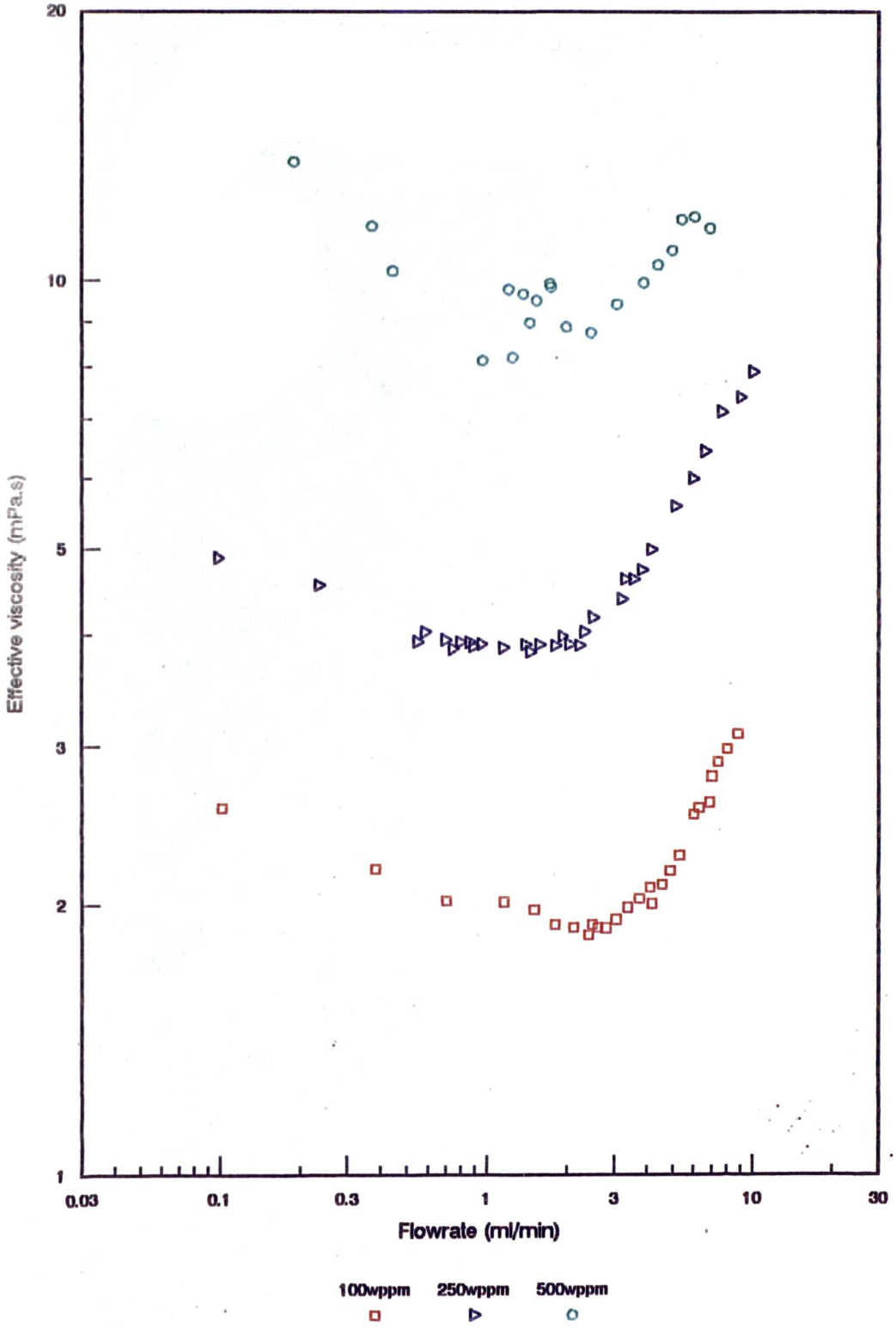

Figure 5.19 Effective viscosity of Polymer B solutions in the low salinity (0.05% NaCl) brine flowing through the 5.0mm rod array

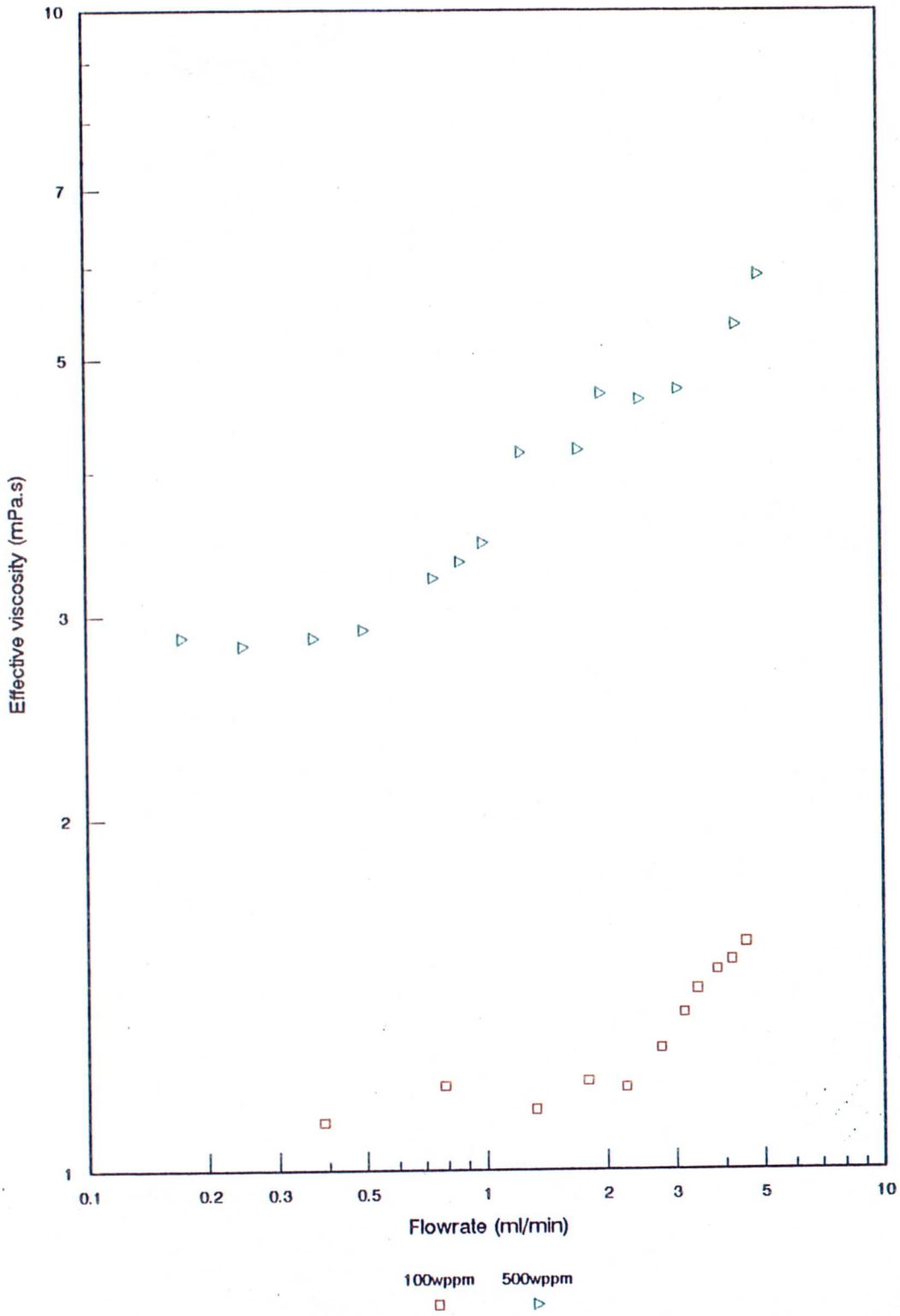

Figure 5.20 Effective viscosity of Polymer B solutions in the high salinity (3% NaCl) brine flowing through the 5.0mm rod array

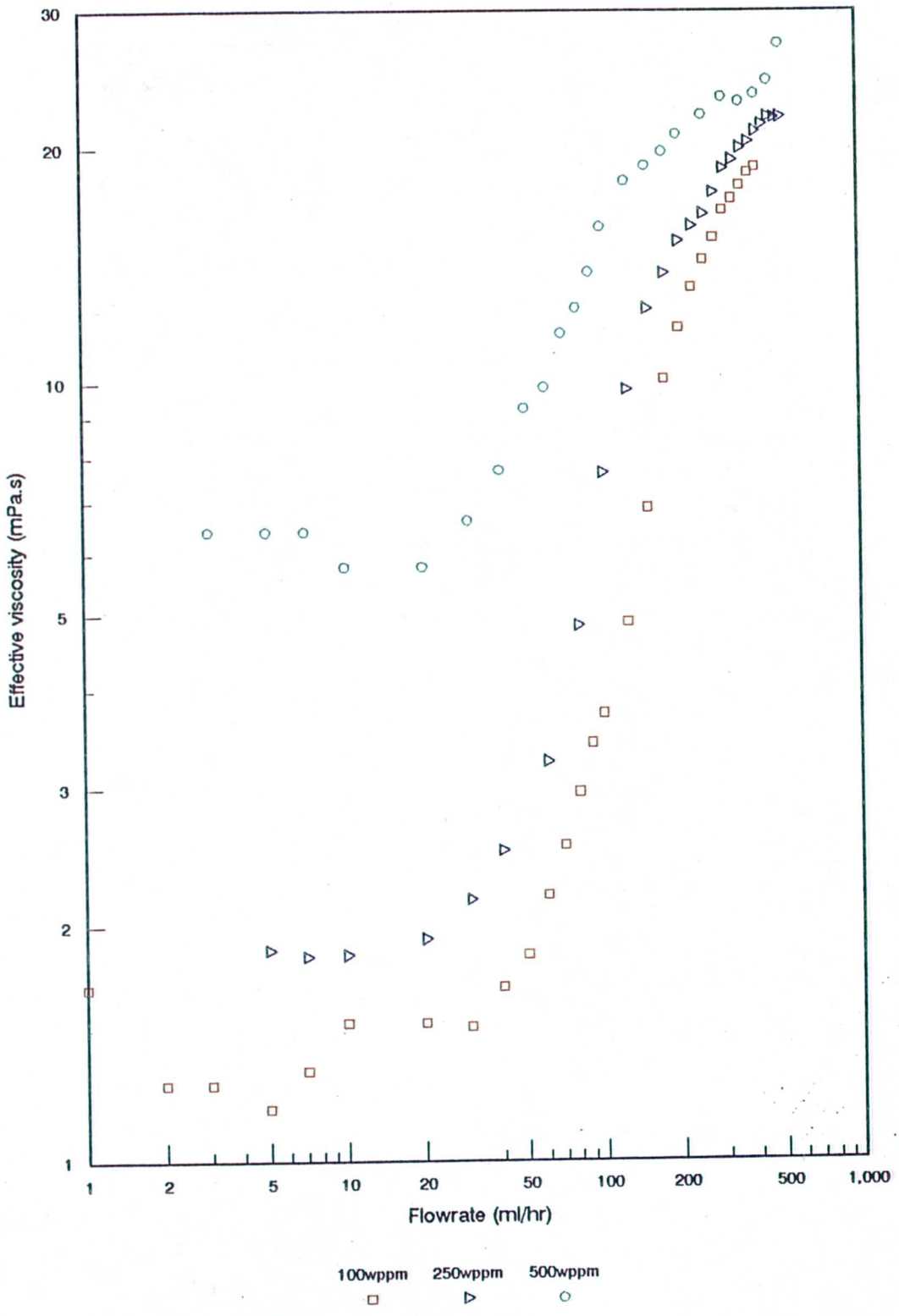

Figure 5.21 Effective viscosity of Polymer B solutions in the low salinity brine flowing through the 0.5mm rod array

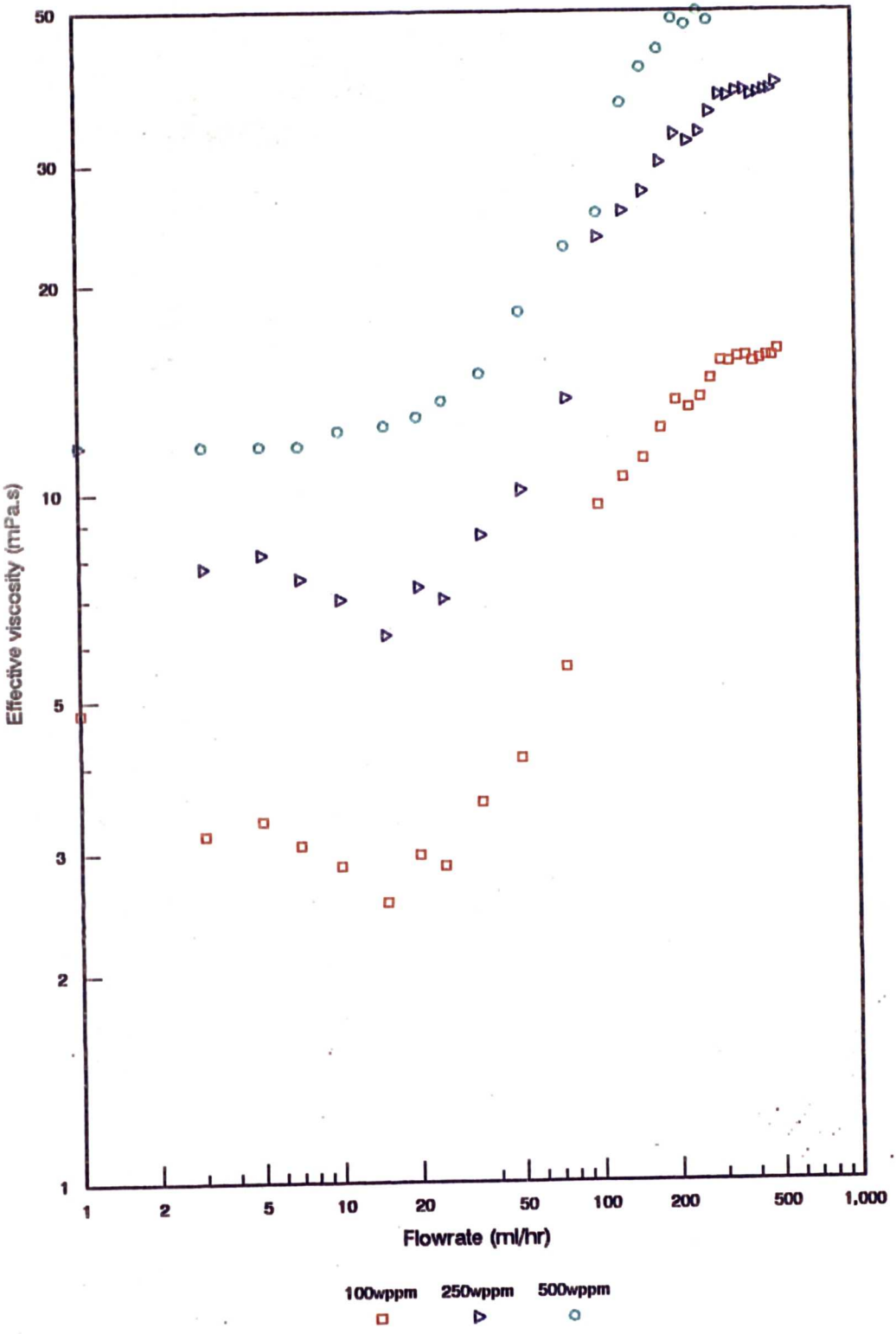

Figure 5.22 Effective viscosity of Polymer B solutions in the high salinity brine flowing through the 0.5mm rod array

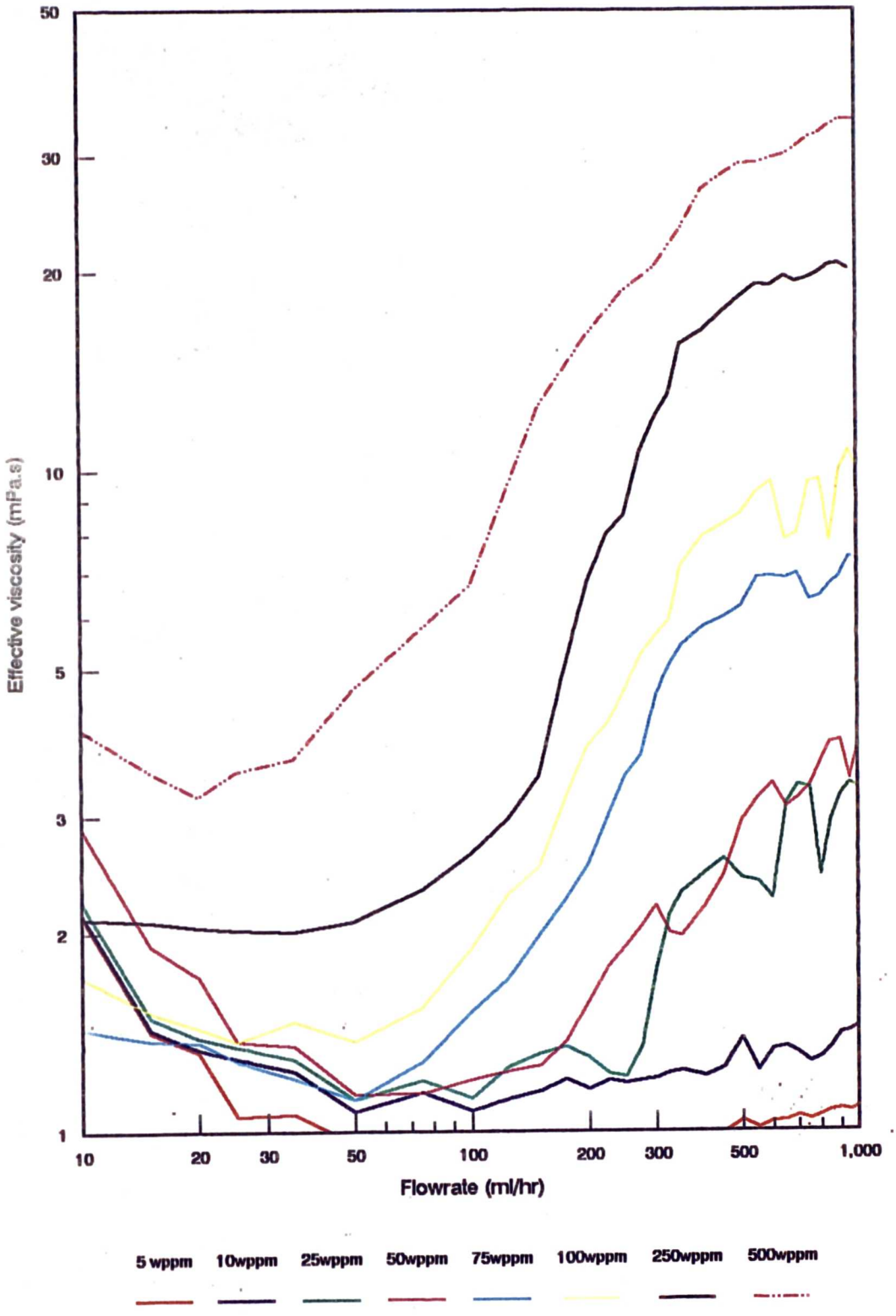

Figure 5.23 Effect of polymer concentration on effective viscosity for solutions of Polymer B in the high salinity brine flowing through the 0.5mm rod array

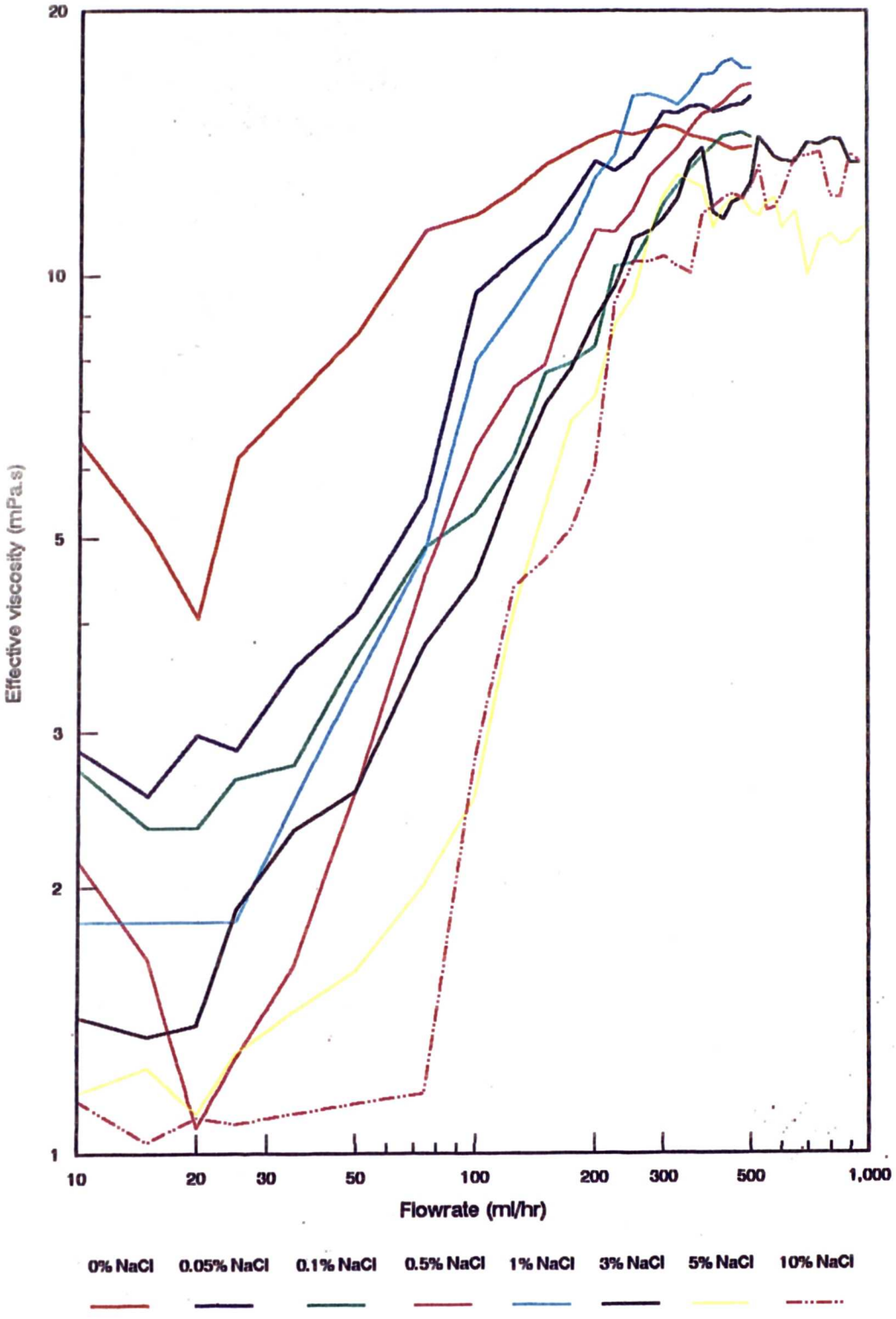

Figure 5.24 Effect of salinity concentration on effective viscosity for a 100wppm solution of Polymer B flowing through the 0.5mm rod array

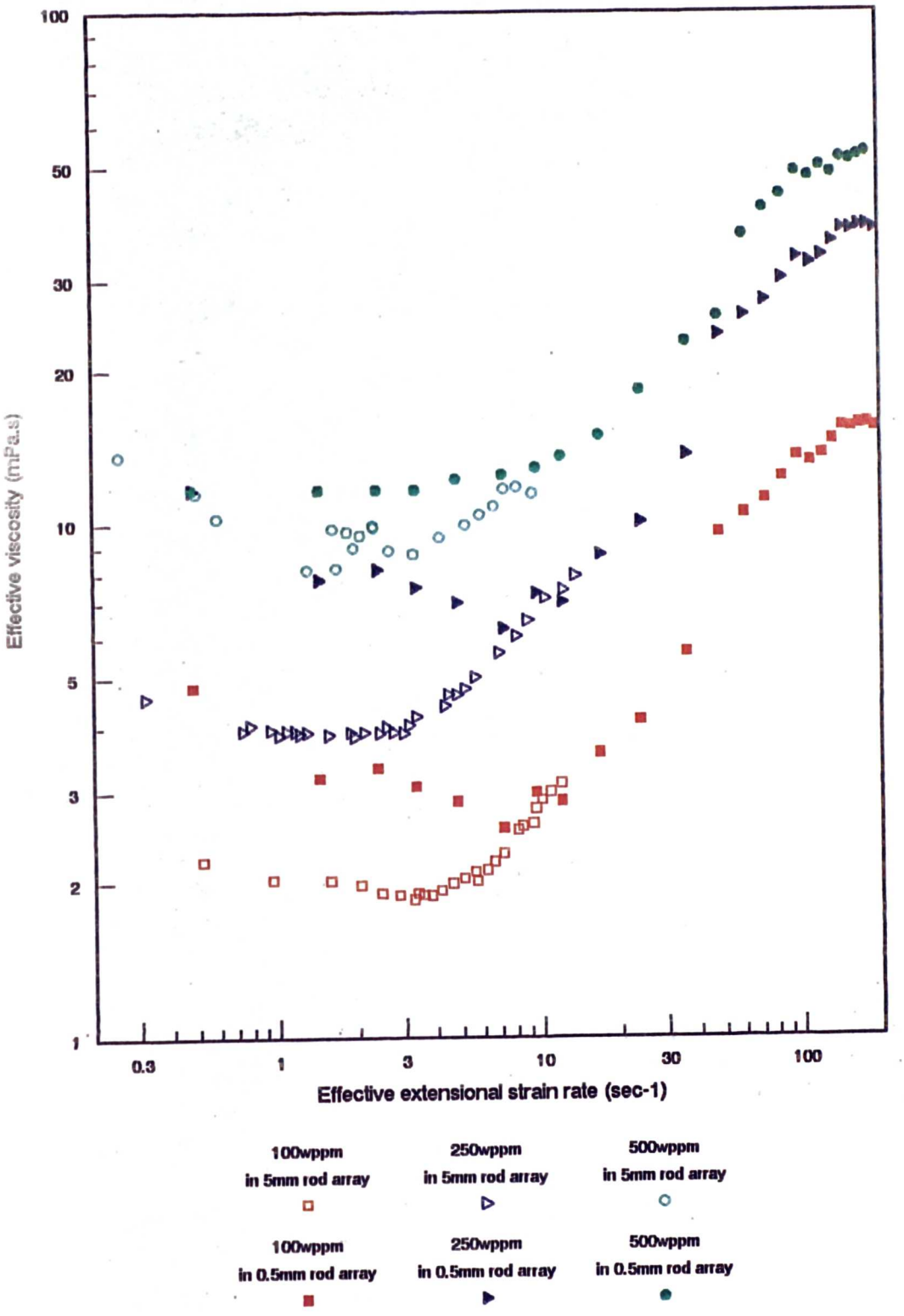

Figure 5.25 Comparison of the effective viscosities of solutions of Polymer B in the low salinity brine in both flow cells

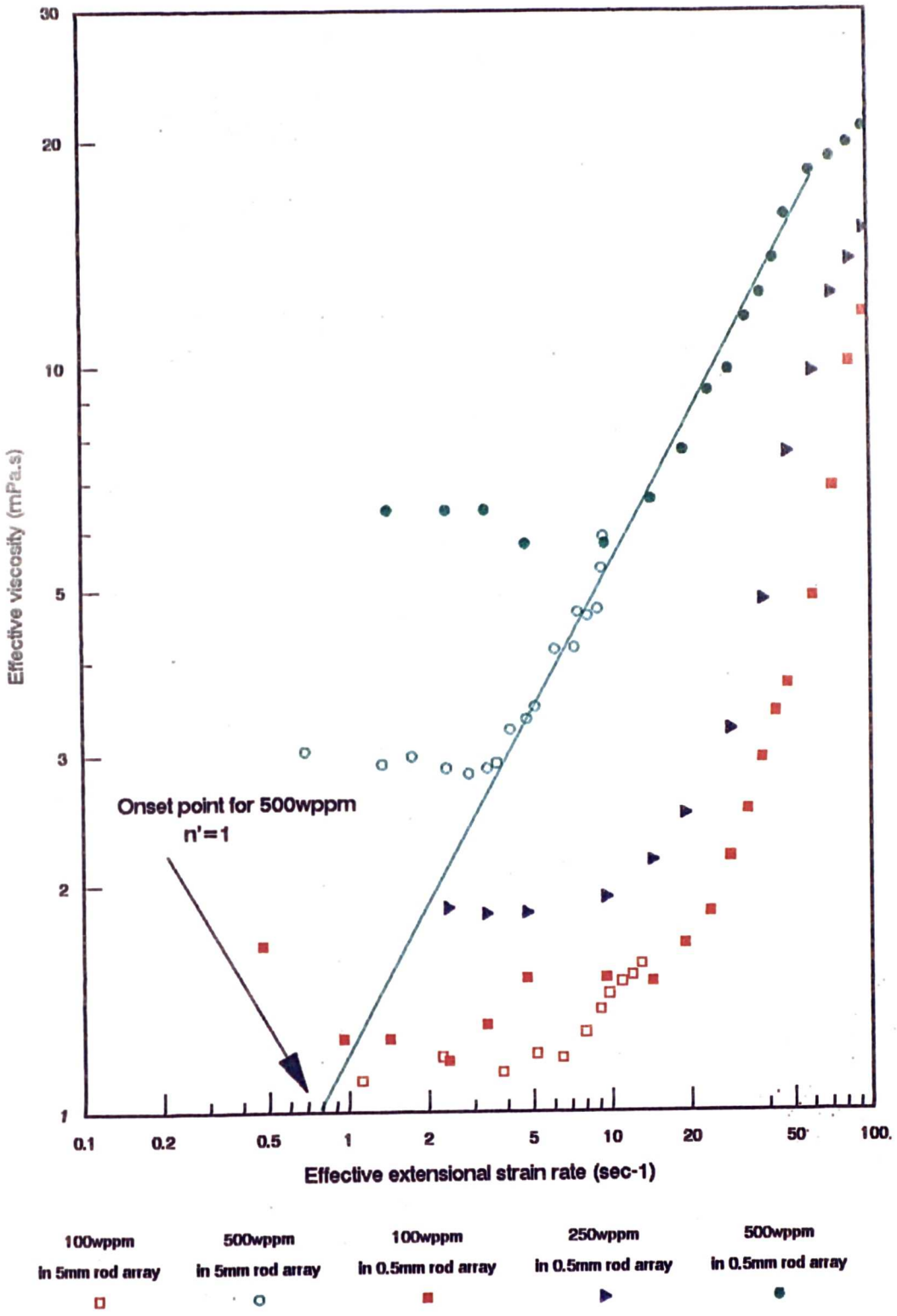

Figure 5.26 Comparison of the effective viscosities of solutions of Polymer B in the high salinity brine in both flow cells, showing the onset point for the 500wppm solution

5.4 Bead Pack Experiments

Degradation of high molecular weight polymers in solution can usually be characterised by a loss in solution shear viscosity. This scission will affect the extensional characteristics to a greater extent because of the reduction in average molecular weight. However, shear viscosity monitoring alone is not a reliable method of determining degradation as processes such as adsorption and retention through filtration can produce similar reductions in shear viscosity. Where possible these processes are identified, but when not possible the term degradation will be used to encompass all losses.

5.4.1 86μm bead diameter pack

A variety of tests were run in this pack, which was calibrated initially at a permeability of 6.8 Darcies, with a porosity of 39%. As with the other apparatus calibration coefficients were defined and calculated prior to the injection of the test solution, and were subsequently remeasured once the pack had been waterflushed. The variation in these coefficients from run to run was minimal (figure 5.27) after the pack had been flushed with the dilute hydrogen peroxide solution to remove any polymer. Polymer was injected until a stable pressure trace was obtained indicating that equilibrium had been reached.

5.4.1.1 Low salt content solvent polymer solutions

Initial runs using three concentrations of Polymer A in deionised water were conducted at 30°C. Although increases in the resistance to flow were observed at higher flowrates (figure 5.28) the resulting viscosities were still less than that of the bulk solution. For these tests no analytical method was available for determining effluent polymer concentrations, and so shear viscometry was used. This did show reductions in the effluent viscosity of upto 40% of the original value, indicating either severe degradation of the polymer had occurred in the pack or a large concentration was lost through adsorption. The phenomena of degradation of polyacrylamide has been studied before (90,89,87), and is reasonably well documented. Solutions in low ionic strength solvents are particularly susceptible because of the very open nature of the molecule - at high ionic strengths the more coiled conformation reduces the chances of chain scission.

No attempt was made to use dilutions of polymer B in deionised water in the bead pack apparatus due to the very high solution shear viscosities. As was stated above, the addition of 0.05% by weight sodium chloride reduced the shear viscosity to manageable proportions, similar to those of polymer A in deionised water. As can be seen from figure 5.29, clear evidence was observed of increases in viscosity above those of the bulk solution, at higher flowrates. As was the case above, the effluent was analysed by shear viscometry and showed some degradation, of the order of 15%. Reductions in shear viscosity are likely to occur from chain scission of molecules in general, thereby reducing the average molecular weight. Extensional viscosity, on the other hand, is dependant on the higher molecular weight chains present in the solution - hence reductions in shear viscosity (indicating degradation of high molecular weight molecules) are likely to result in a lower magnitude of extensional behaviour than expected.
The increases in flow resistance themselves do not appear very dramatic when compared to some of the earlier work. However, the magnitude of the extensional component is the actual result after allowing for the extrapolated shear viscosity, which for these solutions is still highly shear thinning.
It was originally intended to test the variation in this behaviour with temperature. Unfortunately this was not possible due to differential expansion of the acrylic tube compared to that of the glass beads, resulting in a path of low resistance being set up between the outside of the pack and the inside of the tube.

5.4.1.2 High salt content solution tests

Only solutions of polymer B were used at the higher salt concentrations in this apparatus.
The lower viscosities of these solutions allowed a greater flowrate range to be explored in the beadpack, with a maximum flowrate of 1 l/hr compared with 0.5l/hr for the previous runs. The pressure transducers were the limiting factor in these tests.
Three solutions, 100, 250 and 500wppm polymer, were made up in the 3% brine. Effluent polymer concentration analysis was available for these runs, using a manual titration technique carried out by BP Sunbury. This meant that injection and desaturation profiles could be obtained, as shown in figure 5.30. The reduction in molecular (conformation) size at this ionic concentration resulted in no further

observable reduction in the effluent shear viscosity. The observed shear viscosities (figure 5.31) for all three concentrations in the bead pack are in good agreement with those of the bulk. Increases in flow resistance to about 5 times that of the bulk solution were recorded, compared to about 3 times for the lower ionic strength solvents, before either the flowrate or high pressure limit was reached.
For the definition of onset adopted, that is the rate at which the extrapolated behaviour is seen to increase above the solvent viscosity line, the is a clear dependance on concentration, with the 500wppm solution exhibiting an increase at about one third of the flowrate required to induce (observable) extensional behaviour in the 100wppm solution. As was analysed above, the slopes of the extensional behaviour were fitted to a power law, with the exponent 'm' recorded in table 5.6 below. (The data points where the curves start to flatten out were ignored in the calculation of the best fit)

0.05% NaCl solvent

	$m_{5.0mm}$	$m_{0.5mm}$	m_{cap}	m_{sf}	$m_{86\mu m}$
100 wppm	1.41	1.86	1.385	1.521	-
250 wppm	1.52	1.80	1.338	1.476	-
500 wppm	1.58	1.71	1.432	1.486	-

3% NaCl solvent

	$m_{5.0mm}$	$m_{0.5mm}$	m_{sf}	$m_{86\mu m}$	$m_{48\mu m}$
100 wppm	1.42	2.48	1.83	2.36	2.52
250 wppm		2.40	1.855	2.33	
500 wppm	1.65	1.84	1.833	1.92	

- indicates information not calculable as flow not fully extensional

Calculated from power law best fits in the form $\eta = \lambda q^{m-1}$.

Table 5.6 Comparisons of extensional power law exponent m for polymer B between experiments.

5.4.2 48μm bead diameter pack

The initial permeability of this pack was found to be 3.4 Darcies, with a porosity of 38.3%.

5.4.2.1 High salt content solution tests

Only one polymer concentration, 100wppm polymer B in 3% NACl was used in this apparatus. As before effluents were analysed for both concentration and shear viscosity. The results of the concentration analysis are shown with those of the other bead pack in figure 5.30. Although no degradation in shear viscosity was observed once the pressure trace had stabilised, several pore volumes of solution had to be injected to reach equilibrium. The greater injection required for stability is indicative of some form of polymer retention, which would result in higher than expected values for the shear dominated part of the flow curve. The final, post polymer test, value of permeability (after copious flushing with solvent) was in the range 1.3 to 1.9 Darcies, with the pack less permeable at higher flowrates. With a pore radius (the largest circle that will fit in the pore space) of almost 4μm for this case, it is unlikely that molecular filtration at pore level is the cause for this delay in reaching injection concentration. As the pores are tricuspid in shape however, it is possible that physical trapping may occur at the pore periphery (the cusps) causing a substantial reduction on the pore throat area which would result in a lower permeability.
Using this final value for determining the calibration coefficient, and for use in the shear rate equation, comparison between the two bead sizes with shear rate are possible (figure 5.32). It can quickly be seen that although the shear viscosities match, and that the slopes of the extensional behaviour are similar (table 5.6) the onsets are not shear rate dependant.

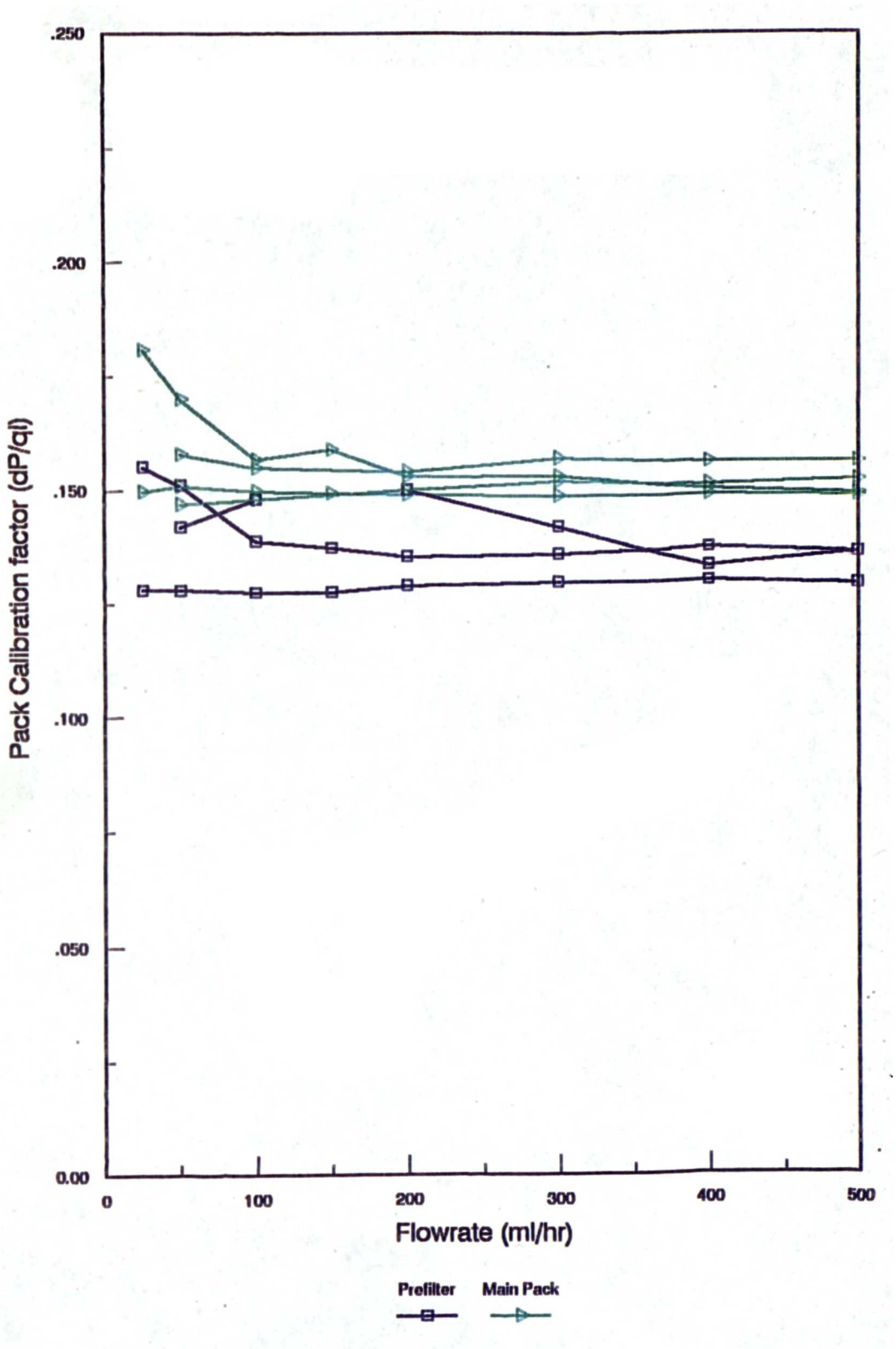

Figure 5.27 Variation in calibration coefficients for the 86μm bead diameter pack

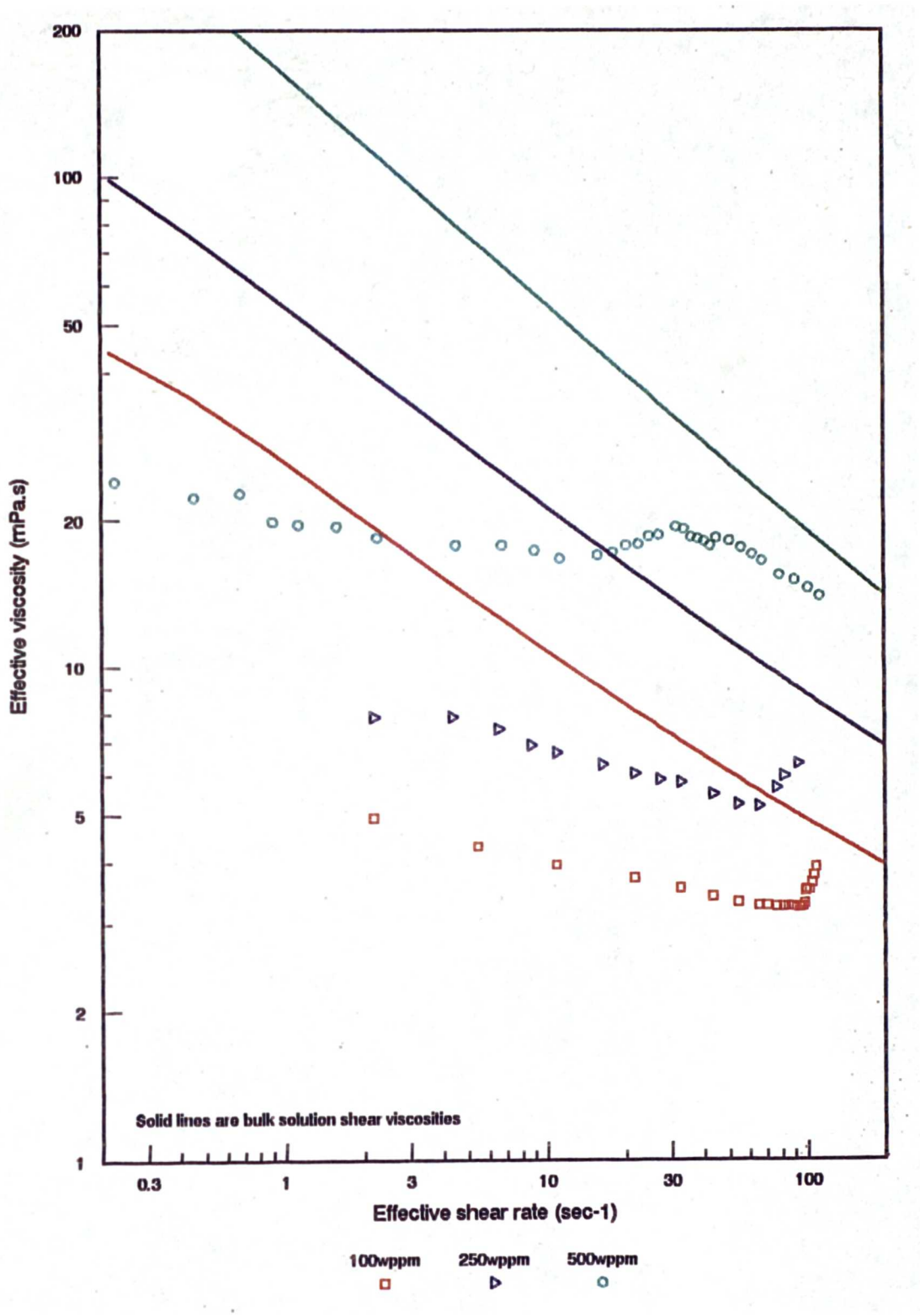

Figure 5.28 Comparisons of observed porous media viscosity of Polymer A in deionised water with those of the bulk solutions in pure shear (86μm bead diameter pack)

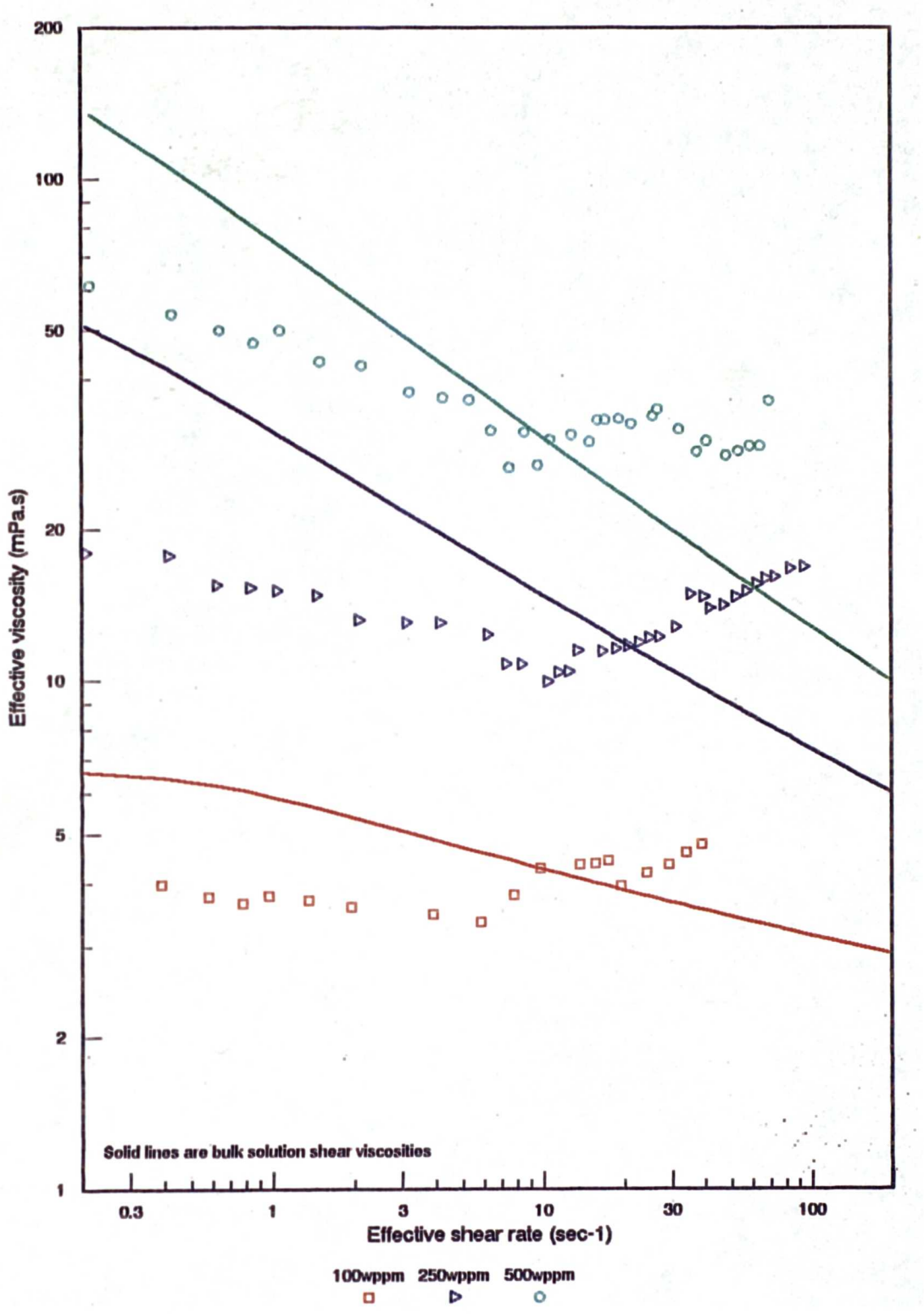

Figure 5.29 Comparisons of observed porous media viscosity of Polymer B in low salinity (0.05%wt) brine with those of the bulk solutions in pure shear (86μm bead diameter pack

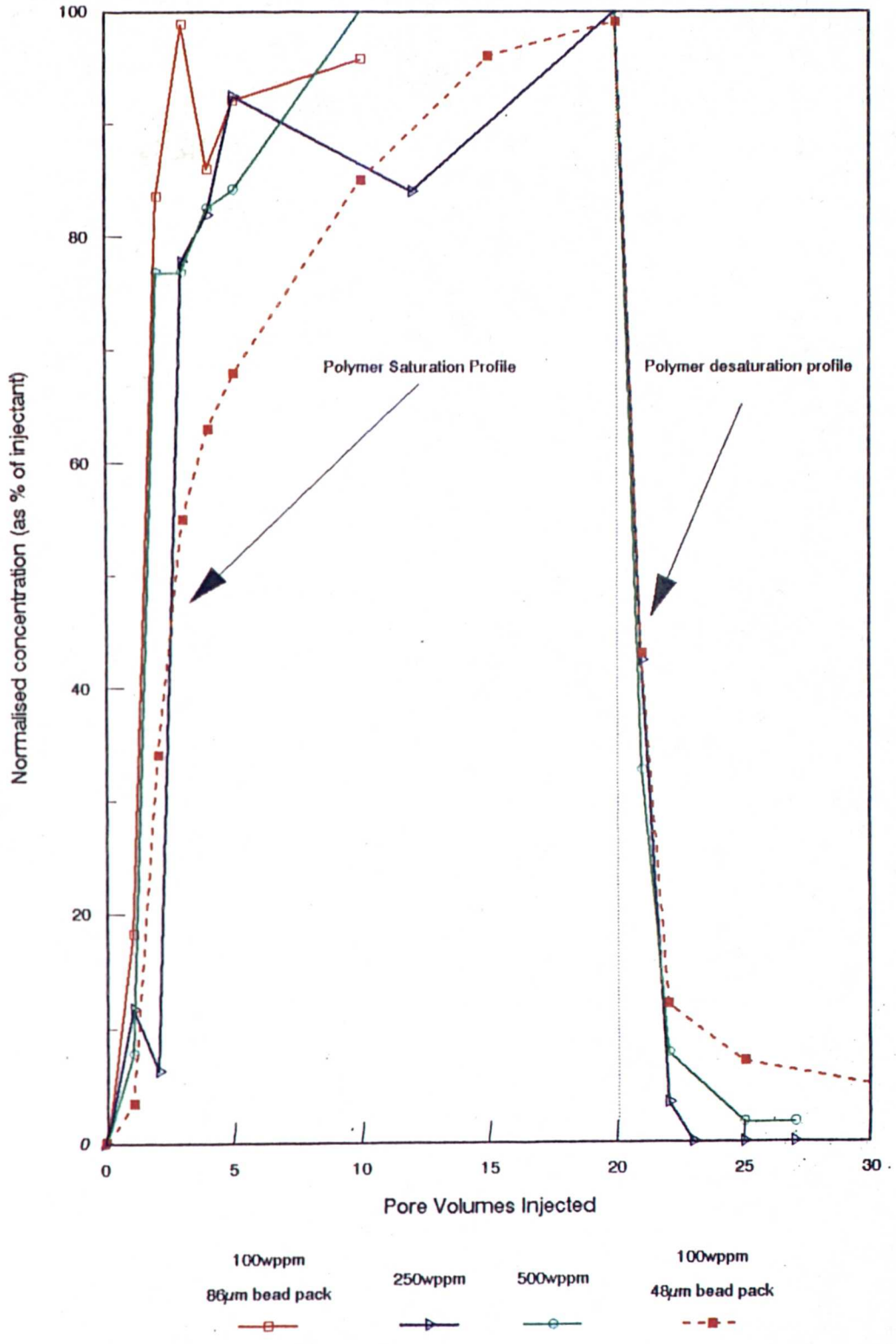

Figure 5.30 Polymer saturation and desaturation profiles for solutions of Polymer B in the high salinity brine in both 86μm and 48μm bead diameter packs

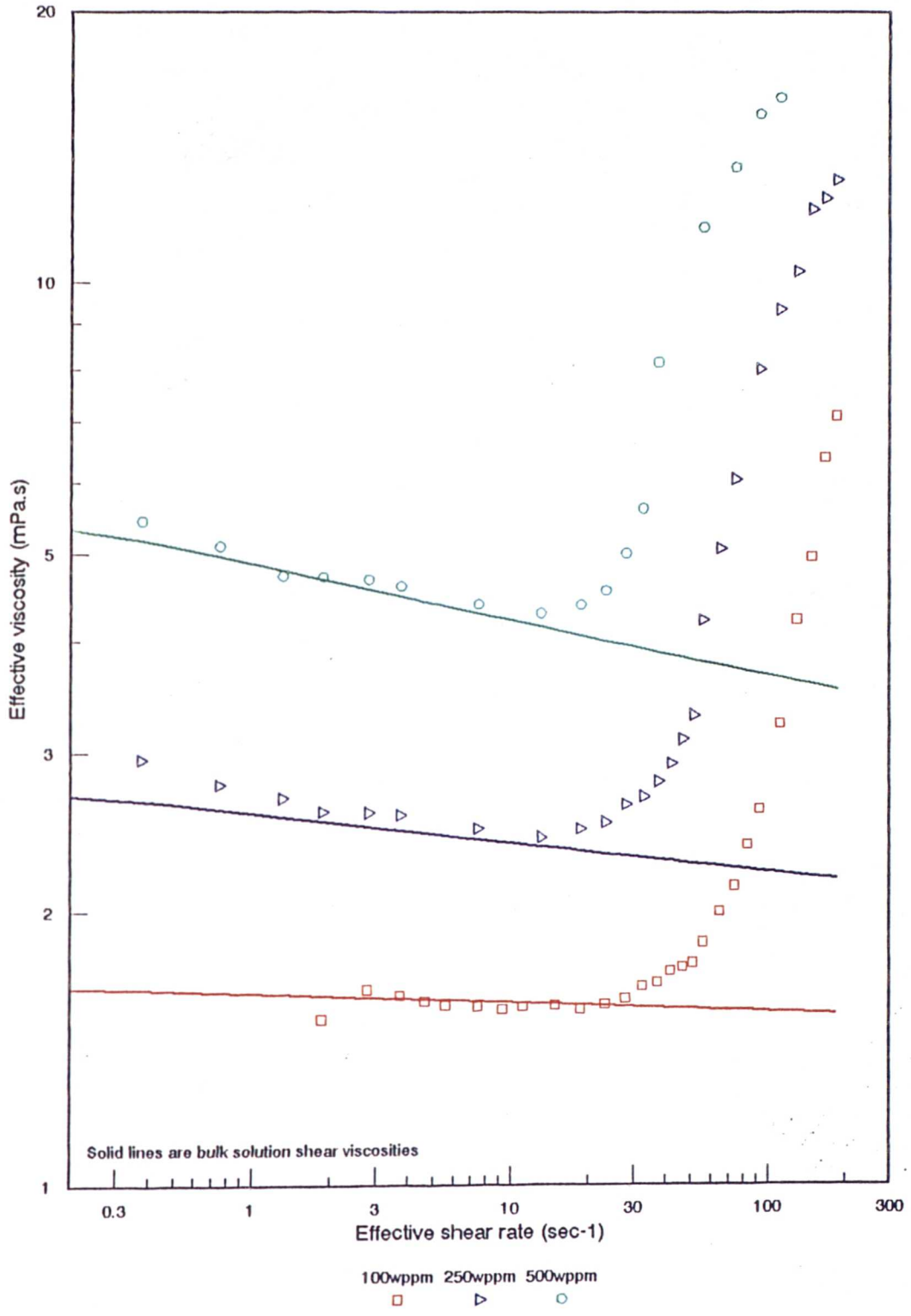

Figure 5.31 Comparisons of observed porous media viscosity of Polymer B in high salinity (3%wt) brine with those of the bulk solutions in pure shear (86μm bead diameter pack)

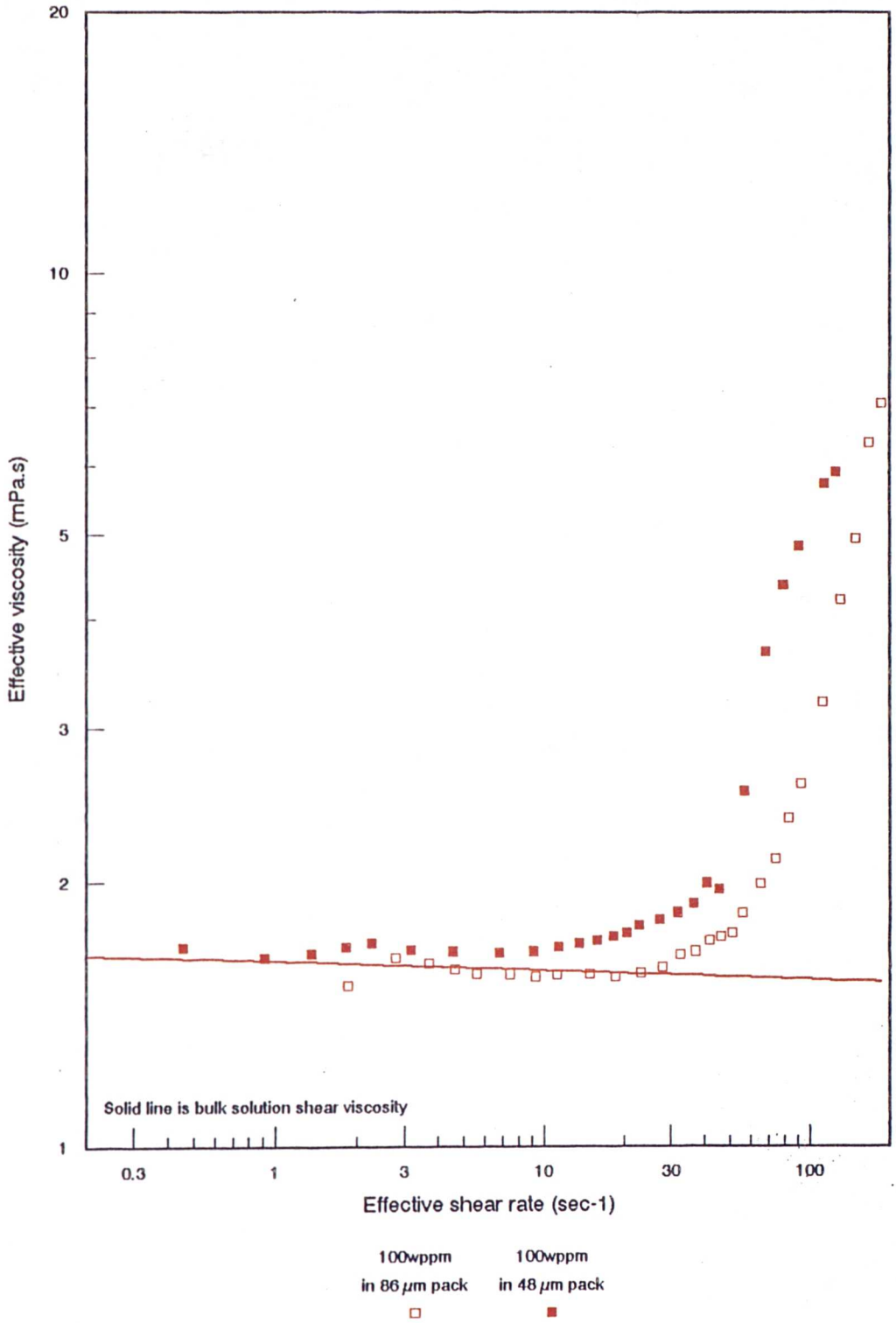

Figure 5.32 Comparison of the observed behaviour of 100wppm solutions of Polymer B in 3%wt.brine between the 86μm bead pack and the 48μm bead pack

5.4.3 Comparison of bead pack results

Comparisons may be made between concentrations as well as between bead sizes. Many published works have presented data using the Ergun co-ordinates (that is a Reynolds number - friction factor plot), or have modified them for their own purposes. Unless there is good agreement between the experimentally observed values of viscosity and that of the bulk solution for highly shear thinning fluids the data will appear scattered with no apparent cause on an N_{Re} vs f plot. When the solution is almost Newtonian, as is the case for the more saline solutions, a plot of f against N_{Re} will reveal any similarities between the flows, and will also allow any solvent inertia effects to be noticed, by a change in slope of the solvent curve. Figure 5.33 compares the results for the different bead packs and concentrations in the 3% brine. It can be seen that no observable inertia effects are present in the solvent flow (light blue line) over the range used, and that the Reynolds number required for onset decreases with increasing concentration, and decreasing bead diameter. Other than the fact that prior to onset all test solutions lie on the line $f.N_{Re}=180$, no firm conclusions as to onset criteria can be drawn from this plot. A plot of $f.N_{Re}$ against N_{Re}, (figure 5.34) as used by Durst, Haas et al (22,24,31,33) does highlight the similarity in slopes between solutions but again other than highlighting inertia no additional information may be gained other than what was available in the effective viscosity vs flowrate plots used above. However, when the extensional strain rate analysis is applied, as seen in figure 5.35, more information about the flow behaviour is revealed, with the two 100wppm solutions almost overlaying each other. Thus it can be seen that in order to compare solutions in differing pore dimensions, plots of extensional strain rate against viscosity are the most effective.

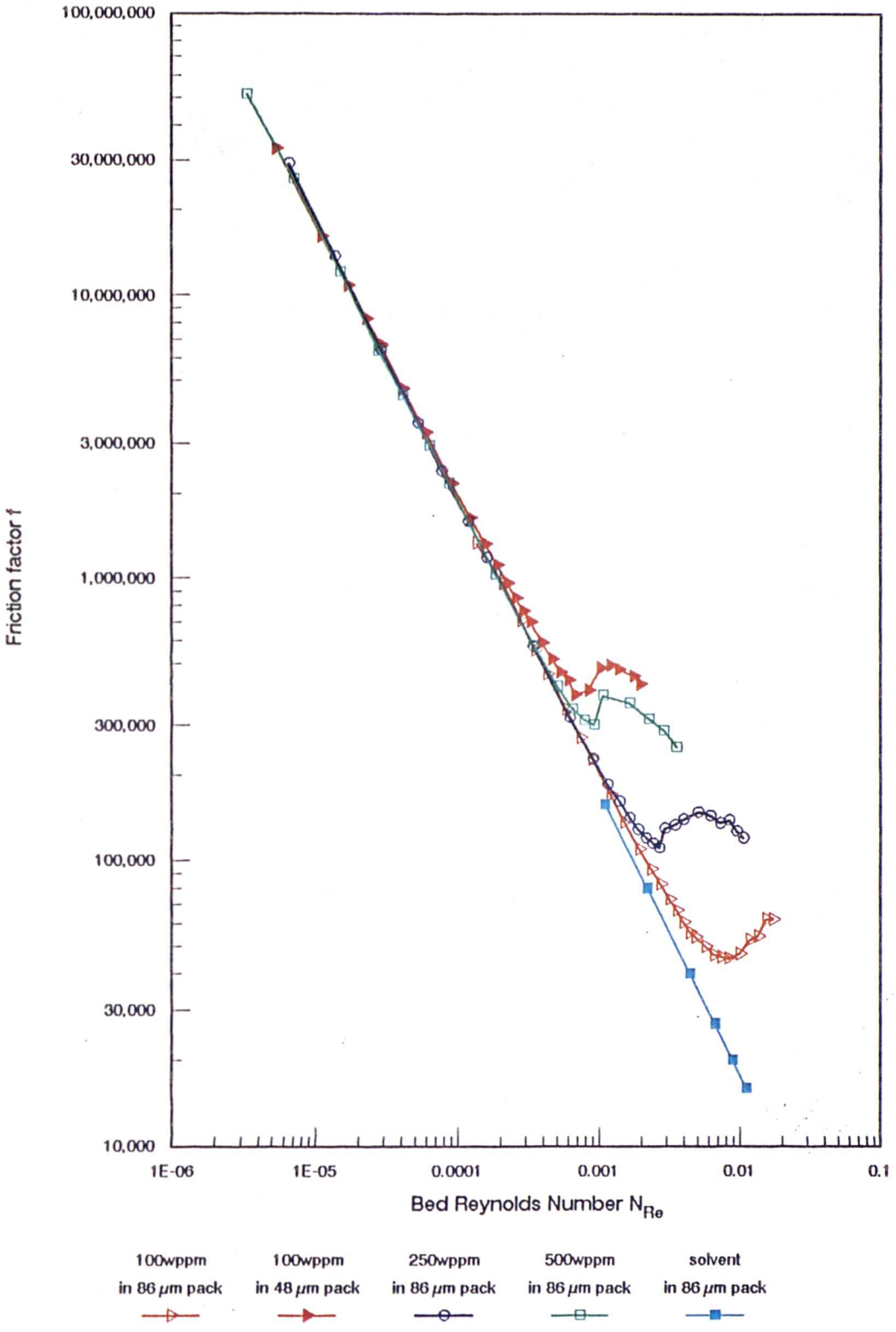

Figure 5.33 Variation of friction factor with Reynolds number (plotted as Ergun coordinates) for solutions of Polymer B in the high salinity brine

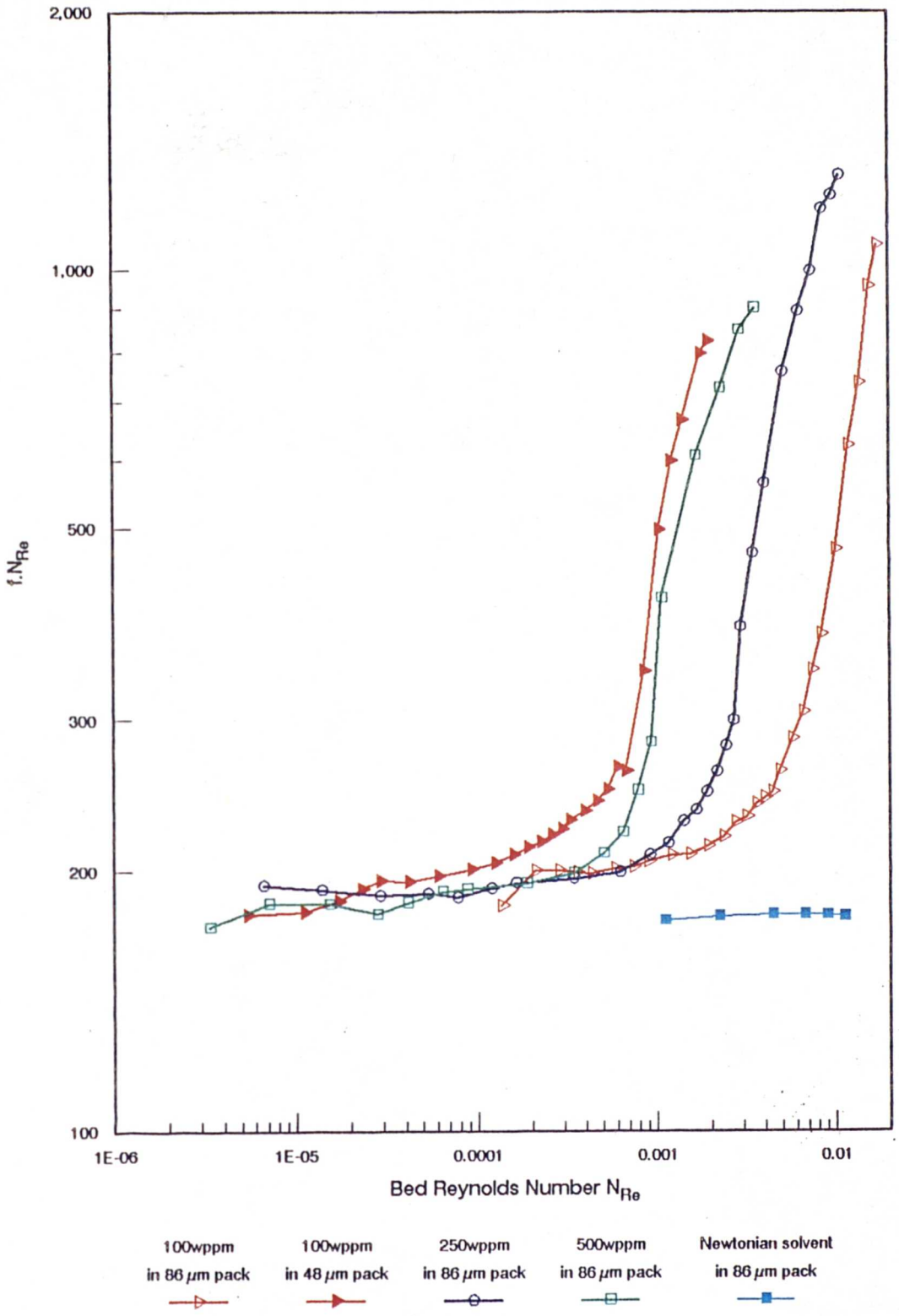

Figure 5.34 Variation of $f.N_{Re}$ with Reynolds number for solutions of Polymer B in the high salinity brine

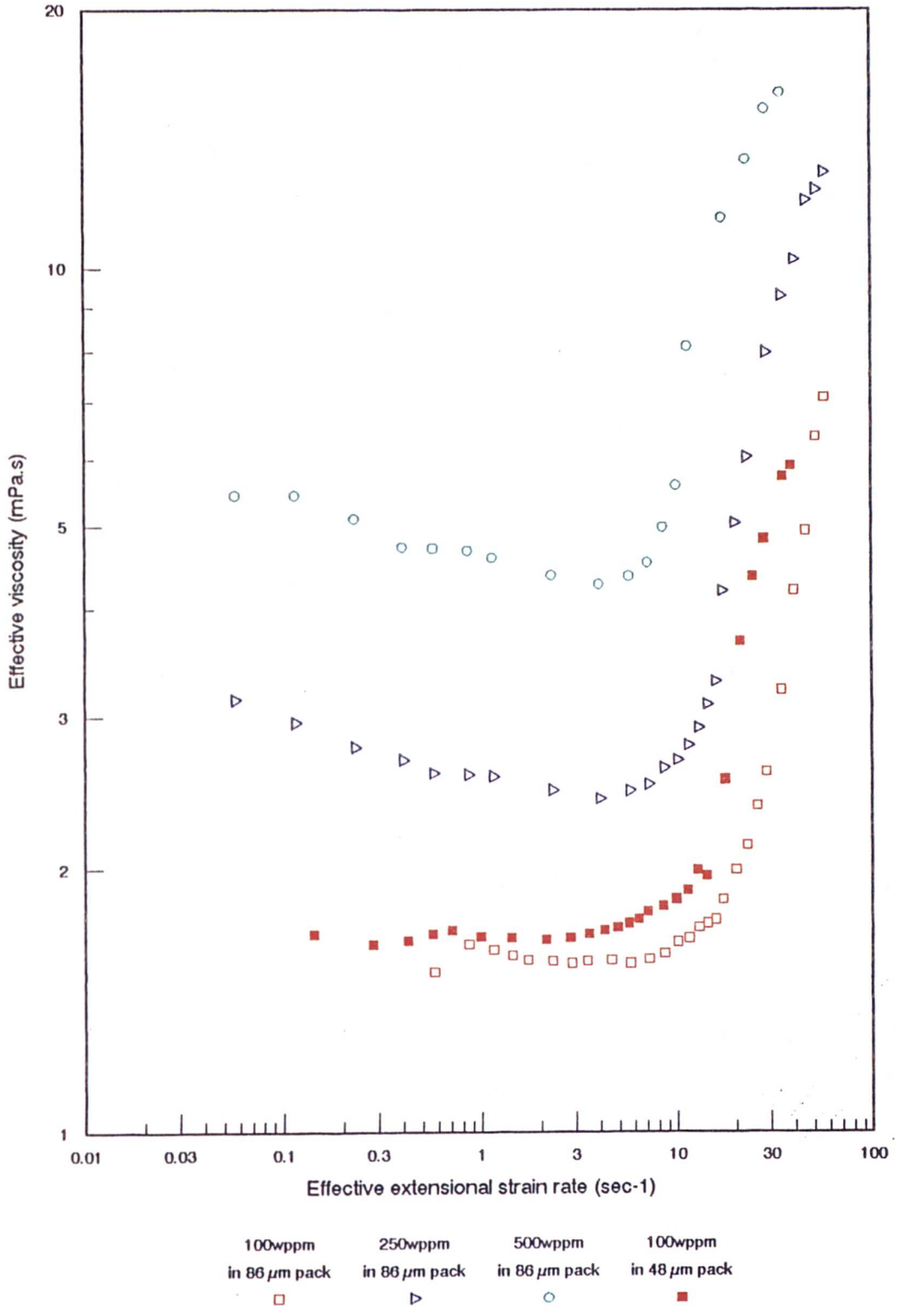

Figure 5.35 Variation of effective viscosity with Extensional strain rate $\dot{\xi}$ (as calculated in Chapter 3) for solutions of Polymer B in the high salinity brine.

5.5 Flow Visualisation Studies

Studies were conducted, in the main, using polymer solutions made up in the lower ionic strength brine (0.05% wt/wt NaCl). Several works have been published (56,58,4,45) using abrupt geometries, so effort was concentrated on the curvilinear geometries, as shown in figure 5.36. This figure also displays the direction conventions used in the following images.

5.5.1 Axisymmetric Contraction Flow

The visualisation studies presented for this geometry are of three concentrations of polymer B in 0.05% wt/wt brine. To enable an easy comparison of the effects of the visualised flow regimes, coefficients of the pressure drop per unit flowrate for the solutions are presented in figure 5.37.

Plates 5.1 to 5.3 illustrate the changes in flow domain for the brine solution, with no inertia effects in plate 5.1, through to totally inertia dominated flow in plate 5.3. Plate 5.2 illustrates the effect of increasing inertia (from the high Reynolds number flow in the fine bore capillary), and how it affects the flow in the subsequent chamber. The 'no inertia' to 'high inertia' dominated transition has a profound effect on the pressure drop across the section. For the low flowrate case, where no inertia is visible, the pressure drop is still proportional to the flowrate, as shown by the constant factor '$\Delta P/Q$' in figure 5.37. The high flowrate case, depicted in plate 5.3, however, has a calibration factor which is highly flowrate dependant, and laminar flow equations obviously do not apply. It is interesting to note in plate 5.3 that at this flowrate sufficient inertia is created to form a 'shear tube' which in effect continues the capillary right across the expansion chamber, with the majority of the flow travelling at high velocity through this tube and not expanding out. It can also be seen that the velocities in the annular region are much lower, characterised by only small movement recorded in the 1/15th second exposure time.

Plates 5.4 to 5.6 are the observations for a 100wppm solution in 0.05% brine of polymer B, over a similar flow range to those of the solvent above. The increased shear viscosity of this fluid depresses Reynolds numbers, with the flow totally laminar over a greater range. The flow in plate 5.4, at a **capillary** wall shear rate of 180 sec^{-1}, is already exhibiting a divergence from the pure shear pseudoplastic

behaviour of the bulk when the pressure drop/flowrate coefficient for this rate is examined. It is possible that a longer time exposure may have captured some detail lost in the 1/2 second exposure. A six fold increase in flowrate, plate 5.5, produces dramatic recirculation zones as the fluid leaves the expansion chamber. These cannot be attributed to fluid inertia, as this would appear at the fine bore capillary exit (the entrance to this chamber). It would appear that with the setting up of these recirculations, two distinct flow regimes are set up in the cell, with a constant velocity profile in one half having little or no effect on the accelerating field set up in the other half. Vortex size was observed to be strongly dependant on flowrate, which may be attributed to a minimising of extensional stresses by reducing the extensional strain rate. Indeed by the time the flowrate is increased a further 2.5 fold the flow in the chamber is apparently totally unstable, with some inertia present, but in the main dominated by the fluid's desire to set up and maintain a 'shear tube' where the bulk of the fluid undergoes little or no expansion. Two dimensional slices of the flow cannot fully reveal the tortuosity of this tube,as it actually extends in other planes not illuminated. This results in a fluid path between leaving the capillary on one side and regaining it on the other of length much greater then that of the chamber itself. This limiting of the extensional effects can be seen by the levelling off of the $\Delta P/Q$ curve in figure 5.37.

Plates 5.7 to 5.10 are for the 250wppm Polymer B solution, again over a similar flowrate range. Plate 5.7, at a capillary wall shear rate of 315 sec^{-1} does exhibit some small recirculation zones just at the inlet to the subsequent capillary, although the pressure per unit flowrate curve is still in decline indicating pseudoplasticity. The doubling of the flowrate, from plates 5.7 to 5.8 again shows the strong vorticies displayed in the lower concentration solution above - however the vortex size is obviously not only flowrate dependant but also concentration dependant. This can be seen from the vortex sizes in plates 5.8 and 5.5, which are of a similar size, but the flowrate in 5.5 is twice that of 5.8. As was mentioned previously these vorticies become unstable and tend to rotate about the capillary entrance above some flowrate. Plate 5.9 catches the inception of these instabilities, at a capillary wall shear of 780 sec^{-1}. As was the case in plate 5.6, plate 5.10 seems to indicate no coherent pattern to the flow, whereas the flow is actually normal to the illuminated slice upon leaving the capillary, and then tortuously follows some path

before exiting the chamber in another plane not illuminated. Once more the dilatent behaviour has been limited by the formation of these long tubes, and the corresponding $\Delta P/Q$ has also plateaued.

Plates 5.11 to 5.13 present similar results for the 500wppm Polymer B solution. It is again worth noting the greater vortex size at a lower flowrate than was the case above.

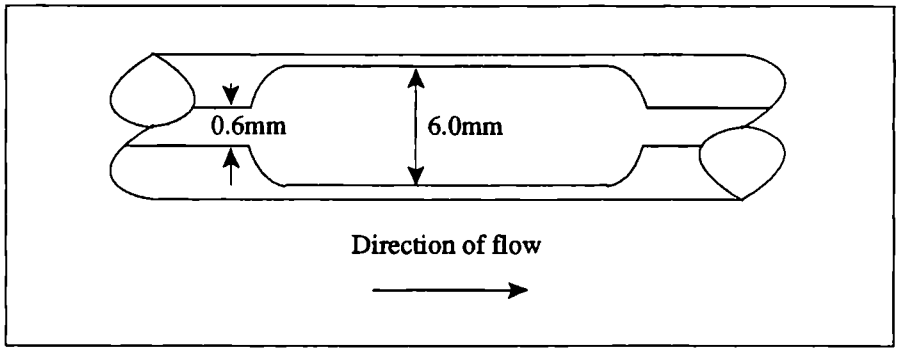

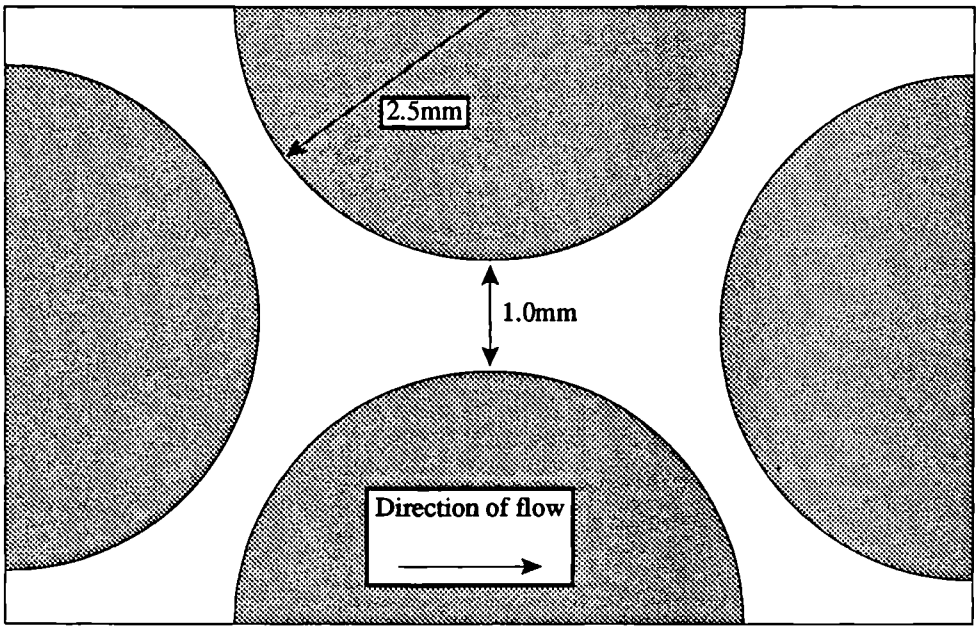

Figure 5.36 Cell sizes and flow directions in the following images

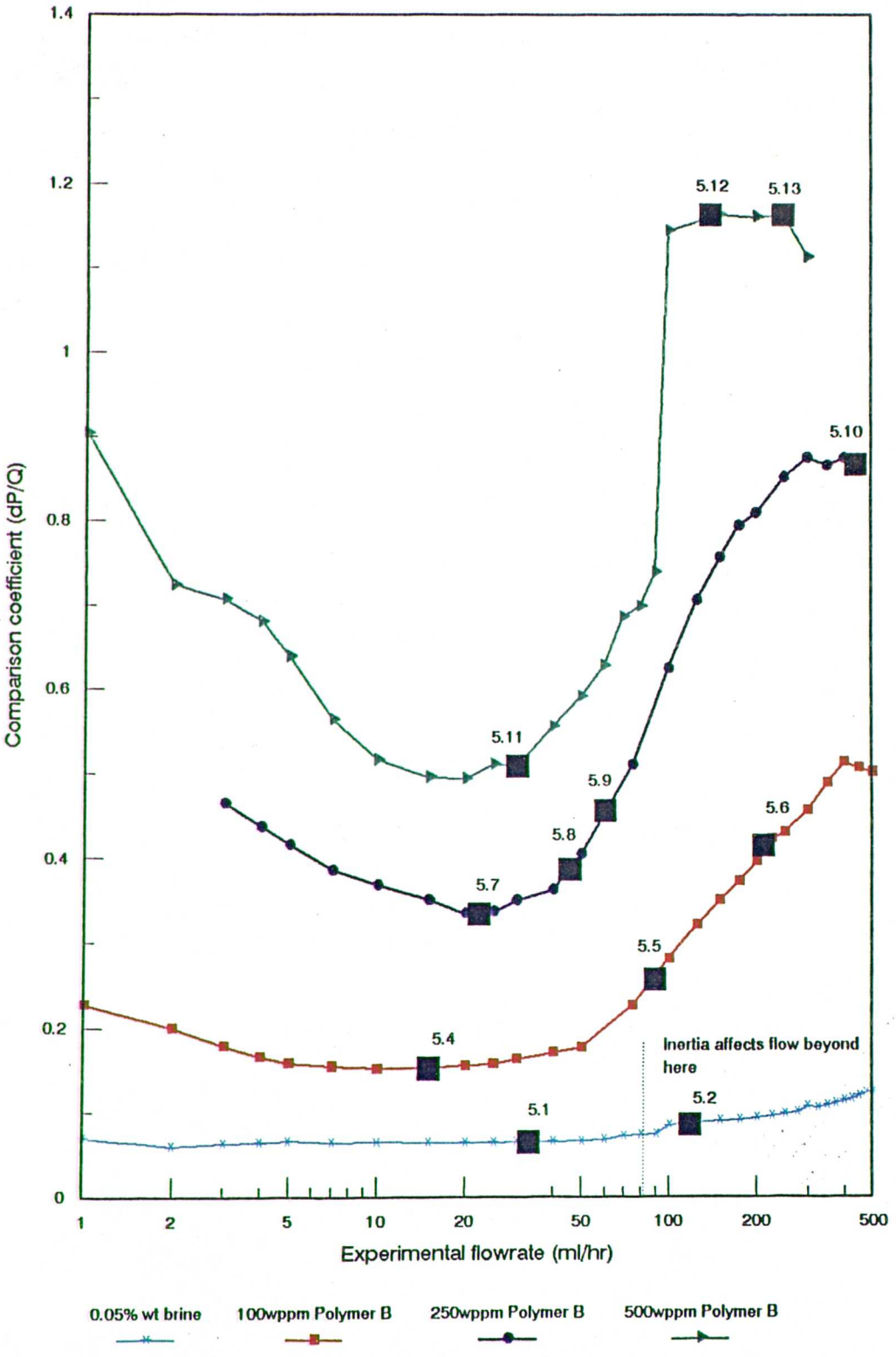

Figure 5.37 ΔP/Q coefficients to enable direct comparison between plates for the test solutions used (■marks plate reference points)

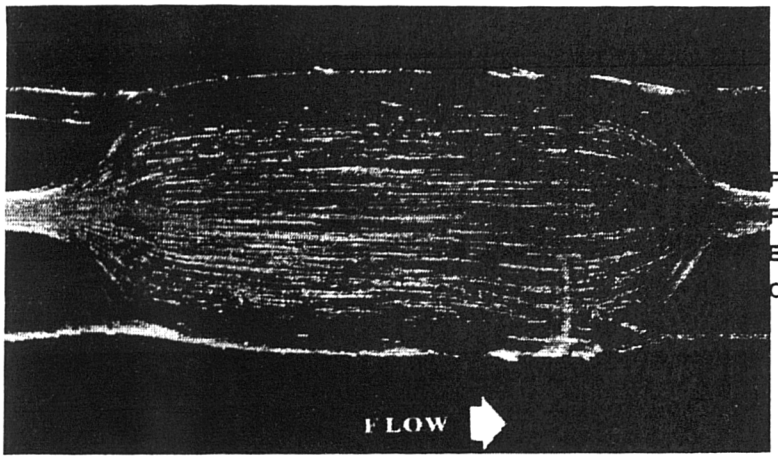

Plate 5.1
Flowrate : 36 ml/hr
Exposure time : 4 sec
Capillary wall shear rate :
470 sec-1

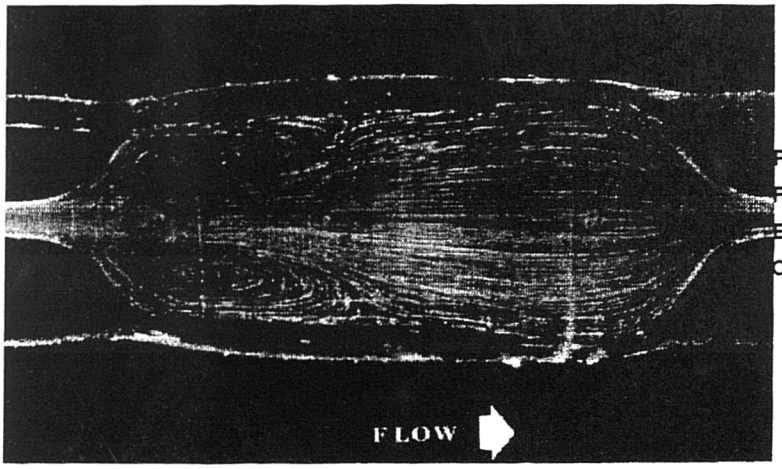

Plate 5.2
Flowrate : 111 ml/hr
Exposure time : 4 sec
Capillary wall shear rate :
1500 sec-1

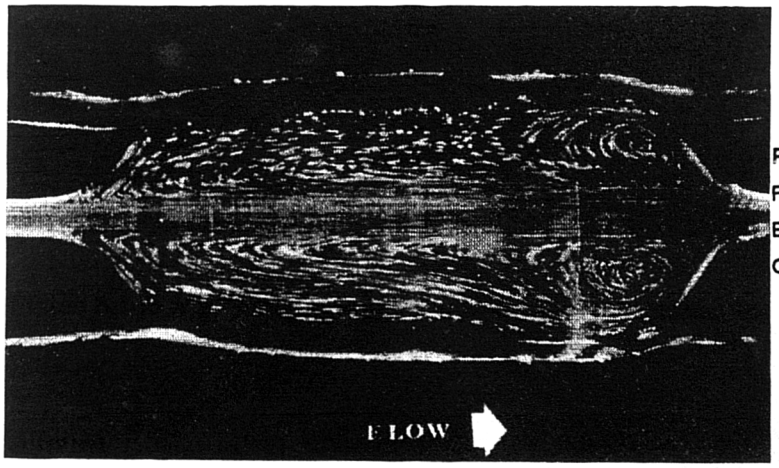

Plate 5.3
Flowrate : 900 ml/hr
Exposure time : 1/15th sec
Capillary wall shear rate :
12000 sec-1

Plates 5.1 to 5.3 Brine flowing through profiled contraction apparatus

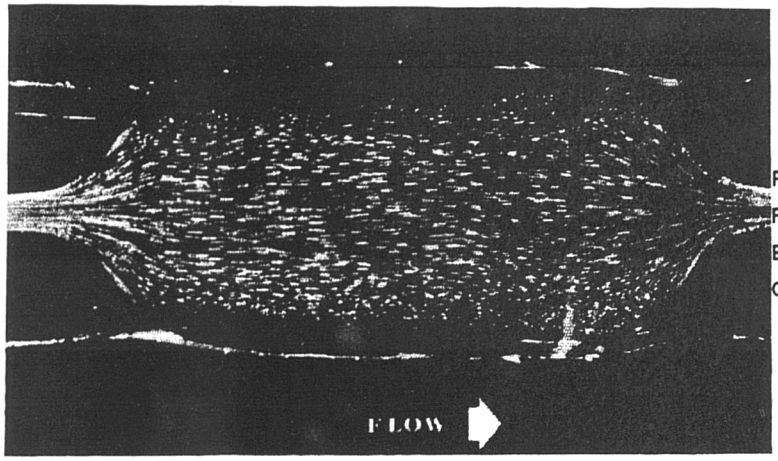

Plate 5.4
Flowrate : 14 ml/hr
Exposure time : 1/2 sec
Capillary wall shear rate :
180 sec-1

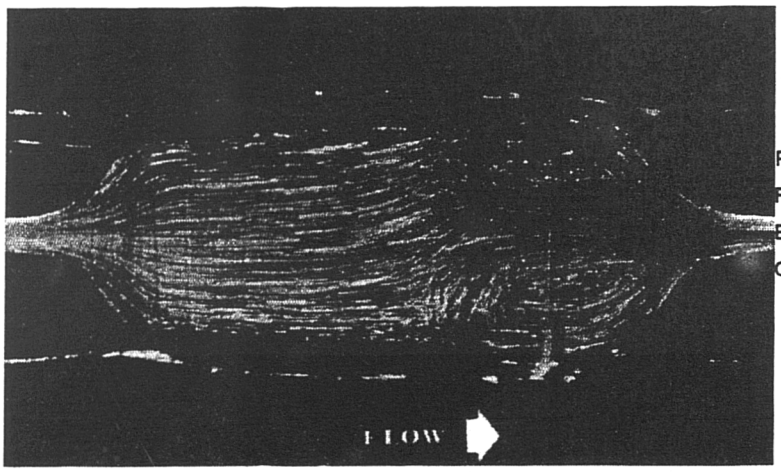

Plate 5.5
Flowrate : 89 ml/hr
Exposure time : 1/2 sec
Capillary wall shear rate :
1200 sec-1

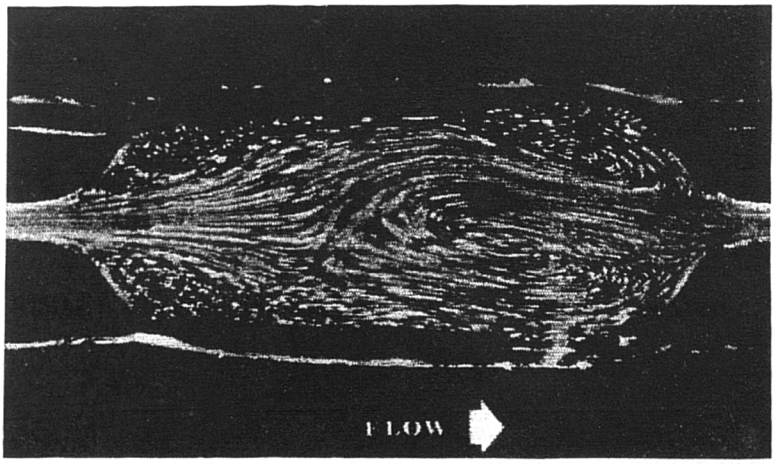

Plate 5.6
Flowrate : 206 ml/hr
Exposure time : 1/60th sec
Capillary wall shear rate :
2700 sec-1

Plates 5.4 to 5.6 100ppm P'mer B flowing through profiled contraction apparatus

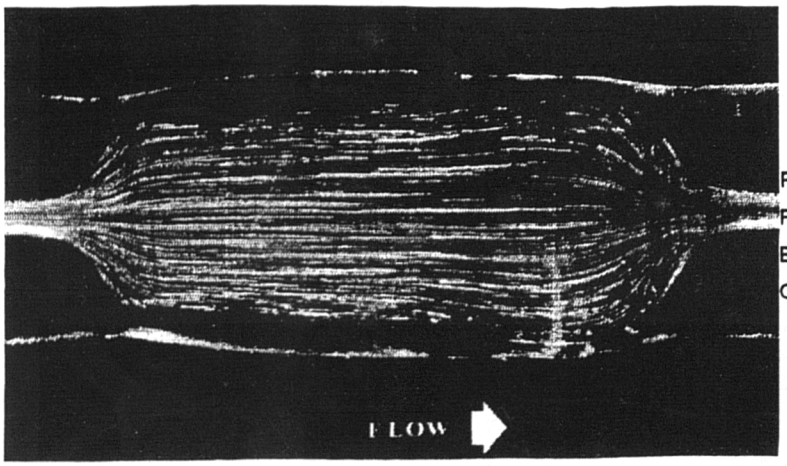

Plate 5.7
Flowrate : 24 ml/hr
Exposure time : 4 sec
Capillary wall shear rate :
315 sec-1

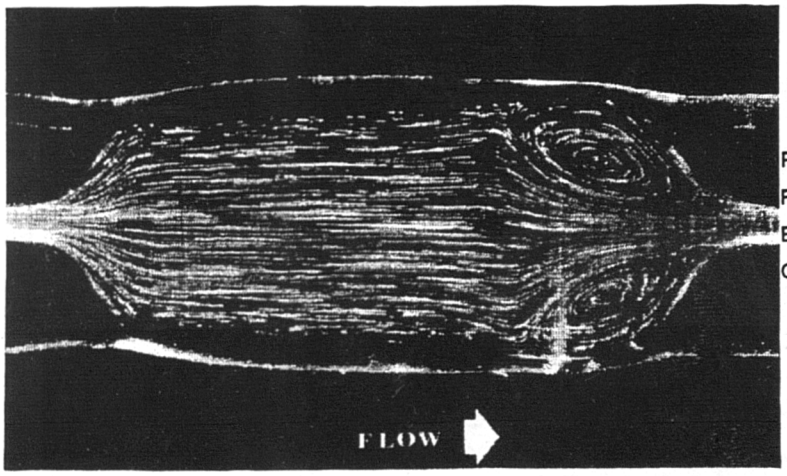

Plate 5.8
Flowrate : 46 ml/hr
Exposure time : 1 sec
Capillary wall shear rate :
600 sec-1

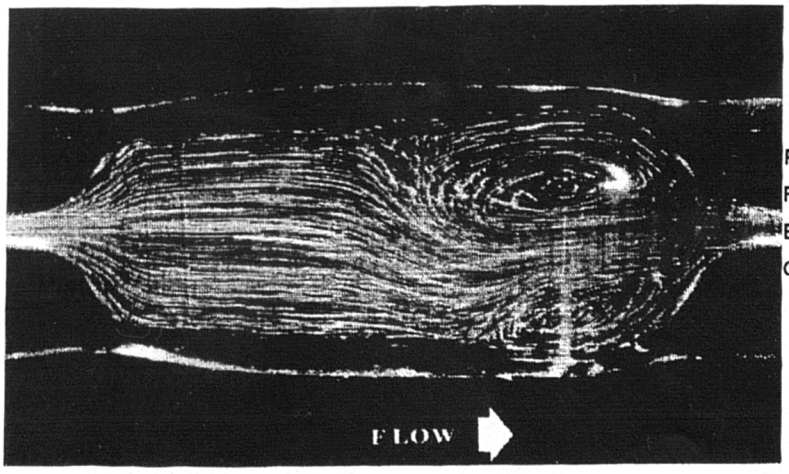

Plate 5.9
Flowrate : 60 ml/hr
Exposure time : 1 sec
Capillary wall shear rate :
780 sec-1

Plates 5.7 to 5.9 250ppm P'mer B flowing through profiled contraction apparatus

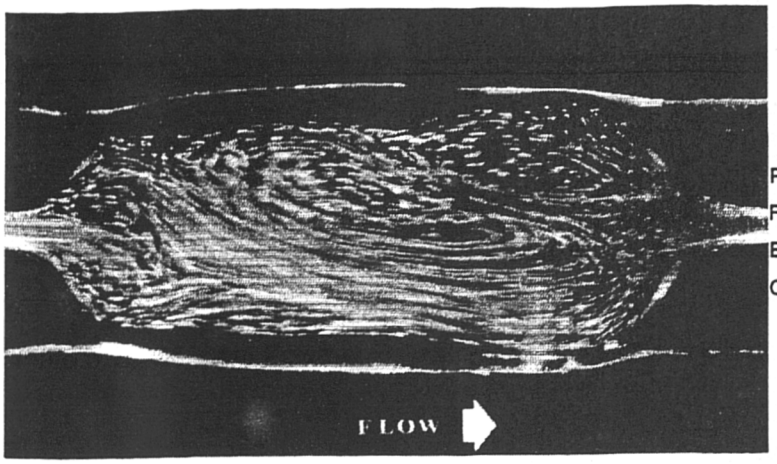

Plate 5.10
Flowrate : 436 ml/hr
Exposure time : 1/15th sec
Capillary wall shear rate :
5710 sec-1

Plate 5.10 250ppm Polymer B flowing through profiled contraction apparatus

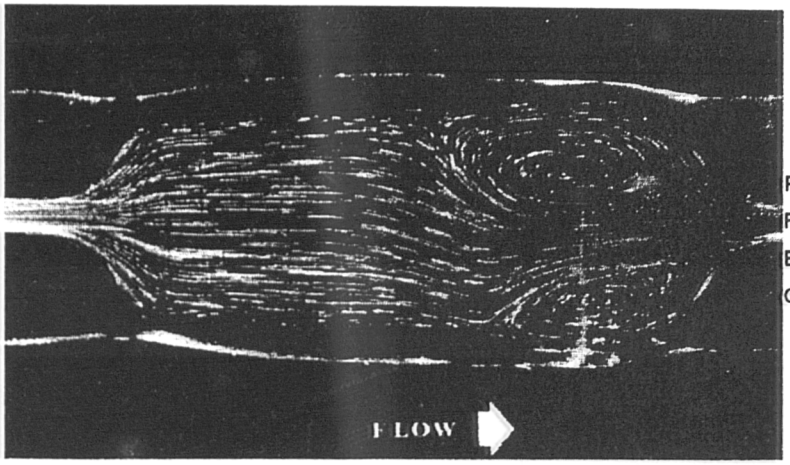

Plate 5.11
Flowrate : 34 ml/hr
Exposure time : 1 sec
Capillary wall shear rate :
440 sec-1

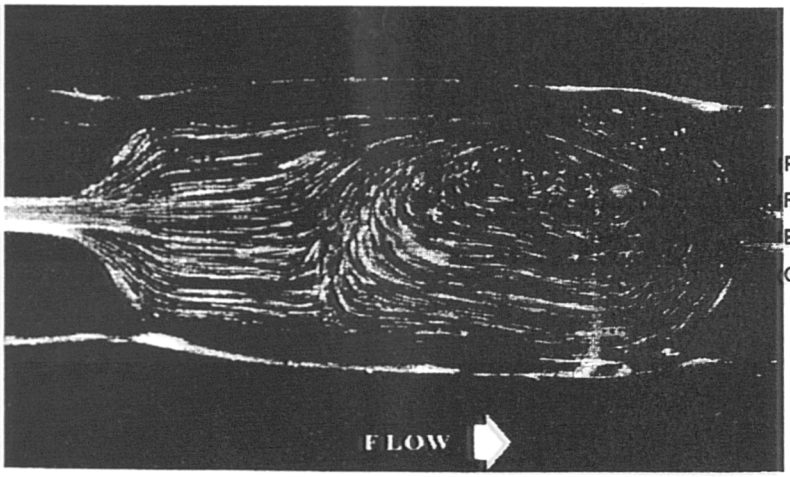

Plate 5.12
Flowrate : 133 ml/hr
Exposure time : 1/2 sec
Capillary wall shear rate :
1740 sec-1

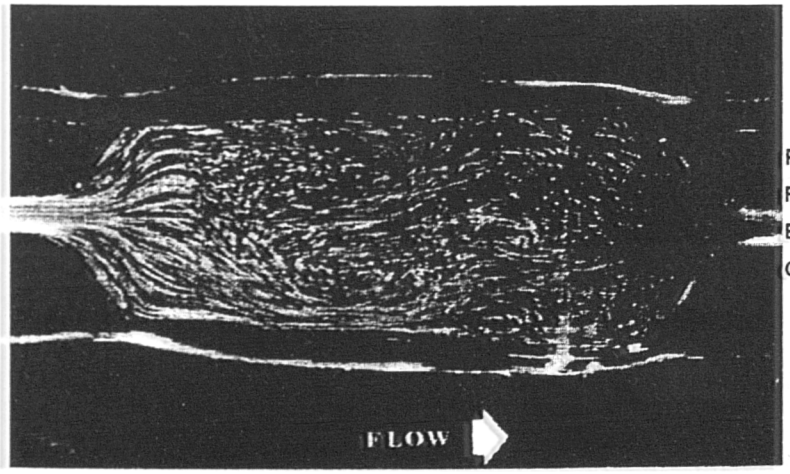

Plate 5.13
Flowrate : 240 ml/hr
Exposure time : 1/4 sec
Capillary wall shear rate :
3140 sec-1

Plates 5.11 to 5.13 500ppm P'mer B flowing through profiled contraction apparatus

5.5.2 Planar Contractions

A comparison between the low salinity brine and a 500wppm Polymer B solution are presented for this geometry. To enable an easy comparison of the effects of the visualised flow regimes, coefficients of the pressure drop per unit flowrate for the solutions are presented in figure 5.38.

Plates 5.14 to 5.19 illustrate the changes in flow regime that occur for the brine solution over the flowrate used. It can be seen from plates 5.14 to 5.16 steady laminar flow was achieved for the low flows. At the higher flowrates, plates 5.17 to 5.19, it can be seen that significant disturbances were created. These can be seen in the main in the form of a large separation region at the tail of the preceding rod. Vortex separation was observed in this region from flowrates of 1200 ml/hr upwards. At these flowrates there was a tendency for the fluid to flow primarily through the upper passage into the neighbouring passages. At the highest flowrates tested this became very pronounced with very little flow in the lower passage.

Plates 5.20 to 5.23 illustrate the changes in flow regime for the 500wppm Polymer B solution over a similar range of flowrates. It can be seen, as was the case for the flow of solvent, steady laminar flow was achieved in the lower flowrates. However, in comparison to the solvent which appeared to prefer to flow through the upper passage, the polymer solution flowed through the lower passage. This 'preference' for the lower passage can be seen in the very slow flow of plate 5.20, and is very obvious in plate 5.21, where the flowrate is about 2.25 times that in the previous plate. A similar increase in flowrate, to plate 5.22, creates a definite pattern, with very little or no flow actually moving through the upper passage. This effect cannot be attributed to unevenness in the flows approaching this passage throat, as it can be seen that the flows mix along the passage centre line. If this was the cause also, this would have been apparent for the solvent flow as well. The pattern stayed largely constant until the flow was increased to over 2500ml/hr, when the fluid appeared to switch between passages. Unfortunately, also at this level more light was being reflected and made photography very difficult. This switching effect can just be seen in plate 5.23. An explanation as to the cause of these observed phenomena can be found in chapter 6.

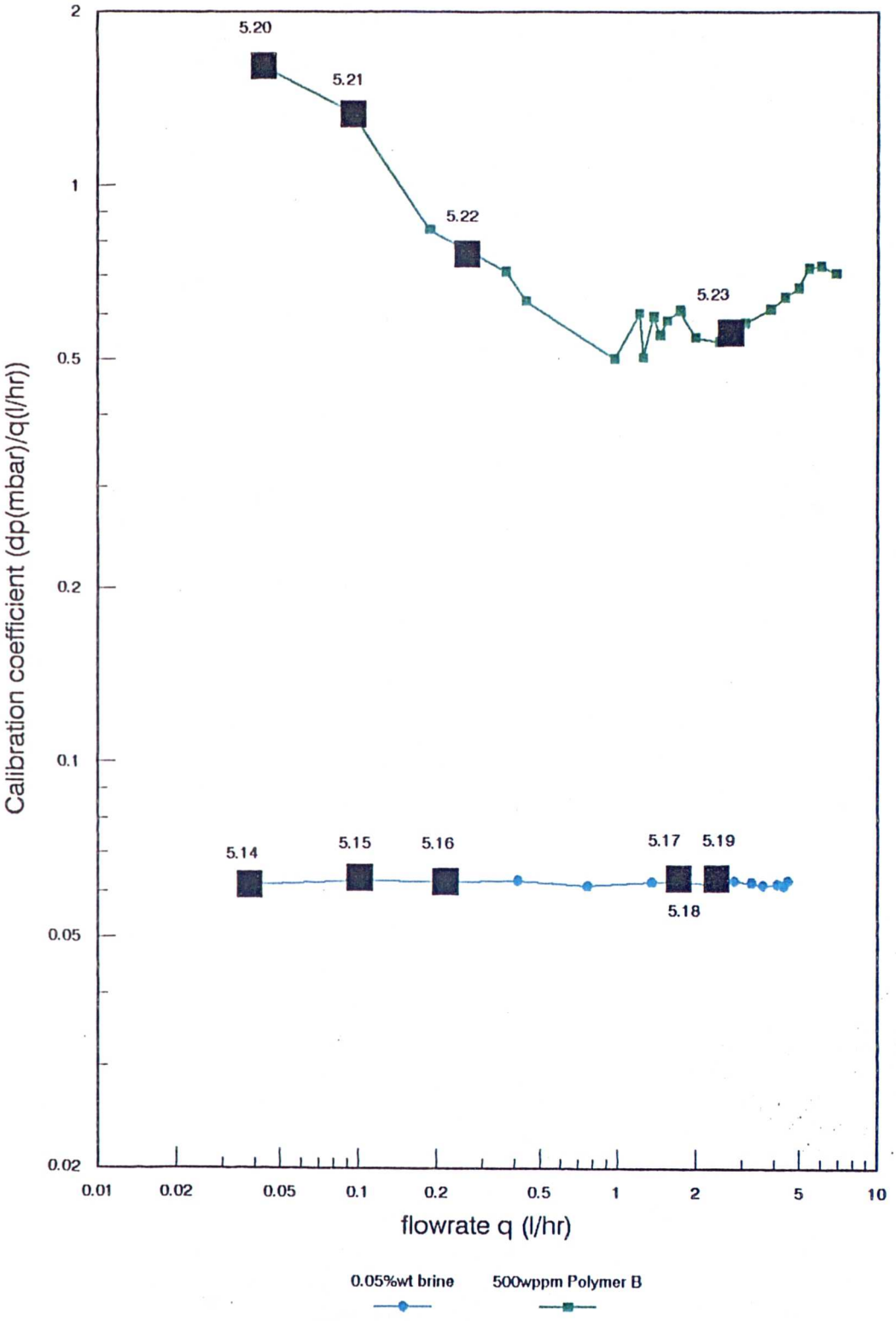

Figure 5.38 ΔP/Q coefficients to enable direct comparison between plates for the test solutions used (■ marks plate reference points)

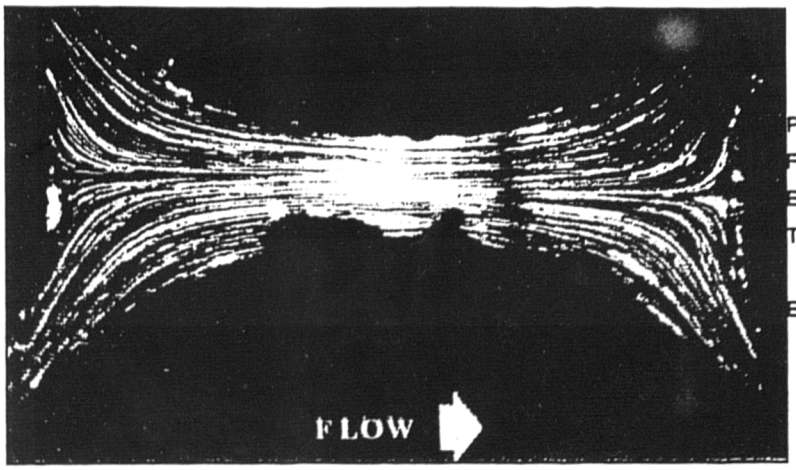

Plate 5.14
Flowrate : 39 ml/hr
Exposure time : 1/2 sec
Throat wall shear rate :
6.5 sec-1
Extensional strain rate:
0.5 sec-1

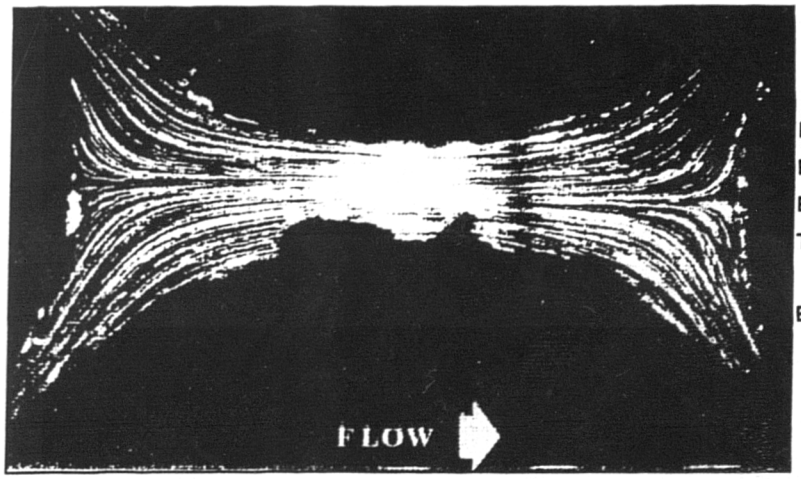

Plate 5.15
Flowrate : 98 ml/hr
Exposure time : 1/2 sec
Throat wall shear rate :
16.07 sec-1
Extensional strain rate:
1.3 sec-1

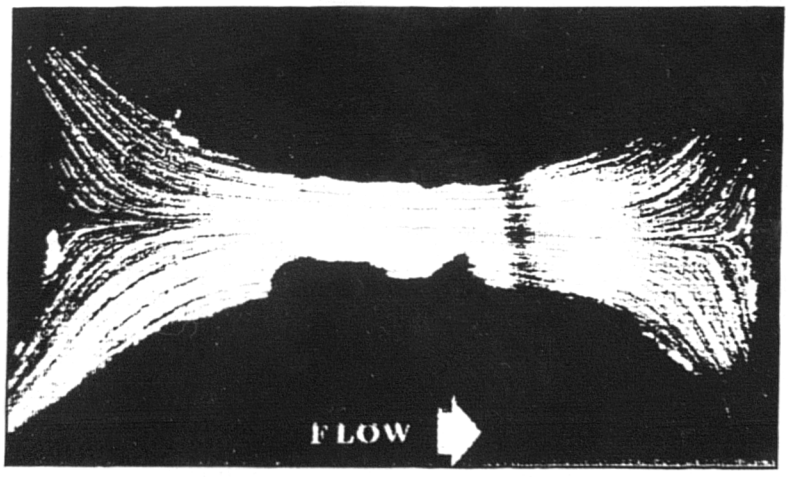

Plate 5.16
Flowrate : 212 ml/hr
Exposure time : 1/2 sec
Throat wall shear rate :
35 sec-1
Extensional strain rate:
2.9 sec-1

Plates 5.14 to 5.16 Brine flowing through planar contraction apparatus

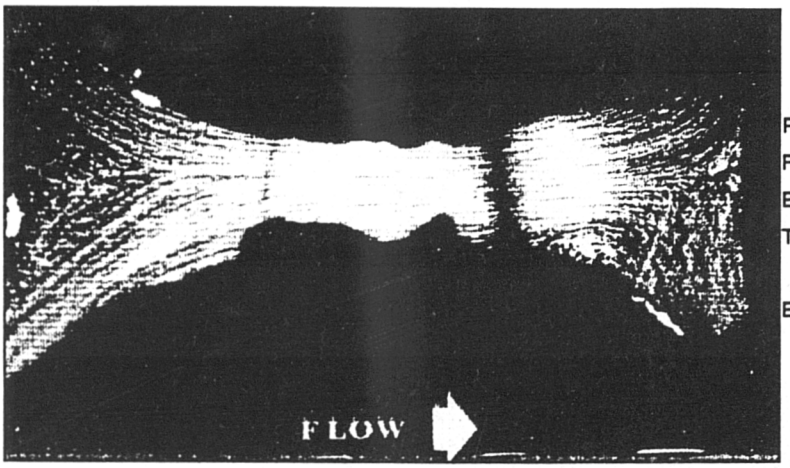

Plate 5.17
Flowrate : 1768 ml/hr
Exposure time : 1/2 sec
Throat wall shear rate :
291 sec-1
Extensional strain rate:
24 sec-1

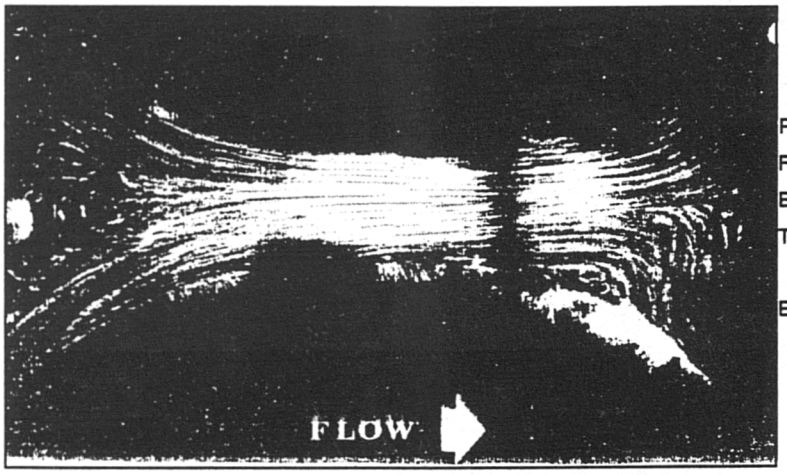

Plate 5.18
Flowrate : 1770 ml/hr
Exposure time : 1/30th sec
Throat wall shear rate :
291 sec-1
Extensional strain rate:
24 sec-1

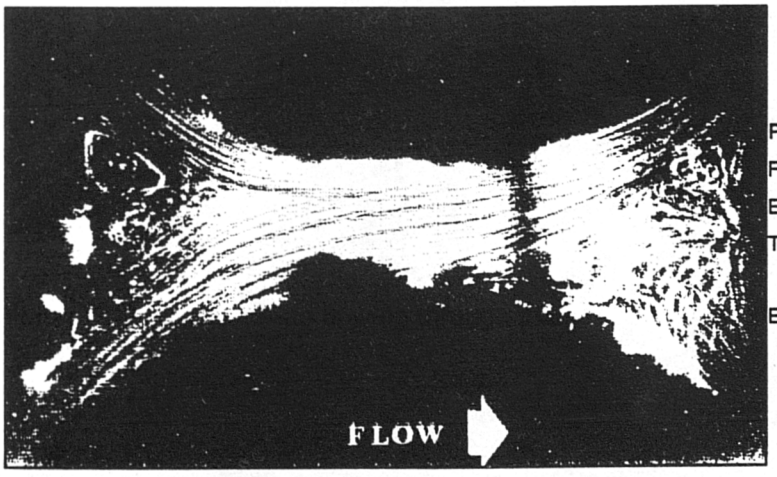

Plate 5.19
Flowrate : 2340 ml/hr
Exposure time : 1/30th sec
Throat wall shear rate :
385 sec-1
Extensional strain rate:
32 sec-1

Plates 5.17 to 5.19 Brine flowing through planar contraction apparatus

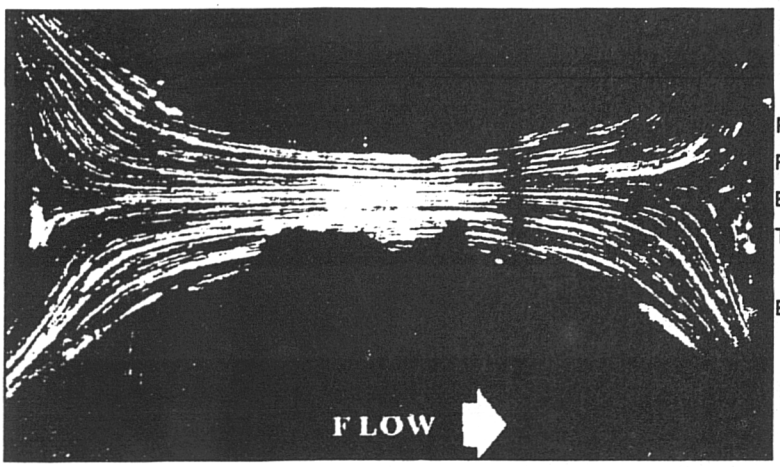

Plate 5.20
Flowrate : 42 ml/hr
Exposure time : 1/2 sec
Throat wall shear rate :
7 sec-1
Extensional strain rate:
0.6 sec-1

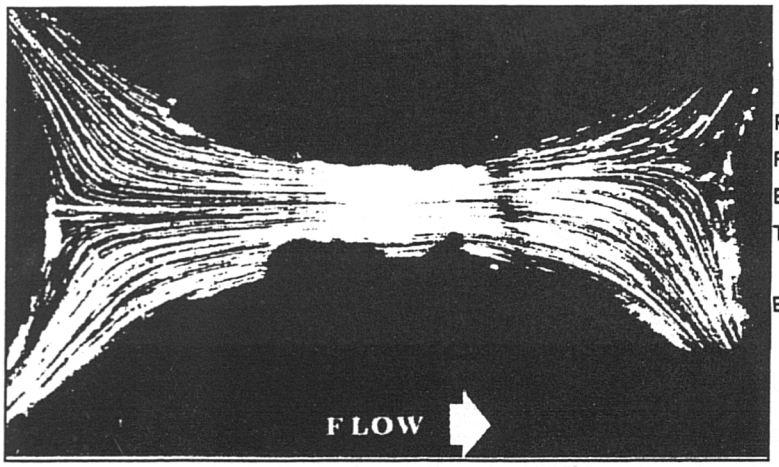

Plate 5.21
Flowrate : 94 ml/hr
Exposure time : 1/2 sec
Throat wall shear rate :
15.5 sec-1
Extensional strain rate:
1.3 sec-1

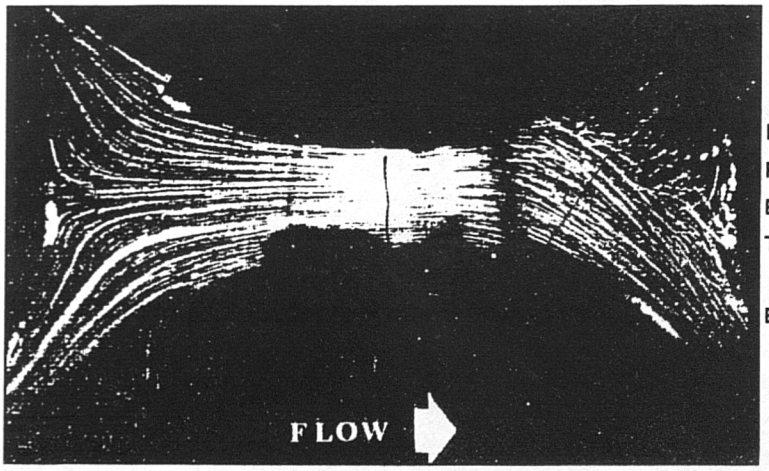

Plate 5.22
Flowrate : 266 ml/hr
Exposure time : 1/2 sec
Throat wall shear rate :
44 sec-1
Extensional strain rate:
3.6 sec-1

Plates 5.20 to 5.22 500ppm P'mer B flowing through planar contraction apparatus

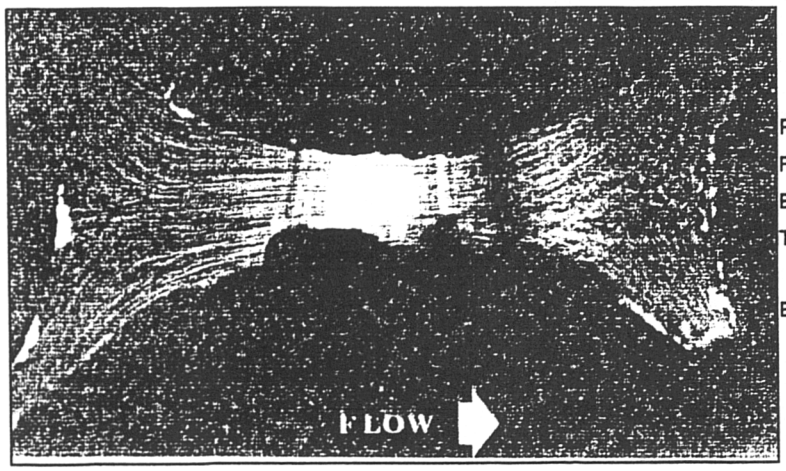

Plate 5.23
Flowrate : 2906 ml/hr
Exposure time : 1/15th sec
Throat wall shear rate :
281 sec-1
Extensional strain rate:
23 sec-1

Plate 5.23 500ppm Polymer B flowing through planar contraction apparatus

5.6 Comparisons of Equal Concentrations between Experiments

As was carried out for the case of the two sizes of rod arrays above, it should now be possible to compare solutions similar in concentration and solvent salinity. For the extensional strain analysis developed here to be correct the extensional behaviour observed in one experiment must match that found in others. We have already seen that good agreement between passages an order of magnitude is obtained through the rod array work. However, the passages in the bead pack are an order of magnitude smaller again.

Figures 5.39, 5.40 and 5.41 present the comparison of behaviour for the 100wppm, 250wppm and 500wppm solutions of Polymer B in the low salinity brine. As can be seen from the plots the behaviour does not quite reach such high extensional strains as were possible in the rod arrays. However the tendency does appear to be towards the rod array behaviour, with increases in flow resistance, rather than the continuation of shear thinning which was observed at lower flowrates. Obviously in a heterogeneous bead pack, at a given overall flowrate the flow in individual pores will vary from passage to passage as sizes will not be constant. This will result in apparent instabilities in the pressure trace as extensional stresses will be setup first in the smaller pores, which will create an increased pressure loss in that locality.

Figures 5.42 to 5.44 compare the behaviour of the 100, 250 and 500wppm Polymer B solutions in the high salinity brine. Extensional behaviour here is obvious, with quite good agreement in terms of onset extensional strains. Again, any spread in the bead size distribution will create uncertainties in the extensional strain analysis. However perturbations in the viscosity observations from the beadpacks are not obvious from these plots and so differences in pore flowrates were not significant. The most striking feature about these plots is the fact that the slopes of the extensional behaviour are so similar, particularly for the case of the 100wppm solutions.

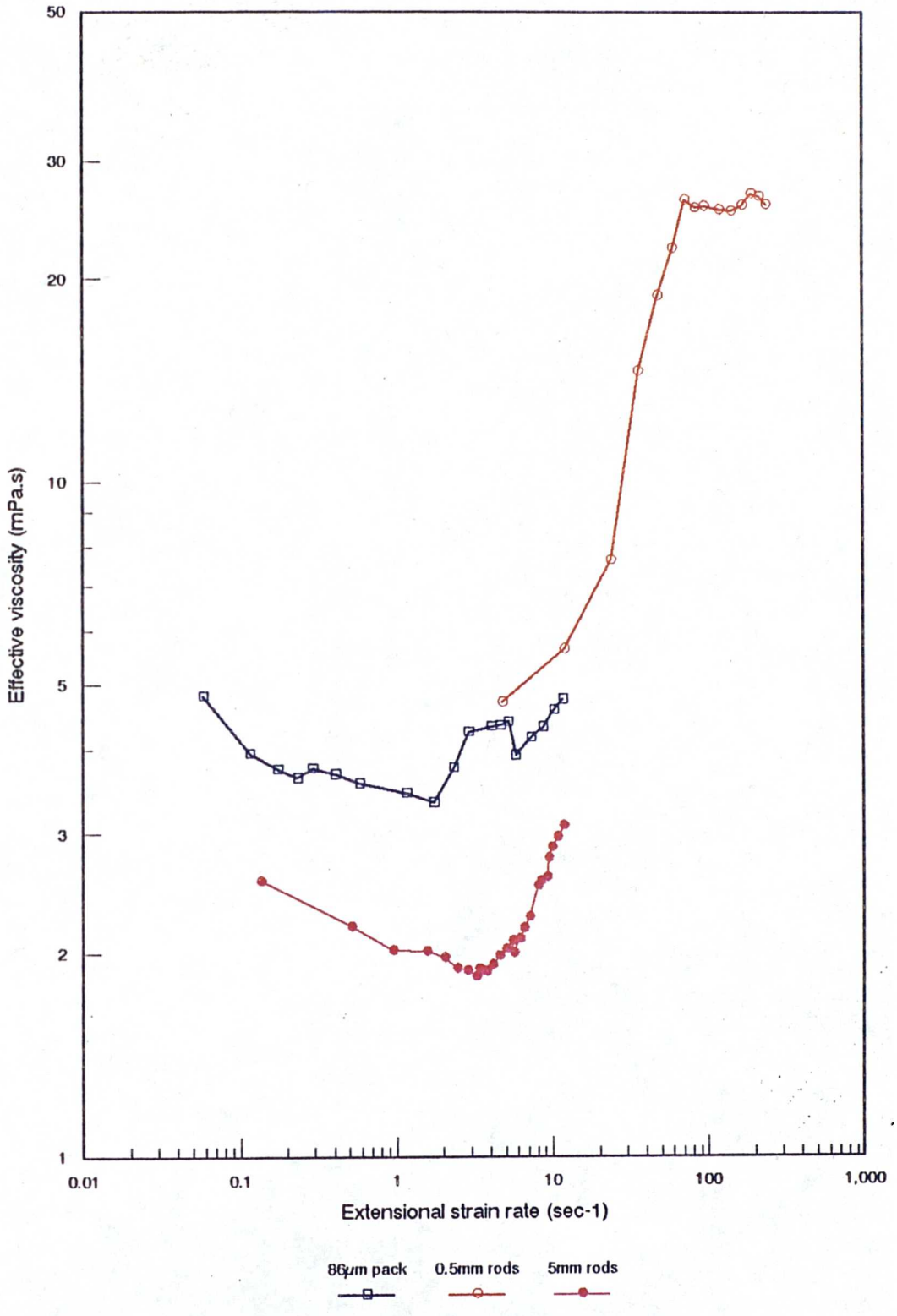

Figure 5.39 Comparison based on extensional strain rate $\dot{\xi}$ for 100wppm solutions of Polymer B in the low salinity brine between the 86μm bead pack and the rod arrays

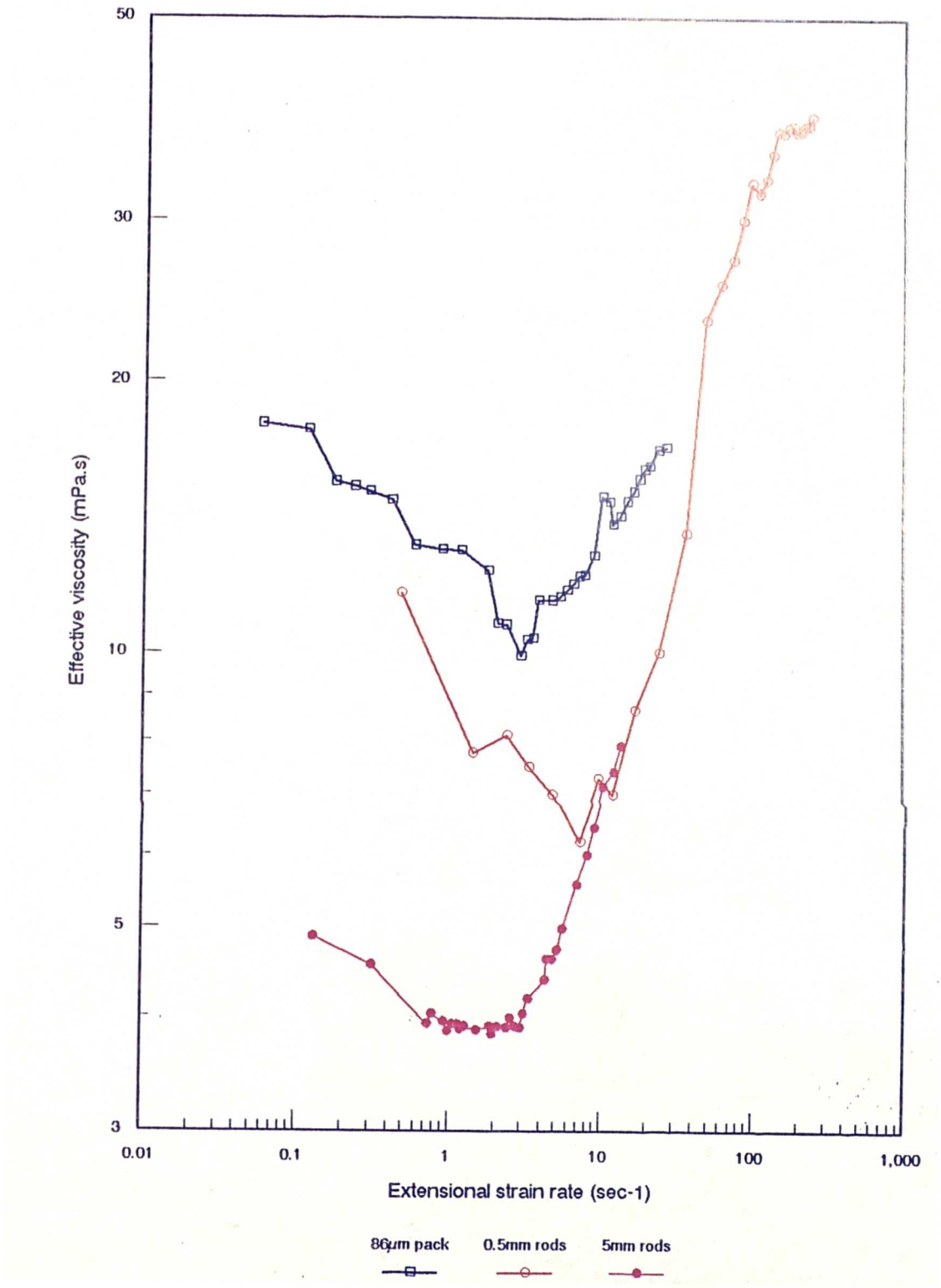

Figure 5.40 Comparison based on extensional strain rate $\dot{\xi}$ for 250wppm solutions of Polymer B in the low salinity brine between the 86μm bead pack and the rod arrays

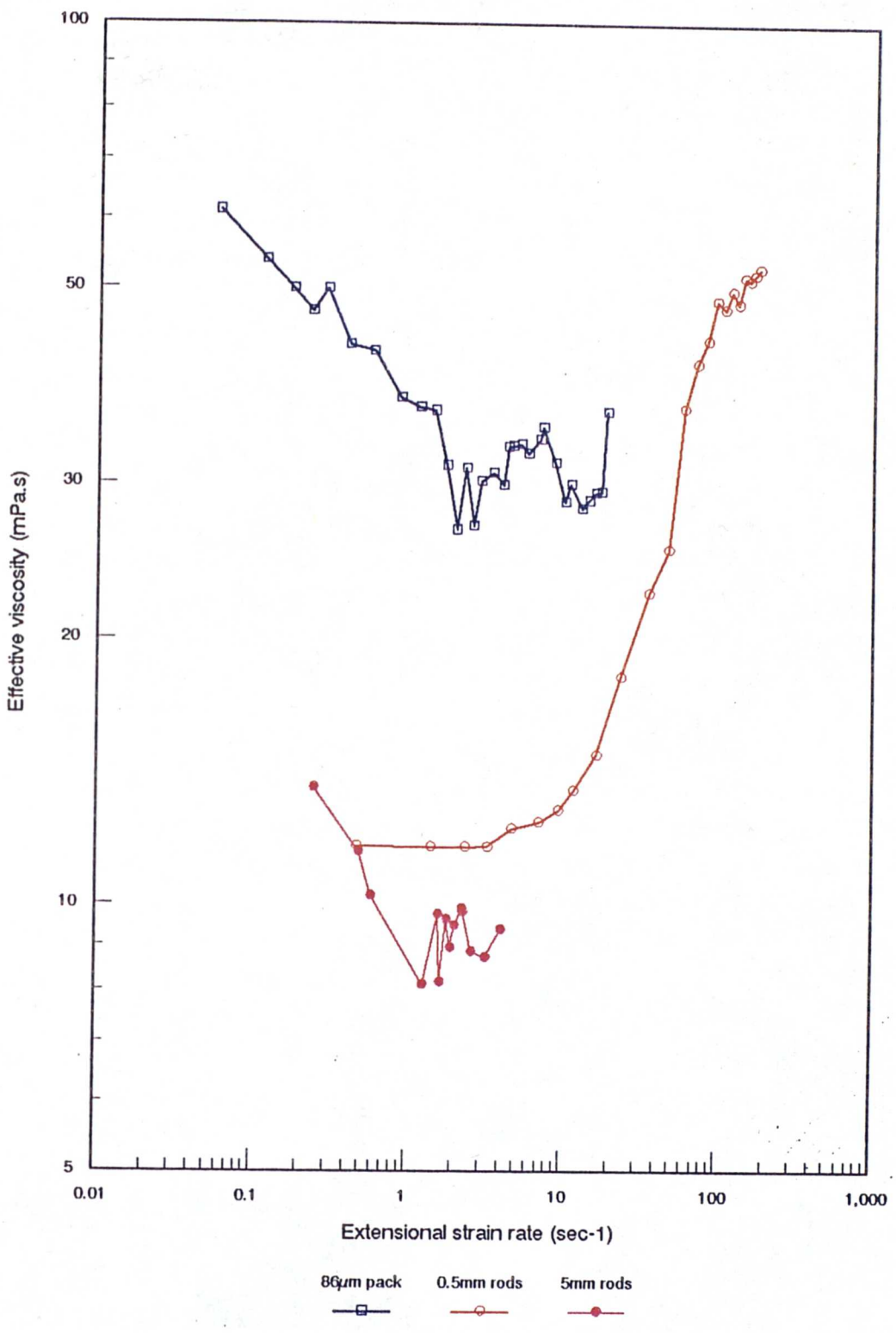

Figure 5.41 Comparison based on extensional strain rate $\dot{\xi}$ for 500wppm solutions of Polymer B in the low salinity brine between the 86μm bead pack and the rod arrays

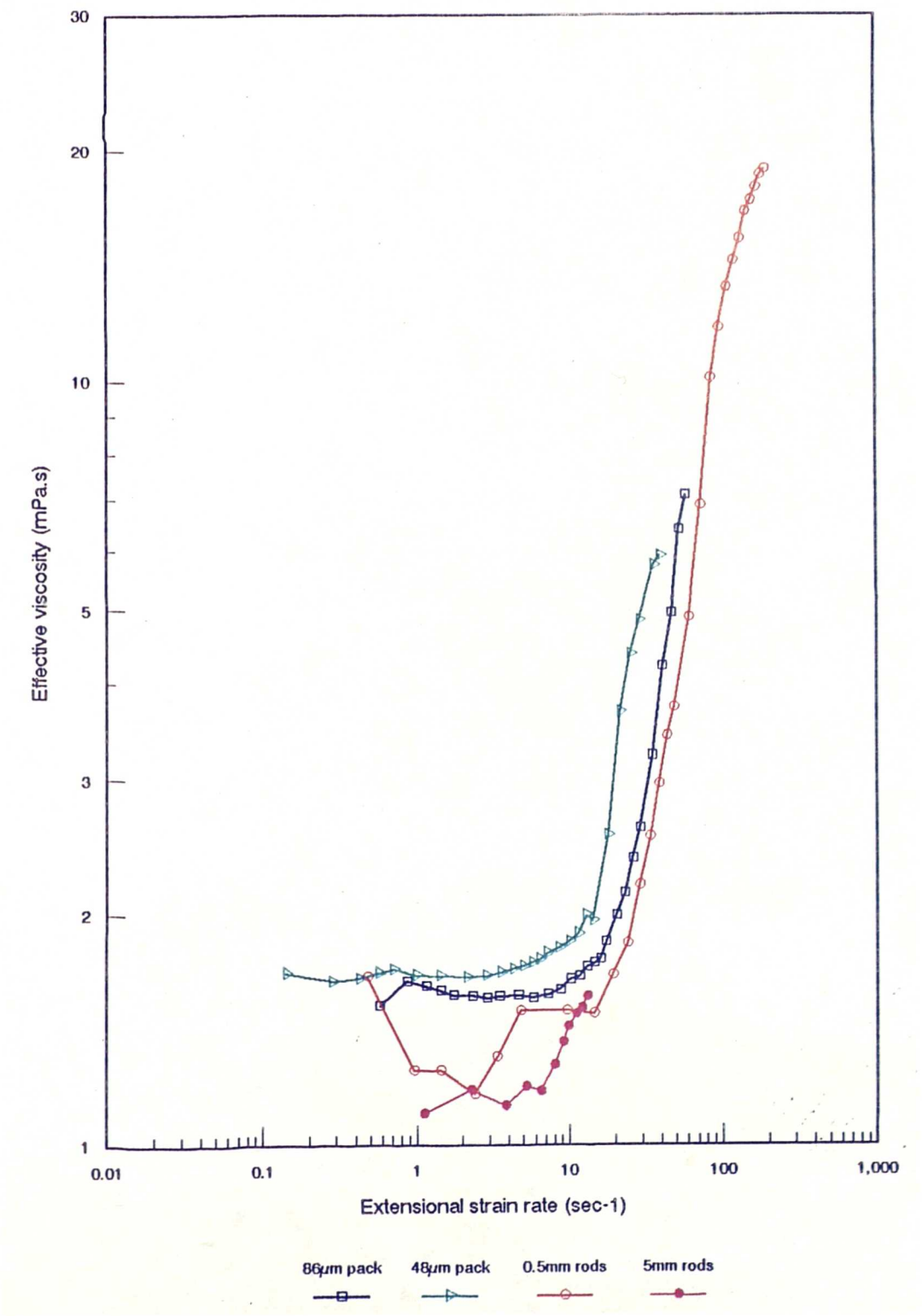

Figure 5.42 Comparison based on extensional strain rate $\dot{\xi}$ for 100wppm solutions of Polymer B in the high salinity brine between the bead packs and rod arrays

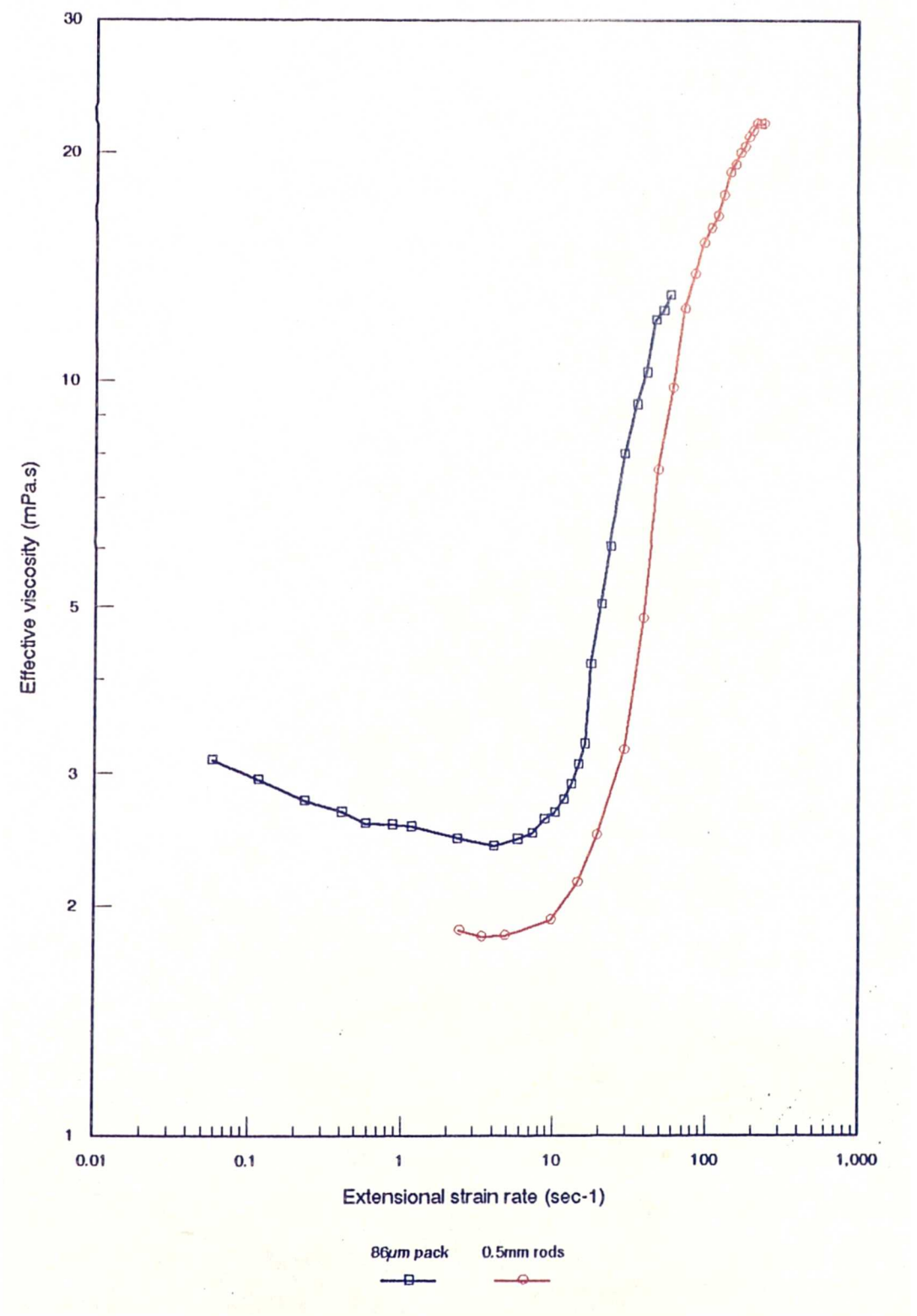

Figure 5.43 Comparison based on extensional strain rate $\dot{\xi}$ for 250wppm solutions of Polymer B in the high salinity brine between the 86μm bead pack and the small rod array

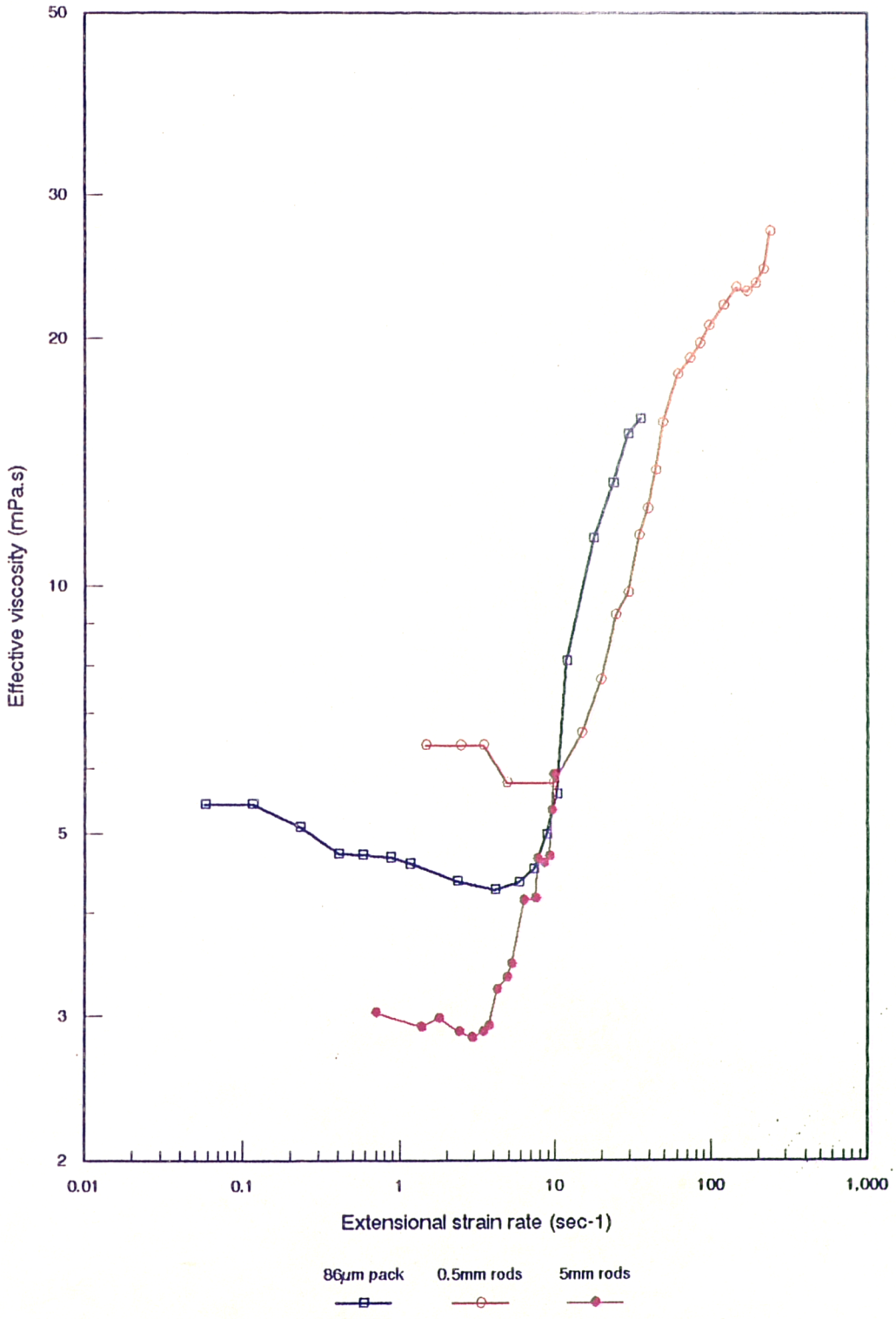

Figure 5.44 Comparison based on extensional strain rate $\dot{\xi}$ for 500wppm solutions of Polymer B in the high salinity brine between the 86μm bead pack and the rod arrays

5.7 Estimation of Errors

As such in all the tests only two variables were measured - flowrate and pressure. Temperature was measured for all the tests, and it is unlikely that errors greater then 0.5°C existed. At room temperature such a small difference would cause no more than a 0.5% change in the shear viscosity of the test solutions.
Errors in flowrate are possible as the flowrate was not constantly monitored. However, the pumps used were calibrated on a regular basis and were never out by more than 1%. If a leak existed in the system then this could seriously affect the results and so effluent flowrates were also monitored. Again, the error between the flowrate set on the pump and that measured was never greater than 5%, and usually less than 1.5%. If the flowrate was out by greater than 5% the run was stopped and the leak solved.
Pressure measurement was carried out using very accurate transducers with only a small range. The transducers were calibrated on a regular basis using the equipment described in chapter 4. Given that the linear micrometer scales read to within 1/100 mm the largest possible error in calibration would be from precisely contacting the water surface. Three water level readings at each height were taken. If one reading varied by more than 0.05mm the three readings were repeated. Thus given that both micrometers may have been out by the same amounts a maximum error of 0.1mm could have existed. Even for the lowest range transducer, 10mbar, this only represented 0.1% deflection and so it is very unlikely that errors above this size existed for the transducers themselves. The transducer output was always displayed on a 4 digit display, so again errors of less than 0.1% fsd are unlikely unless grossly misread. Obviously 0.1% fsd of a 200mbar transducer is 0.2mbar which for the majority of this work would be significant. To overcome this two transducers were used in parallel, one 200mbar and either a 20mbar or a 10mbar. This should reduce actual pressure measurement inaccuracies to less than 0.02mbar. Zero drift are most likely to contribute the most to pressure errors. Again the use of two transducers does reduce this somewhat. However zero drift was apparent with movements of upto 1% fsd. To counteract this problem a series of valves was set up around the transducers so that they could be zeroed insitu, by closing them off from the apparatus. It is possible that zero drift may have contributed pressure errors of upto 0.1mbar. This level of pressure drop was only observed for the very low flowrates in the bead pack, where shear stresses were dominant. In the areas of interest, that is around the onset of extensional behaviour, this 0.1mbar error does not represent more than 0.1%.

6. DISCUSSION

Conditions which affect the prediction of polymer flow resistance factors, or their apparent viscosity, will be discussed here.
Particular emphasis will be placed on the difference in flow regimes between the experiments and the consequences of this on the scale up of parameters.
Comparisons of these experimental results with those of published work are examined.
Factors affecting the viscoelasticity of polyacrylamide solutions in a constantly varying velocity field will be considered and conclusions drawn from the comparison of results from the different flow geometries.

6.1 Previous published works.

6.1.1 Axi-symmetric contraction flow.

Although several workers (26,30,21) have proposed similar geometries as an alternative to the capillary bundle representation of porous media flow, only a few have published results in such repeated geometries (56,58).
The importance of accelerating flows to die design has produced many papers on abrupt contraction flows of polymer melts, and of concentrated solutions as found in foodstuffs. These works, although applicable in terms of theoretical approach, will not be considered here.
Chauveteau and his co-workers have published work (56,58) where the contraction ratio, together with chamber length, and the number of such units was varied. A polyacrylamide, of molecular weight close to $7x10^6$ g/mol, was used in various solvents at 2% NaCl. For a given polymer concentration they found that the onset of *shear thickening behaviour* for different length/radius ratios and for differing numbers of contraction/expansions occurred at similar wall shear rates, which they called γ^*. The additional losses encountered at the entrance/exit pairs were accounted for in a term called the end pressure loss - a linear term equivalent to an extra length of capillary. Bagley (2) proposed a method by which this could be estimated by carrying out experiments in capillaries of the same radius but of differing lengths. This method was adopted and refined by Chauveteau to produce a relationship which required only one length/radius ratio to be used. One

drawback with this approach is that the polymer solution rheogram must already be known, as the relative viscosity (η_r) at a given wall shear rate is required. The relationship proposed by Chauveteau *et al* allowed the additional loss factor per contraction to be predicted.

Ghoniem (26) studied the flow of polyacrylamide, polyethyleneoxide and xanthan solutions in a plexiglass column having a succession of enlargements and contractions, as well as in a sand pack. Although the majority of his solutions were of higher concentrations (2000wppm), and in deionised water, his solution 8, a 400wppm partially hydrolysed polyacrylamide in 2% brine is comparable to those of this work. This solution exhibited upto a 10 fold increase in 'apparent viscosity' when flowed through the plexiglass model. No increases in observed viscosity were reported for the xanthan solution over the same flow range. A new group, S_G, was proposed to predict the onset of viscoelastic behaviour. S_G, equal to the ratio of the stretch rate multiplied by the inverse shear rate at the onset of pseudoplasticity to the residence time of the solution in the extensional flow field, was found to have a value of 100. This value, he found, was irrespective of polymer type, concentration and solvent conditions.

At a similar time, Choplin and Sabatie (11) carried out tests on solutions of Pusher 700, a HPAM with a molecular weight of 7 million, in a water/glycerol solvent. Rather than looking at tension thickening, they observed 'shear thickening', and postulated that it was caused by a change in molecular conformation from a statistical coil to a deformed coil state. The effect of this shear thickening results in only a marginal increase in effective viscosity with an increase of ~50%, opposed to that caused by the coil-stretch transition, where increases of more than 1000% are observed.

Most recently, work by Walters *et al* at UCW, Aberystwyth, has been published (44) with geometries similar to the abrupt interrupted capillaries of this work. The geometries used in their work consist of rectangular channels with obstructions placed in the flow path.

Although one of the obstacle sets, cylinders, is more akin to the next section of this thesis, all geometries will be considered here. Their S1 geometry, figure 6.1, resulting in two long narrow passages along the outside walls of the section, with a 10:1 contraction ratio, shows no increase in resistance for the very high molecular weight HPAM used. However, when these long narrow pores are broken up, and the flow allowed to expand momentarily, an increase in resistance is observed. The magnitude of these resistance factors was seen to increase with decreasing pore

length (that is an increase in the number of contractions).
Visualisation studies were also undertaken by Walters *et al* in the rectangular duct with a Newtonian liquid, a 1250wppm Xanthan solution and a 250wppm solution of HPAM.
The most noticeable difference between the flow of the solvent and that of the 250ppm solution of HPAM is that the polymer solution tends to affect the flow to a much lesser extent in the passages normal to the principal flow direction. Where the flow is disturbed it is only by the deflection of the streamlines and no recirculation zones are observable. This is in contrast to the flow of the Newtonian solvent, where strong vorticies dominate these cross passages. The 1250ppm solution of xanthan gum is very similar in flow behaviour to that of the Newtonian solvent.

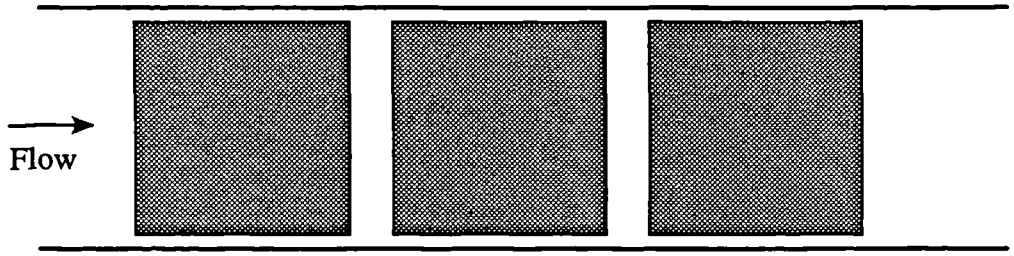

Figure 6.1 Geometry 'S1' as used by Walters *et al* in (44)

The second and third geometries used by Walters consist of either square or cylindrical obstructions placed as to present the flow with either a wide flow path and a low contraction ratio or a narrow path with the correspondingly much higher contraction ratio, as shown in figure 6.2. Once more comparing the flow of the Newtonian solvent to that of the HPAM solution highlights the ability of this polymer solution to depress the size of the stagnation region, by flowing around the obstacles as opposed by separating from them as in the flow of xanthan or the solvent. The flow of the polyacrylamide solution can also be seen to follow the path with the lowest contraction ratio, and hence extensional stresses, with very little flow passing through the narrow passages. This compares to the flow of the other solutions which appear to flow at a similar rate through both passages.

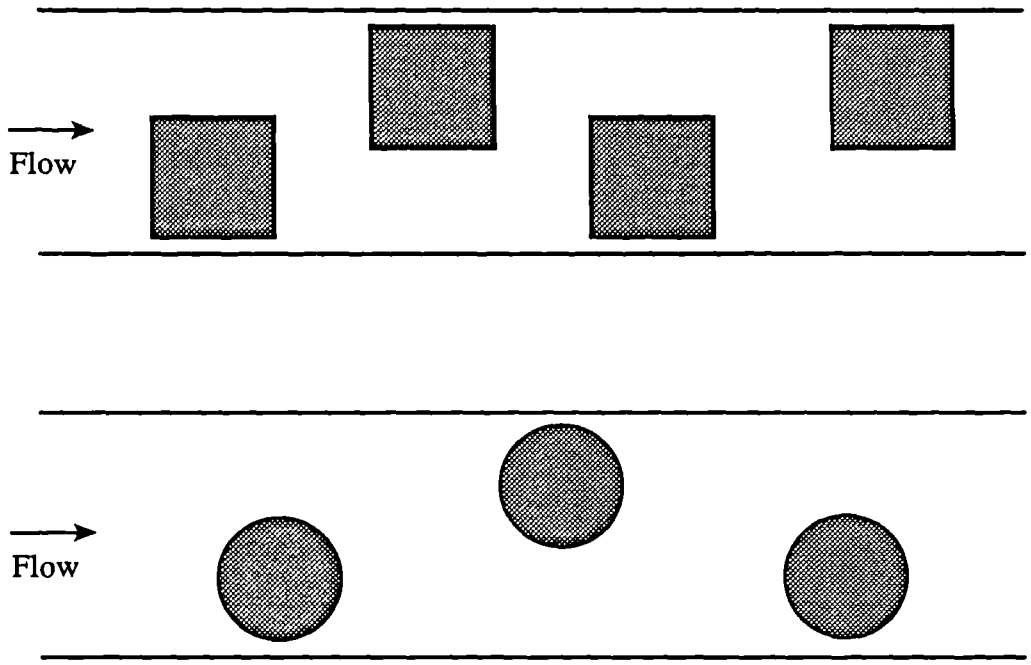

Figure 6.2 Square and cylindrical 'obstacle type' geometries as used by Walters *et al* in (44)

6.1.2 Planar Contraction Flow

This simple geometric configuration has not been used to a great extent in the literature. Barboza *et al* (3) did use cylinder arrays to study the flow of Seperan AP-30, a synthetic polymer with a molecular weight of around 1.5×10^6. Only one data set is presented, where they show that the 'additional viscosity' μ_{extra} was about three times that of the shear. It is likely that this extra viscosity was a form of extensional viscosity - the factor three is the same as the Trouton ratio between the shear and elongational viscosity of Newtonian fluids.

Vossoughi and Seyer published a paper in 1974 which used 36 rows of 6mm diameter glass rods with a wetted length of 56mm, which is a similar diameter to the larger flow cell used in this current work. A 2000 wppm solution of HPAM (Seperan AP273) was made in 'domestic tap water'. An approach was made to theoretically predict the behaviour, using areal porosity and tortuosity functions, by modelling the media as a bed of parallel plates. The tortuosity function, however, produced a value of 0.22, that is the path length would have to be less than the linear distance. A friction factor was defined which allowed the data to be presented in the usual Reynolds number format. No observable inertia effects were noted for the Newtonian solvents below N_{Re}=.1, using their definition. However the polyacrylamide solution did show considerable divergence, with a friction factor an order of magnitude greater than expected. Plotting these results against a Deborah number function, they obtained an onset criterion of N_{De}=0.2. Considering the crudity of their stretch rate analysis [(throat velocity-zero)/(distance between stagnation point and throat)] this results is surprisingly close to those of more recent publications and of this current work. Their comparison of the work to the results of others in sintered bronze disks with pore sizes at least an order of magnitude lower shows a difference in onset Deborah number of a factor of 3. The authors did acknowledge that visualisation studies in such a geometry 'may provide significant information concerning the effect of polymer elasticity on flow distribution and in immiscible displacements.

Visualisation studies have been carried out on single rods, or cylinders, in a free stream. However work on cylinders in regular arrays, or at only nominal spacings, have only been reported occasionally. The visualisation studies undertaken by

Barboza *et al* (3) used either two or five rods, of unreported diameter. Although the photographs are of only mediocre quality, the five rod array highlights the phenomena found in this current work that viscoelastic solutions tend to suppress the stagnation region to only a small zone. this observation can also be made of the work of Walters *et al* (44), where the 250wppm solution of polyacrylamide 1175 flows the obstacle contours much more closely than the Newtonian liquid or Xanthan gum solutions used.

6.1.3 Polyacrylamide flow through Porous Media

Glass bead, or ballotini, packs have been widely used to study fluid flow in porous media. An abundance of literature has been published on polymeric solution flow of both flexible coil and rigid rod polymers.

Although widely used in the field in the USA, little literature has been published on polyacrylamide flow through rock cores. Much work, however, has been carried out and reported on the flow of xanthan solutions in both outcrop cores, such as Berea and Clashach, and in reservoir cores (7,14,35,36).

Since the developments by Christopher and Middleman in 1965 many papers have been published which present data in the form of a bed Reynolds number plotted against a friction factor (12). More recently, work by Durst, Haas *et al* in Germany has concentrated on presenting the data with a normalised resistance factor plotted as the absicca. Their work in the main has used dilute solutions of polyacrylamide (concentration range 10→200wppm) in packs of beads varying in diameter from 200 to 5000μm. They found that the onset of elongational behaviour, using the definitions of extensional strain, occurred at a Deborah number of 0.5.

Chauveteau *et al* (9) on the other hand characterises onset as when the inverse of the maximum stretch rate overcomes the polymer relaxation time (Hence N_{De}=1.0). They then state that this only indicated a tendency for the macromolecules to stretch in the flow direction.

Extensional behaviour, that is an increase in apparent viscosity beyond that of the bulk, has been reported by Durst, Haas *et al* in solutions as low as 10wppm polymer (22). A similar polymer concentration also exhibited large increases in the opposed jets set up of Odell *et al* (97). Such concentrations are deemed dilute (that

is $C\times[\eta]<<0.1$), and as such little or no molecular chain interaction occurs. Thus the observed increases are due to the summation of the energies involved in stretching the individual molecular chains, in contrast to chain A acting on chain B etc, which would result in an effective molecular weight many times that of one chain.

In all of the literature concentrations of 100wppm or greater in high (>1%) ionic strength solvents have indicated increase in flow resistance of an order of magnitude or greater. These increases diminish with solvents of lower ionic strength. Polymer concentration has also been shown to affect behaviour - working with a bead pack of 392μm diameter ballotini Interhal and Haas in 1981 reported a decrease in onset Reynolds Number with increasing polymer concentration. Their work also reported a decrease in the maximum normalised resistance factor with lower polymer concentrations.

6.2 Observed flow phenomena

The observed phenomena of dilatency exhibited by certain polymer solutions flowing through porous media is usually attributed to molecular elasticity. Fluids that display viscoelasticity, that is a resistance to deformation (viscous) and reversible stress/strain behaviour (elastic) are therefore dependent on changes in pore geometry, and on the time it takes for the changes to occur. Obviously polymer solutions with short relaxation times have to be strained to a greater degree before displaying elastic behaviour in a flowing situation, than those which recoil more slowly. This can be seen by comparing solutions of the same polymer in different solvents. Polyelectrolytes tend to coil more tightly as the ionic content of the solvent increases, screening charges along the molecule's length, thereby reducing the electrostatic repulsions between the charged sites. This results in a lowering of the relaxation time, as the chain can recoil more rapidly. Conversely it is more difficult to stretch the chain in the first instance, and hence a higher strain rate has to be applied before the chain will uncoil. Thus for a given porous matrix, observance of extensional behaviour would be expected to occur at a lower flowrate than one with a higher salt concentration. Allied to this is the extent to which the chains can be unravelled - in low ionic strength solutions the molecule

exists in a more open manner, and therefore has less uncoiling to do than a more tightly entwined one. This accounts for the greater increases seen in solutions made up in more concentrated brines.

6.2.1 Axi-symmetric contraction studies

Observations of the flow patterns found in the capillary geometries used in this work provide a useful background for understanding the complexities of viscoelastic flow. As could be seen from the plates in the previous chapter, at low flowrates all solutions exhibited purely viscous laminar flow. At higher flowrates, however, increasingly different flow patterns were observed, with the more concentrated polymer solutions exhibiting dramatic contraction vortex growth. The growth of these vorticies, dependant on both flowrate and polymer concentration can be seen to occur as the behaviour diverges from that of the solution in pure shear. Thus it may be said that the inception of these contraction vorticies indicates a change in flow regime from that of shear to a mixture of shear and extensional flows. Once contraction vortices become established and extensional behaviour dominates then small increases in flowrate result in proportionately larger increases in the recorded pressure differential. Conversely it can be said that larger increases in the applied stress (driving/differential pressure) become necessary to produce small increments in flowrate. Thus for a given flow increment the stresses set up in the flow will be greater when the fluid is undergoing extensional flow then if it was in pure shear. Trouton (74) noted this, finding that for a Newtonian fluid the resultant extensional viscosity was three times the magnitude of its shear viscosity. Therefore for a fluid flowing through a continuously changing diameter pore, the lower energy state, and hence the preferred state, will be one of shear and not of extension. If we now consider how vortex length affects the magnitude of extensional strain, it is possible to see how extensional stresses are minimised by increasing the distance over which the contraction occurs.

Figure 6.3 shows the extensional strain regime for 6 typical vortex lengths for a 10:1 abrupt contraction - it can quickly be seen from the lower plot that the extensional strain at a given flowrate is dramatically reduced when the length over which the contraction occurs is extended. The peak extensional strain for the 0.5mm vortex length is 10.3 times that experienced when the contraction length increases to 5mm.

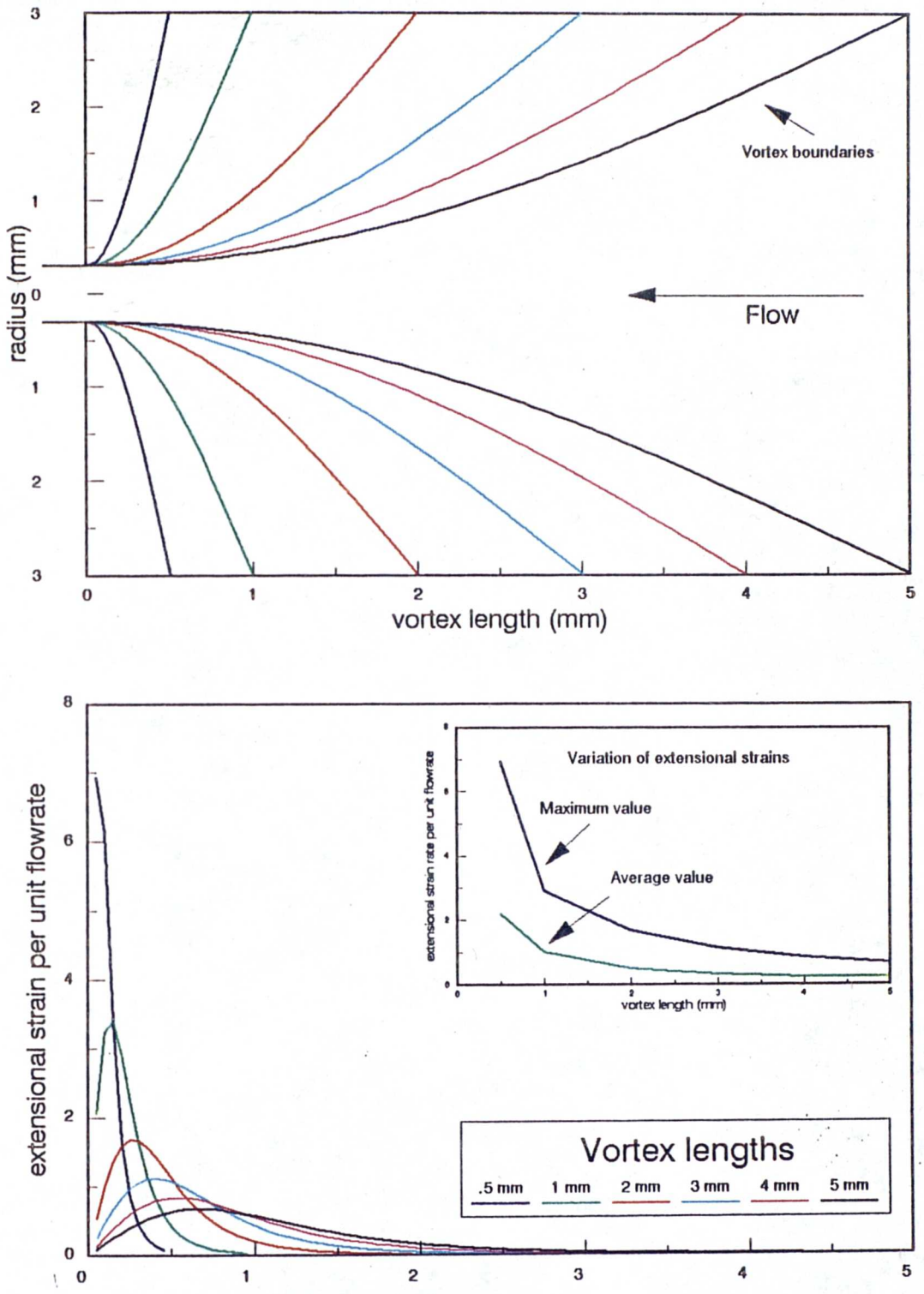

Figure 6.3 Variation in extensional strain with increasing vortex length

If we now consider the effect the extensional stress component has on the flow in terms of total applied stress, and hence apparent viscosity.
Consider that both shear and extensional stress components may be represented by a power law, with the exponent for the shear stress less than unity, and greater than unity for the extensional case.
It can be said in the case of a time averaged steady state that;

$$\sigma_{total} = \sigma_{shear} + \sigma_{extensional}$$

replacing the shear and extensional components with power laws give,

$$\sigma_{total} = \kappa \dot{\beta}^n + \lambda \dot{\beta}^m$$

where $\dot{\beta}$ is the strain rate. Now, replacing the power laws by viscosities,

$$\sigma/\dot{\beta} = \eta_{shear} + \eta_{ext}$$

or,

$$\eta_{total} = \eta_{shear} + \eta_{ext} \qquad - 6.1$$

The results of this can be seen in figure 6.4, where it is clear that at low rates of strain shear behaviour dominates, but as the rate of strain is increases extensional forces become the more dominant. A more detailed discussion on these effects can be found later.

If we now use the Carreau model for shear viscosity to replace the term in equ 6.1 above, and define the extensional behaviour as a power law, with slope m, and constant λ, we get;

$$\eta_{eff} = \frac{\eta_0}{(1 + (t_1\dot{\gamma})^2)^{(1-n)/2}} + \lambda \dot{\zeta}^m \qquad - 6.2$$

where η_{eff} is the observed viscosity.

If we now consider the flow in the capillary chambers once more, we can see that by limiting the rate of extensional strain it is possible that the total fluid stresses and therefore the observed viscosity will be reduced. Once the extensional viscosity becomes dominant the fluid can have two different flow regimes which result in the same overall applied stress.

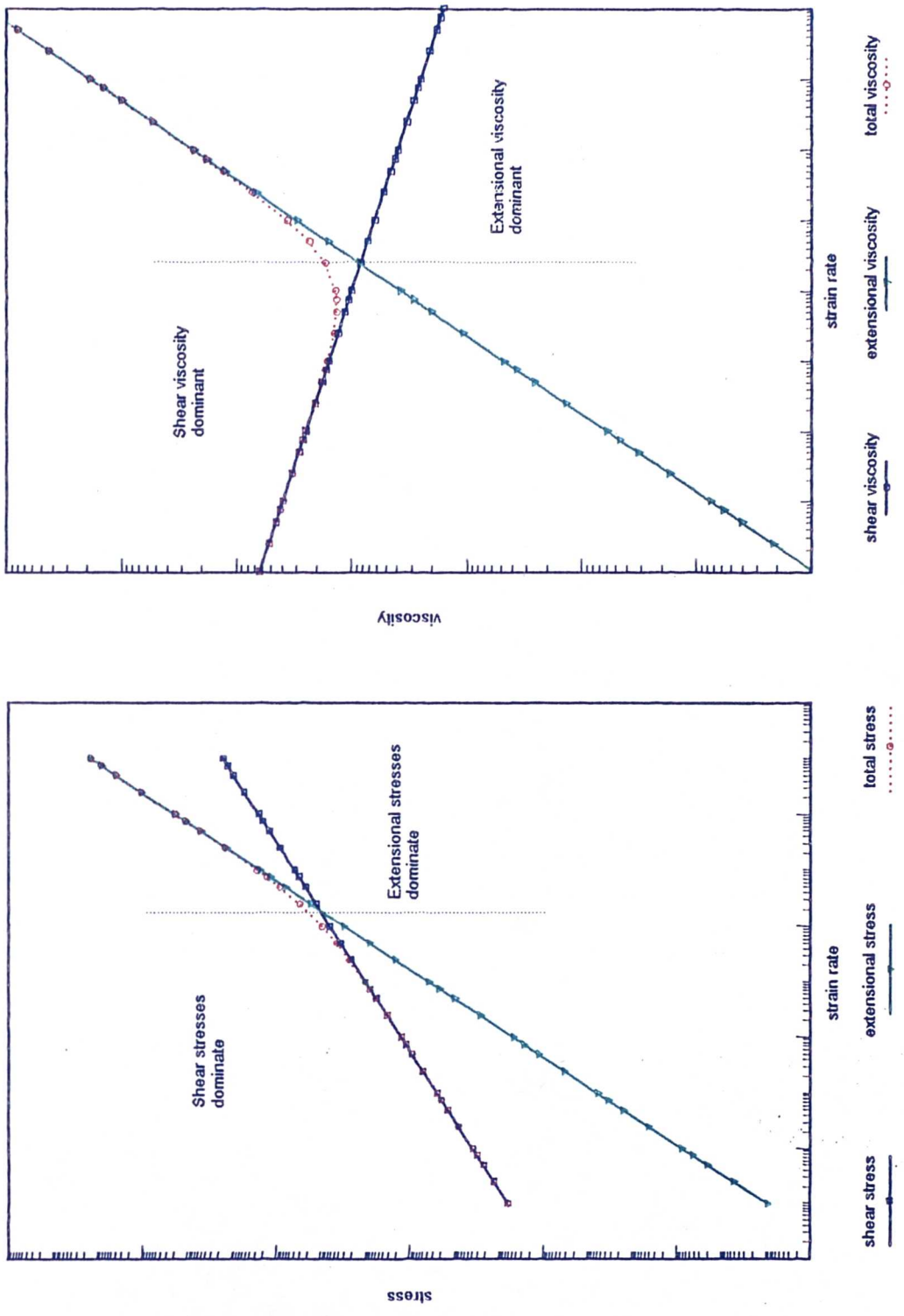

Figure 6.4 Summation of stress components and viscosity components

As the vortex length increases in order to decrease the extensional stresses, a point is reached where the flow from the inlet to the chamber begins to affect the flow, as shown in figure 6.5 below. Upon a further increment in flowrate the vortex cannot grow and hence extensional stresses significantly increase. However, a similar stress level could be reached if shear stresses were increased as significantly. Now, as the polymer solutions are in general shear thinning, the rate of change of shear stress with flowrate decreases as the flowrate increases, and as such the flowrate would have to significantly change to produce such a change in stress (- this increase in flowrate would also cause a further increase in extensional strain leading to a growth in that stress as well). Clearly this cannot happen, however shear stresses can be increased by keeping the same flowrate but by increasing the length over which the shear occurs. As was mentioned above, the shear viscosity of these solutions is higher at low strain rates, which are found for instance in the vorticies, which create two distinct flow regimes, with the flow in the centre flowing much faster. Thus by the setting up of 'shear tubes' where the fluid, still taking the path of least resistance, actually creates a tortuous tube within the expansion chamber the same overall stress level can be achieved. This can be schematically seen in figure 6.6, or in plates 5.6, 5.10, 5.12 and 5.13.

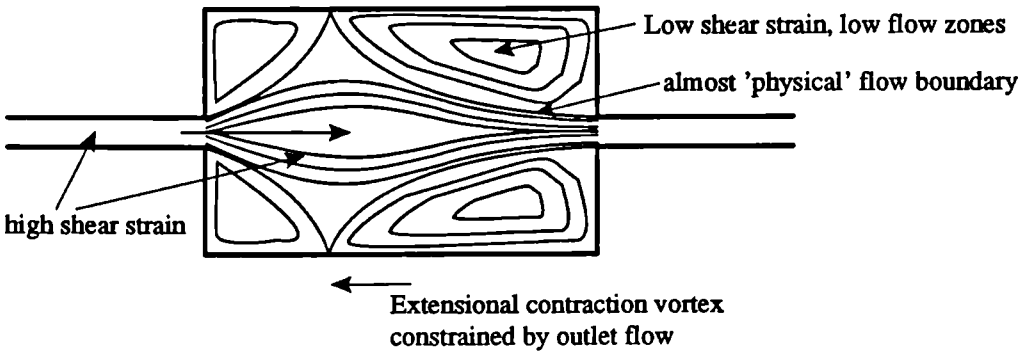

Figure 6.5 Impingement of contraction extensional flow vorticies on the flow expansion from the capillary.

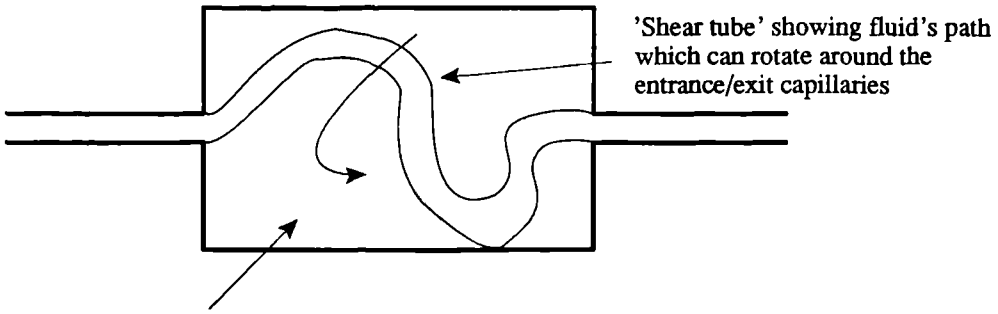

Figure 6.6 Schematic diagram of 'shear tubes' as found in the capillary expansion/contraction flow.

This phenomena produced other interesting results which were not recorded on file. Rather than forming a single tube, occasionally bifurcated flow was formed, with the two tongues of flow rotating not only axially but also radially. Fluid rotation was noticed on a number of occasions, this was particularly obvious when a small air bubble became trapped in the contraction vortex and was seen to rotate about axially. Rotation of the fluid once it had formed the apparent shear tube was the rule, which made recording the image difficult when only illuminating a single plane, - at the higher flowrates the flow appeared to stop in the plane of view.
This limiting of the extensional stresses can be clearly seen from the variation of effective viscosity with flowrate (figures 5.14 to 5.17). A similar effect, but due to a different reason, was observed for the solvent (Newtonian) flow. At very high flowrates the fluid inertia gained in the fine bore capillaries was sufficient to cause a jet which reached the following capillary entrance. This is apparent in plate 5.3, where very high velocities can be seen in the inertia jet, with much lower velocities in the annulus.
Other workers whilst observing increases in effective viscosity in such apparatus for dilute polymer solutions have not commented on this stress limiting behaviour.

6.2.2 Planar contraction studies

The flow regime set up in the flow through the rod arrays is clearly one where extensional forces are always present. By forcing the fluid to flow in a tortuous fashion reduces the possibility of stress limiting changes as were described above. Comparison of the flow visualisation studies does show a difference in behaviour, with the 500wppm polymer solution suppressing the stagnation region, as was seen in the work of Walters *et al*. If plates 5.16 and 5.22 are compared, where the flowrates through the cell are at a similar value, the effects of shear thinning on the flow can be clearly seen. The flow of the brine is almost equally divided between the two exit passages. This is in complete contrast to the 500wppm polymer case, where the majority of the flow is seen to pass through the lower passage. This effect can also be seen in plates 5.15 and 5.21. This can be attributed to shear thinning only because the passage widths were found to be 10% different - the centre of the right hand rod was misplaced by around 0.1mm. This difference in passage width results in a higher shear strain rate for a given flowrate in the lower passage, which for shear thinning solutions results in a lower fluid stress. Conversely, if plates 5.19 and 5.23 are compared the fluid is now flowing in both cases through the upper passage. As can be seen from figure 5.38, the flow in plate 5.23 is entering the extensionally dominated flow regime. This now means that where flowrates through individual passages are higher compared to its neighbour, the extensional stresses produced result in an increased fluid stress. Thus by flowing through the other, larger passage marginally smaller extensional stresses are exerted. Although not captured on film the flow was seen to oscillate between these two passages, where for a while a reduction in stress was possible by switching to the passage that had little or no flow, and thus was seeing a much reduced extensional strain. As the flow in this passage increased a point was reached where less resistance was offered by the other passage. Plate 5.23 also illustrates the stagnation zone size suppression where the streamlines are seen to follow closely the rod's form, rather than separate as for the solvent (plate 5.19).

The viscosity characteristics observed in these rod arrays produces dramatic changes of slope when sufficient extensional strains are encountered. The smaller cell was of particular use here enabling quite accurate determination of the exact point of departure from the shear viscosity curve.

As can be seen in figure 5.23 the magnitude of the peak viscosity is dependant on polymer concentration. However, for all but the lowest polymer concentrations the slope of the extensional flow curve is constant within experimental limits. As was mentioned in chapter 5, the 5 and 10wppm solutions can be considered totally dilute with no chain-chain interactions. Higher concentrations, however, cannot be considered as isolated molecules with chain-chain interactions resulting in a non linear increase in peak reading with concentration. Similar results to the variation in peak viscosities have been recorded by Durst and Haas with solutions of polyacrylamide with a 13.5 million molecular weight flowing through a 392μm bead diameter pack. Quantitative comparison of the two polymers is not possible because of the differences in molecular weight and in solvent ionic strength, however there is at least a qualitative agreement between the results, as shown in figure 6.7 below. Similar observations about the slopes of the extensionally dominated regions can be made for their work, with solutions of 25, 50, 100 and 200wppm increasing at uniform rates.

Peaking of the viscoelastic behaviour has been attributed to stretch limit in the dumbbell model of the molecular chain, as proposed by Bird *et al* (5). However, it is possible that this expression which includes an empiricism over compensates for limits on the extensional stresses which are due to changes in flow regime. It is not the intention of this work to study peak effective viscosities for viscoelastic fluids. Once extensional behaviour is dominant, that is some change in conformation has occurred, the effect of the solvent ionic strength becomes less significant. The variation of slopes of the curves in figure 5.24 between 0.05%wt brine to 10% brine is less than 10%. It is possible that this result does mask some effect of the solvent may have on the extensional behaviour as slopes with a greater variation were found in the screen factor work.

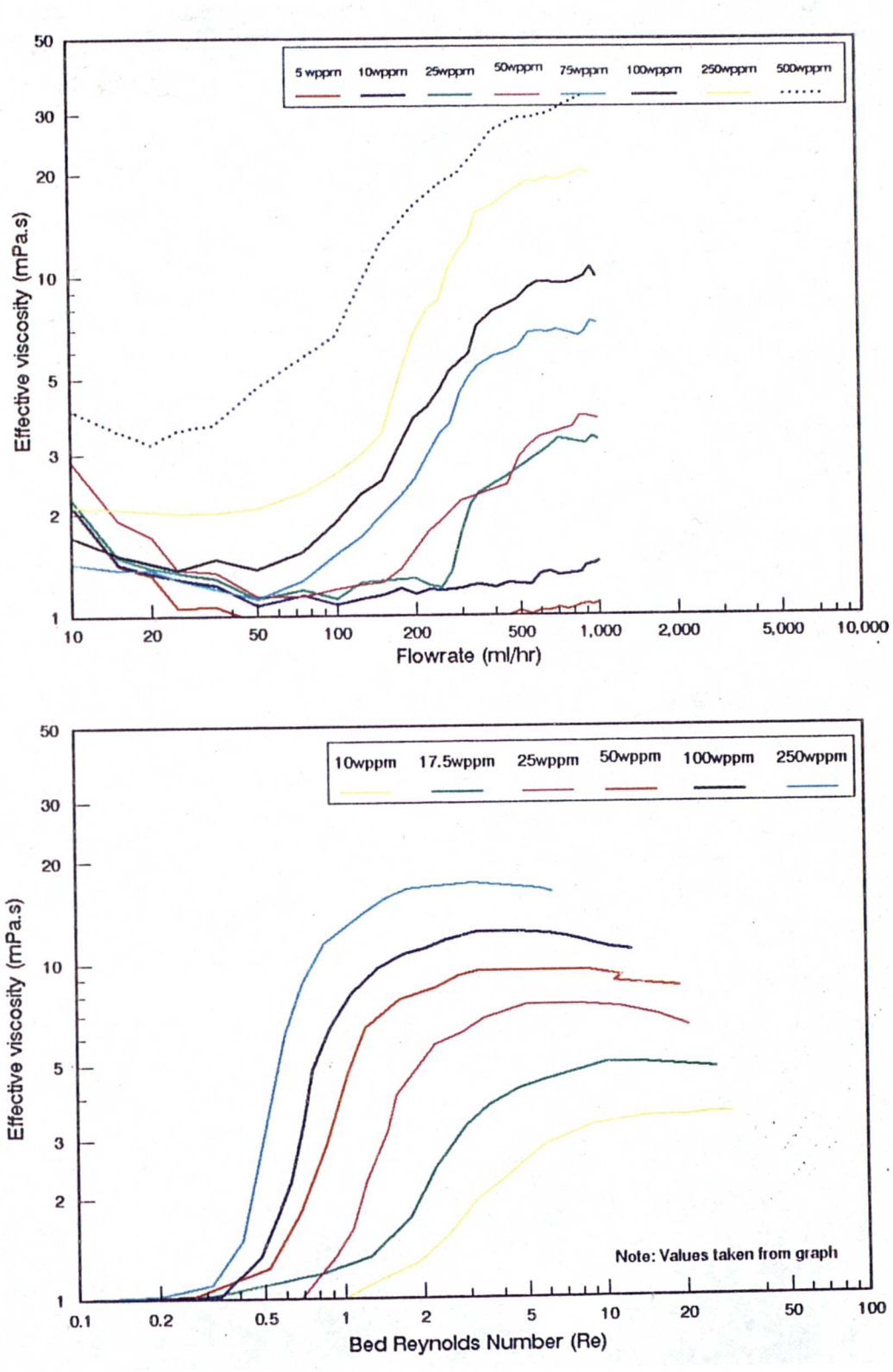

Figure 6.7 Comparison of variation of viscoelastic characteristics between this work (top), and the work of Durst and Haas (REF) (bottom).

Comparison of the effective viscosity behaviour of the polymer solutions in the 2 sizes of rod array clearly shows that passage sizes do not affect the flow greatly when an extensional strain comparison is made. Figure 5.25 does highlight the effect different shear rate regimes have on the flow. For a given extensional strain the flow was under a greater shear strain in the large capillary apparatus than in the smaller cell. This is an effect of the not exact scale up of the cells where the height of the larger cell is not 10 times that of the smaller cell. Good continuity is obtained in the behaviour on going from the larger cell to the smaller cell. Unfortunately not enough overlap in recorded behaviour between the cells is present in order to make definite statements that the extensional component is directly scaleable. It is felt, however, that given the evidence present in the other experiments, there is sufficient evidence to say that the extensional behaviour is scaleable.

6.2.3 Screen Factor Analysis

The results produced by this apparatus give the lowest variation in the spread of the extensional power law exponent 'm'. The apparatus itself is very simple to use and can give a very rapid indication of the presence of viscoelastic behaviour. Only relatively small volumes of test solution are required to carry out the flow tests as settling times are much shorter than in most of the other tests. These factors make this very desirable to use as an initial rheometric test to obtain solution properties. The main disadvantage of the apparatus is that due to problems with numerically determining the rate of change of area with distance travelled. This produces a problem when the relationship between the flowrate and the rate of extensional strain is sought. The most straight forward way to obtain this relationship in this case is to use an empirical constant. If the extensional behaviour of a given fluid is known then this may be used to determine the coefficient so that flowrate may be replaced by extensional strain rate. This coefficient will be valid for all fluids in this apparatus until it is dismantled, or the arrangement of the screens changed. For this work it was assumed that the flow in the small planar contraction cell would provide the known behaviour so that the screen coefficient could be obtained. Figure 6.8 shows the fit between the screen apparatus results and the 0.5mm rod array for the 3% brine tests when the flowrate is converted into extensional strain using a factor 7.8, where;

$$\dot{\xi} = 7.8 * Q$$

Similarly, for the 0.05%wt brine, the following factors were used;

100wppm polymer: $\dot{\xi} = 8.2 * Q$

250wppm polymer: $\dot{\xi} = 11.75 * Q$

500wppm polymer: $\dot{\xi} = 10.1 * Q$

The variation in factor is caused by the dismantling of the screens between tests. These results can be seen in figure 6.9.

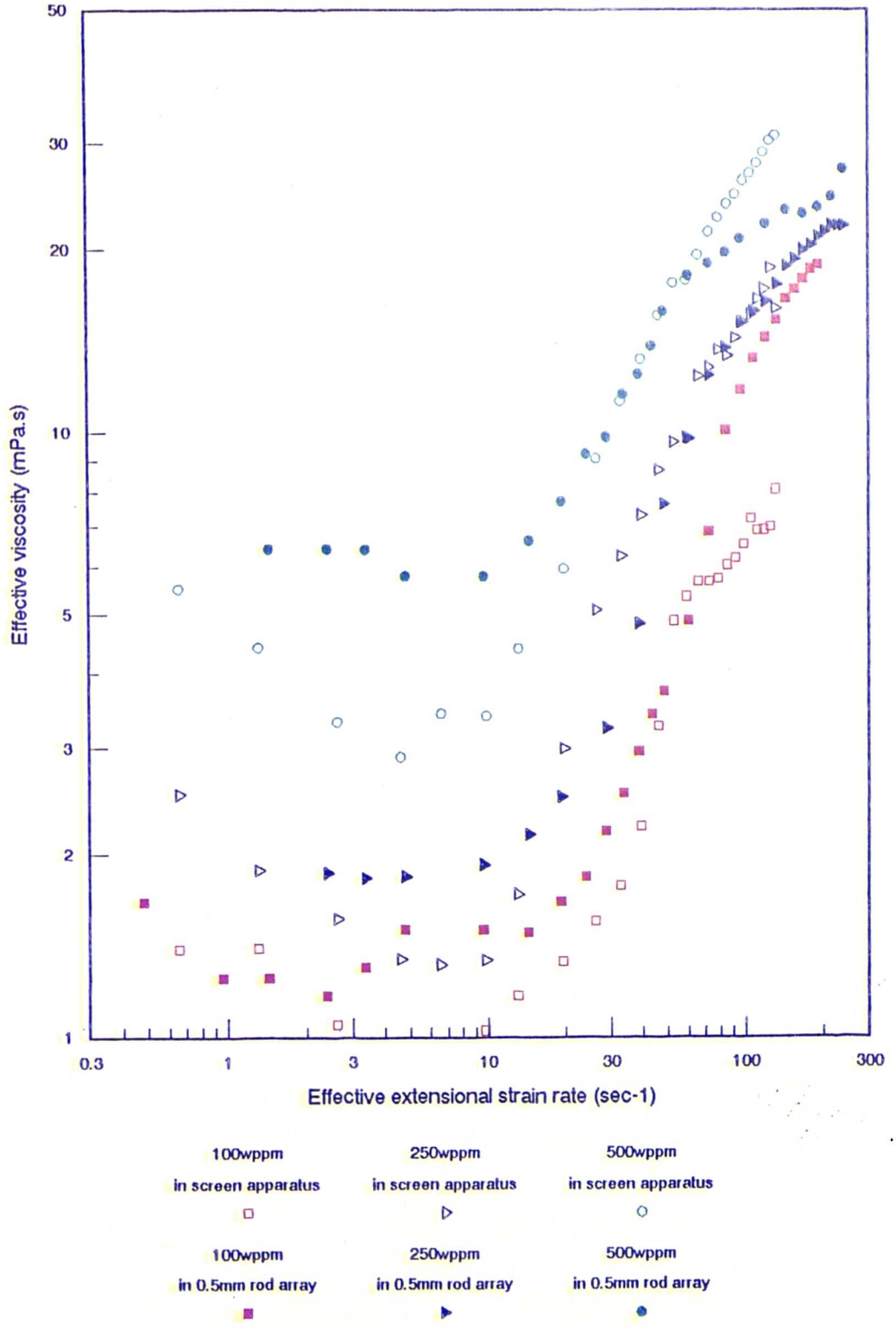

Figure 6.8 Calibration of screen factor apparatus for the polymer solutions made up in 3% brine using the results from the 0.5mm rod array

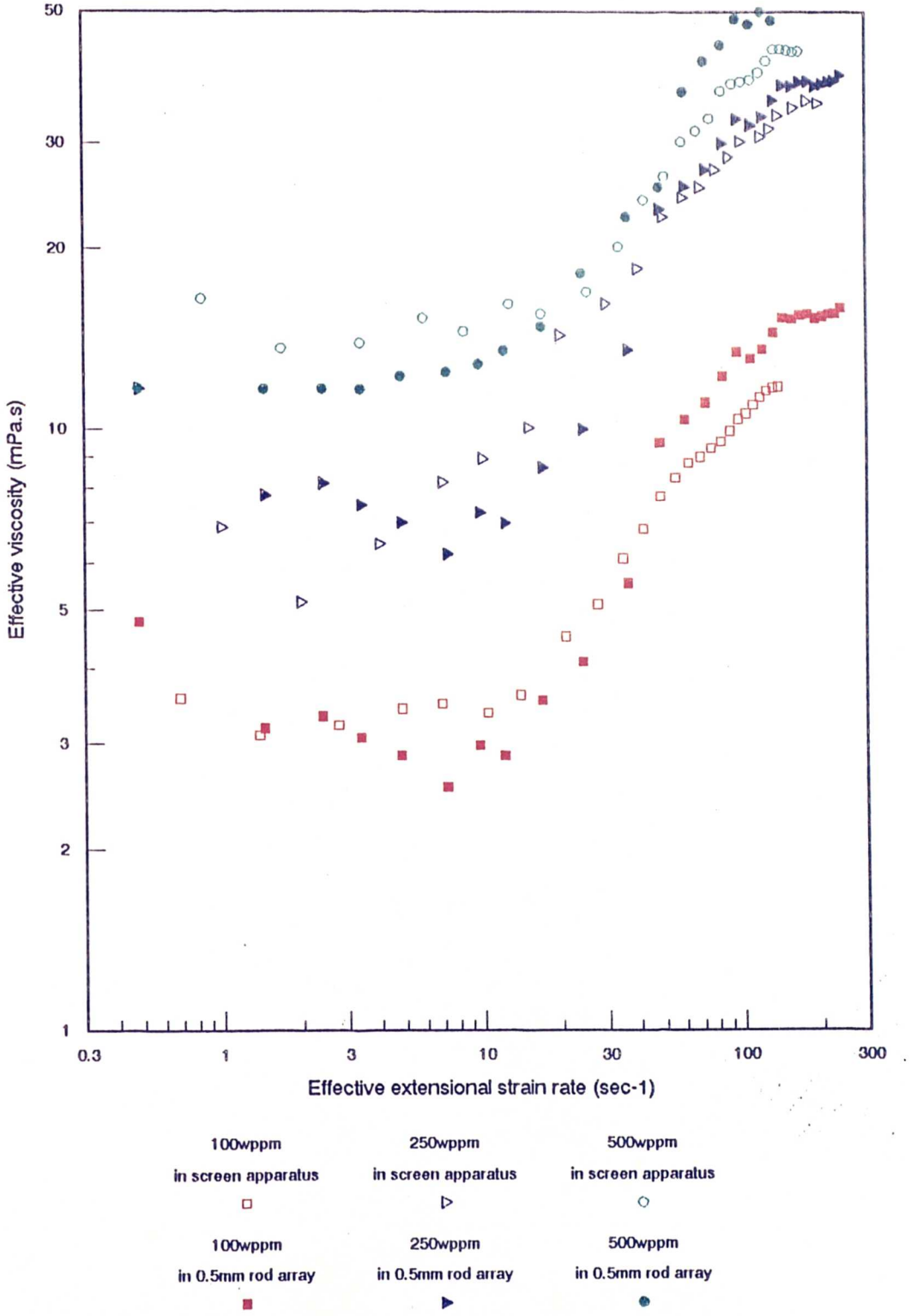

Figure 6.9 Calibration of screen factor apparatus for the polymer solutions made up in 0.05% brine using the results from the 0.5mm rod array

As can be seen the range in conversion factor is not too large; it is likely that the factor will always lie in the range 7 to 12, which is ±20% about the average 9.5. Although this scatter may seem large more careful control of how the screens are placed through the joining of them together by some means should reduce the spread. Figure 6.8 also reveals that at the higher extensional strain rates there appears to be a reduced tendency for the viscosity to flatten off in this apparatus.

6.2.4 Bead Pack Flow

The results obtained in this work, as well as in the literature clearly show the usefulness of columns of tightly packed glass balls in studying liquid flow. Although not monodisperse, the beads produce a medium whose pores are similar in shape and size, allowing direct comparison between the results of different researchers. The constantly changing pore cross sectional area produces an ideal medium for studying viscoelastic effects, where inertia can be minimised.

The flow of polymer solutions in porous media has been shown to be a more complex case than the flow through the above apparatus. Several works (8,10) have reported on the apparent difference in the viscosity observed in the porous media to that obtained in rheometers. Most recently the work by Sorbie (71) has shown that if account is taken of the region near the pore wall where the molecules are sterically restricted from entering then a much better fit is achieved. Steric hindrance is most prominent where large molecular chains are present, in particular where these chains are rigid rather than flexible. The polyacrylamides used in this work fall into the flexible group, unlike Xanthan gum which is a rigid molecule with a double helix for a backbone. The fact that polyacrylamides are flexible however should not preclude the possibility of some steric hindrance, particularly when the molecules are open in conformation, as is the case in low ionic strength solvents. With the molecule in this state it is unlikely that the concentration near the wall in a small pore will be at the concentration of the bulk. With a smaller conformation, as exists in the higher salinity brines the molecules may approach the wall more, and hence the apparent viscosity will be nearer to that of the bulk.

Steric hindrance for solutions of Xanthan gum can reduce the observed viscosity by upto 50% if the permeability of the porous media is low (c 20mD). The viscosity loss observed for the solutions of Polymer A in deionised water are of a far greater magnitude that as could be explained by the limited steric hindrance it would encounter. Adsorption levels of polyacrylamide on quartzic materials are low, so any loss must be attributed to either shear degradation or polymer retention through face blocking. Although the permeability to water after the flow of polymer was less than before by a factor of 1.8, a value of this magnitude is not indicative of significant loss of polymer through retention/filtration effects on the front faces of the packs. It is therefore most likely that the viscosity loss must be attributed to shear degradation of the polymer whilst flowing through the pipes and pores of the apparatus. For a polymer to be of use in an oilfield application its resistance to shear degradation must be high, otherwise little viscosity enhancement will remain once the solution has passed through the perforations were shear strains of the order of 10000 sec^{-1} are present. It should be noted here though that the majority of polymer treatments of oilfields are carried out in highly saline (3%wt +) brines where less degradation will occur because of the different molecular conformation. The results of Polymer B in the 0.05% brine show how degradation is reduced as solvent salinity increases. In this series of tests the viscosity loss was around 50% at the low shear rate limits. Given that the molecular weight of this particular polyacrylamide is larger than that of Polymer A a greater loss may have been expected. By reducing the conformational size less degradation has occurred.
If we now consider the flow of solutions of Polymer B made up in the 3% brine, no loss of viscosity is observed, with the 500wppm solution matching the shear behaviour very well.
The viscoelasticity of the solutions in the 0.05% brine does appear somewhat muted compared to the tests in the other apparatus. Even the response of the 250wppm polymer solution results in only a doubling of the observed pre-extensional onset value. However, with all three test solutions resistance factors greater than those predicted by shear viscosity alone it may be said that a change in behaviour has occurred.

The results in figure 5.31, clearly showing the elastic behaviour, compare very well with those published in the literature. Choosing the convention of Durst and Haas (24) of plotting Reynolds Numbers against friction factor multiplied by Reynolds Number (as in figure 5.34) allows a comparison of this work to theirs possible. Comparing identical polymer concentrations is not possible as their published data is on 50wppm solutions of a similar molecular weight polyacrylamide. Figure 6.10, comparing the 100wppm polymer solutions used here to their 50wppm solution does show a clear pattern of the onset point occurring at a lower Reynolds Number as the bead diameter decreases. For the extensional strain analysis presented here to be verified other workers results must show a coincident onset point for different bead pack sizes. As insufficient raw data is available from the work by Durst *et al*, the extensional strain relationship will be modified to allow qualitative comparison of the different pack sizes when not all the required parameters are known.
Since,

$$N_{Re} = \frac{\bar{u}\, d_b \rho}{\eta(1-\phi)}$$

from the definition used by Durst and Haas, and

$$\dot{\xi} = 93.2 * \sqrt{3}\, \bar{u} / 4 * d_b$$

from combining equations 3.70 and 3.74,
we can say that by substituting for $\bar{u}/d_b$;

$$\dot{\xi} = \frac{93.2\sqrt{3}}{4\rho}\, \eta (1 - \phi) \quad \frac{N_{Re}}{d_b^2}$$

For a bead pack the porosity is usually within .39 to .42 and so can be assumed constant, as can be the density and fluid shear viscosity by taking the values for the solvent.

Hence we have;

$$\dot{\xi} = 2.42e\text{-}5 \frac{N_{Re}}{d_b^2}$$

The results of this comparison can be seen in figure 6.11, for the same fluids as used in the Reynolds Number comparison of figure 6.10.

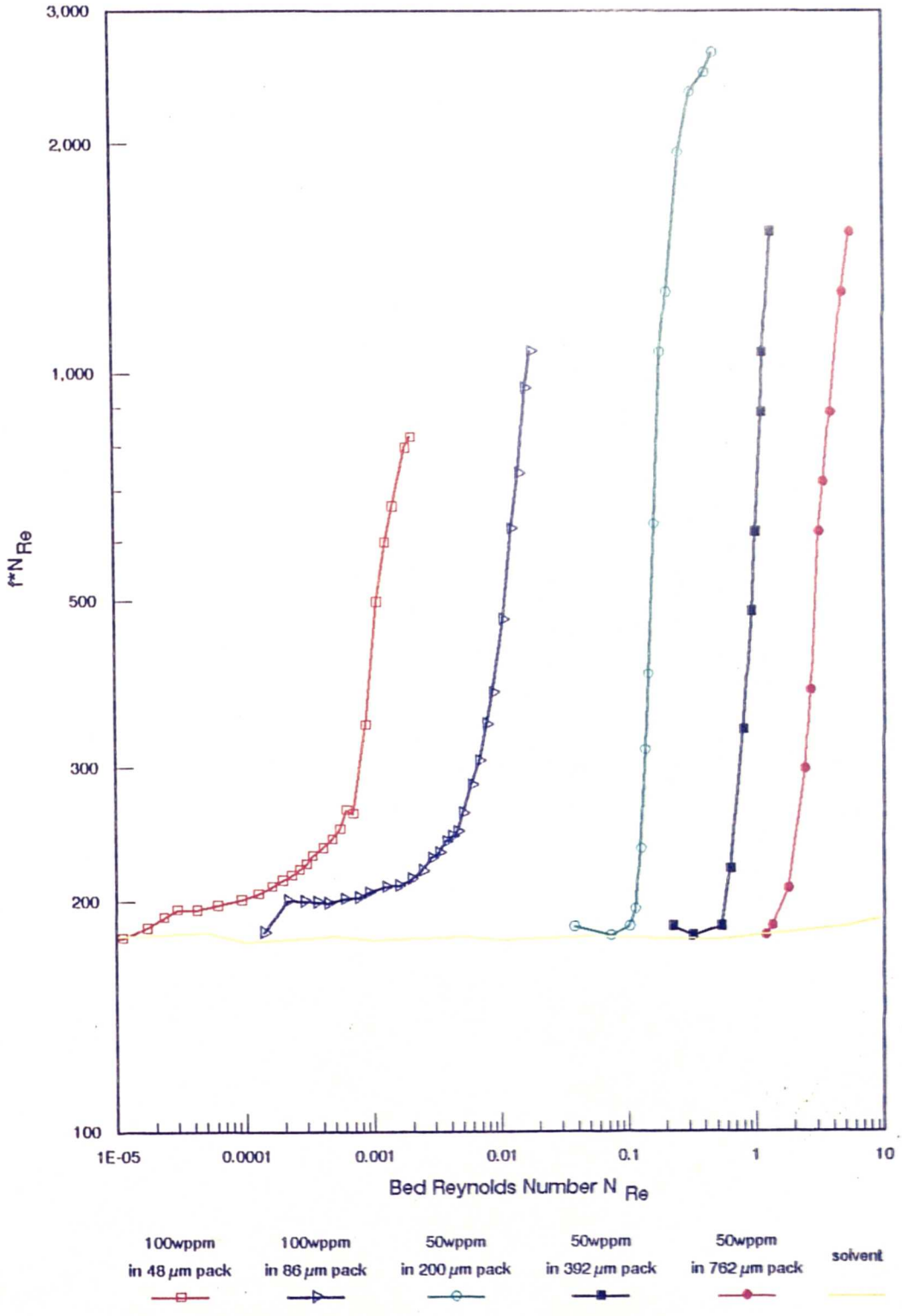

Figure 6.10 Comparison of onset Reynolds Numbers between this work and that of Durst *et al.*

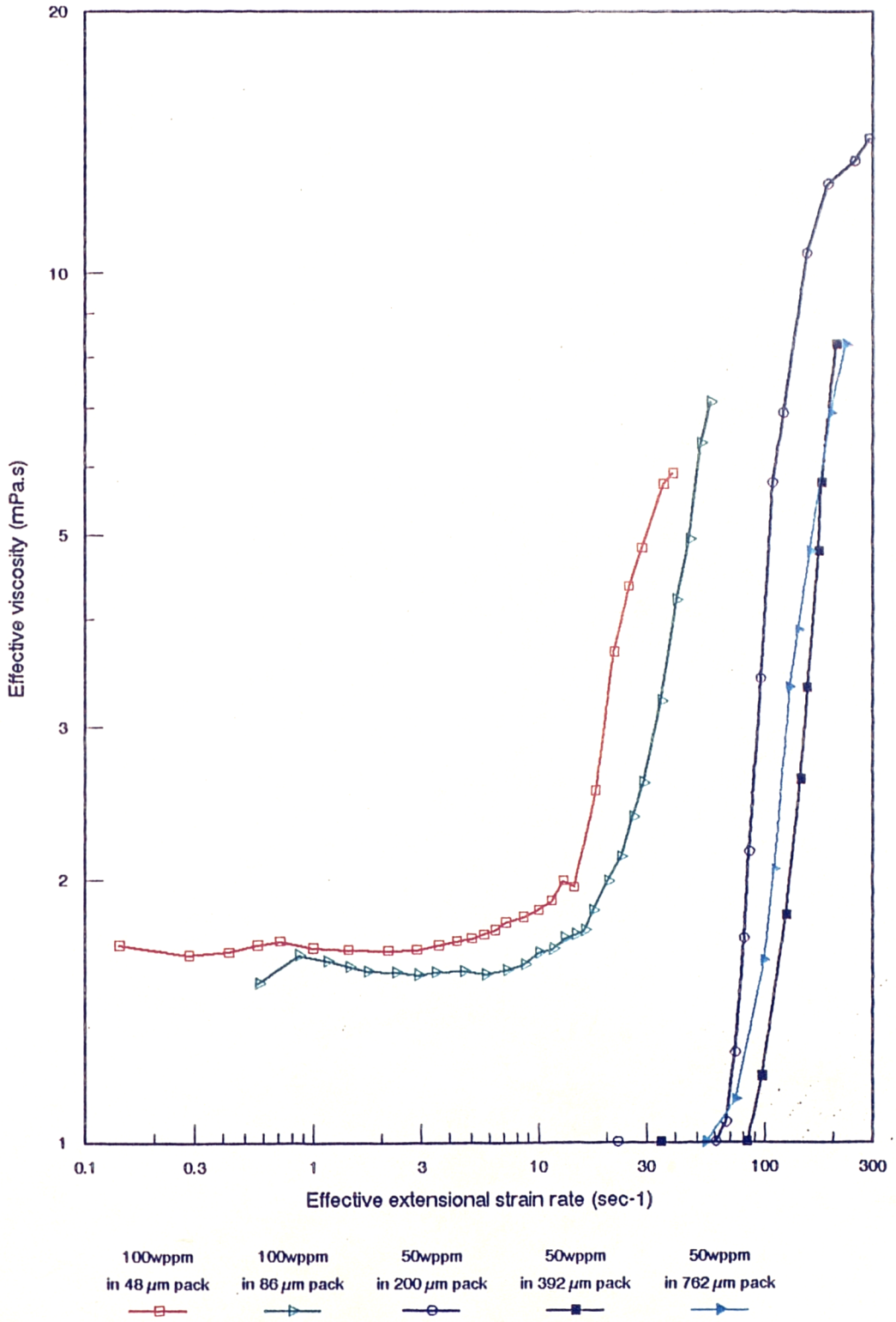

Figure 6.11 Comparison of extensional strains between this work and that of Durst *et al.*

Figures 6.10 and 6.11 also show that the extensional power law exponent for the 50wppm polymer solutions of Durst *et al* are of similar values. Figure 6.11 shows clearly that the analysis developed to provide a measure of extensional strain which allows direct transposition of results from one apparatus to another of completely different size is valid.

In order to test for viscoelastic behaviour in solutions of xanthan gum results previously collected by another researcher in the laboratory (55) were re-analysed using this method. As can be seen in figure 6.12 no evidence of viscoelasticity was observed for the 500wppm Xanthan solution over the same range of extensional strains as was used in this work. Xanthan because of its rigid nature and neutral charge is affected much less by changes in solvent ionic content than polyacrylamides. This results in a lower bulk solution viscosity for solutions in fresh waters compared to polyacrylamides, but at higher ionic strengths the coiling of the polyacrylamide reduces its viscosity and hence the Xanthan solution now is more viscous. This can be seen in figure 6.12 where, until extensional behaviour dominates, the viscosity of the Xanthan solution is double that of the polyacrylamide. Published works have shown no tendency for Xanthan to exhibit viscoelasticity over much wider flow ranges.

As was found above at the higher extensional strain rates the observed viscosity began to level out. This has been noticed for porous media flow for solutions of polyethyleneoxide (PEO) (40) as well as for polyacrylamides. Given that all these works are subjecting the flow to a shear as well as extensional strain, care must be taken to account for the relative effects of both. Pure simple shear is relatively easy to quantify, however in the majority of cases extensional strains are accompanied by some level of shear strains. The next section of this discussion will look specifically at the behaviour of polyacrylamides under as near pure extension as possible.

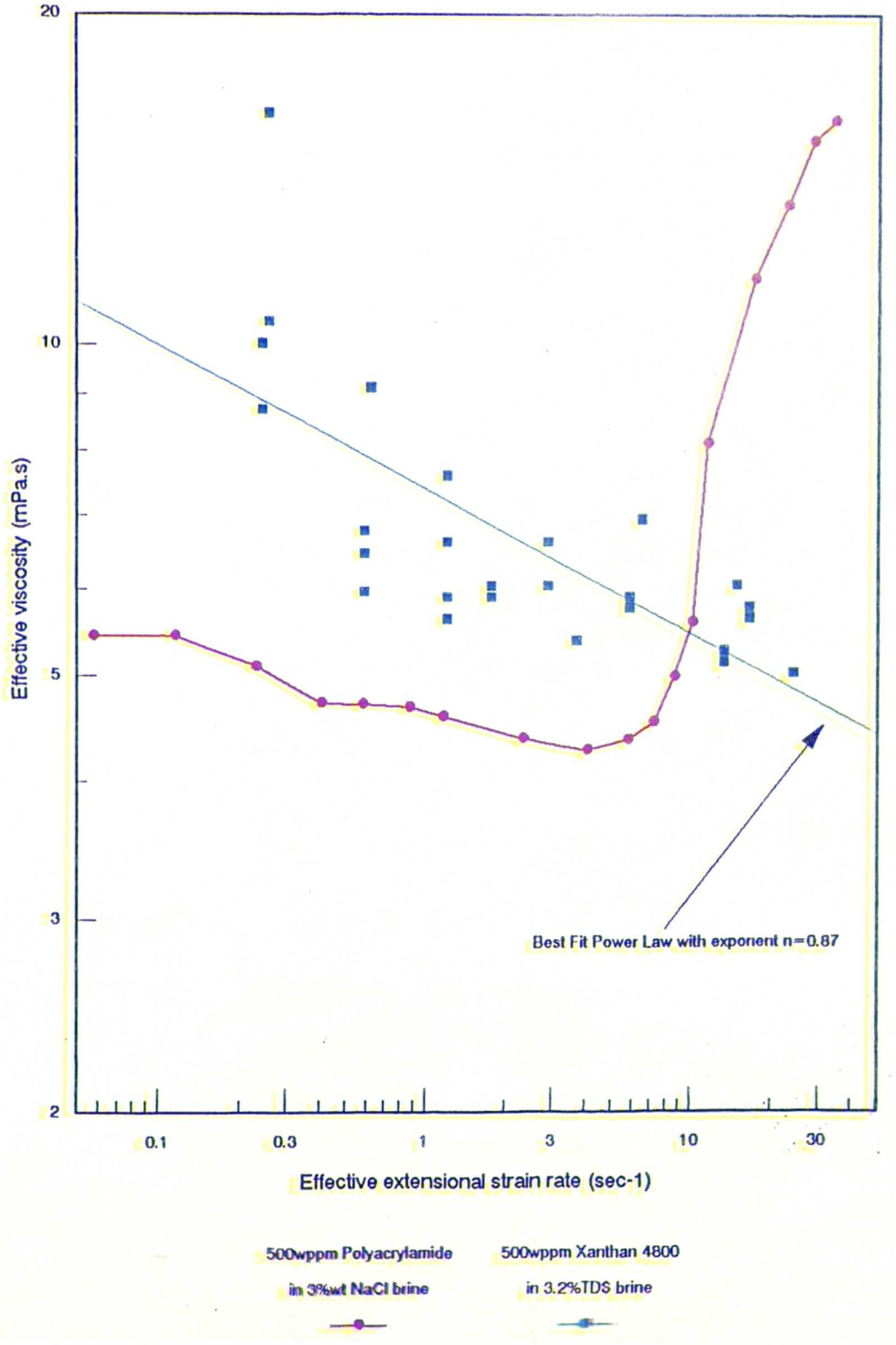

Figure 6.12 Comparison of behaviour of a 500wppm Polyacrylamide solution and a 500wppm solution of Xanthan gum in 3%wt brine.

6.2.5 Deborah Number Considerations

The Deborah number has been widely used in published work to predict the onset of elastic behaviour. However a range of values have been quoted for the onset point, from N_{De}=0.05 (61), to N_{De}=0.5 (31) or N_{De}=1.0 (9). Although the definition, the ratio of the duration of fluid memory (relaxation time) to the duration of deformation (inverse of stretch rate) has not changed various researchers have used different groups for both time intervals. At high Deborah numbers an elastic molecule deforms more rapidly than it can relax, and hence assumes a permanently deformed state. Conversely at low Deborah Numbers the molecule relaxes quickly to the original state. Chauveteau (9) states that a Deborah number of one only actually means that the fluid has a tendency to extend as the rate of deformation is greater than the relaxation rate. This being said however, at Deborah numbers around unity a transition between the two states occurs which is observed in many cases by a large change in pressure drop for only a small increment in flowrate.

The duration of deformation has been variously defined as the residence time of the fluid in a given geometry, or as a ratio of a length to a characteristic velocity. The following definitions are among the many published;

1. $t = L/(U/\phi_s)$ (98)
   for a 2-D medium where L is the distance between the rods and ϕ_s is the planar porosity.

2. $t = D/\bar{u}$ (29)

3. $t = 4R_H/\bar{u}$ (99)

4. $t = D/U$ (100)

5. $t = 1/\dot{\zeta}$ (23)
   where $\dot{\zeta} = k_1 U/D$ and $2 \leq k_1 \leq 200$, with k_1=4 taken to empiricise.

6. $t = 1/\dot{\gamma}$ (101)

With the exception of the empirical relationship (5) above, no account is taken of the rate of change of flow boundaries which means that the same deformation duration would be experienced whilst flowing through a long plain capillary as to one with a sinusoidal variation in diameter. Clearly account must be taken of the pore geometry if any analysis is to be correct. The definition for the duration of deformation in this work is the inverse of the extensional strain rate (relationship 5). This definition is used because at a given flowrate through a pore if the time taken for the chain to relax is greater than the time it is exposed to stretching, permanent deformation occurs. This permanent deformation will result in extensional stresses being setup within the flow, with the corresponding results. The other expressions are more analogous to shear strain durations.

At the onset Deborah number all data should collapse onto a single curve. A single value exists for a given polymer at any concentration or in any solvent for the onset N_{De}, as the relaxation time takes account of differences due to concentration and solvent changes.

If we initially compare the results for the series of tests carried out in the 3%wt brine as shown in figure 6.13. Variations in shear viscosity are not accounted for, and so scatter will occur due to the differences in shear regimes between the experiments. It can be seen that the behaviour of all solutions is very similar, with an onset point of around $N_{De} = 0.1$. Once the polymer solution is in the extensional regime the scatter that was experienced due to shear viscosity differences disappears, and very good agreement is reached. Figure 6.14 shows the results for the polymer solutions in the 0.05%wt brine. It can be seen that a much greater scatter due to shear viscosity differences is present here, but as above, much less scatter is observed in the extensional regime.

Figure 6.15 compares the data for the polymer solution tests in both brine strengths. Although slightly scattered it can be seen that at $N_{De} > 0.1$ extensional viscosities dominate the flow. Variations in the Deborah Number itself will be a cause of some of the scatter. A small difference in for example the assumed average bead diameter will make a corresponding difference in N_{De}. Considering the sizes of pore throats vary from 1mm to 0.01mm across the four experiments a very good agreement is obtained.

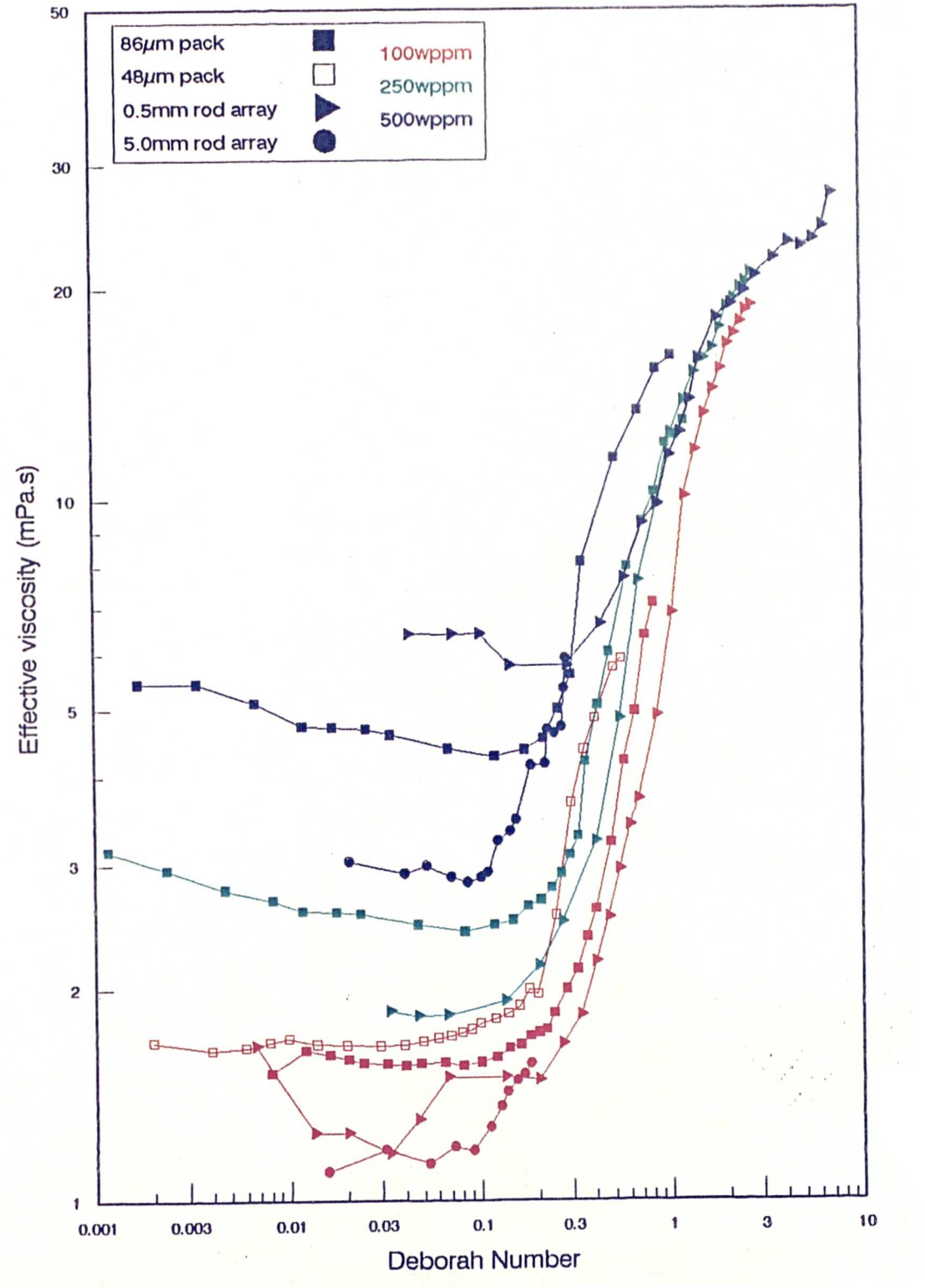

Figure 6.13 Deborah Number comparison between experiments for polymer solutions in 3%wt brine.

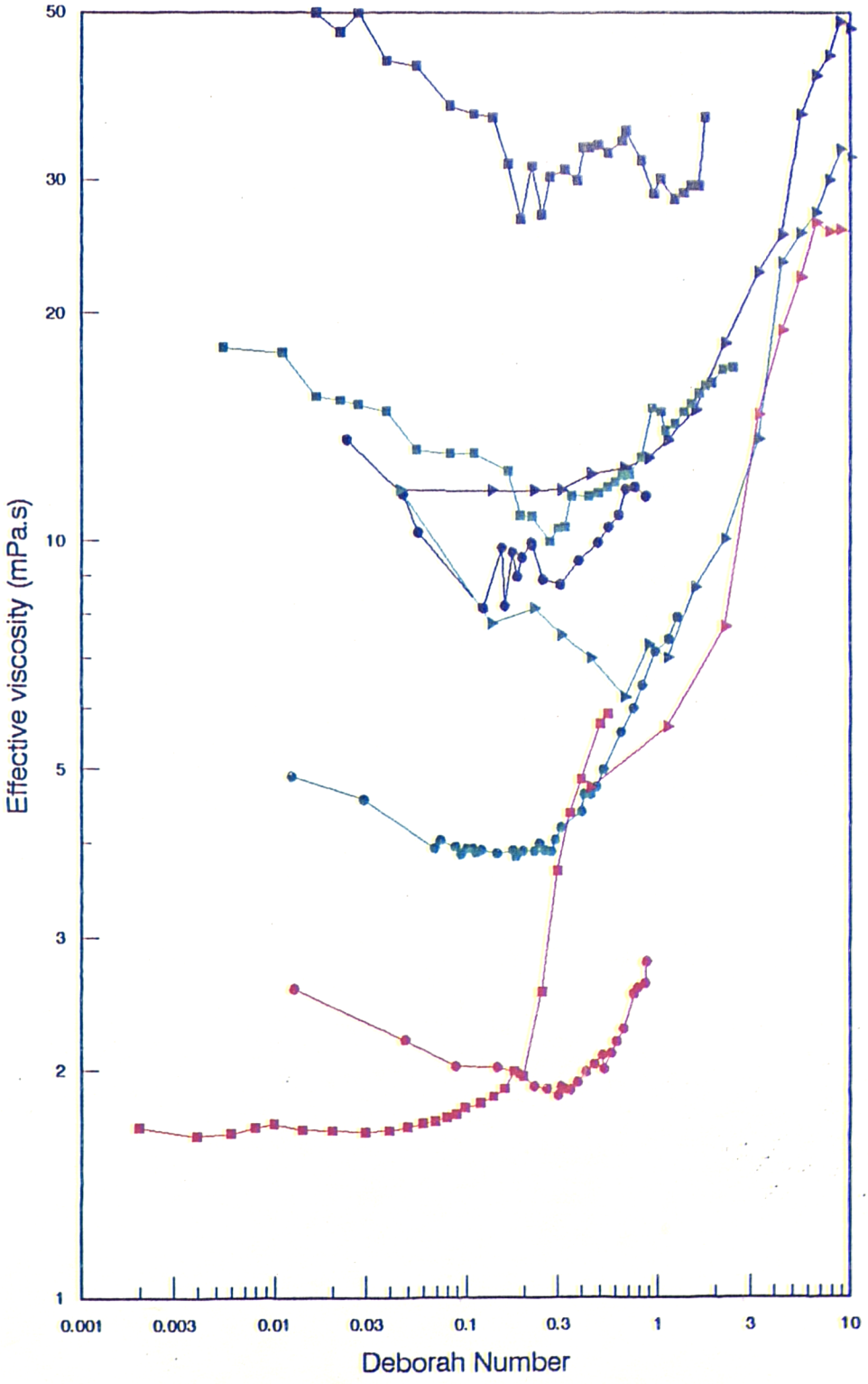

Figure 6.14 Deborah Number comparison between experiments for the polymer solutions in the 0.05%wt brine.
(Note: Same symbol and colour convention as previous figure)

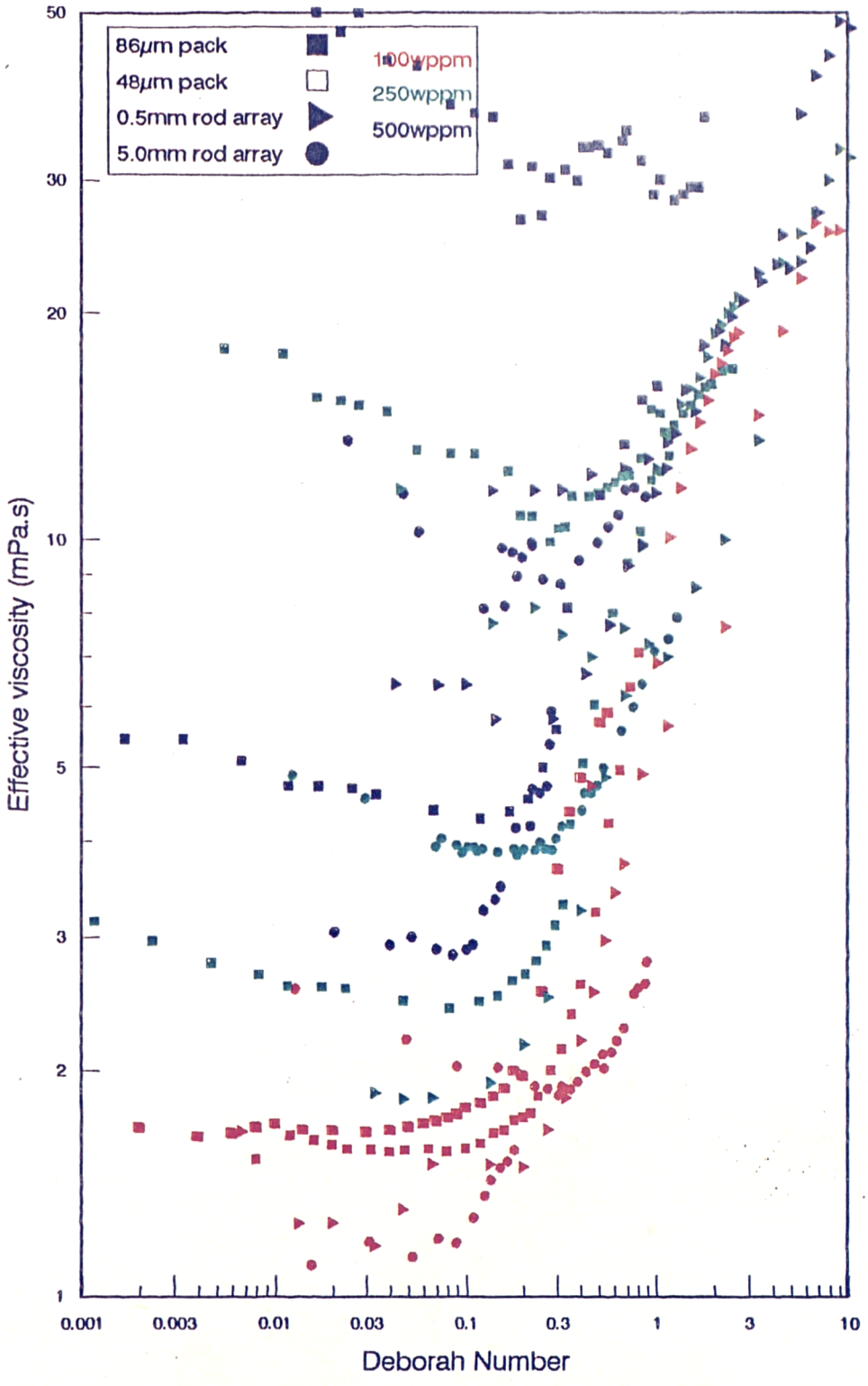

Figure 6.15 Deborah Number comparison between experiments for polymer solutions in the two brine strengths used.

6.3 Analysis of 'pure' Extensional flow

The recent paper by Walters and Jones (44) presents results obtained on an instrument called a spin line rheometer. This instrument consists of a rotating drum which catches and pulls a thread from a nozzle which is linked to a reservoir of the test solution. By monitoring the thread width, and knowing the forces applied by the drum it is possible to gain an estimate of extensional rheology. Obviously at very low rates of extensional strain it is impossible to pull a thread without shear at the nozzle being more significant, and therefore low extensional rates cannot be studied. This limitation means that under no circumstances can the low strain plateau of

$$\eta_e \big|_{\xi \to 0} = 3\eta_{shr} \big|_{\gamma \to 0}$$

be reached without the encroachment of significant shear stresses. This prevents a direct determination of the onset point at which the extensional viscosity ceases to be governed by the 3η continuum mechanics rule above. Therefore although it is acknowledged that at low extensional strain rates a constant value of η_e exists no precise onset point can be obtained, and hence one has to be defined. If we look at the data presented in this paper several factors in common with this work are visible. Figure 6.16 presents the extensional stress/strain behaviour for solutions of polyacrylamide 1175 in deionised water. This is a very high molecular weight (c 18million) polymer that is used in polymer augmented waterflooding of oil reservoirs.

The results show clearly that the behaviour obtained can be modelled by a power law over the specified range, with only a small spread of values of the exponent m. The data as presented does not include the low extensional strain limiting value which has been added from data generated with the same polymer in this work. It can be seen by adding the behaviour for the 125 and 250wppm polymer solutions (higher solutions could not be measured due to viscosities beyond the upper limit of the apparatus) that extensional onset points are only just outside the limits of the spin line rheometer. Quantification of the onset points for these two solutions is now possible by extending the behaviour produced by Walters. This presents a slight anomaly where the onset point for the more dilute solution is less than the

other. However, if the other concentrations are considered, where the shear viscosity is higher, it can be envisaged that the onsets will occur at lower extensional strains as the polymer concentration increases. It is possible that the extensional stress/strain behaviour for either the 125ppm or the 250ppm solution is in error. The authors of the paper do acknowledge that the extensional behaviour is very difficult to measure.

Distinct similarities between the behaviour recorded by Walters and this work exist. The extensional power law exponent of the behaviour for the 125wppm solution used is m=1.62, which is within the range encountered in this work. For the 250wppm solution the slope is m=1.99 which is only marginally higher than those found here. Also the point at which extensional behaviour is apparent, the onset point, is very similar with between 3 and 10 sec^{-1} for Walters' work and, using the definition of onset adopted for this work, between 0.1 and 10 for the full range of solutions used here.

It can be said therefore that good agreement between the simplified analysis of this work allowing transposition of results from one scale to another, and those of almost pure extensional flow is obtained.

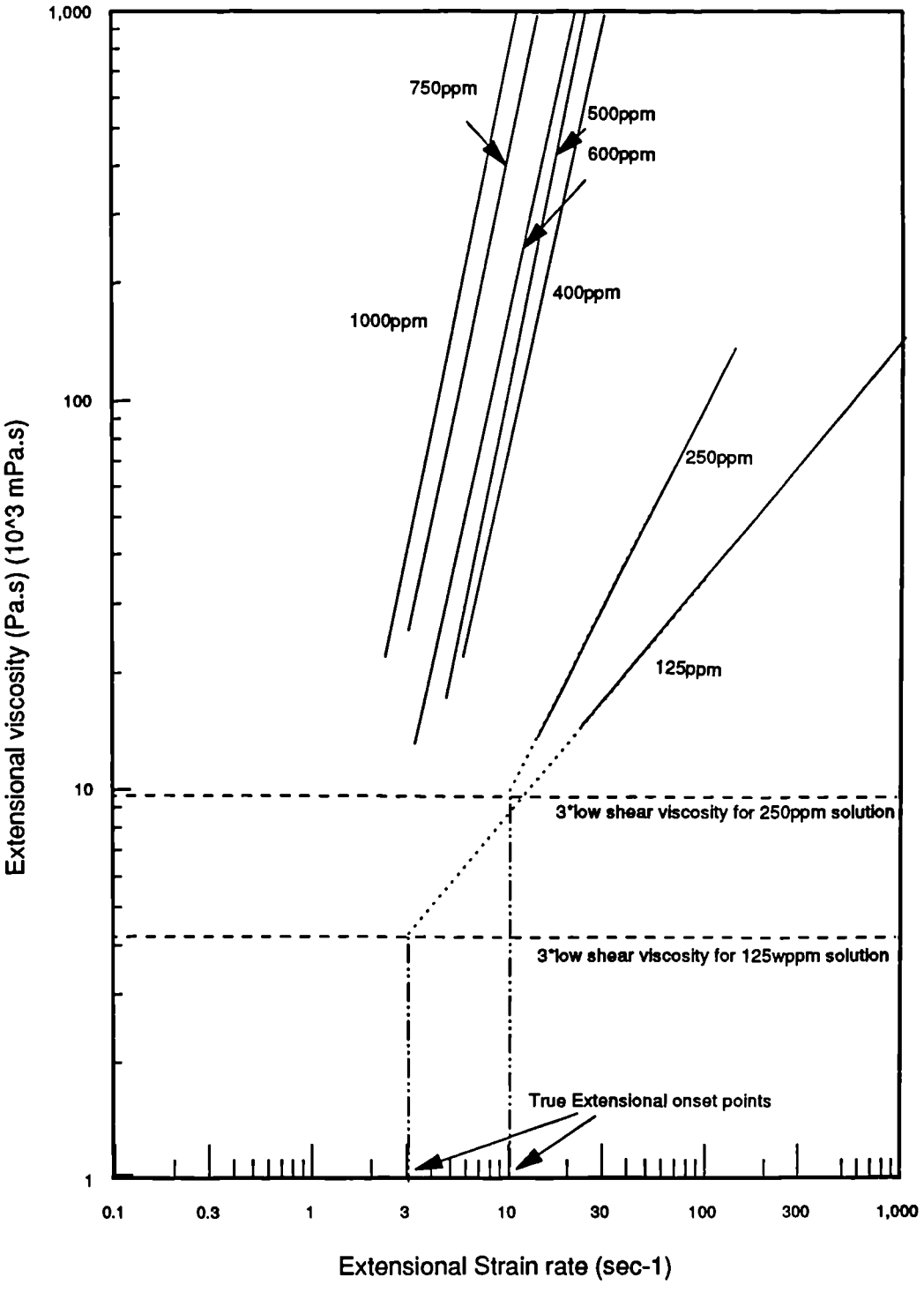

Figure 6.16 Extensional stress/strain data for Polyacrylamide 1175 in deionised water from the work of Walters *et al* with the low strain rate plateaux of $3^*\eta_0$ added for two solutions.

6.4 Application of proposed viscosity model

Equation 6.2, repeated below, combining the shear and extensional viscosities can be used in any situation to provide information as to the expected viscosity behaviour. It is not intended to be applicable over the full range of extensional strains as the power law relationship chosen does not take account of the low extensional strain plateau and also the apparent limiting value at higher extensional strains. Basic information about the power law exponent, which may be quickly determined using a screen factor apparatus, and also the constant λ which may be found by calibrating the screens, allows determination of the onset point in a variety of geometries.

Figures 6.17, 6.18 and 6.19 use the exponent m, and constant λ found from the screen factor flow to compare the predicted behaviour of solutions of 100wppm, 250wppm, 500wppm Polymer B in 3%wt brine in three differing geometries. The plots show good agreement between the behaviour predicted and that actually recorded. For these set of plots a single m, λ pair was used, as the apparatus was not stripped down between runs.

$$\eta_{eff} = \frac{\eta_0}{(1 + (t_1\dot{\gamma})^2)^{(1-n)/2}} + \lambda\zeta^m \qquad - 6.2$$

where η_{eff} is the observed viscosity.

The variables in the above equation, η, λ, m, n, can all be found from either shear rheometry (η & n), or screen factor flow (λ & m). The calculation of the rates of shear and extensional strain, although not trivial, can be made using equations presented in this thesis.

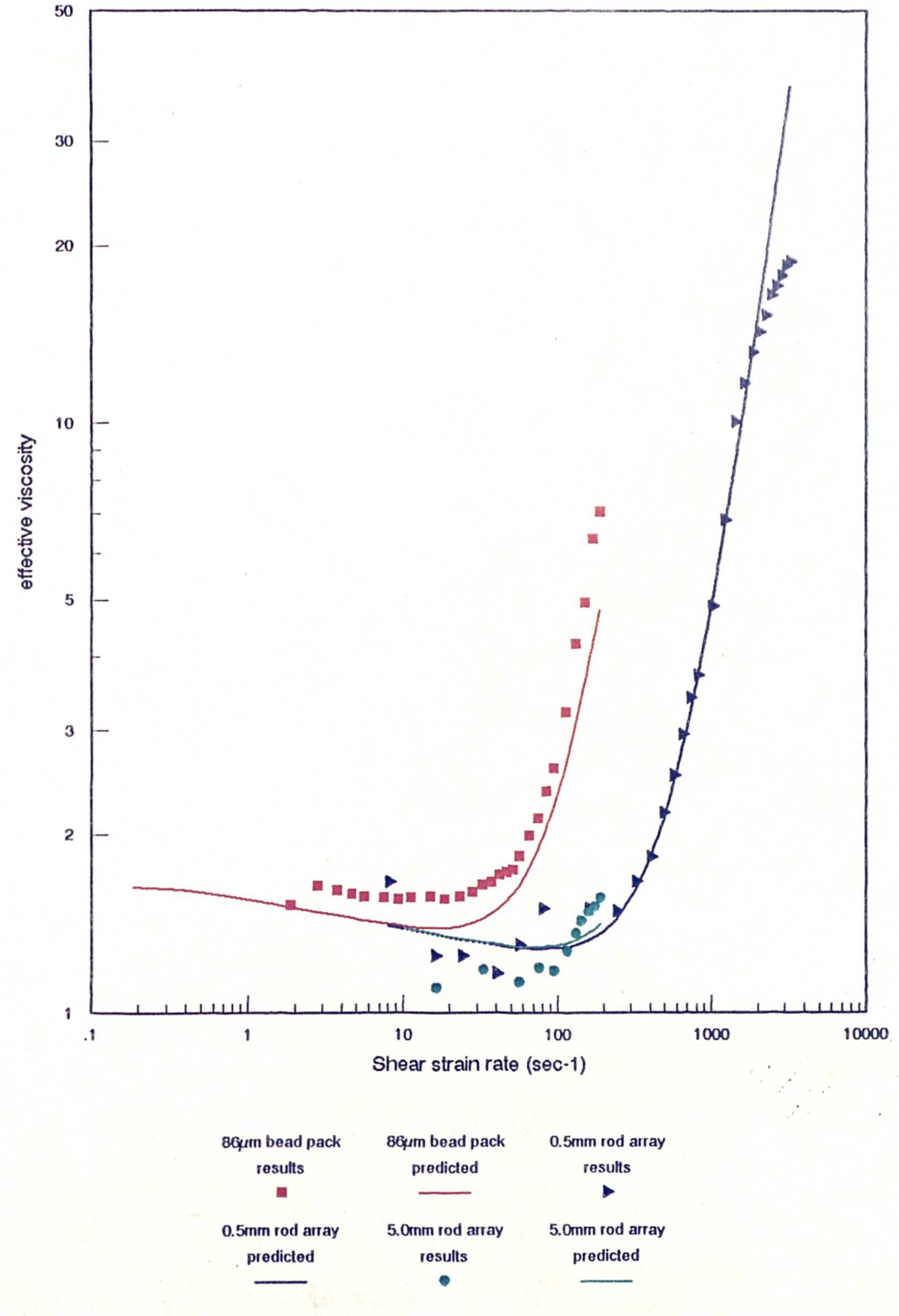

Figure 6.17 Comparison of predicted and observed values for a 100wppm solution of Polymer B in 3%wt brine.

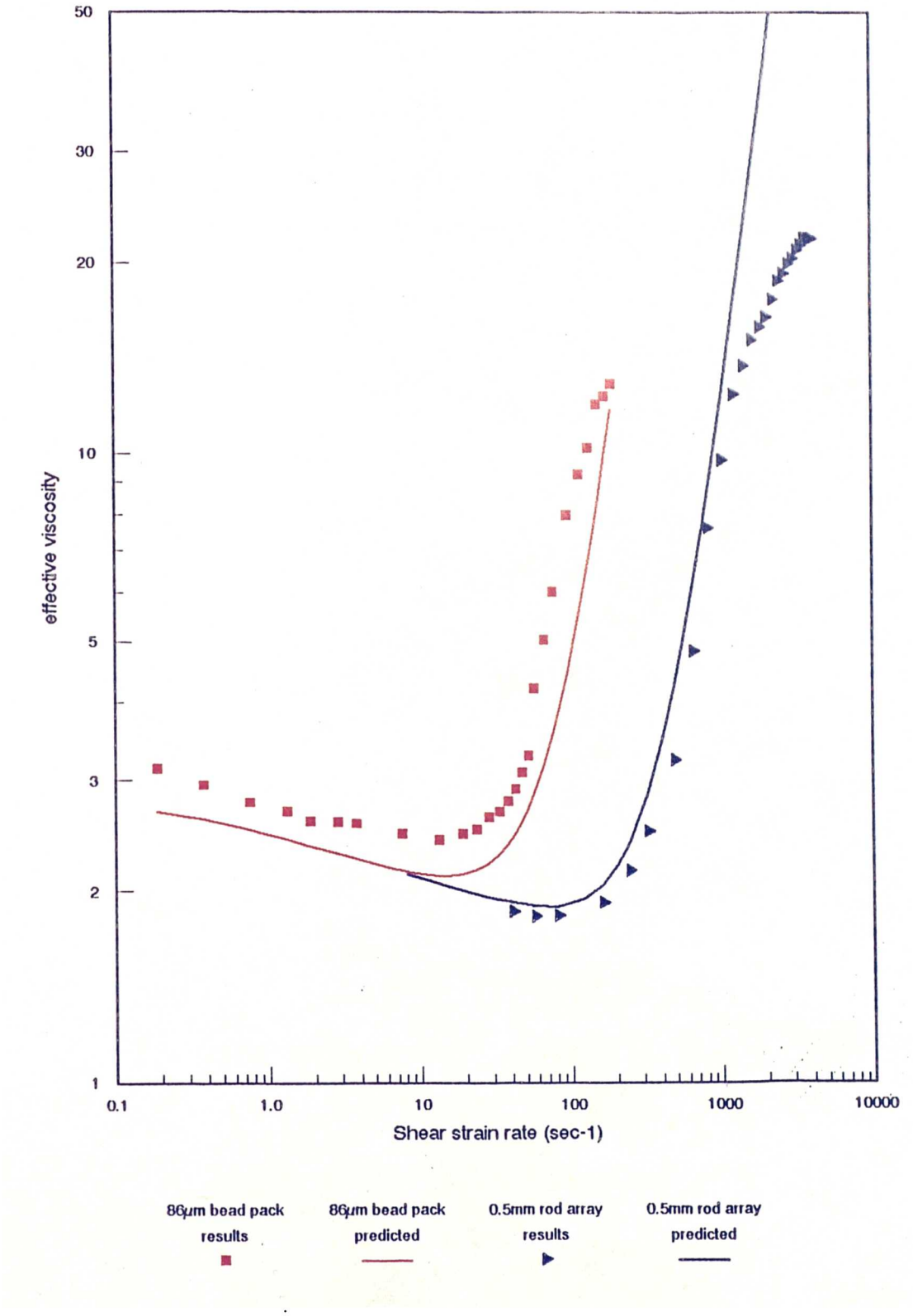

Figure 6.18 Comparison of predicted and observed values for a 250wppm solution of Polymer B in 3%wt brine.

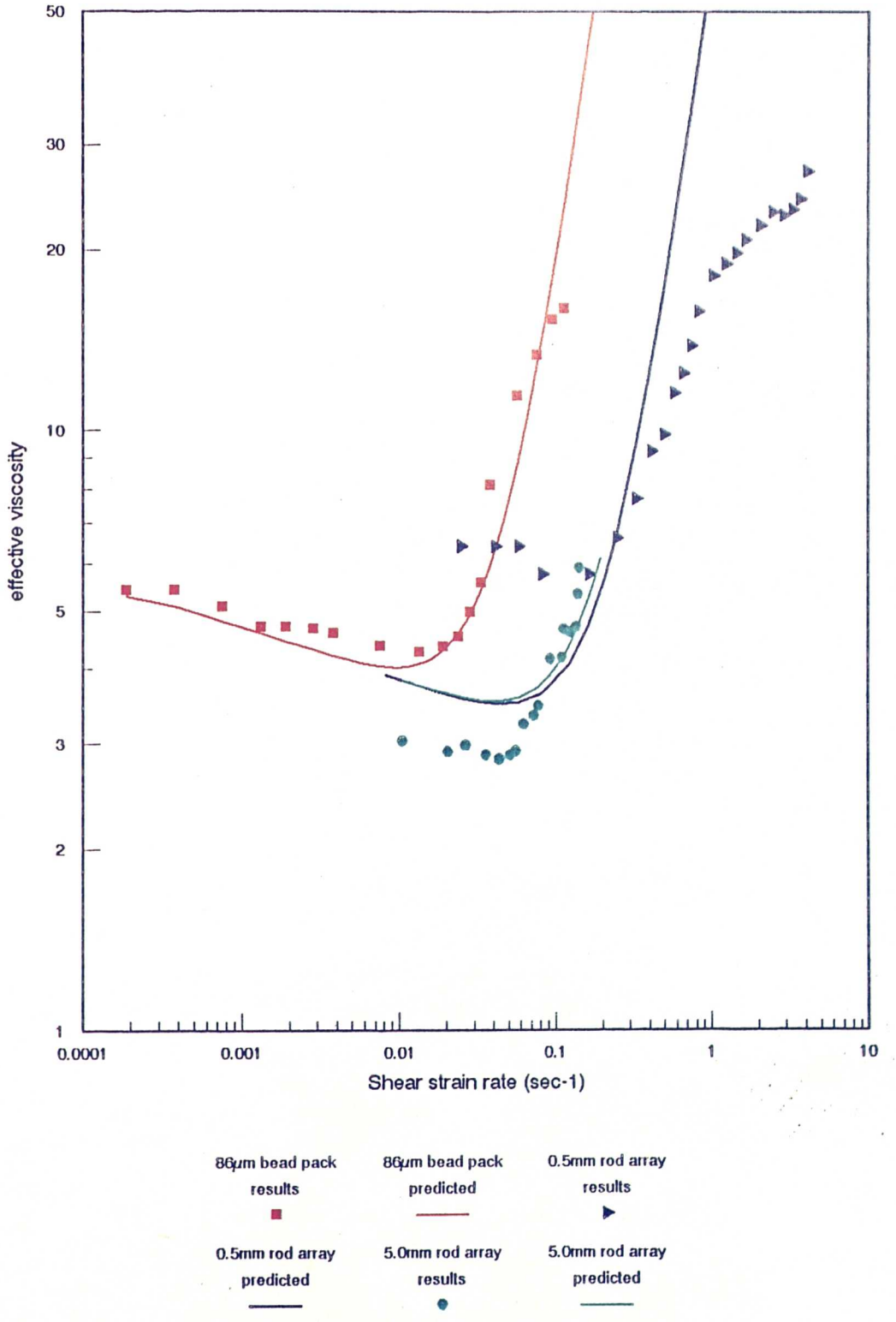

Figure 6.19 Comparison of predicted and observed values for a 500wppm solution of Polymer B in 3%wt brine.

7. CONCLUSIONS

7.1 The use of Polyacrylamide for Augmenting Waterflooding.

7.1.1 Polyacrylamide can be used as a viscosifying agent in injection waters typical of those tested here. Typical viscosity enhancements would be of about 5 x that of the solvent for a 500wppm polymer solution. Apparent viscosity loss through steric hindrance as affects other EOR polymers was not observed in high salinity brines.

7.1.2 Severe degradation of these solutions is likely when made up in low salinity brines. This will be more severe in the field than experienced in this work because of the decreased permeability of the porous media. Most reservoir rocks are less than a tenth of the permeability of the bead packs used here.

7.1.3 The most severe limitation of these polymers will be the necessary reduction in injection rates in order to prevent extensional effects whilst pumping these solutions through the perforations. Typical frontal advance rates near well can be greater than the maximum obtained here. To overcome the onset of elasticity injection rates (and hence production rates) may have to be reduced by half. It is not feasible to allow injection pressures to rise to compensate for the extra pressure loss as too high an injection pressure will result in well fracture. It is unlikely that lower molecular weight polymers will present these problems.

7.1.4 Such high molecular weight polymers could find application in fracture treatment of injectors. If solutions were pumped down under a low rate to fill the well bore, and then the rate rapidly increased fracturing could occur. The elastic properties would mean that a very rapid rise in pressure ensued.

7.2 Experimental

7.2.1 The screen factor apparatus has been shown to yield very useful information of the viscoelastic behaviour of these solutions. This is of particular benefit as the time required to test a solution is low. Thus the screen factor is ideal as an initial screening test as well as providing extensional rheological parameters.

7.2.2 Both planar and axi-symmetric contraction flows provide useful information on the behaviour of these fluids across the strain rate range. Visualisation studies are highly beneficial in increasing understanding of the flow processes.

7.2.3 The non-use of ferric materials from the construction of this equipment did not present problems. The use of transparent materials permitted problems to be identified early.

7.3 Analytical

7.3.1 The shear behaviour of the solutions in the bead pack in low ionic strength brines is poorly modelled using existing relationships. Further work needs to be carried out on the effects of retention and adsorption levels, together with viscosity loss through degradation.

7.3.2 In high salinity brines the shear behaviour is adequately modelled by existing relationships. These do not take account of the influence of extensional strain.

7.3.3 The extensional behaviour of polyacrylamides can be modelled by a power law type relationship. Values of the constant and exponent can be determined from one experiment and successfully applied to another flow regime.

7.3.4 The derivation of extensional strain presented here can be modified to suit any regular geometry. Conversion of the local variables to more global ones is possible. Provided the correct extensional strain expression is used there appears

no problem in scaling the flow behaviour. The values of extensional strain found here agree well with those obtained on 'pure' extensional apparatus. Use of the extensional strain analysis presented here has been shown to produce an onset Deborah Number of 0.1. This value is in good agreement with values in the literature.

7.3.5 Extensional behaviour is not restricted to those solutions where chain interactions occur. Increased viscosities were observed in solutions as low as 10wppm polymer in a 3%wt NaCl solvent. However, careful experimental procedures must be adapted to detect changes at this level.

LITERATURE REFERENCED

Abbreviations used :

SPE n	Society of Petroleum Engineers Paper n,
JPT	Journal of Petroleum Technology
JNNFM	Journal of Non-Newtonian Fluid Mechanics
SPE Res Eng	SPE Reservoir Engineering
SPE Form Eval	SPE Formation Evaluation
AIChEJ	American Institute of Chemical Engineers Journal
SPEJ	Society of Petroleum Engineers Journal
JFM	Journal of Fluid Mechanics

1
Archer J S, Wall C G
Petroleum Engineering
Publ Graham and Trotman (ISBN 0-86010-665-9)

2
Bagley E B
End corrections in the capillary flow of polyethylene
J of App Phys 28(5) pp624-627

3
Barboza M Rangel C Mena B
Viscoelatic effects in flow through porous media
J of Rheology 23(3) pp281-299 (1979)

4
Binding D M
An approximate analysis for contraction and converging flows
JNNFM 27 (1988) 2 pp173-190

5
Bird R B Armstrong C Hassager O Curtiss C F
Dynamics of Polymeric Liquids (Vol.1 - Fluid Mechanics Vol.2 - Kinetic Theory)
Wiley NY 1977
"Dynamics of Polymeric Liquids (v1&2) pub 1977 Wiley NY

6
Budd P M
Determination of average molecular weights of a polyelectrolyte by meniscus depletion sedimentation equilibrium
Brit Poly J 20 (1988)

7
Chauveteau G
Molecular interpretation of several different properties of flow of coiled polymer solutions thro porous media in oil recovery conditions
SPE 10060 (1981)

8
Chauveteau G
Rodlike polymer solution flow thro fine pores : Influence of pore size on Rheological behaviour
J of Rheology 26(2) pp 111-142 (1982)

9
Chauveteau G Moan M
Onset of dilatant behaviour in non inertial flows of dilute polymer solutions through channels with varying cross section
J Phys (Paris) Lett v42 (1981) 10 pp201-204

10
Chauveteau G Zaitoun A
Basic rheological behaviour of xanthan polysaccharide solutions in porous media : effects of pore size and polymer concentration
Proc 1981 European Symp on EOR pp197-212 publ Elsevier 1981

11
Choplin L Sabatie J
Threshold type shear thickening in polymeric solutions
Rheol Acta 25 (1986) pp570-579

12
Christopher R H Middleman S
Power law flow thro a packed tube
I&EC Fundam 4 4 (Nov 1965) pp422-426

13
Cogswell F N
Converging flow and stretching flow : a compilation
JNNFM 4 (1978) pp23-38

14
Cohen Y Christ F R
Polymer retention and adsorption in the flow of polymer solutions thro' porous media
SPE Res Eng March 1986 pp113-118

15
Davison P Mentzer E
Polymer flooding in North Sea reservoirs
SPE 9300 (1980)

16
de Gennes P G
Coil stretch transition of dilute flexible polymers under velocity gradients
J of Chem Phys v60 n12 (15/06/74) pp5030-5042

17
Deiber J A Schowalter W R
Flow through tubes with sinusoidal axial variations in diameter
AIChEJ 25 (1979) 4 pp638-645

18
Deiber J A Schowalter W R
Modeling the flow of viscoelastic fluids through porous media
AIChEJ 27 (1981) 6 pp912-920

19
Dominquez J G Willhite G P
Mechanisms of poymer retention in porous media
"polymer retention in porous media pp511-554

20
Dreher K D Gogarty W B
An overview of mobility control in micelar/polymer enhanced oil recovery processes
J of Rheol 23 (1979) 2 pp209-229

21
Duda J L Hong S A Klaus E E
Flow of polymer solutions in porous media - Inadequecy of capillary model
Ind Chem Fundam 22 (1983) pp299-305

22
Durst F Haas R Interthal W
The nature of flows through porous media
JNNFM 22 (1987) pp169-189

23
Durst F Haas R Interthal W
Laminar and turbulent flows of dilute polymer solutions : a physical model
Rheol Acta 21 (1982) pp575-577

24
Durst F Haas R Kaczmar B U
Flow of dilute hydrolysed polyacrylamide solutions in porous media under various solvent conditions
J Appl Polym Sci 26 (1981) pp3125-3149

25
Ergun S
Fluid flow thro packed columns
Chem Eng Progr 48 (1952) pp89

26
Ghoniem S A
Extensional flow of polymer solutions through porous media
Rheol Acta 24 (1985) pp588-595

27
Gogarty W B
Micellar/polymer flooding - An overview
JPT Aug 1978 pp1089-1101

28
Graton L C Fraser H J
Systematic packing of spheres - with particular relation to porosity and permeability
J Geolgy 43 (1935) 8 pp785-909

29
Greenkorn R A
Steady flow through porous media
AIChE J 27 (1981) 4 pp529-545

30
Gupta R K Sridhar T
Viscoelastic effects in non newtonian flows through porous media
Rheol Acta 24 2 (1985) pp148-151

31
Haas R Durst F
Viscoelastic flow of dilute polymer solutions in regularly packed beds
Rheol Acta 21 (1982) pp566-571

32
Haas R Durst F Interthal W
Effects of dilute polymer solutions on porous media flows Pt 2: theory of molecule-flow-interaction and its verification
Proc EuroMech 143/Delft/Sept 1981 pp163-168

33
Haas R Kulicke W M
Flow behaviour of dilute polyacrylamide solutions through porous media. 2. Indirect determination of extremely high molecular weights and some aspects of viscosity decrease over long time intervals
Ind Eng Chem Fundam 23 (1984) pp316-319

34
Harrington R E Zimm B H
Degredation of polymers by controlled hydrodynamic shear
J of Phys Chem v69 (1) 1965 pp161-175

35
Hirasaki G J Pope G A
Analysis of factors influencing mobility and adsorption in the flow of polymer solution through porous media
SPEJ Aug 1974 pp337-346

36
Hong S A Duda J L Klaus E E
The influence of bulk rheology on the flow of polymer solutions in porous media
Poly Prepr 22 (1981) 2 p20-23

37
Horn A F Merrill E W
Midpoint scission of macromolecules in dilute solution in turbulent flow
Nature v312 (8-11-84) pp140-141

38
Interthal W Haas R
Effects of dilute polymer solutions on porous media flows Part 1: Basic concepts and experimental results
Proc Euromech 143/Delft/Sept 81 p157-162

39
James D F McClaren D R
The laminar flow of dilute polymer solutions through porous media
J Fluid Mech 70 (1975) 4 pp733-752

40
James D F Saringer J H
Elongational flow of dilute polyox solutions
JNNFM 5 (1979) p409

41
James D F Saringer J H
Extensional flow of dilute polymer solutions
J Fluid Mech 97 (1980)

42
James D F Saringer J H
Flow of dilute polymer solutions through converging channels
JNNFM 11 (1982) p317-339

43
Jennings R R Rogers J H West T J
Factors influencing mobility control by polymer solutoins
JPT March 1971 pp391-401

44
Jones D M Walters K
Extensional Viscosity effects in EOR
SPE 18070 (October 1988)

45
Jones W M
The flow of dilute aqueous solutions of macromolecules in various geometries VIII.
Mechanisms of resistance in porous media
J Phys -D 12 (1979) 3 pp383-393

46
Jones W M
Flow of dilute polymer solutions thro porous beds
EOR by displacement with saline solns. BP Ed services p123-135

47
Jones W M
Polymer additives in reservoir flooding for oil recovery : shear thinning or shear thickening
letter in J Phys D : Appl hys 13 (1980) L87

48
Keller A Odell J A
The extensibility of macromolecules in solution : A new focus for macromolecular science
(1985) ?

49
Kemblowski Z Michniewicz M
A new look at the laminar flow of power law fluids thro granular beds
Rheol Acta 18 (1979) pp730-739

50
Kulicke W M Haas R
Flow behaviour of dilute polyacrylamide solutions through porous media Pt.1
Influence of chain length, concentration and theromdynamic quality of solvent
Ind & Eng Chem Fund 23 (1984) 3 pp308-315

51
Lake L W Pope G A
Status of micellar-polymer field tests
Pet Eng Int 51 (1979) 13 pp38-60

52
Lange W Rehage G
Recent results on the use of polymers in tertiary oil recovery in brines of high salinity
SPE 8983 (1980)

53
Langhaar H L
Steady flow in the transition length of a straight tube
J appl Mech 9, 55-8 (1942)

54
Lim T Uhl J Prud'homme R K
The interpretation of screen factor measurements
SPE Res Eng May 1986 pp272-276

55
Little C E
Macromechanics of Xanthan solution flow
PhD Thesis, University of Bristol 1986

56
Magueur A Moan M Chauveteau G
Effect of successive contractions and expansions on the apparent viscosity of dilute polymer solutions
Chem Eng Commun 36(1985) pp351-366

57
Martin F D
Mechanical degredation of polyacrylamide solutions in core plugs from several carbonate resevoirs
SPE Form Eval April 1986 pp139-150

58
Moan M Chauveteau G Ghoniem S
Entrance effects in capilary flow of dilute and semi-dilute polymer solutions
JNNFM 5 (1979) pp463-474

59
Mungan N
Rheology and Adsorption of aqueous polymer solutions
Technology (Montreal) Apr/Jun 1969 pp45-50

60
Needham R B Doe P H
Polymer flooding review
JPT Dec 1987 p1503-1507

61
Ouibrahim A Fruman D H
Characteristics of HPAM dilute polymer solutions in three elongational flow situations
JNNFM 7 (1980) pp315-331

62
Polishchuk A M
Effect of iron ions on the viscosity of a polyacrylamide solution
Neft Khoz 5 (1979) May pp42-44

63
Putz A Chevalier J P Stock G Philippot J
Chateaurenard (Fr) microemulsion pilot design and performance
SPE 8198 (1979)

64
Ramsden D K Mckay H
The degredation of polyacrylamide in aqueous solution induced by chemically generated hydroxyl radicals (pt1 - Fentons Reagent .pt2 - Autooxidation of Fe++)
Poly deg + stab 1986 pt1-14pp217-229 pt2-15pp15-31

65
Sadowski T J Bird R B
Non-Newtonian flow through porous media 1. Theoretical
trans Soc Rheol 9 (1965) 2 pp243-250

66
Sadowski T J Bird R B
Non-Newtonian flow through porous media 2. Experimental
trans Soc Rheol 9 (1965) 2 pp251-271

67
Savins J G
Non newtonian flow thro porous media (flow thro porous media symposium)
Ind + Eng Chem v61 (1969) 10 pp18-47

68
Seright R S
The effects of mechanical degredation and viscoelastic behaviour on injectivity of polyacrylamide solutions
SPE 9297 (Sept 1980)

69
Sheffield R E Metzner A B
Flows of nonlinear fluids thro porous media
AIChE J 22 4 (1976) pp736-743

70
Sorbie K
Shear rates for Newtonian and Non-Newtonian fluids in porous media
Report Oil Recovery Projects Divn AEE, Winfrith April 1982

71
Sorbie K S Clifford P Jones E R W
The rheology of pseudoplastic fluids in porous media using network modelling
Internal Report to BP. (To be Published Shortly)

72
Sorbie K S Parker A Clifford P J
Experimental and theoretical study of polymers flow in porous media
SPE 14231 (1985)

73
Sridhar T Gupta R K
A simple extensional viscometer
Rheol Acta 24 (1985) pp207-209

74
Trouton F T
On the coefficient of viscous traction and its relation to that of viscosity
Proc Royal Soc 77 (1906) pp426

75
Unsal E Duda J L Klaus E E Lim H T
Solution properties of mobility control polymers
SPE 6625 (Oct 1977)

76
Chang H L et al
Determination of Oil/Water Bank Mobility in Miceller/Polymer Flooding
JPT 30 (1978) p1055-60

77
Danielson H H et al
Tertiary recovery by the maraflood Process in the Bradford Field
JPT 28 (1976) p129-138

78
Trantham J C
The North Burbank Unit Tract 97 Surfactant/Polymer Pilot Operation and Control
JPT 30 (1978) p1068-74

79
Pfizer Chemicals Ltd
Polymer Floods using 4800C since 1972
Commercial in Confidence - Not available to Public

80
Martin F D et al
Development of Improved Mobility Control Agents for Surfactant/Polymer Flooding. First Annual Report
DOE/BC/00047-9; US Dept of Energy

81
Harris J
Rheology and Non-Newtonian Flow
Publ Longmans, London 1977

82
Van Wazer J R et al
Viscosity and Flow Measurement
Publ J Wiley and Sons NY 1963

83
Jones W M, Ho S P
The flow of dilute Aqueous solutions of macromolecules in various geometries VII. Mechanisms of retention in Porous Media
J Phyd D : Appl Phys 12 (1979) p383-393

84
Seright R S
The effects of mechanical degradation and viscoselastic behaviour on injectivity of polyacrylamide solutions
SPE 9297 (1980)

85
Ward J S Martin F D
Prediction of viscosity for partially hydrolysed polyacrylamides in the presence of calcium and magnesium salts
SPE 8978 (1980)

86
Warner H J Jr
Ind Eng Chem Fundam 11 (1972) 379-

87
Maerker J M
Shear degradation of partially hydrolysed polyacrylamide solutions
SPEJ August 1975 pp311-322

88
Ramsden D K McKay H
The degradation of polyacrylamide in aqueous solution induced by chemically generated hydroxyl radicals
Polymr degradation and Stability (1986) pp15-31,217-229

89
Morris C W
Mechanical Degradation of polyacrylamide solutions in porous media
SPE 7064 (1978)

90
Brennan R L Jennings R R
Hydrodynamic degradation of mobility control polymers
Polym Prepr 22 (1981) pp81-83

91
Scheidegger A E
The Physics of Flow Through Porous Media
Publ Macmillan and Co, New York 1957

92
Darcy H P G
Les Fontaines Publiques de la Ville de Dijon
Publ Paris 1856

93
Mahers E G Wright R J Dawe R A
Visualisation of Behaviour of EOR reagants in displacement in Porous Media
Proc Euro Symp on EOR, Bournemouth England 1981

94
Brinkman H C
A calculation of the viscous force exerted by a flowing liquid on a dense swarm of particles
Appl Sci Research A I (1947) p27-34

95
Wilkinson
Modified Dray Theory of Permeability
Phys Fluids 28 (1985) 4 p1015-1022

96
Sheffield R E Metzner A B
Flows of Nonlinear fluids through porous media
AIChEJ 22 4 (1976) pp736-743

97
Odell G
Personal Discussion with Author on work progressing in Physics Dept, University of Bristol
October 1988

98
Vossoughi S Seyer F A
Prediction of recovery and water saturation distribution during an unstable immiscible displacement of oil from aporous medium
Ind Eng Chem Fundam 23 (1984) pp64-74

99
Tiu C et al
Flow of Non-Newtonian Fluids through beds of various packing geometries (Eds Lindley D and Sutherland A J)
5th Australasian Conference on Hydraulics and Fluid Mechanics, Christchurch, New Zealand 1974 V1 pp411-417

100
Thomas C P
The mechanism of reduction of water mobility by polymers in glass capillary arrays
SPE 5556

101
Killen J M Naudascher E
Onset and saturation of polymer effects in Porous media Flows
Phys of Fluids 20, 10 (1977) 2, s280-s283

Appendix A - Data Listing

Bead Pack Results

Polymer A in 86μm bead diameter pack
Tube internal diameter : 53mm
Temperature : 30°C
Pack Porosity : 0.395

flow ml/hr	100 ppm Δp mbar/m	250 ppm Δp mbar/m	500 ppm Δp mbar/m
Calibration: (mbar/m)/(ml/hr) for solvent	0.302	0.302	0.32
1	-	-	7.66
2	-	-	14.22
3	-	-	21.74
4	-	-	25.34
5	-	-	31.24
7	-	-	43.36
10	14.86	23.76	58.8
20	-	47.52	113.18
25	32.4	-	-
30	-	67.34	170.06
40	-	83.16	220.92
50	59.48	100.3	265.96
70	-	-	378.94
75	-	142.58	-
80	-	-	438.02
90	-	-	509.94
100	111.56	182.16	569.8
110	-	-	650.6
120	-	-	714.2
125	-	221.8	-
140	-	-	865.2
150	159.88	262.68	918.2
160	-	-	944.2
170	-	-	995
180	-	-	1040
190	-	-	1075.5
200	205.06	331.18	1175.1
225	-	-	1302.26
250	249.8	394.64	1402.92
275	-	-	1495.62
300	294.4	469.98	1583.04
325	319.8	-	-
350	342.6	597.92	1725.8
375	367.6	675.82	-
390	382	-	-
400	392	-	1927.42
410	401.08	-	-
420	410.08	-	-

continued ...

flow ml/hr	100ppm Δp mbar/m	250ppm Δp mbar/m	500ppm Δp mbar/m
425	-	811.9	-
430	418.6	-	-
435	423.9	-	-
440	429.76	-	-
445	436.14	-	-
450	446.74	-	2086.4
455	479.16	-	-
460	487.14	-	-
470	497.64	-	-
480	524.86	-	-
490	555.1	-	-
499	586.98	-	2229.4

Polymer B in 3% NaCl in 86μm and 48μm bead diameter packs

flow ml/hr	86μm 100ppm Δp mbar/m	86μm 250ppm Δp mbar/m	86μm 500ppm Δp mbar/m	48μm 100ppm Δp mbar/m
Calibration : (mbar/m)/(ml/hr) for solvent	0.326	0.346	0.352	0.9
1	-	1.08	1.91	1.51
2	-	2.04	3.82	2.95
3	-	-	-	4.46
4	-	3.82	7.18	6.06
5	-	-	-	7.65
7	-	6.47	11.63	10.52
10	4.96	8.92	16.58	14.98
15	8.01	13.34	24.7	22.39
20	10.52	17.68	32.34	29.96
25	12.96	-	-	37.85
30	15.36	-	-	45.89
35	-	-	-	53.94
40	20.44	34.1	61.68	62.31
45	-	-	-	70.84
50	25.38	-	-	80.24
60	30.64	-	-	97.74
70	-	58.32	105.34	116.2
80	40.96	-	-	136
90	-	-	-	161.4
100	50.8	85.1	153.78	176.5
125	64.14	108.2	199.36	285.3
150	78.16	135.76	263.2	495
175	94.02	161.6	344	688
200	108.52	192.04	571.1	871
225	125.6	226.3		-
250	140.96	267.26	-	1287

continued ...

flow ml/hr	100ppm Δp mbar/m	250ppm Δp mbar/m	500ppm Δp mbar/m	100ppm Δp mbar/m
275	156.66	312.66	-	1457
300	180.08	435.7	1208.4	-
350	227.24	611		-
400	277.3	834.1	1881.733	-
450	346.8	-		-
500	421.68	1380.72	2694	-
600	628.84	1928.2	3376	-
700	960	2478.2		-
800	1290.2	3318		-
900	1868.4	3840		-
998	2304	4462		-

Polymer B in 0.05% NaCl: 86 μm bead diameter pack

flow ml/hr	100ppm Δp mbar/m	250ppm Δp mbar/m	500ppm Δp mbar/m
Calibration: (mbar/m)/(ml/hr) of solvent	0.306	0.300	0.302
1	1.454	5.42	18.48
2	2.39	10.68	32.43
3	3.4	14.02	45.18
4	4.4	18.48	56.73
5	5.68	22.8	75.2
7	7.8	31.24	91.1
10	10.8	39.77	127.995
15	-	59	169.915
20	20.9	78.57	221.235
25	-	-	273.9
30	30.32	111.79	285.0333
35	-	113.94	281.12
40	45.6	129.88	377.525
45	-	-	365.26
50	64.42	150.12	456.37
55	-	172.12	-
60	-	188.52	559.86
65	-	224.7	-
70	91.84	-	632.5
75	-	-	749
80	105.34	276.18	800
90	120.04	313.94	904.8
100	118.8	354.6	981.6
110	-	396	-
120	-	440.6	1221.8
125	157.92	-	1313.2
130	-	478.8	-
150	196.5	580.8	1437.4

continued ...

flow ml/hr	100ppm Δp mbar/m	250ppm Δp mbar/m	500ppm Δp mbar/m
170	-	764.2	-
175	242.7	-	1515
190	-	844.4	1722.8
200	287.64	839.04	-
225	-	963.34	1914.8
250	-	1111.56	2171
275	-	1253.4	2440
300	-	1411.2	2664
325	-	1567.4	3556
350	-	1702.8	-
400	-	2027.8	-
450	-	2295.6	-

Capillary Cell Results

Polymer A in deionised water in 6mm capillary diameter cell with 10 repeated abrupt 10:1 contraction/expansion units

flow ml/hr	100 ppm Δp mbar	250 ppm Δp mbar	500 ppm Δp mbar
5	1.2	3.33	6.4
10	2.4	5.07	8.8
15	3.2	6.4	10.8
20	4	7.6	12.4
25	4.8	8.8	14.13
50	8.13	13.6	21.07
75	11.33	18.4	27.6
100	14.4	22.13	33.07
125	17.6	26.4	38.53
150	20.4	30.53	44.53
175	23.2	-	-
200	26	37.87	53.86
225	28.7	-	-
250	31.1	45.33	64.53
275	33.7	-	-
300	36.27	51.87	72.67
325	38.67	-	-
350	41.6	58.7	82
375	43.87	-	-
400	46.8	65.6	90
425	49.3	-	-
450	51.7	73.3	100.67
475	54	-	-
499	56.3	79.3	110

Polymer B in 3% NaCl solvent in two profile geometries of 6mm capillary diameter cell with 10:1 contraction/expansion ratios repeated over 10 units

flow ml/hr	profiled contraction 250 ppm Δp mbar	abrupt contraction 250 ppm Δp mbar
25	1.77	3.24
50	3.63	6.08
75	5.395	9.02
100	8.63	12.07
150	13.24	-
200	18.44	34.4
300	55.62	141.6
350	111.24	-
400	201.3	247.6
499	287.4	336

Polymer B in 0.05% NaCl solvent in three geometries of 6mm capillary diameter cells with 10:1 contraction/expansion ratios

flow ml/hr	profiled 100 ppm Δp mbar	repeated profiled 100 ppm Δp mbar	abrupt 100 ppm Δp mbar
1	0.165	0.284	0.168
2	0.35	0.5	0.34
3	0.45	0.668	0.452
4	0.62	0.831	0.573
5	0.74	0.99	0.69
7	0.99	1.353	0.931
10	1.35	1.9	1.245
15	1.027	2.85	1.806
20	2.51	3.88	2.355
25	3.099	4.91	2.945
30	3.62	6.11	3.5353
40	4.71	8.53	4.765
50	5.76	11	6
75	7.99	21.17	9.61
100	10.1	35.04	13.12
125	12.6	49.97	16.85
150	16.61	65.44	20.85
175	19.68	81.31	24.09
200	23.28	98.7	27.96
225	26.61	118.67	32.36
250	30.21	134.27	37.29
275	34.35	-	43.69
300	37.55	170.9	49.563
325	-	-	56.09
350	47.95	213.6	62.49
375	-	-	67.96
400	55.41	256.2	74.09
425	-	-	78.7
450	63.81	284.3	83.29
475	-	-	87.56
499	73.08	312.3	91.56

flow ml/hr	profiled 250 ppm Δp mbar	int prof 250 ppm Δp mbar	abrupt 250 ppm Δp mbar
1	0.587	-	0.638
2	0.893	-	1.023
3	1.2	1.467	1.293
4	1.44	1.84	1.52
5	1.68	2.187	1.77
7	2.2	2.84	2.22
10	2.866	3.87	2.79
15	3.8	5.52	3.713
20	4.72	7.027	4.6

continued ...

flow ml/hr	profiled 250 ppm Δp mbar	repeated profiled 250 ppm Δp mbar	abrupt 250 ppm Δp mbar
25	5.64	8.84	5.51
30	6.57	11.03	6.34
40	8.16	15.23	8.293
50	9.93	21.23	10.3
75	14.6	40.13	15.45
100	19	65.6	20.79
125	24.67	92.67	26.67
150	30	119.25	33.6
175	35.67	146.05	40.53
200	41	170.05	47.2
225	46.33	-	54.13
250	52.33	223.87	60.8
275	57.33	-	67.3
300	62.33	275.87	73.2
325	67.53	-	77.2
350	74.07	318.5	82
375	79.4	-	87.87
400	86.3	367.7	94.4
425	92.3	-	99.87
450	98.3	410.5	103.87
475	103.4	-	113.2
499	108.5	-	115.6

flow ml/hr	profiled 500 ppm Δp mbar	repeated profiled 500 ppm Δp mbar	abrupt 500 ppm Δp mbar
1	2.07	1.13	1.413
2	2.93	1.81	2.2
3	3.53	2.65	2.76
4	4.07	3.4	3.31
5	4.73	3.99	3.73
7	5.6	4.93	4.53
10	6.8	6.44	5.6
15	8.53	9.27	7.37
20	10.47	12.33	9
25	12.13	15.93	10.53
30	13.47	19	12.24
40	16.67	27.7	14.91
50	20.4	36.87	18.11
60	-	47	-
70	-	59.9	-
75	28.13	-	25.71
80	-	69.7	-
90	-	83	-
100	35.47	143	35.17
125	42.6	-	43.44
150	49.6	218	52.24

continued ...

flow ml/hr	profiled 500 ppm Δp mbar	repeated profiled 500 ppm Δp mbar	abrupt 500 ppm Δp mbar
175	58.27	-	56.93
200	64.27	290	69.48
225	73.6	-	76.8
250	80.27	363	87.47
275	88.93	-	94.8
300	94.27	417	104.1
325	102.27	-	110.1
350	109.87	-	120.8
375	118.9	-	132.1
400	126.3	-	140.13
425	132.9	-	144.13
450	140.93	-	153.41
475	147.6	-	162.8
499	156.9	-	177.47

Solvent Calibration Coefficients in all geometries of the 6mm capillary diameter cells with 10:1 contraction/expansion ratios

flow ml/hr	profiled Δp/q	repeated profiled Δp/q	abrupt Δp/q	repeated abrupt Δp/q
	mbar/(ml/hr)			
1	0.0533	0.0704	0.0638	-
2	0.0665	0.06	0.0644	-
3	0.0673	0.0633	0.0679	-
4	0.0663	0.0646	0.0722	-
5	0.0648	0.066	0.0717	0.1009
7	0.0657	0.0643	0.0722	-
10	0.0622	0.065	0.0711	0.1019
15	0.063	0.0644	0.0725	0.1016
20	0.0632	0.0647	0.0727	0.1047
25	0.0637	0.0647	0.0728	-
30	0.0632	0.0653	0.0726	0.1015
40	-	0.0659	0.0724	0.0983
50	0.051	0.0661	0.0723	0.0966
60	-	0.0676	0.0723	-
70	0.067	0.0718	0.0728	0.0979
80	-	0.0731	0.0731	-
90	0.0676	0.0745	0.0735	-
100	0.0675	0.0846	0.0739	0.0965
125	0.0682	0.0872	0.074	-
150	0.069	0.0902	0.075	0.1049
175	0.0691	0.0912	0.0752	-
200	0.0694	0.0931	0.0754	0.1333
225	0.0697	0.0955	-	-
250	0.070	0.0981	0.0759	0.1756
275	0.0705	0.1003	0.0763	-
300	0.0707	0.1065	0.076	0.2121
325	0.0710	0.1054	0.0763	-
350	0.0715	0.1082	0.0766	0.2435
375	-	0.1106	0.0768	-
400	0.0724	0.1137	0.0773	0.2702
425	-	0.1155	0.0776	-
450	0.0732	0.1193	0.0781	0.2938
475	-	0.1222	0.0787	-
499	0.0738	0.1243	0.0789	0.3208

Typical Solvent Pressure Losses for both planar flow cells

flow ml/hr	0.5mm Δp mbar	5.0mm Δp mbar
50	.115	
100	.2213	
200	.457	
300	.688	
400	.916	
499	1.145	
407		.0257
766		.047
1346		.084
1800		.112
2380		.147
2812		.175
3261		.2023
3614		.222
4091		.253
4337		.266
4500		.281

Pressure Losses for solutions of Polymer B in high salinity brine in the 0.5mm planar flow cell

flow ml/hr	100wppm Δp mbar	250wppm Δp mbar	500wppm Δp mbar
solvent (dp/q) (mbar/ml/hr)	.0016	.00229	.00208
1	0.00266	-	-
2	0.004	-	-
3	0.006	-	0.04
4	0.00933	0.0213	0.066
7	0.0146	0.0293	0.0933
10	0.024	0.042	0.12
20	0.048	0.088	0.24
30	0.0713	0.148	0.413
40	0.1067	0.228	0.64
50	0.1467	-	0.96
60	0.2093	0.444	1.227
70	0.283	-	1.68
80	0.378	0.885	2.07
90	0.491	-	2.59
100	0.595	1.745	3.29
125	0.976	2.796	4.71
150	1.647	4.293	5.91
175	2.82	5.52	7.19
200	3.75	6.93	8.64

continued ...

Pressure Losses for solutions of Polymer B in high salinity brine in the 0.5mm planar flow cell

flow ml/hr	100wppm Δp mbar	250wppm Δp mbar	500wppm Δp mbar
solvent (dp/q) (mbar/ml/hr)	.0016	.00229	.00208
225	4.76	8.16	-
250	5.73	9.4	11.44
275	6.73	11.02	-
300	7.97	12.89	14.44
325	8.93	14.33	-
350	10	15.99	16.64
375	11.13	17.45	-
400	12.07	19.19	19.44
425	-	20.79	-
450	-	22.52	22.77
475	-	23.72	-
499	-	24.95	28.11

Pressure Losses for solutions of Polymer B in high salinity brine in the 5.0mm planar flow cell

flow l/hr	100wppm Δp mbar	500wppm Δp mbar
solvent (dp/q) (mbar/l/hr)	.09373	.0703
0.241	-	0.0533
0.388	0.04	-
0.471	-	0.1
0.611	-	0.133
0.782	0.0866	-
0.825	-	0.173
1.002	-	0.2067
1.178	-	0.247
1.282	-	0.273
1.325	0.14	-
1.44	-	0.34
1.667	-	0.4067
1.788	-	0.453
1.79	0.2	-
2.134	-	0.647
2.237	0.2467	-
2.535	-	0.773
2.605	-	0.8867
2.742	0.3267	-
2.853	-	0.96
3.108	-	1.067

Pressure Losses for solutions of Polymer B in high salinity brine in the 0.5mm planar flow cell

flow l/hr	100wppm Δp mbar	500wppm Δp mbar
solvent (dp/q) (mbar/l/hr)	.09373	.073
3.133	0.4	-
3.214	-	1.253
3.267	-	1.407
3.384	0.453	-
3.793	0.527	-
4.142	0.587	-
4.5	0.66	-

Pressure Losses for solutions of Polymer B in low salinity brine in the 0.5mm planar flow cell

flow ml/hr	100wppm Δp mbar	250wppm Δp mbar	500wppm Δp mbar
solvent (dp/q) (mbar/ml/hr)	.00226	.00229	.00229
1		0.0267	0.267
3	-	0.0533	0.08
5	-	0.093	0.133
7	-	0.12	0.1867
10	0.1067	0.16	0.28
15	-	0.213	0.427
20	-	0.333	0.587
25	0.32	0.4	0.773
35	-	0.693	1.187
50	0.867	1.147	2.08
75	2.48	2.33	3.88
100	4.28	5.33	5.8
125	6.29	7.28	10.47
150	8.91	9.31	14.13
175	10.12	12	17.53
200	11.63	15.07	22.2
225	-	16.53	24.47
300	17.15	25.73	38.07
325	-	27.8	38.07
350	20.41	30.4	41.66
375	-	32.67	45.31
400	24.38	34.27	-
425	-	36.67	-
450	27.05	39.2	-
475	-	41.47	-
499	29.17	44.53	-

Pressure Losses for solutions of Polymer B in low salinity brine in the 5.0mm planar flow cell

flow l/hr	100wppm Δp mbar	250wppm Δp mbar	500wppm Δp mbar
solvent (dp/q) (mbar/l/hr)	.0619	.0619	.0619
0.097	-	0.0293	-
0.101	0.016	-	-
0.187	-	-	0.157
0.232	-	0.0653	-
0.367	-	-	0.261
0.383	0.052	-	-
0.44	-	-	0.279
0.543	-	0.132	-
0.581	-	0.145	-
0.692	-	0.169	-
0.703	0.088	-	-
0.742	-	0.177	-
0.791	-	0.192	-
0.853	-	0.207	-
0.887	-	0.2127	-
0.947	-	0.229	-
0.96	-	-	0.483
1.142	-	0.273	-
1.16	0.1446	-	-
1.2	-	-	0.725
1.24	-	-	0.628
1.36	-	0.334	0.811
1.44	-	0.341	0.798
1.506	0.184	-	-
1.53	-	-	0.898
1.565	-	0.377	-
1.714	-	-	1.051
1.727	-	-	1.05
1.791	-	0.4307	-
1.81	0.213	-	-
1.905	-	0.4693	-
1.97	-	-	1.08
2.028	-	0.4893	-
2.118	0.2473	-	-
2.204	-	0.53	-
2.308	-	0.5747	-
2.41	0.276	-	-
2.44	-	-	1.318
2.48	-	0.6413	-
2.5	0.294	-	-
2.62	0.306	-	-
2.805	0.327	-	-
3.06	0.3646	-	1.778
3.176	-	0.8613	-
3.273	-	0.9347	-

continued ...

Pressure Losses for solutions of Polymer B in low salinity brine in the 5.0mm planar flow cell

flow l/hr	100wppm Δp mbar	250wppm Δp mbar	500wppm Δp mbar
solvent (dp/q) (mbar/l/hr)	.0619	.0619	.0619
3.38	0.4153	-	-
3.529	-	1.008	-
3.74	0.47	-	-
3.789	-	1.108	-
3.84	-	-	2.358
4.114	0.5323	1.268	-
4.18	0.5186	-	-
4.36	-	-	2.805
4.57	0.595	-	-
4.88	0.6586	-	-
4.93	-	-	3.291
5.07	-	1.748	-
5.29	0.742	-	-
5.37	-	-	3.878
5.901	-	2.188	-
6	0.9353	-	4.363
6.26	0.992	-	-
6.54	-	2.6013	-
6.86	1.102	-	4.846
7.02	1.205	-	-
7.384	1.315	-	-
7.58	-	3.34	-
8	1.475	-	-
8.78	1.682	-	-
8.94	-	4.088	-
9.93	-	4.848	-

Pressure Losses for solutions of Polymer B in high salinity brine in the 0.5mm planar flow cell - varying concentration

flow ml/hr	5wppm Δp mbar	10wppm Δp mbar	25wppm Δp mbar	50wppm Δp mbar	75wppm Δp mbar	100wppm Δp mbar	250wppm Δp mbar
solvent (dp/q) (mbar/ml/hr)	0.00225	0.00223	0.00214	0.0021	0.00214	0.0021	0.00214
3	.02	.02	.0267	.033	.008	.0133	.017
5	.033	.033	.04	.04	.016	.0267	.031
7	.04	.04	.04	.053	.02	.04	.04
10	.053	.053	.053	.067	.034	.04	.05
15	.053	.053	.053	.067	.049	.053	.074
20	.066	.066	.066	.08	.065	.067	.097
25	.066	.08	.08	.08	.076	.08	.12
35	.093	.107	.107	.11	.1	.12	.167
50	.12	.133	.133	.133	.133	.16	.247
75	.187	.213	.213	.2	.227	.27	.413
100	.24	.267	.267	.28	.36	.44	.625
125	.293	.347	.373	.36	.507	.666	.883
150	.36	.427	.467	.44	.707	.88	1.23
175	.413	.52	.56	.56	.93	1.293	2.093
200	.48	.573	.613	.73	1.2	1.787	3.213
225	.547	.666	.653	.93	1.6	2.17	4.28
250	.613	.733	.72	1.11	2.04	2.71	5.07
275	.666	.813	.88	1.31	2.413	3.37	6.93
300	.733	.893	1.25	1.53	3.24	3.92	8.51
325	.8	.987	1.64	1.51	3.91	4.49	9.95
350	.853	1.07	1.91	1.613	4.51	5.85	12.87
400	1	1.2	2.33	2.03	5.51	7.39	15.4
450	1.12	1.387	2.76	2.56	6.37	8.656	18.49
500	1.293	1.71	2.87	3.43	7.37	9.99	21.67
550	1.387	1.68	3.11	4.08	8.97	11.85	24.93
600	1.55	1.97	3.2	4.69	9.84	13.45	27.13
650	1.68	2.16	4.83	4.67	10.57	11.85	30.27
700	1.84	2.27	5.53	5.2	11.57	13.05	32.07
750	1.95	2.36	5.87	5.8	11.31	16.72	43.73
800	2.11	2.56	4.63	6.73	12.24	17.99	37.8
850	2.28	2.81	5.96	7.67	13.52	15.45	41.13
900	2.43	3.13	6.89	8.16	14.77	20.92	43.87
950	2.55	3.33	7.56	7.53	16.63	23.59	45.45
998	2.71	3.56	7.83	8.87	17.31	23.52	-

Pressure Losses for solutions of 100wppm Polymer B in increasing salinity brine the 0.5mm planar flow cell.
(Salinity as % NaCl by weight)

flow ml/hr	0% Δp mbar	0.05% Δp mbar	0.1% Δp mbar	0.5% Δp mbar	1% Δp mbar	3% Δp mbar	10% Δp mbar
solvent (dp/q) (mbar/ml/hr)	0.0052	0.00503	0.00308	0.00336	0.00315	0.0028	0.0021
1	.1066	.0267	.013	0.013	-	-	-
3	.173	.0533	.04	0.033	.033	0.033	0.0267
5	.227	.093	.053	0.053	.04	0.053	.04
7	.273	.12	.08	0.0667	.053	0.066	.053
10	.373	.16	.093	0.08	.08	0.08	.0666
15	.44	.213	.12	0.093	.12	0.093	.093
20	.467	.333	.16	0.08	.16	0.12	.12
25	.893	.4	.227	0.12	.16	0.1467	.16
35	-	.693	.33	0.213	.307	0.253	.213
50	2.48	1.147	.627	0.48	.6	0.4	.333
75	4.87	2.33	1.253	1.267	1.267	0.88	.52
100	6.77	5.33	1.827	2.36	2.79	1.4	.813
125	9.03	7.28	2.653	3.48	4.01	2.29	1.28
150	11.6	9.31	3.97	4.43	5.45	3.32	1.65
175	14.01	12	4.76	6.41	6.91	4.27	2.09
200	16.53	15.07	5.68	8.39	9.04	5.55	2.813
225	18.93	16.53	7.87	9.4	10.77	6.8	4.89
250	20.87	19	8.826	11.05	13.97	8.56	6.04
275	23.27	22.27	10.48	13.32	15.44	9.6	6.64
300	25.67	25.73	12.41	15.08	16.71	10.83	7.35
325	27.53	27.8	14.08	16.92	17.77	12.4	7.75
350	29.13	30.4	15.81	19.19	19.77	14.66	8.21
375	31	32.67	17.48	21.32	22.17	16.27	10.28
400	32.87	34.27	19.21	23.05	23.71	14.67	11.15
425	-	36.67	20.95	24.92	25.97	15.33	12.15
450	36.2	39.2	22.28	27.05	27.71	16.93	13.01
475	-	41.47	23.61	29.12	28.57	18.13	13.55
500	40.47	44.53	24.55	30.97	30.04	19.73	14.68
525	-	-	-	-	-	23.47	16.28
550	-	-	-	-	-	24	15.21
600	-	-	-	-	-	24.37	16.05
650	-	-	-	-	-	25.2	17.27
700	-	-	-	-	-	27.2	20.55
750	-	-	-	-	-	30.8	22.41
800	-	-	-	-	-	32.93	24.15
850	-	-	-	-	-	35.6	22.95
900	-	-	-	-	-	37.73	24.35
950	-	-	-	-	-	37.6	28.95
998	-	-	-	-	-	39.67	29.88

Appendix B - Planar Contraction Force Balance

Consider an element $\delta x, \delta y, \delta z$, flowing through a planar contraction :

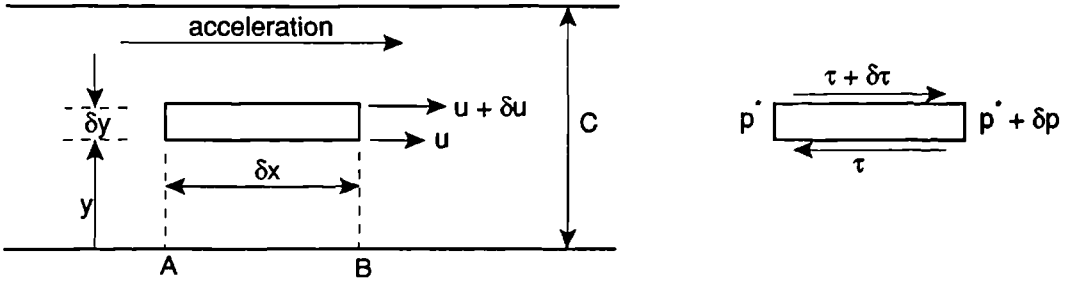

The total force on the element (where δz is the elemental thickness into the page) is given by :

$$(p^* - (p^* + \delta p))\delta y \delta z + ((\tau + \delta\tau) - \tau))\delta x \delta z = \rho \delta x \delta y \delta z * \text{acceleration}$$

assuming δx is small enough so that the restraining boundaries may be considered parallel.

Thus we get,

$$-\delta p \delta y + \delta\tau \delta x = \rho \delta x \delta y * \text{acceleration}$$

or,

$$-\frac{\delta P}{\delta x} + \frac{\delta \tau}{\delta y} = \rho * \text{acceleration}$$

The acceleration of a fluid particle is a function of both position and time - if a particle moves from A to B then its velocity changes, also a particle at B has a different velocity than one at A at the same instant in time. Again, during the time taken to travel from A to B the velocity at B may change.

Therefore we have,

$$\delta u = \frac{\partial u}{\partial x} \cdot \delta x + \frac{\partial u}{\partial t} \cdot \delta t$$

where δu is the change in velocity

δx is the distance between A and B (assumed very small)

δt is the time take to travel from A to B

so, in the limit as $\partial t \to 0$, the acceleration becomes

$$\frac{du}{dt} = \frac{\partial u}{\partial x}\frac{dx}{dt} + \frac{\partial u}{\partial t}$$

but as $\frac{dx}{dt} = u$

we get

$$\text{acceleration} = \frac{du}{dt} = \frac{\partial u}{\partial x}.u + \frac{\partial u}{\partial t}$$

where $\frac{\partial u}{\partial x}.u$ is known as the convective acceleration - that is the rate of increase due to a particles change of position

$\frac{\partial u}{\partial t}$ is the local acceleration - that is the rate of increase wrt time at a particular point in the flow

$\frac{du}{dt}$ is the substantial acceleration

If we assume a global time averaged steady state (an assumption already made in the flow through these rod arrays), then we can set $\partial u/\partial t = 0$

thus,

$$\text{acceleration} = \frac{du}{dt} = \frac{\partial u}{\partial x}.u$$

Now, substituting for acceleration into the force balance equation, gives

$$\frac{\partial \tau}{\partial x} - \frac{\partial p}{\partial y} = \rho u \frac{\partial u}{\partial x}$$

Assuming a power law fluid, that is

$$\tau = \kappa \left(\frac{\partial u}{\partial y}\right)^n$$

we get;

$$\frac{\partial}{\partial y}\left(\kappa\left(\frac{\partial u}{\partial y}\right)^n\right) = \rho u \frac{\partial u}{\partial x} + \frac{\partial p}{\partial x}$$

Integrating wrt y gives

$$\kappa \left(\frac{\partial u}{\partial y}\right)^n = \rho u y \frac{\partial u}{\partial x} + y \frac{\partial p}{\partial x} + A$$

thus

$$\frac{\partial u}{\delta y} = \left(\frac{\rho u y}{\kappa} \frac{\delta u}{\partial x} + \frac{y}{\kappa} \frac{\partial p}{\partial x} + \frac{A}{\kappa}\right)^{1/n}$$

which due to the split infinitive is considered beyond the scope of this work to solve.

If a Newtonian fluid is considered however, the relationship may be simplified by substituting for n=1 and $\kappa=\mu$. Thus we get;

$$\frac{\partial u}{\partial y} = \frac{\rho u y}{\mu} \frac{\partial u}{\partial x} + \frac{y}{\mu} \frac{\partial p}{\partial x} + \frac{A}{\mu}$$

Integrate with respect to y

$$u = \frac{\rho u y^2}{2\mu} \frac{\partial u}{\partial x} + \frac{y^2}{2\mu} \frac{\partial p}{\partial x} + \frac{A y}{\mu} + B$$

Applying Boundary Conditions;

y=0, u=0 - 1

y=C, u=0 - 2

1 gives;

$$0 = 0 + 0 + 0 + B$$

$$\therefore B = 0$$

2 gives;

$$0 = 0 + \frac{\partial p}{\delta x} \frac{C^2}{2\mu} + \frac{AC}{\mu}$$

$$\therefore A = -\frac{C}{2} \frac{\partial p}{\partial x}$$

Resulting in;

$$u = \frac{y^2}{2\mu}\left[\rho u\frac{\partial u}{\partial x} + \left(1 - \frac{C}{y}\right)\frac{\partial p}{\partial x}\right]$$

Converting the local velocity u into flowrate by introducing the rod height 'h', such that;

$$\partial Q = h\, u\, \partial y$$

which gives the flowrate per incremental step ∂y. Obviously the increments with the highest flowrates produce the highest resultant velocities.

Substituting the flowrate term for the velocity u in the pressure drop equation above gives;

$$\int_0^Q \partial Q = \int_0^C \frac{hy^2}{2\mu}\left[\rho u\frac{\partial u}{\partial x} + \left(1 - \frac{C}{y}\right)\frac{\partial p}{\partial x}\right]\partial y$$

upon integration we get

$$Q = \frac{h\rho u}{2\mu}\frac{\partial u}{\partial x}\left[\frac{y^3}{3}\right]_0^C + \left(\frac{h}{2\mu}\left[\frac{y^3}{3}\right]_0^C - \frac{Ch}{2\mu}\left[\frac{y^2}{2}\right]_0^C\right)\frac{\partial p}{\partial x}$$

$$= \frac{h\rho u}{2\mu}\frac{\partial u}{\partial x}\frac{C^3}{3} + \left(\frac{h}{2\mu}\frac{C^3}{3} - \frac{C^3 h}{4\mu}\right)\frac{\partial p}{\partial x}$$

$$= \frac{h\rho u}{2\mu}\frac{\partial u}{\partial x}\frac{C^3}{3} + \frac{C^3 h}{12\mu}\left(-\frac{\partial p}{\partial x}\right)$$

$$\boxed{Q = \frac{hC^3}{12\mu}\left[2\mu\rho\frac{\partial u}{\partial x} + \left(-\frac{\partial p}{\partial x}\right)\right]}$$

In order to estimate the differences between the Newtonian and non-Newtonian case we need to solve for the shear rate $\dot{\gamma}$ to see which region of the rheological behaviour of the polymer solution is encountered.

Now, $\dot{\gamma} = \frac{\partial u}{\partial y}$

substituting this, and for the constant of integration A, before integrating with respect to y gives;

$$\frac{\partial u}{\partial y} = \dot{\gamma} = \frac{\rho u y}{\mu}\frac{\partial u}{\partial x} + \frac{y}{\mu}\frac{\partial p}{\partial x} - \frac{C}{2\mu}\frac{\partial p}{\partial x}$$

The maximum rate of shear will occur at the wall, therefore boundary conditions are;

$\dot{\gamma}_{wall}$ occurs at $y = 0$ (or $y = C$)

$u = 0$ at wall, $\therefore \partial u/\partial x = 0$ also

which when applied give;

$$\dot{\gamma} = \frac{C}{2\mu}\left(-\frac{\partial p}{\partial x}\right)$$

If we now use this result, with the above condition of $\partial u/\partial x = 0$ which occurs at the instant the flow passes through the neck, we may obtain a relationship between the flowrate Q and the maximum shear strain rate $\dot{\gamma}$.

$$Q = \frac{hC^2}{6}\dot{\gamma}_{max}$$